Universitat Autònoma de Barcelona

Development and application of modern pure shift NMR techniques and improved HSQC/HSQMBC experiments

Laura Castañar Acedo

Doctoral Thesis
Ph.D. in Chemistry
Chemistry Department
Faculty of Sciences

2015

Supervisors:
Teodor Parella Coll
Albert Virgili Moya

PUBLICATION 8

Pure in-phase heteronuclear correlation NMR experiments

Laura Castañar, Josep Saurí, Robert Thomas Williamson,
Albert Virgili and Teodor Parella.
Angew. Chem. Int. Ed., **2014**, *53*, 8379-8382.

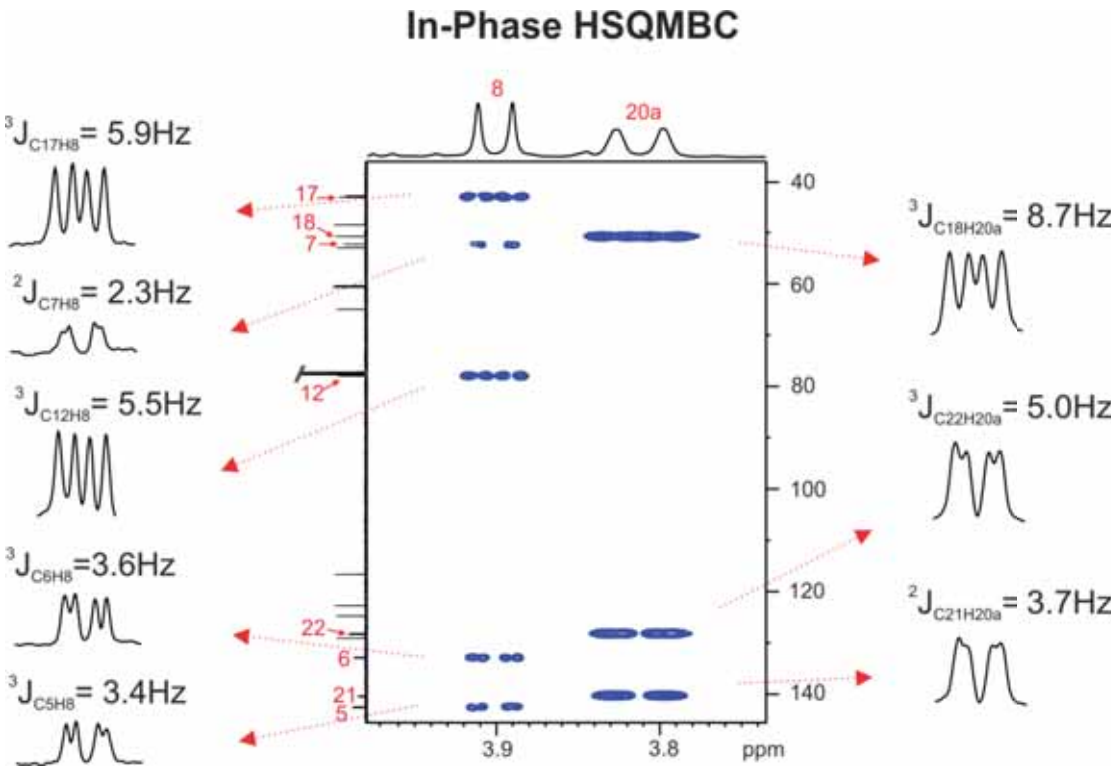

Introduction

The most serious drawback of HSQC and HSQMBC experiments is that the phase of 2D cross-peaks appear strongly distorted due to that the observable magnetization just before acquisition is a mixture of IP and AP components (see Eq.1.12 in section 1.2.1.1). This communication reports a simple and general solution to obtain heteronuclear correlation spectra that yield truly pure absorption lineshapes and IP multiplet structures for all available cross-peaks with respect to both J_{CH} and al the passive J_{HH} coupling constants along the detected dimension. The proposal is based on a conventional HSQC/HSQMBC pulse train with and appended adiabatic *z*-filter[94] applied just before acquisition.

The use of adiabatic *z*-filters was proposed to remove the *Zero-Quantum Coherences* (ZQCs) which give rise to AP dispersive components, thereby reducing the effective resolution, introducing misleading correlation, and obscuring wanted features. Although ZQCs are not detected, they can be transferred into observables signals producing AP dispersive components in the final spectrum. This ZQ filter is based on the simultaneously application of a swept-frequency 180° pulse (CHIRP pulse) and a soft PFG flanked by two 90° ^{1}H pulses (Figure 22).

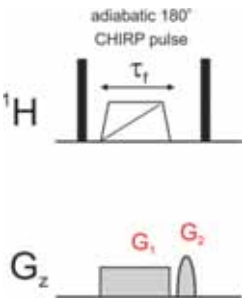

Figure 22: ZQ-filter scheme that consists of a simultaneous CHIRP 180° ^{1}H pulse and a purging gradient (G_1) followed by a single short gradient (G_2), all they placed between two 90° ^{1}H pulses.

The way in which this swept-pulse/gradient pair works can be envisaged in the following way. The application of the gradient (along the *z*-axis) results in that the Larmor frequency becomes a function of the *z*-position into the NMR tube. The swept-frequency 180° pulse will therefore flip the spins at different positions in the sample at different times. Thus, the top of the sample might experience the 180° pulse at the start of the sweep, the middle of the sample at time $\tau_f/2$, and the bottom at time τ_f, where τ_f is the duration of the sweep. The result is that in different parts of the sample the zero-quantum has evolved for different times, and so has acquired a different phase. If

[94] M. Thrippleton, J. Keeler. *Angew. Chem. Int. Ed.*, **2003**, *42*, 3938.

the range of these phases across the sample is large enough, the net result will be the cancelation of the ZQCs.

The experimental results shown in this publication confirm that the adiabatic *z*-filter incorporated at the end of the conventional HSQC/HSQMBC pulse train is an efficient tool to suppress unwanted homo- and heteronuclear AP contributions. The proposed PIP-HSQC and PIP-HSQMBC experiments yield undistorted in-phase cross-peaks that are amenable for a more accurate extraction of small coupling constant values. All these methods can be recorded in full automation mode without any prior calibration and they offer a general implementation on a large variety of isotropic and anisotropic sample conditions.

Angewandte Chemie

NMR Spectroscopy

DOI: 10.1002/anie.201404136

Pure In-Phase Heteronuclear Correlation NMR Experiments**

*Laura Castañar, Josep Saurí, Robert Thomas Williamson, Albert Virgili, and Teodor Parella**

Abstract: *A general NMR approach to provide pure in-phase (PIP) multiplets in heteronuclear correlation experiments is described. The implementation of a zero-quantum filter efficiently suppresses any unwanted anti-phase contributions that usually distort the multiplet pattern of cross-peaks and can hamper their analysis. The clean pattern obtained in PIP-HSQMBC experiments is suitable for a direct extraction of coupling constants in resolved signals, for a peak-fitting process from a reference signal, and for the application of the IPAP technique in non-resolved multiplets.*

Long-range proton–carbon correlations routinely extracted from HMBC spectra are key elements in the structural characterization of small and medium-sized molecules in solution.[1] However, the accurate quantitation of such interactions from these spectra has been problematic due to the characteristic mixed phases of the resulting HMBC cross-peaks, which lead to difficult data analysis.[2] As an alternative, the long-range optimized HSQC experiment, referred to as HSQMBC,[3] has been preferred to measure small proton–carbon coupling constants, $^{n}J(CH)$ ($n > 1$), although it is not free of inconveniences. In both HMBC and HSQMBC experiments, the main source of problems arises from the fact that proton–proton coupling constants, $J(HH)$, that have similar magnitudes to $^{n}J(CH)$ (typically ranging from 0–15 Hz), also evolve during the defocusing/refocusing periods. This unwanted modulation can introduce undesired effects in both the multiplet phase and the transfer efficiency. In order to avoid or minimize such interferences, several approaches have been reported such as the use of a BIRD-INEPT element,[4] CPMG pulse trains,[5] or selective 180° ^{1}H pulses.[6]

HMBC and HSQMBC experiments are usually recorded under non-refocusing conditions and the resulting cross-peaks are related to anti-phase (AP) multiplet patterns. Recently, a frequency-selective CLIP-HSQMBC experiment has been proposed to obtain undistorted pure in-phase (PIP) patterns that are easier to analyze but this approach requires the recording of multiple experiments to monitor all protons in the molecule of interest.[7] Here we report a simple and general solution to obtain heteronuclear correlation spectra that yield truly pure absorption lineshapes and IP multiplet structures for all available cross-peaks with respect to both $J(CH)$ and all passive $J(HH)$ coupling constants along the detected dimension (Figure 1). The proposal is based on a conventional HSQC pulse train with an appended adiabatic z-filter[8] applied just before a refocusing gradient perfect-echo element[9] and acquisition. Modification of HSQC and HSQMBC pulse sequences to include a PIP-module affords experiments that can be referred to as PIP-HSQC when the Δ delay is optimized as a function of $^{1}J(CH)$ or as PIP-HSQMBC when Δ is optimized as a function of $^{n}J(CH)$.

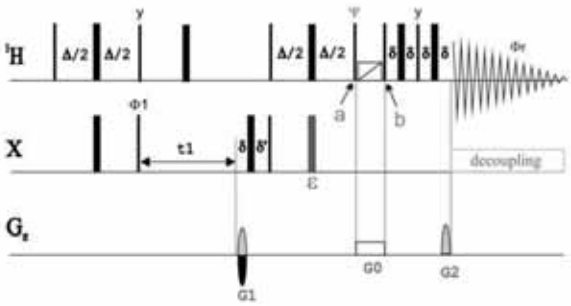

Figure 1. Pulse sequence designed to obtain pure in-phase (PIP) cross-peaks in heteronuclear correlation experiments. The delay Δ is set to $1/[2\,^{1}J(CH)]$ or $1/[2\,^{n}J(CH)]$ in PIP-HSQC or PIP-HSQMBC experiments, respectively. The z-filter includes a chirped adiabatic 180° ^{1}H pulse applied simultaneously with a purging G0 gradient, and broadband heteronuclear decoupling during proton acquisition is optional. A complete detailed description of the experiment can be found in the Supporting Information.

The HSQC scheme is easily analyzed by product operator formalism considering a heteronuclear three-spin H_1, H_2 and C system, with $J(H_1H_2)$ and $J(CH_1)$ coupling values. At the end of the refocusing INEPT period (point a in Figure 1), the magnetization of spin H_1 can be described as a mixture of IP and AP components:

$$H_{1x}\,c^2s'^2 - 2H_{1y}C_z\,c^2s'c' + 2H_{1y}H_{2z}css'^2 + 4H_{1x}H_{2z}C_z\,csc's' \qquad (1)$$

where c is $\cos(\pi J(H_1H_2)\Delta)$, s is $\sin(\pi J(H_1H_2)\Delta)$, c' is $\cos(\pi J(CH_1)\Delta)$, s' is $\sin(\pi J(CH_1)\Delta)$, and Δ is the J evolution period. The last three terms explain why cross-peaks appear strongly distorted in F2-coupled HSQC spectra of a test sample of the alkaloid strychnine (**1**) (Figure 2 A). The use of the CLIP technique (a 90° ^{13}C purging pulse applied just before the acquisition)[10] or heteronuclear decoupling during acquisition

[*] L. Castañar, J. Saurí, Prof. A. Virgili, Dr. T. Parella
Servei de RMN and Departament de Química
Universitat Autònoma de Barcelona
08193 Bellaterra (Spain)
E-mail: teodor.parella@uab.cat
Dr. R. T. Williamson
NMR Structure Elucidation, Process & Analytical Chemistry
Merck & Co. Inc.
126 E. Lincoln Avenue, Rahway, NJ 07065 (USA)

[**] Financial support provided by MINECO of Spain (project CTQ2012-32436) is gratefully acknowledged. We thank SeRMN, Universitat Autònoma de Barcelona, for allocating instrument time to this project and R. R. Gil for a sample of PMMA gel.

Supporting information for this article is available on the WWW under http://dx.doi.org/10.1002/anie.201404136.

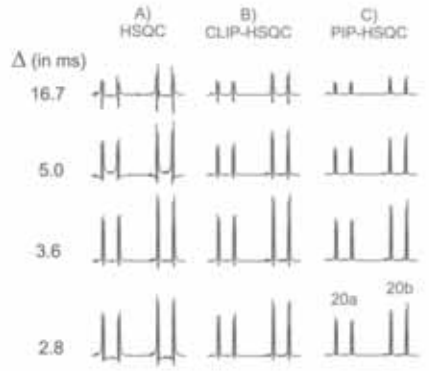

Figure 2. 1D traces extracted at the C20 chemical shift of (**1**) showing the phase distortions in A) conventional HSQC, B) CLIP-HSQC, and C) PIP-HSQC spectra with Δ optimized to several ^{1}J(CH) values: 2.8 ms (180 Hz), 3.6 ms (140 Hz), 5 ms (100 Hz), and 16.7 ms (30 Hz). Experimental values of the diastereotopic CH_2 group: ^{2}J(H20a-H20b) = 14.9 Hz, ^{1}J(C-H20a) = 138.8 Hz, ^{1}J(C-H20b) = 138.7 Hz.

efficiently removes the second and the fourth terms, but a mixture consisting of $H_{1x}+2H_{1y}H_{2z}$ still remains (Figure 2B). In practice, due to the difference of magnitudes between ^{1}J(CH) and J(HH), these unwanted contributions are small and they have been traditionally omitted in cross-peak analysis in CLIP-HSQC or in conventional decoupled HSQC experiments. It is shown experimentally and by simulations that a gradient-based ^{1}H z-filter before acquisition[11] would improve the result by partially removing the double-quantum contribution in the third term but PIP peaks are still not achieved (Supporting Information, Figures S1–S6). These perturbations could become critical when measuring ^{1}J(CH) in the presence of large J(HH) values (Figure S3), as could be found in the measurement of Residual Dipolar Couplings (RDCs) for weakly aligned samples in anisotropic media, or in experiments involving longer Δ delays (Figures S4–S6). For instance, for J(HH) = 5 Hz and ^{1}J(CH) = 140 Hz, the contribution of the ZQ term is only about 3% in a 140 Hz optimized HSQC experiment. However, in the case that ^{n}J(CH) = 8 Hz, this percentage increases to 75% in an 8 Hz optimized experiment.

As a further enhancement, it is shown here that all unwanted homo- and heteronuclear dispersive AP contributions are completely removed (Figure 2C) by applying a z-filter consisting of a 90°$_y$(^{1}H)–[adiabatic 180° ^{1}H pulse/purge gradient]–90°$_x$(^{1}H) element.[8] The remarkable benefits from the use of a z-filter for obtaining high-quality spectra has already been demonstrated for a number of NMR experiments.[9,12] Thus, after the 90°$_y$(^{1}H) pulse the above four components are converted to

$$-H_{1z}\,c^{2}s'^{2}-2H_{1y}C_{z}\,c^{2}s'c'+2H_{1y}H_{2x}\,css'^{2}-4H_{1z}H_{2x}C_{z}\,csc's' \qquad (2)$$

where the second and fourth terms represent transverse AP heteronuclear magnetization and the third element represents a mixture of homonuclear ZQ and DQ coherences, which are also eliminated by the effect of the simultaneous adiabatic 180° ^{1}H pulse and the purging G0 gradient pair. As a result, only the first term representing the desired IP magnetization remains detectable after the z-filter (point b in Figure 1). To maintain the pure IP character during detection, the classical δ-180°$_x$(^{1}H)-G2 block has been replaced by a perfect gradient echo element, in the form of δ-180°$_x$(^{1}H)–δ-90°$_y$(^{1}H)–δ-180°$_x$(^{1}H)-G2, where J(HH) should be fully refocused.[9] Using gradients with a duration of 1 ms, the unwanted anti-phase J(HH) contribution should be about 3% for a J(HH) = 5 Hz using a conventional gradient echo (Figure S7).

The interference of J(HH) effects is more obvious when the size of J(CH) and J(HH) are of the same order, as found in long-range heteronuclear correlation experiments. The importance of the z-filter is illustrated with the superior IP performance of the 8 Hz PIP-HSQMBC experiment over conventional, CLIP and z-filtered HSQMBC experiments acquired under the same conditions (Figure 3). It must be emphasized that the apparent reduced sensitivity of the PIP spectrum is not due to relaxation associated to the z-filter, but rather to the elimination of all dispersive components.

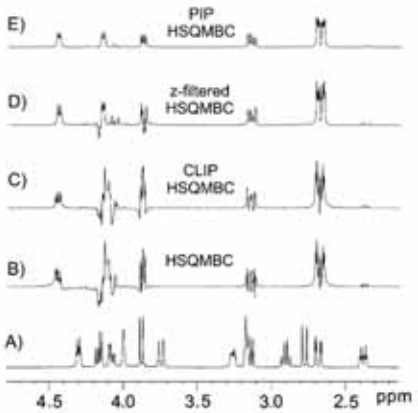

Figure 3. A) ^{1}H NMR spectrum of (**1**); B–E) 1D traces extracted at the C12 chemical shift showing the signal distortions in B) HSQMBC, C) CLIP-HSQMBC, D) z-filtered HSQMBC, and E) PIP-HSQMBC spectra (all experiments were optimized to 8 Hz (Δ = 62.5 ms)).

The inspection of some selected traces along the F2 dimension belonging to the 8 Hz PIP-HSQMBC spectrum of (**1**) clearly reveals that all cross-peaks display a clean IP character (Figure 4B). The expansion observed for the H8 and H20a cross-peaks (Figure 4C) exhibits well resolved multiplets, where the additional IP splitting (in these simple signals all observed cross-peaks become double-doublets) allows a direct and easy determination of the ^{n}J(CH) value, analogous to measuring J(HH) in conventional 1D ^{1}H spectra. Note the rough proportionality between signal intensity and ^{n}J(CH) values. Under these conditions, even a small coupling value of 2.3 Hz can be directly measured for the two-bond C7/H8 correlation. Experimentally, a different delay optimization can be useful in the event that expected correlations are missing (Figure S8).

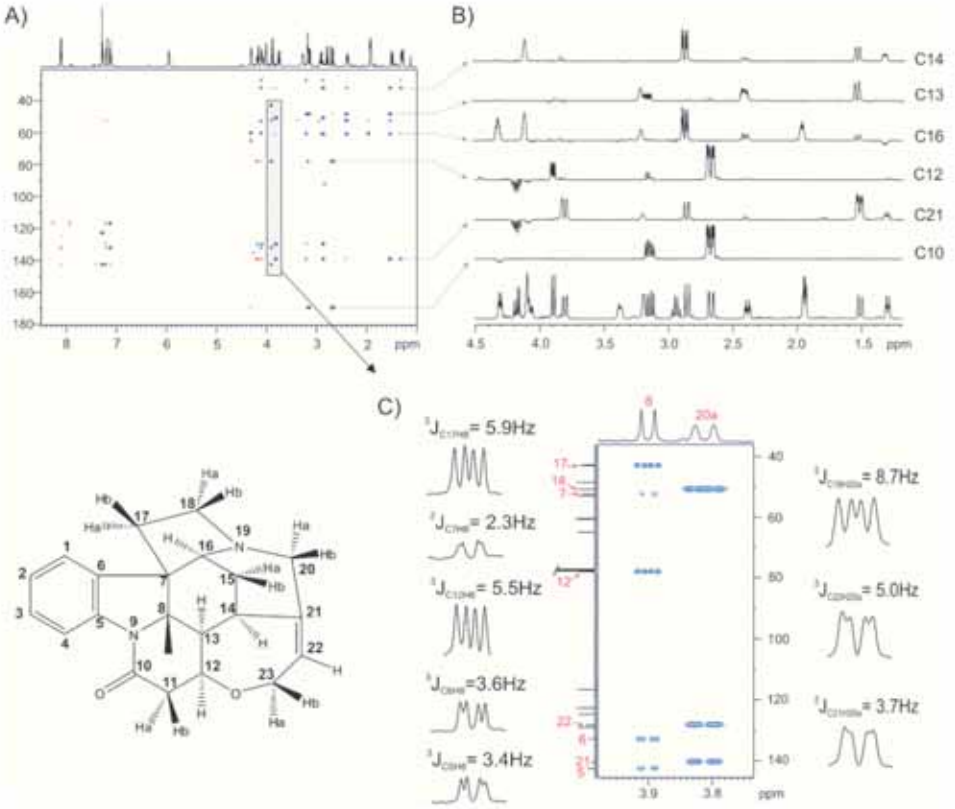

Figure 4. A) 8 Hz optimized PIP-HSQMBC spectrum of (**1**) acquired with a BIRD cluster in the initial INEPT period to minimize direct responses. B) 1D row slices taken at different ^{13}C frequencies showing in-phase multiplet patterns for all observed cross-peaks. C) Expanded area showing how the magnitude of ^{n}J(CH) can be easily determined from direct analysis of undistorted and resolved IP peaks.

The extraction of ^{n}J(CH) in more complex or non-resolved multiplets can be performed with several established methods: 1) measuring overall multiplet widths, 2) fitting/matching them to an external reference cross-peak obtained from the same sequence with broadband ^{13}C-decoupling during acquisition,[13] or 3) from the internal satellite lines corresponding to the direct ^{1}J(CH) responses, if available, without need to acquire a second reference spectrum. Alternatively, a simple approach relies on the implementation of the IPAP technique,[6] which is achieved by recording two separate IP and AP datasets as a function of the last 180° ^{13}C pulse (marked with ε in Figure 1). Figure 5 and S9–S10 compare the success of all these analytical methods from some selected cross-peaks. Similar results are obtained in experiments where the basic INEPT period has been replaced by other heteronuclear echo periods such as INEPT-BIRD,[4] CPMG,[5] or CPMG-BIRD[5] elements (Figures S11–S14).

The performance of the proposed PIP methods has been also verified under anisotropic conditions, using a sample of **1** weakly aligned in a reversible compressed poly(methyl methacrylate (PMMA) gel swollen in $CDCl_3$ (Figures S15–S17).[14] Although broader and more complex ^{1}H signals are typical for RDC experiments, experimental splittings arising from CH couplings in the range 110–190 Hz and to large HH

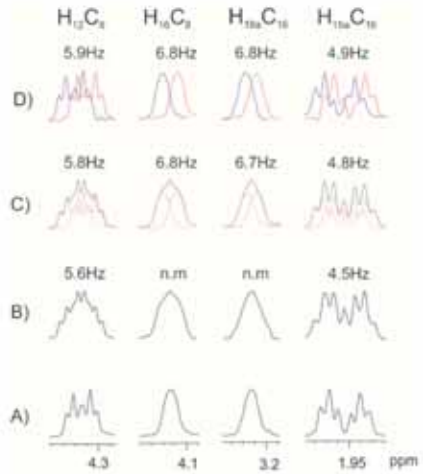

Figure 5. Comparison of several methods for the measurement of ^{n}J(CH) values in non-resolved or complex multiplets. PIP-HSQMBC cross-peaks obtained A) with and B) without ^{13}C decoupling during acquisition; C) fitting process performed from the decoupled multiplets in A to match the experimental coupled multiplets in B; D) overlaid α and β multiplets obtained after IP ± AP data combination in an IPAP experiment, respectively.

couplings up to 35 Hz can be measured (Tables S1–S3). In particular, special focus is made for the analysis and precise determination of $^{1}D(CH)$ and $^{2}D(HH)$ RDCs from undistorted cross-peaks belonging to diasterotopic CH_2 groups. The H11a/H11b protons of **1** are a good example to evaluate the more accurate measurement of their homonuclear ($^{2}D(HH) = -12.5$ Hz) and heteronuclear ($^{1}D(C_{11}H_{11a}) = +7.7$ Hz and $^{1}D(C_{11}H_{11b}) = -18.2$ Hz) RDCs, facilitating determination of their unequivocal orientation and stereoselective assignment. It is shown that errors in the measurement of up to 10% Hz can be introduced from distorted cross-peaks in conventional F2-coupled CLIP-HSQC and F2-decoupled HSQC spectra. These errors are avoided in the undistorted PIP-HSQC cross-peaks. In addition, a PIP-HSQMBC spectrum has been recorded under these challenging conditions to quantitatively measure a number of small long-range CH RDCs values, thus opening the door for the application of these parameters to superior structure determination and refinement (Figures S19–S21).

In conclusion, it has been shown that a *z*-filter is an extremely efficient tool to suppress unwanted homo- and heteronuclear anti-phase contributions in HSQC-like experiments. The proposed PIP-HSQC and PIP-HSQMBC experiments yield undistorted in-phase cross-peaks that are amenable for a more accurate extraction of small coupling constant values. All these methods can be recorded in full automation mode without any prior calibration and they offer a general implementation on a large variety of isotropic and anisotropic sample conditions. In addition, the method can be implemented in other inverse-detected NMR experiments, including HMQC-type experiments or involving other heteronuclei than carbon.

Received: April 9, 2014
Published online: June 24, 2014

Keywords: coupling constants · heteronuclear long-range correlation · HSQC · HSQMBC · pure in-phase NMR

[1] a) A. Bax, M. F. Summers, *J. Am. Chem. Soc.* **1986**, *108*, 2093–2094; b) R. C. Breton, W. F. Reynolds, *Nat. Prod. Rep.* **2013**, *30*, 501–524.
[2] a) T. Parella, J. F. Espinosa, *Prog. Nucl. Magn. Reson. Spectrosc.* **2013**, *73*, 17–55; b) B. L. Márquez, W. H. Gerwick, R. T. Williamson, *Magn. Reson. Chem.* **2001**, *39*, 499–530.
[3] a) R. T. Williamson, B. L. Márquez, W. H. Gerwick, K. E. Kövér, *Magn. Reson. Chem.* **2000**, *38*, 265–273.
[4] a) J. R. Garbow, D. P. Weitekamp, A. Pines, *Chem. Phys. Lett.* **1982**, *93*, 504–509; b) V. Lacerda, Jr., G. V. J. da Silva, M. G. Constantino, C. F. Tormena, R. T. Williamson, B. L. Márquez, *Magn. Reson. Chem.* **2006**, *44*, 95–98.
[5] a) H. Koskela, I. Kilpelainen, S. Heikkinen, *J. Magn. Reson.* **2003**, *164*, 228–232; b) K. E. Kövér, G. Batta, K. Fehér, *J. Magn. Reson.* **2006**, *181*, 89–97; c) K. Kobzar, B. Luy, *J. Magn. Reson.* **2007**, *186*, 131–141.
[6] a) S. Gil, J. F. Espinosa, T. Parella, *J. Magn. Reson.* **2010**, *207*, 312–313; b) S. Gil, J. F. Espinosa, T. Parella, *J. Magn. Reson.* **2011**, *213*, 145–150; c) J. Saurí, J. F. Espinosa, T. Parella, *Angew. Chem.* **2012**, *124*, 3985–3988; *Angew. Chem. Int. Ed.* **2012**, *51*, 3919–3922.
[7] J. Saurí, T. Parella, J. F. Espinosa, *Org. Biomol. Chem.* **2013**, *11*, 4473–4478.
[8] M. J. Thrippleton, J. Keeler, *Angew. Chem.* **2003**, *115*, 4068–4071; *Angew. Chem. Int. Ed.* **2003**, *42*, 3938–3941.
[9] A. M. Torres, G. Zheng, W. S. Price, *Magn. Reson. Chem.* **2010**, *48*, 129–133.
[10] A. Enthart, J. C. Freudenberger, J. Furrer, H. Kessler, B. Luy, *J. Magn. Reson.* **2008**, *192*, 314–322.
[11] K. E. Kövér, O. Prakash, V. J. Hruby, *J. Magn. Reson.* **1993**, *103*, 92–96.
[12] a) Ref [5c]; b) A. J. Pell, R. A. E. Edden, J. Keeler, *Magn. Reson. Chem.* **2007**, *45*, 296–316; c) B. Luy, *J. Magn. Reson.* **2009**, *201*, 18–24; d) A. M. Torres, R. D. Cruz, W. S. Price, *J. Magn. Reson.* **2008**, *193*, 311–316.
[13] K. E. Kövér, V. J. Hruby, D. Uhrín, *J. Magn. Reson.* **1997**, *129*, 125–129.
[14] J. D. Snider, E. Troche-Pesqueira, S. R. Woodruff, C. Gayathri, N. V. Tsarevsky, R. R. Gil, *Magn. Reson. Chem.* **2012**, *50*, S89–S91.

Angewandte Chemie
Eine Zeitschrift der Gesellschaft Deutscher Chemiker

Supporting Information

69451 Weinheim, Germany

Pure In-Phase Heteronuclear Correlation NMR Experiments**

*Laura Castañar, Josep Saurí, Robert Thomas Williamson, Albert Virgili, and Teodor Parella**

anie_201404136_sm_miscellaneous_information.pdf

Table of Contents:

- **Figure S17:** Comparison of 1D traces extracted from F2-decoupled (A) conventional HSQC and (B) PIP-HSQC spectra in anisotropic conditions.
- **Table S1:** ^{1}J(CH)/ ^{1}T(CH) values extracted from the PIP-HSQC spectra of strychnine recorded in isotropic and anisotropic conditions.
- **Table S2:** ^{2}J(HH)/ ^{2}T(HH) vàlues of diasterotopic CH_2 groups extracted from the PIP-HSQC spectra of strychnine recorded in isotròpic and anisotropic conditions.
- **Table S3:** Comparison of ^{2}J(HH)/ ^{2}T(HH) values extracted from the conventional HSQC, CLIP-HSQC and PIP-HSQC spectra of strychnine recorded in isotropic and anisotropic conditions.
- **Figure S18:** Plot showing the correlation between the experimental and calculated ^{1}D(CH) data for strychnine.
- **Figure S19:** 8-Hz optimized PIP-HSQMBC spectrum of strychnine in anisotropic conditions
- **Figure S20:** Comparison of 1D traces extracted from (B) HSQMBC, (C) CLIP-HSQMBC and (D) PIP-HSQMBC spectra in anisotropic conditions.
- **Figure S21:** Measurement of $^{n}T_{CH}$ values of (**1**) in anisotropic conditions in complex multiplets.
- Pulse program code for Bruker spectrometers.

Experimental Section

All NMR experiments were recorded on a BRUKER DRX-500 spectrometer equiped with a 3-channel 5-mm cryoprobe incorporating a z-gradient coil. The test sample was 25 mg of strychnine (**1**) in 0.6 ml of $CDCl_3$.

Details of pulse sequence of Fig. 1: Pulse phases are x unless indicated otherwise (Ψ=y) and a basic two-step phase cycling scheme is applied: Φ_1=x,-x, Φ_r=x,-x. The z-filter includes a chirped adiabatic 180º ^{1}H pulse applied simultaneously with a purging G0 gradient. Gradient echo/anti-echo and coherence selection was achieved by switching gradients according to G1/G2=γ_H/γ_X, where γ is the gyromagnetic ratio. δ stands for the duration of the gradient and its recovery delay and $\delta'=\delta+t_1$. TPPI-like incrementation with the echo/anti-echo recording scheme was achieved by simultaneous inversion of ^{13}C pulses applied prior to the variable t_1 period. Broadband heteronuclear decoupling during proton acquisition is optional. The IPAP technique can be applied by recording separately two complementary IP (ε=on; Ψ=y) and AP (ε=off; Ψ=x) data sets, which are further added/subtracted in the time domain followed by conventional processing to give two separate α/β spectra.

PIP-HSQC and PIP-HSQMBC spectra were recorded using the same pulse program (see Fig. 1), with an interpulse delay optimized to 140 Hz ($\Delta=1/2*{}^1J_{CH}$=3.57 ms) and 8 Hz (($\Delta=1/2*{}^nJ_{CH}$=62.5 ms), respectively. The recycle delay was of 1 s and 4 scans were collected for each one of the 128 t_1 increments, with 4096 data points in each t_1 increment. Prior to Fourier-transformation, zero-filling to 1024 points in F1, 8192 points in F2 and a squared sine-bell apodization phase-shifted 90º in both dimensions were applied. The final resolution along the detected F2 dimension was of 0.4 Hz. The total experimental time was about 13 min. Gradients G1 and G2 with a duration of 1 ms (δ) are used for echo-antiecho coherence selection, and G0 is applied simultaneously to a CHIRP pulse (30 ms) to remove undesired transverse and ZQ contributions. The proportionality between gradients G1:G2:G0 were set to ±80:20.1:3. ^{13}C 180º pulses are applied as CHIRP inversion and refocusing pulses of 500 μs and 2000 μs of duration, respectively. For the IPAP technique, IP and AP-HSQMBC datasets were separately recorded and then added/subtracted in the time-domain to provide two separate α/β data. Several fitting processes, simulations, some experimental spectra and the pulse sequence code are contained in the Supporting information.

We have also evaluated other possible long-range correlation pulse schemes where the basic INEPT period has been replaced by other heteronuclear echo periods such as INEPT-BIRD, CPMG, or CPMG-BIRD elements (Fig. S11). In all of these approaches and in the absence of the z-

filter, a severe degree of multiplet distortions were always observed due to dispersive AP contributions. These interferences occurred even when using a CPMG element with short inter-pulse delays but these approaches are particularly problematic because the consecutive application of simultaneous ^{1}H and ^{13}C pulses at high rates can produce sample heating and signal distortion. A comparison of all these versions shows that the z-filter completely removes any unwanted AP contribution and, in all cases, the resulting IP signals can be analyzed with superior accuracy (Fig. S12-S14).

For the measurement of RDCs, 4 mg of strychnine was weakly aligned in a poly(methyl methacrylate) (PMMA) gel swollen in 200ml of $CDCl_3$ using the reversible compression relaxation method. The ^{2}H quadrupolar splitting ($\Delta\upsilon_Q$) for the $CDCl_3$ signal was of 26 Hz. PIP-HSQC and PIP-HSQMBC experiments were recorded using the same pulse program, with an interpulse delay optimized to 140 Hz ($\Delta=1/2*{}^{1}J_{CH}$=3.57 ms) and 8 Hz (($\Delta=1/2*{}^{n}J_{CH}$=62.5 ms), respectively. The recycle delay was of 1 s and 64 scans were collected for each one of the 128 t_1 increments, with 4096 data points in each t_1 increment. Prior to Fourier-transformation, zero-filling to 1024 points in F1, 8192 points in F2 and a squared sine-bell apodization phase-shifted 90º in both dimensions were applied. The final resolution along the detected F2 dimension was of 0.4 Hz. The total experimental time was about 3h 30min. All spectra and experimental and calculated values can be found in figures S15-S21 and tables S1-S3.

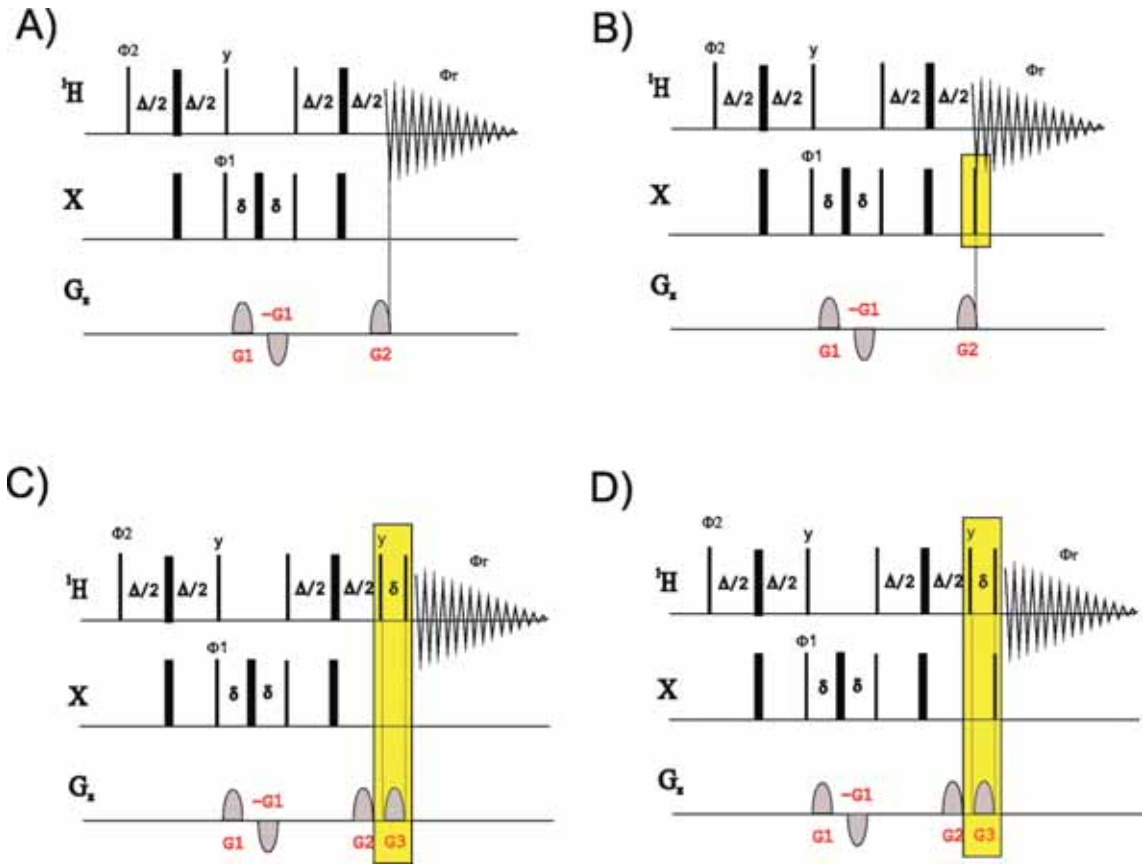

Figure S1: 1D HSQC pulse sequences used in the simulations: A) Conventional F2-coupled HSQC; B) CLIP-HSQC; C) HSQC including a z-filter, and D) HSQC including a z-filter and a CLIP ^{13}C pulse. All simulations were performed using the NMRSIM module included into the Bruker's Topspin (v3.1) software package. Pulse phases are x unless indicated otherwise. A basic four-step phase cycle was applied: Φ1=x,-x,x,-x; Φ2=x,x-x,-x; Φ r=x,-x,-x,x. Gradient ratios with a duration of 1 ms (δ) were set to G1:G2:G3=2:1:0.3 and the inter-pulse delay was optimized to Δ=1/[2*(J(CH)]. Simulations of the z-filter including the adiabatic pulse were not possible with this program.

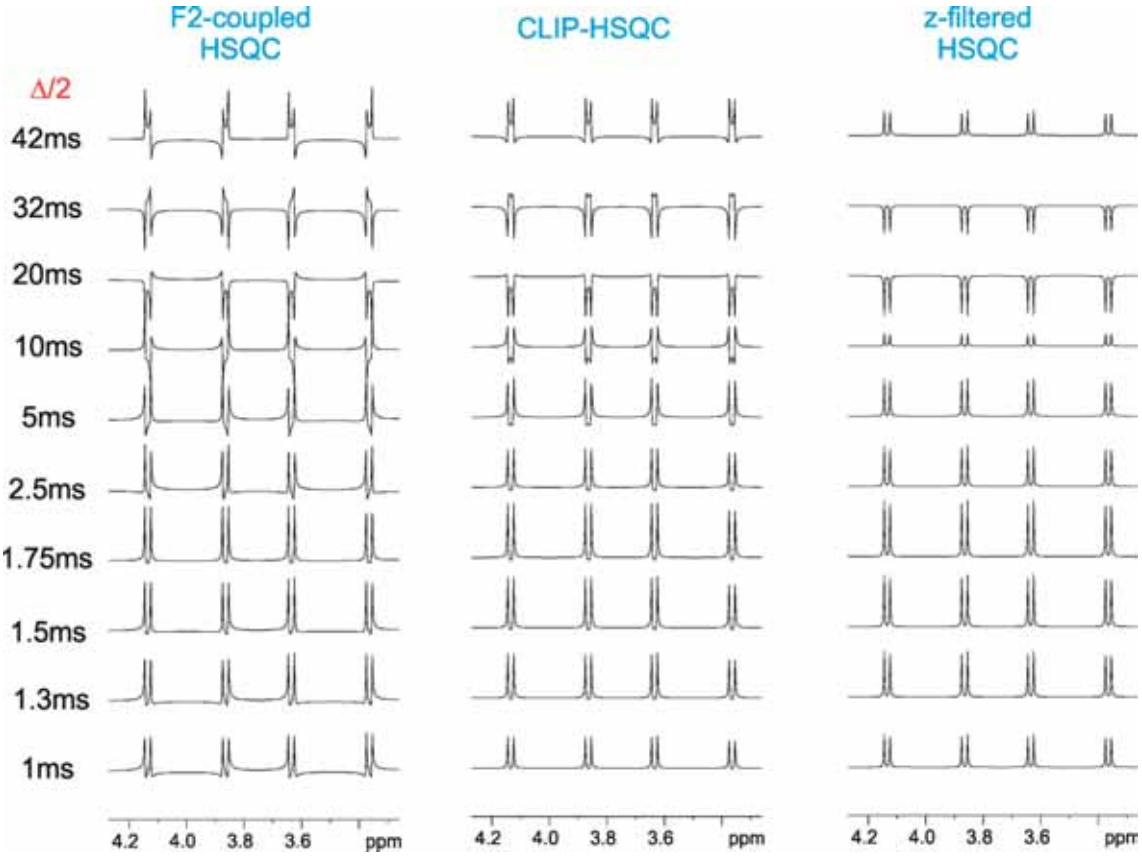

Figure S2: Simulations showing the effects of J(HH) as a function of the inter-pulse delay optimization in 1D F2-coupled A) conventional HSQC, B) CLIP-HSQC and C) z-filtered HSQC experiments (see pulse schemes in Fig. S1). Simulation parameters of the diastereotopic CH_2 group: $\delta(H_A)$=4.0 ppm, $\delta(H_A)$=3.5 ppm, $J(H_AH_B)$=10 Hz, $^1J(CH_A)$= $^1J(CH_B)$=135 Hz.

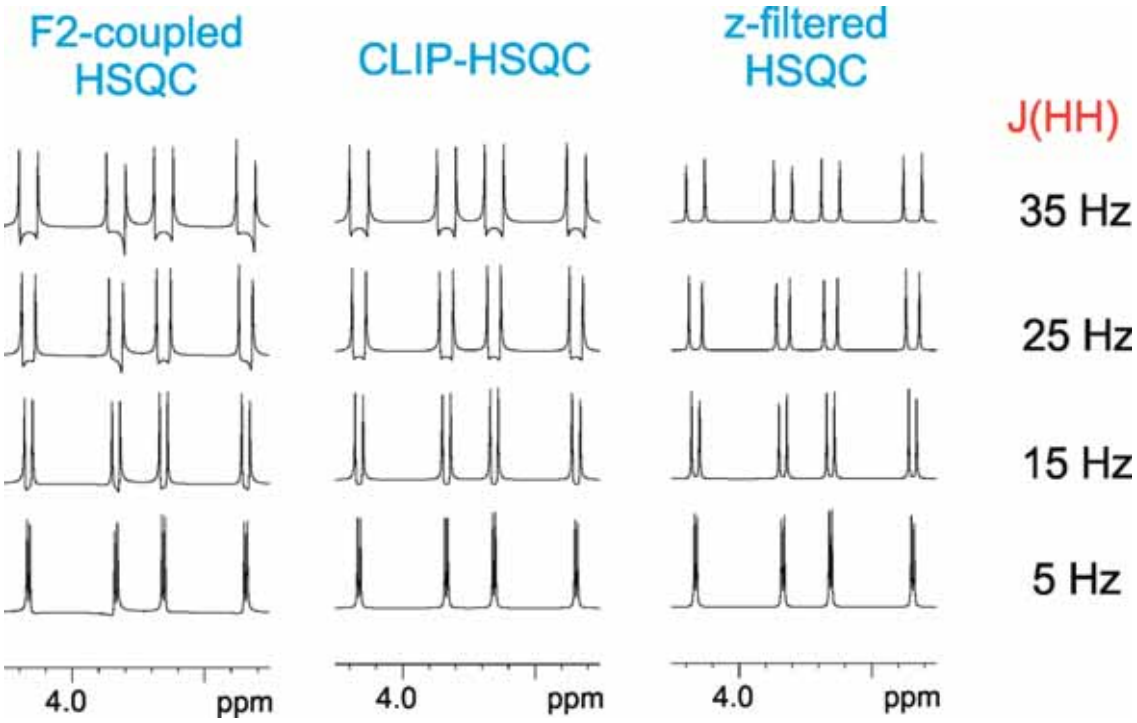

Figure S3: Simulations showing the effects of the size of J(HH) in 140-Hz optimized F2-coupled HSQC, CLIP-HSQC and z-filtered HSQC experiments. Simulation parameters: $\delta(H_A)$=4.0 ppm, $\delta(H_A)$=3.5 ppm, $^1J(CH_A)$=155 Hz, $^1J(CH_B)$=165 Hz and Δ=3.5 ms.

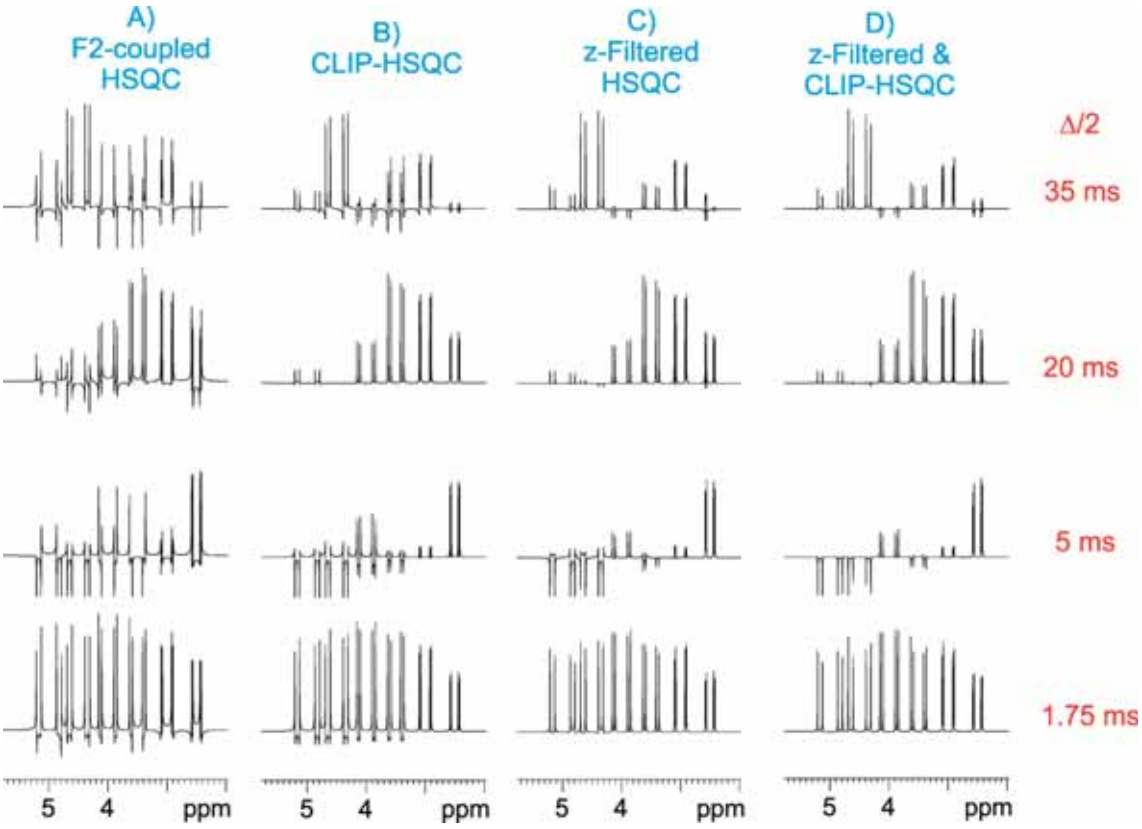

Figure S4: Simulations showing the effects of a wide range of J(HH) and J(CH) values in F2-coupled A) HSQC, B) CLIP-HSQC, C) z-filtered HSQC and D) z-filtered & CLIP-HSQC experiments as a function of the inter-pulse delay optimization. Simulation parameters: $\delta(H_A)$=2.5, $\delta(H_B)$=3.0, $\delta(H_C)$=3.5, $\delta(H_D)$=4.0, $\delta(H_E)$=4.5, $\delta(H_F)$=5; $^1J(CH_A)$=70 Hz, $^1J(CH_B)$=90 Hz, $^1J(CH_C)$=110 Hz, $^1J(CH_D)$=130 Hz, $^1J(CH_E)$=150 Hz, $^1J(CH_F)$=170Hz; $^2J(H_AH_B)$=10 Hz, $^2J(H_CH_D)$= 25 Hz, $^2J(H_EH_F)$=40 Hz.

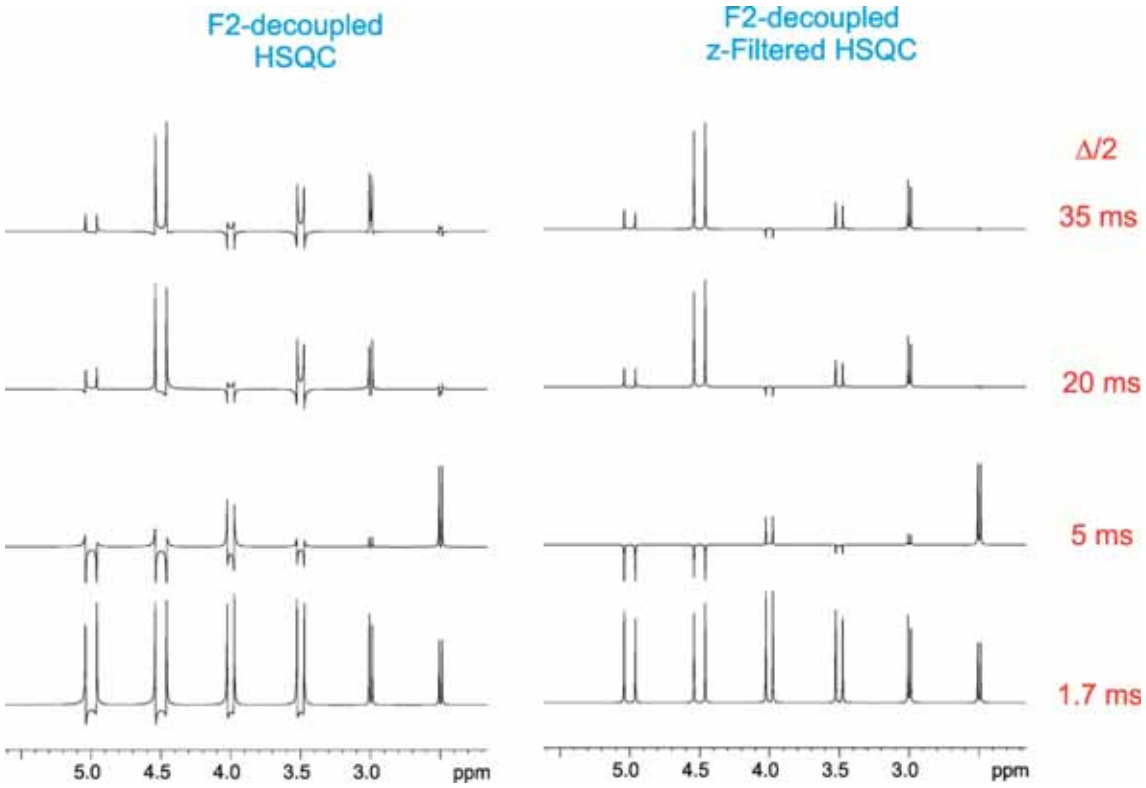

Figure S5: Simulations showing the effects of a wide range of J(HH) and J(CH) values in broadband decoupled HSQC and z-filtered HSQC experiment as a function of the inter-pulse delay optimization. We used the same spin system as described in Fig. S4.

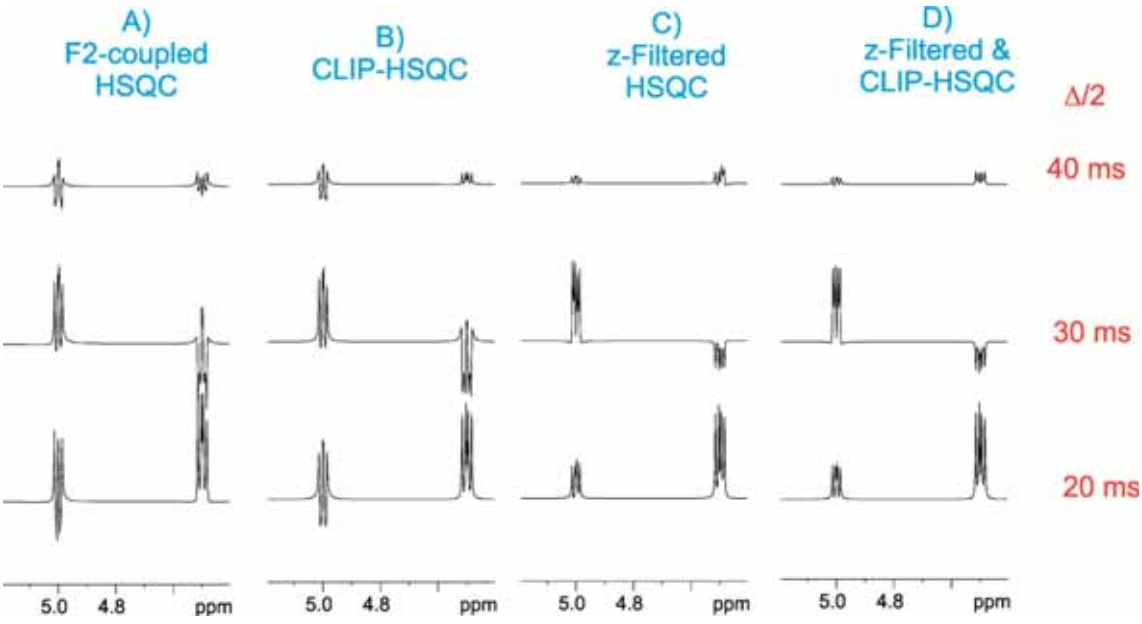

Figure S6: Simulations showing the effects of the inter-pulse delay optimization on small long-range J(CH) coupling constants in A) F2-coupled HSQC, B) CLIP-HSQC, C) z-filtered HSQC and D) z-filtered & CLIP-HSQC experiments. Simulation parameters: $\delta(H_A)$=4, $\delta(H_B)$=4.5, $\delta(H_C)$=5.0; $^{1}J(CH_A)$=140 Hz, $^{n}J(H_AH_B)$=6 Hz, $^{n}J(H_AH_C)$= 5 Hz, $^{n}J(CH_B)$=10 Hz, $^{n}J(CH_C)$=8 Hz.

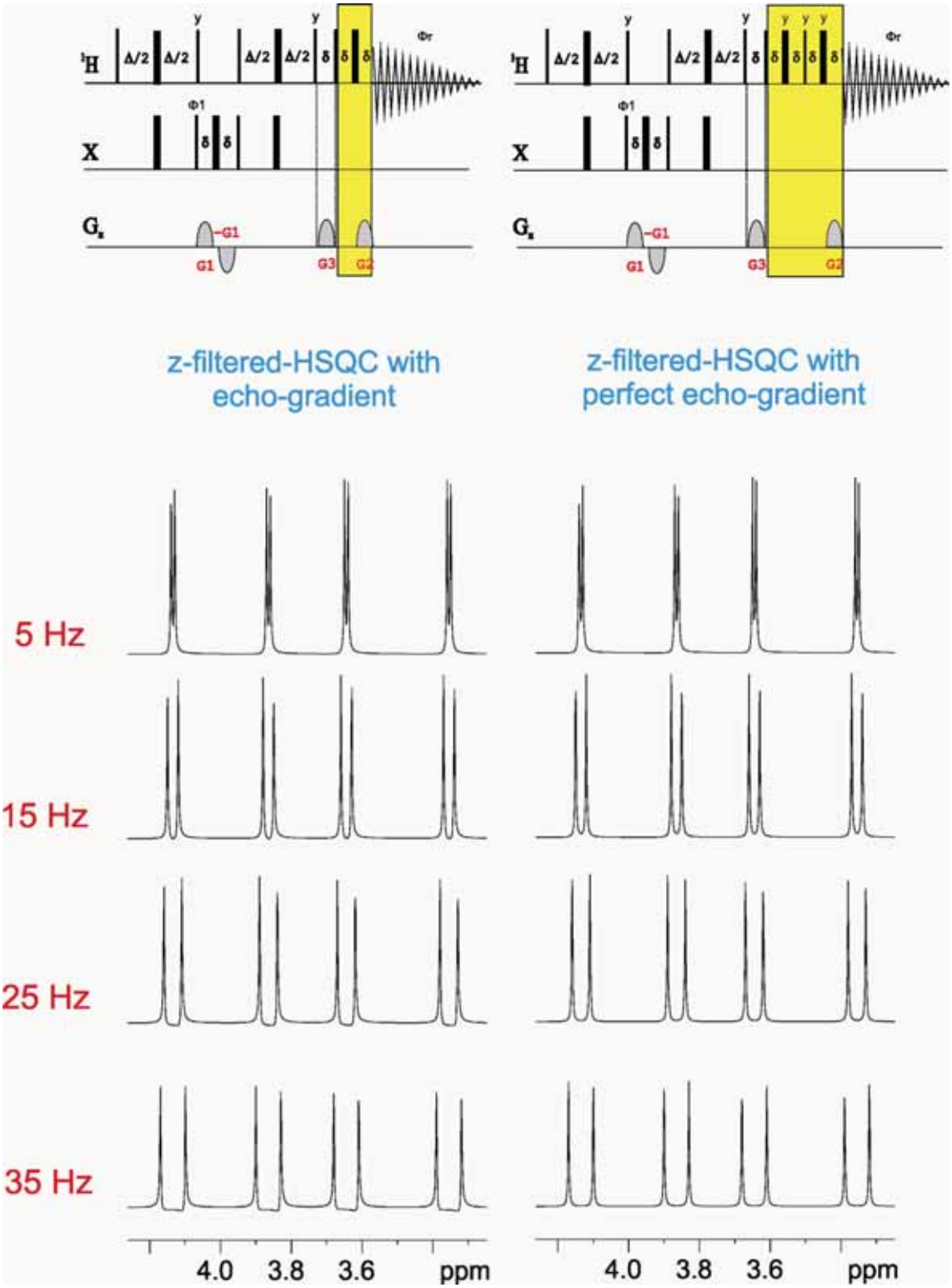

Figure S7: Simulations showing the effects of J(HH) evolution in a F2-coupled z-filtered HSQC experiment with A) a conventional echo gradient and B) a perfect-echo gradient. Simulation parameters: $\delta(H_A)$=4.0 ppm, $\delta(H_A)$=3.5 ppm, $^1J(CH_A)$=135 Hz, $^1J(CH_B)$=145 Hz,Δ=3.57 ms (optimized to 140 Hz), the duration of the gradient was 1ms and the recovery delay was set to 100µs (δ=1.1ms).

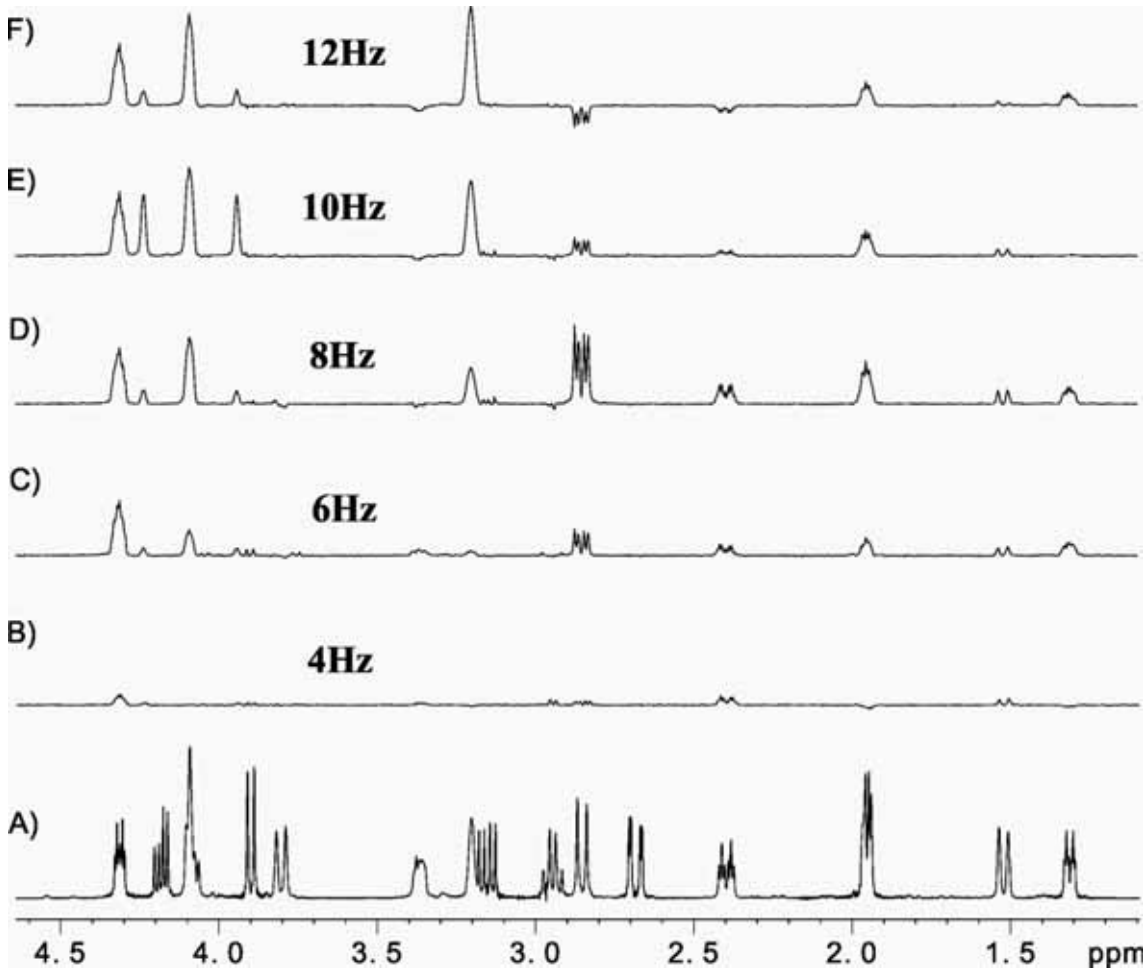

Figure S8: 1D traces extracted at 60.1 ppm (corresponding to the C8 and C16 carbons) as a function of inter-pulse Δ delay optimization in the PIP-HSQMBC experiment. A) Conventional ^{1}H, B) 4 Hz (Δ=125 ms), C) 6 Hz (Δ=83.3 ms), D) 8 Hz (Δ=62.5 ms), E) 10 Hz (Δ=50 ms) and E) 12 Hz (Δ=41.7 ms).

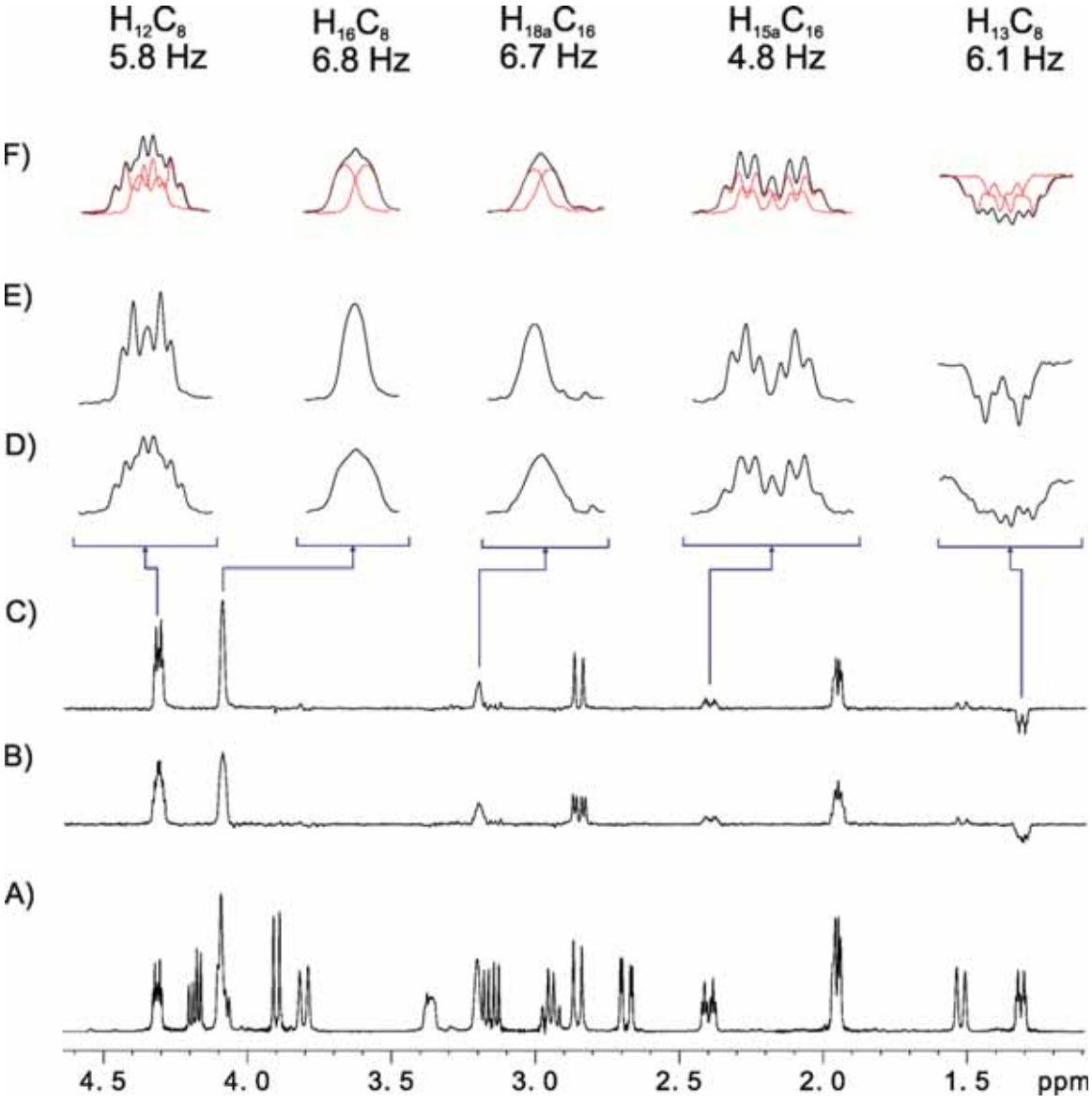

Figure S9: A) ^{1}H spectrum of strychnine at 500.13MHz. B-C) Comparison of the 1D slices extracted at 60.1 ppm (C8 and C16 carbons) from PIP-HSQMBC spectra acquired without (B) and with (C) heteronuclear decoupling during proton acquisition in Fig. 1 (Δ=62.5 ms). D-E) Expansion of some signals extracted from B and C, respectively. F) The decoupled multiplets can be used as a reference for a fitting process in cases where the additional splitting due to the active ^{n}J(CH) cannot be directly extracted from the non-decoupled multiplet.

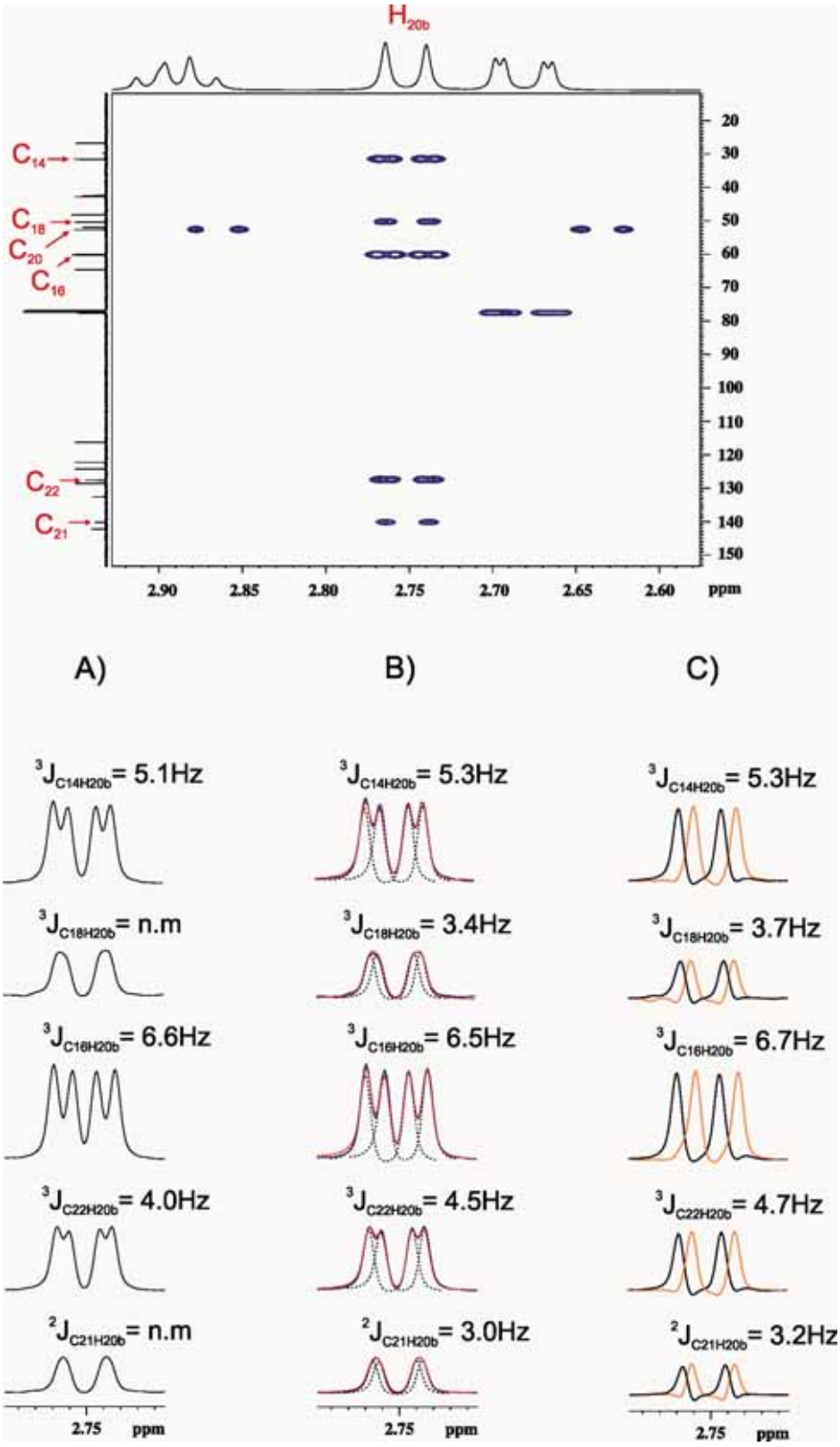

Figure S10: Comparison of methods for the measuring of small heteronuclear coupling constants taking some multiplet patterns from an 8 Hz optimized PIP-HSQMBC spectrum: A) direct extraction, B) fitting from the internal satellite lines and, C) IPAP methodology. The resolution along the detected F2 dimension was of 0.4Hz.

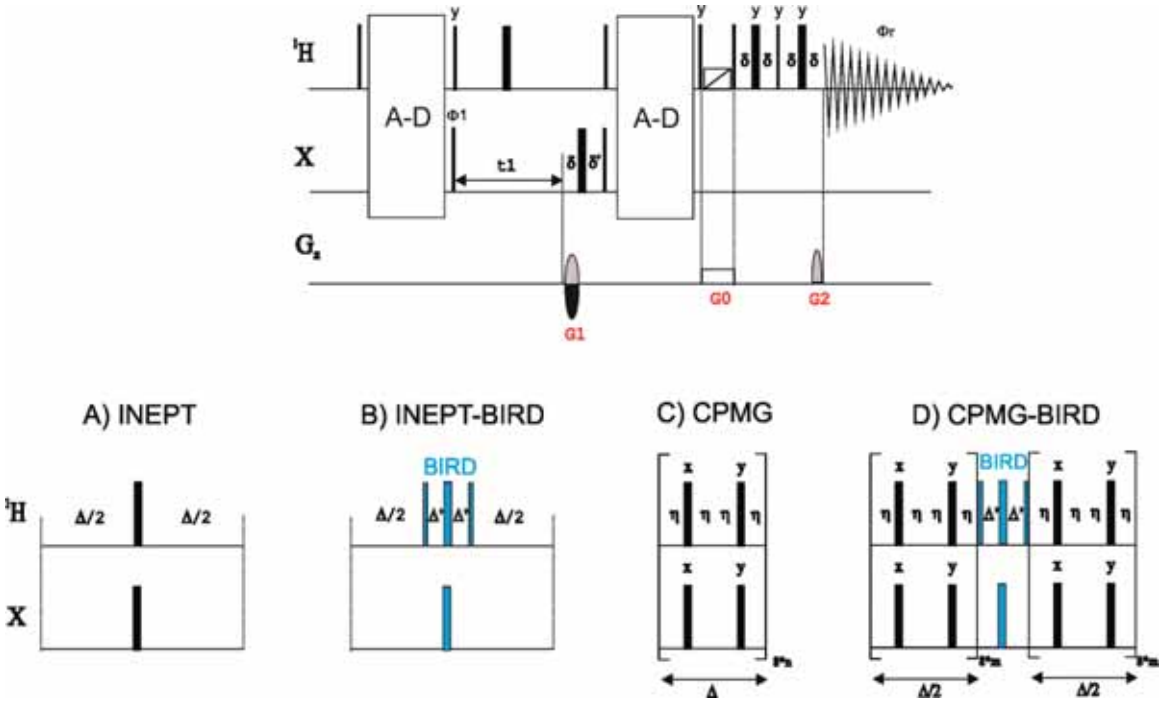

Figure S11: 2D pulse schemes to obtain PIP heteronuclear long-range correlation spectra. All these variants use the basic HSQMBC pulse train with a final zero-quantum filter after the refocusing period and just before the refocusing gradient echo and the acquisition. Several elements have been evaluated for the defocusing/refocusing of the heteronuclear coupling constants during the period $\Delta=1/[2*{}^{n}J(CH)]$: A) the basic INEPT; B) the INEPT-BIRD block ($\Delta'=1/[2*{}^{1}J(CH)]$); C) the CPMG XY-16 super cycle consisting of simultaneous ^{1}H and ^{13}C pulses applied at intervals 2η; D) the CPMG-BIRD element combining the features of B and C.

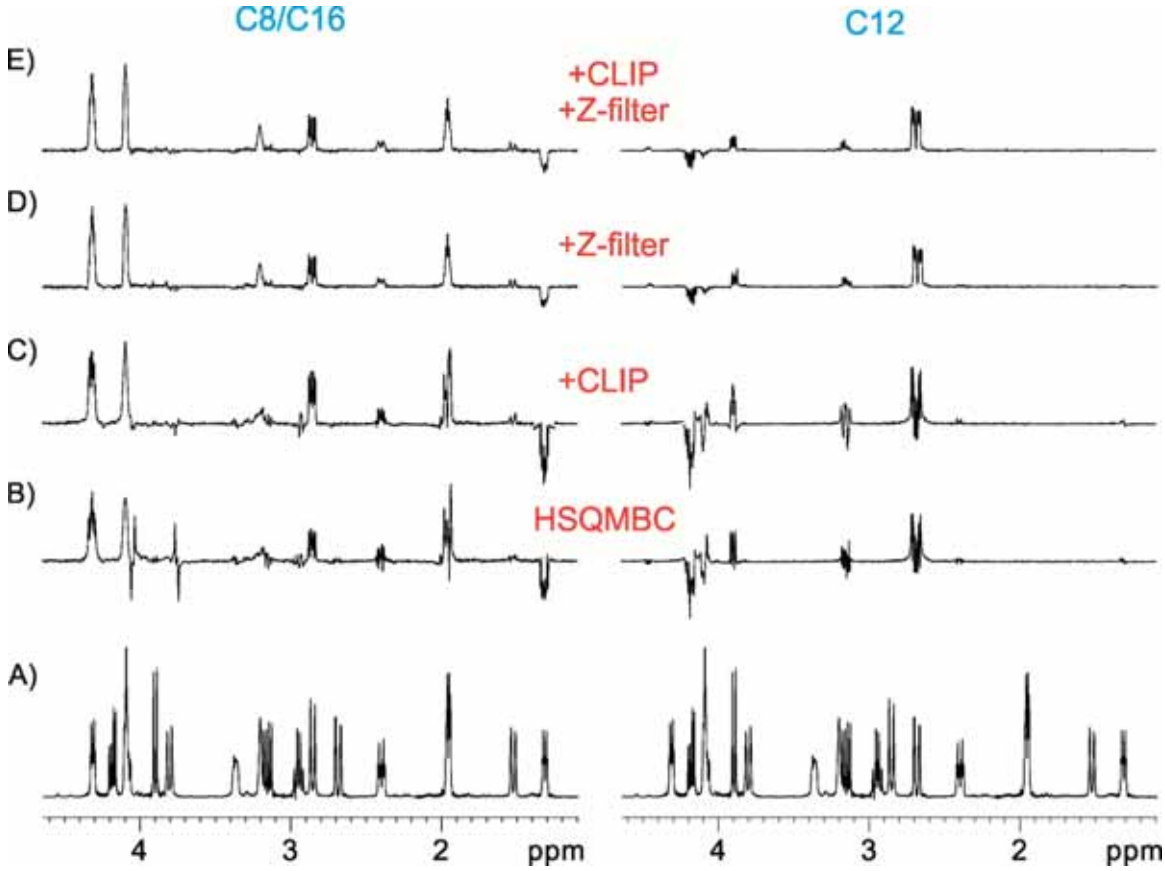

Figure S12: A) ^{1}H spectrum of strychnine at 500.13 MHz. B-E) Experimental effects on the application of the z-filter and a purging 90º ^{13}C pulse just before acquisition. 1D slices were extracted at 60.1 and 77.7 ppm (C8/C16 and C12 carbons, respectively) corresponding to the following 8 Hz optimized PIP-HSQMBC experiments: B) without adiabatic z-filter and CLIP pulse; C) with CLIP pulse; D) with adiabatic z-filter; E) with CLIP pulse and adiabatic z-filter. In all cases, data were acquired and processed under the same conditions (see experimental section) and the corresponding slices have been plotted at the same vertical scale to compare real sensitivity levels.

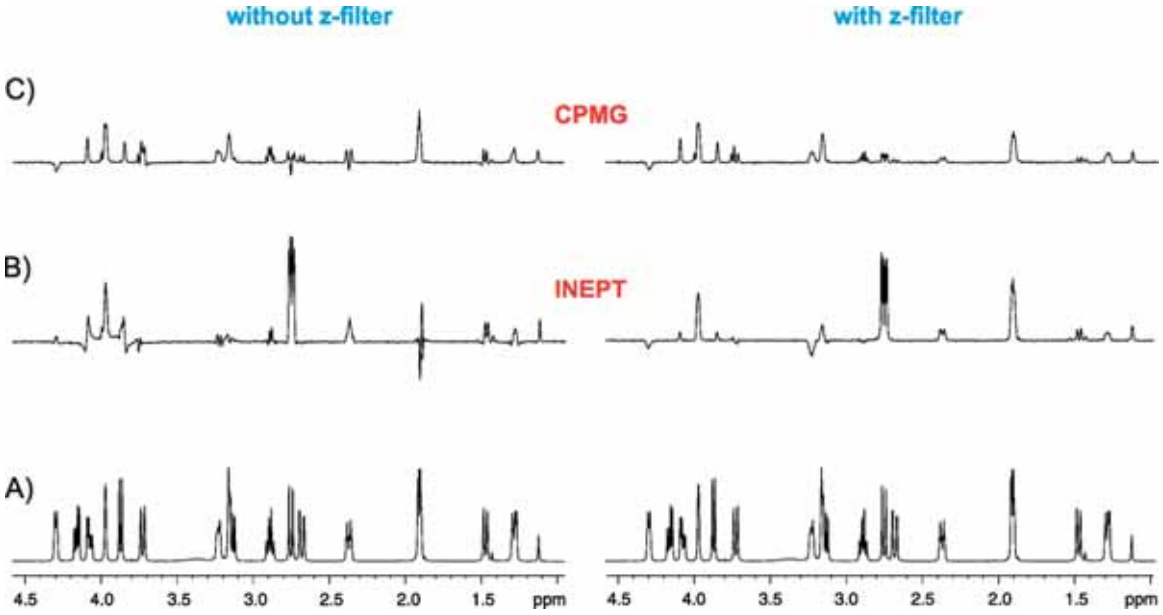

Figure S13: A) Conventional ^{1}H NMR; B-D) 1D slices extracted at 60.1 ppm (C8 and C16 carbons), corresponding to the following 8-Hz optimized PIP-HSQMBC experiments with and without z-filter: B) HSQMBC with INEPT (Fig. S11A); C) HSQMBC with CPMG (Fig. S11C with η=300 μs). In all cases, data were acquired and processed under the same conditions (see experimental section). The corresponding slices have been plotted at the same vertical scale to compare real sensitivity levels.

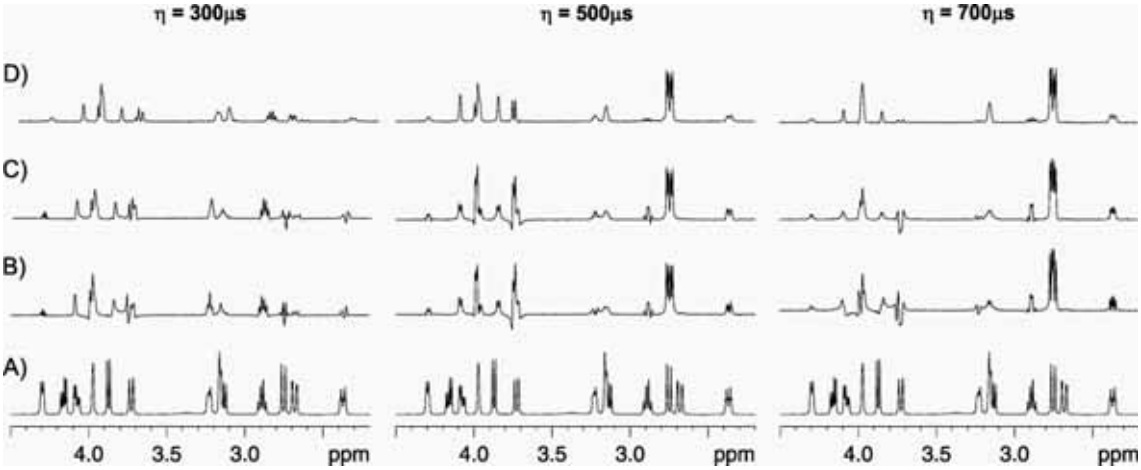

Figure S14: Experimental effects on the influence of the inter-pulse delay setting (η) in the success of the 8 Hz optimized B) HSQMBC-CPMG, C) HSQMBC-CPMG-CLIP and D) PIP-HSQMBC-CPMG experiment. All NMR experiments were acquired with the same experimental conditions described in figure S13.

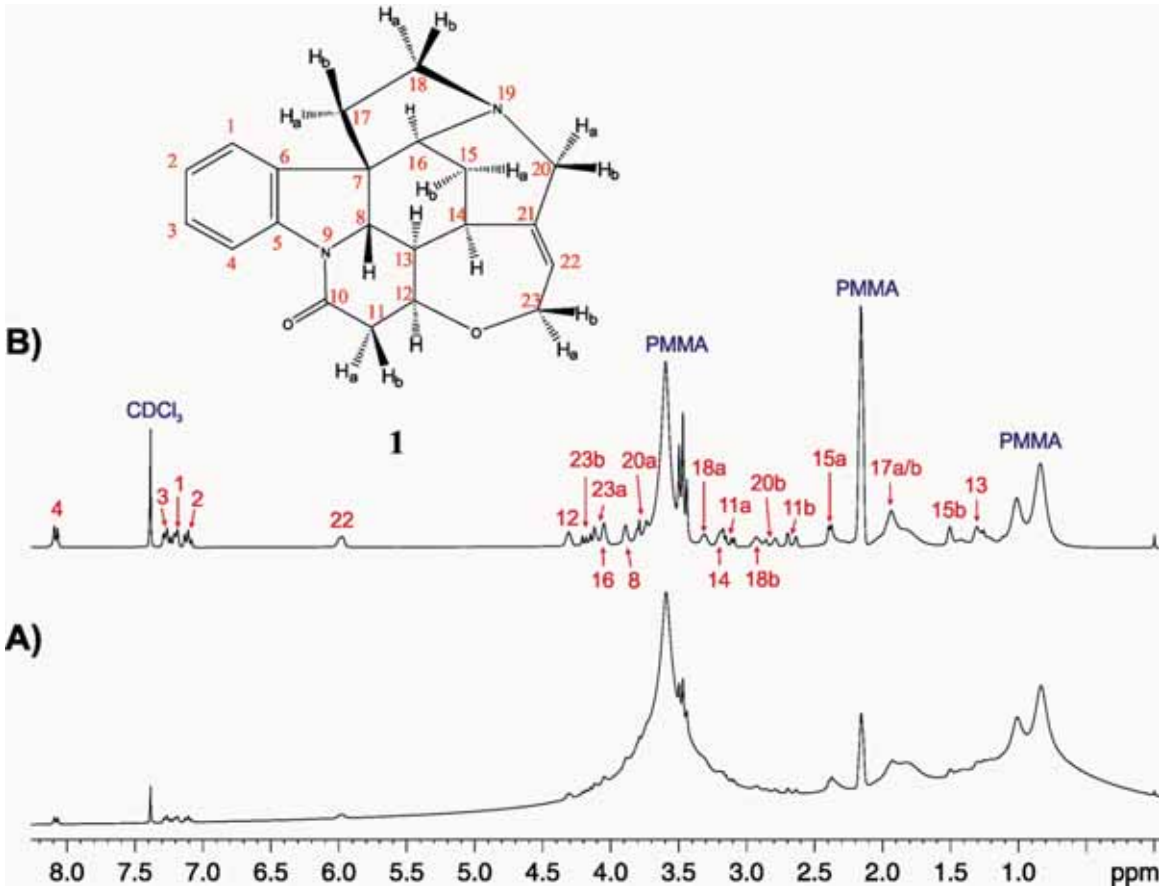

Figure S15: (A) conventional ^{1}H and (B) CPMG-PROJECT spectra of 4 mg of strychnine weakly aligned in PMMA gel swollen in $CDCl_3$. The 1D CPMG spectrum was acquired with a total echo time of 12 ms. Both experiments were collected using 4 scans.

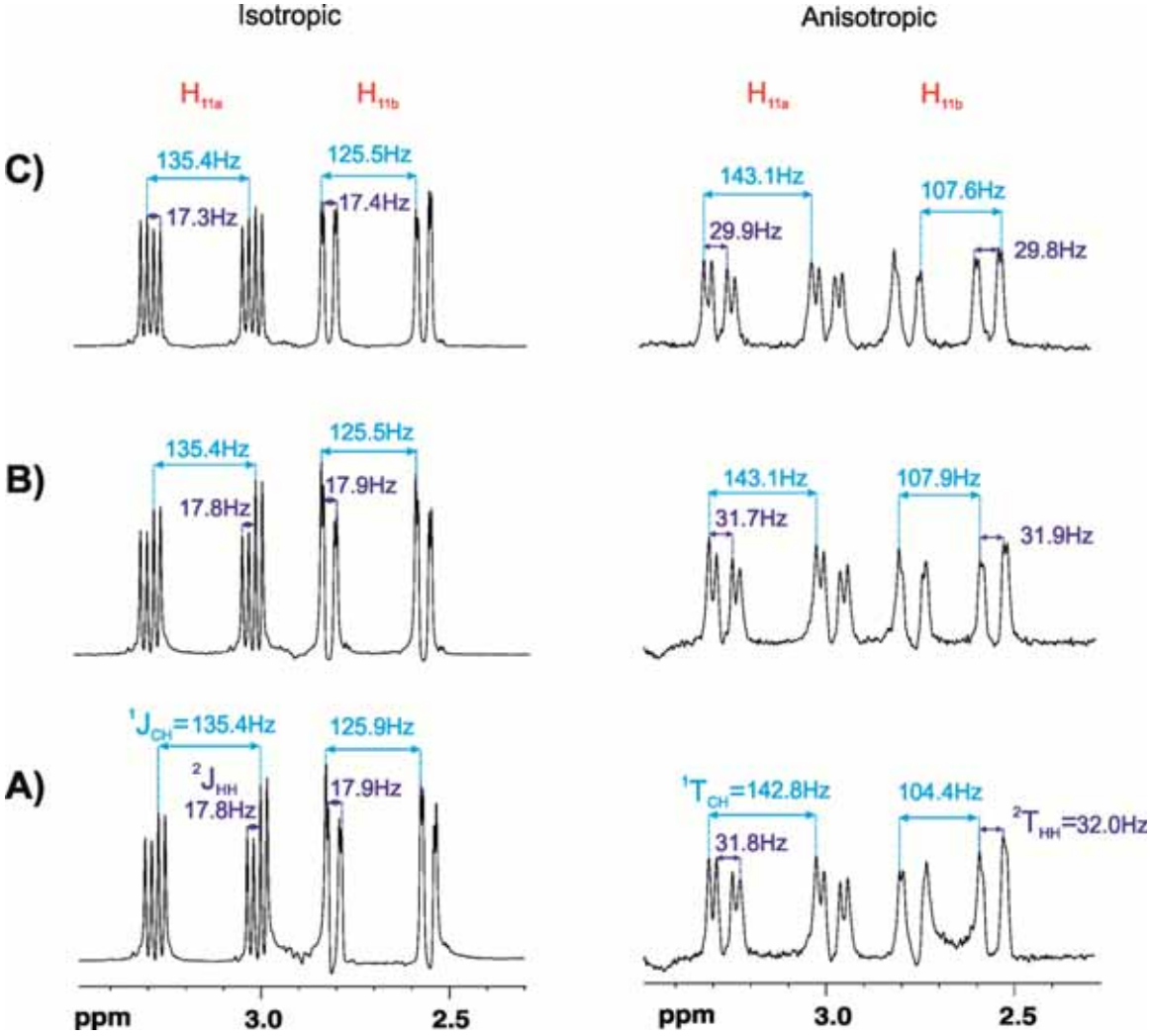

Figure S16: 1D traces extracted at the C11 chemical shift of (**1**) in isotropic and anisotropic conditions showing the signal distortions originated in (A) conventional HSQC, (B) CLIP-HSQC, and (C) PIP-HSQC spectra recorded with Δ set to 3.6 ms ($^{1}J_{CH}$=140 Hz).

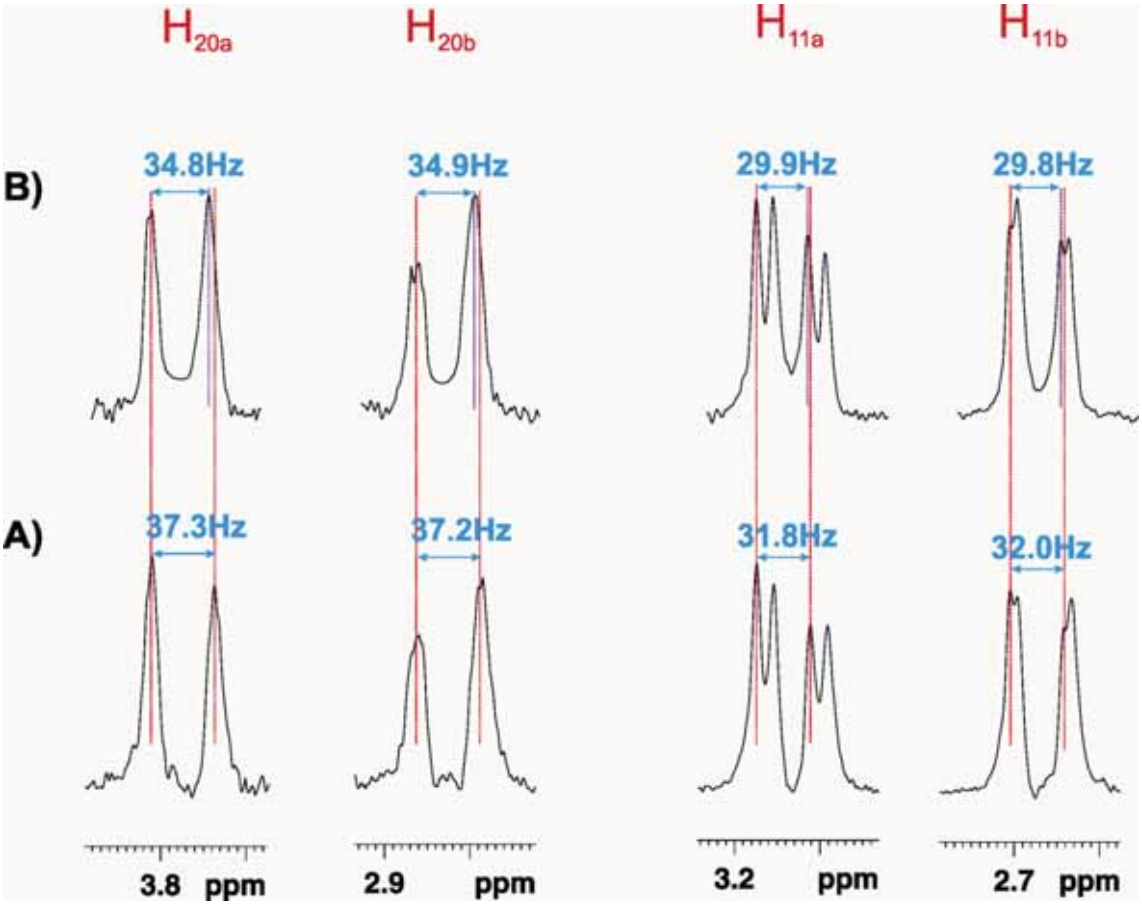

Figure S17: 1D traces extracted at the C11 and C20 chemical shift of (**1**) in anisotropic conditions from F2-decoupled (A) conventional HSQC and (B) PIP-HSQC spectra with Δ optimized 3.6 ms ($^{1}J_{CH}$=140 Hz). The elimination of all dispersive components in (B) allows carrying out the measurement of ^{n}JHH more accurately. J_{HH} splittings extracted from ^{1}H-PROJECT spectrum were $^{2}J_{H20aH20b}$=34.8Hz and $^{2}J_{H11aH11b}$=30.0Hz.

Table S1: Experimental $^{1}J(CH)$/ $^{1}T(CH)$ values extracted from the PIP-HSQC spectra of strychnine recorded in isotropic and anisotropic conditions.

				PIP-HSQC				
				Isotropic	Anisotropic		Predicted[c]	Others [ref.1]
C	δ (ppm)	H	δ (ppm)	$^{1}J_{CH}$ (Hz)	$^{1}T_{CH}$ (Hz)	$^{1}D_{CH}$ (Hz)	$^{1}D_{CH}$ (Hz)	$^{1}D_{CH}$ (Hz)
C_1	122.3	H_1	7.16	158.3	174.8	+16.5	+12.2	+21.0
C_2	124.2	H_2	7.09	160.8[a]	163.7[a]	+2.9	+2.2	+12.3
C_3	128.6	H_3	7.25	159.2[a]	163.5[a]	+4.3	+3.2	+10.0
C_4	116.2	H_4	8.08	168.4	187.1	+18.7	+13.9	+21.6
C_8	60.1	H_8	3.86	144.9	133.7	-11.2	-8.6	-9.8
C_{11}	42.5	H_{11a}	3.12	135.4	143.1	+7.7	+5.9	+10.0
		H_{11b}	2.66	125.5	107.6	-18.2	-14.1	-18.0
C_{12}	77.6	H_{12}	4.28	150.0	134.2	-15.8	-12.3	-20.6
C_{13}	48.2	H_{13}	1.27	124.8	118.9	-5.9	-4.6	-4.9
C_{14}	31.6	H_{14}	3.15	131.3	117.9	-13.4	-10.4	-20.7
C_{15}	26.8	H_{15a}	2.36	130.9	135.0	+4.1	+3.2	+2.0
		H_{15b}	1.47	129.9	131.0	+1.1	+0.9	+4.5
C_{16}	60.2	H_{16}	3.98	146.7	158.2	+11.5	+9.0	+14.0
C_{17}	42.8	$H_{17a/b}$	1.90	133.2	139.1	+5.9	+4.6	+1.38
C_{18}	50.3	H_{18a}	3.25	146.3	148.1	+1.8	+1.4	0.0
		H_{18b}	2.88	131.7	143.4	+11.7	+9.0	+13.0
C_{20}	52.7	H_{20a}	3.73	138.8	ov[b]		-7.7	-10.0
		H_{20b}	2.76	138.7	132.9	-6.2	-4.6	-6.0
C_{22}	127.6	H_{22}	5.93	158.8	156.4	-2.4	-1.8	-1.1
C_{23}	64.6	H_{23b}	4.15	145.5	148.9	+3.4	+2.6	+8
		H_{23a}	4.05	137.2	111.7	-25.5	-19.4	--

[a] Strong coupling effect
[b] Overlapped with PMMA signals
[c] The predicted values have been calculated with MSpin program (MESTREALAB RESEARCH SL, Santiago de Compostela, Spain. http://www.mestrelab.com).

[1] J. D. Snider, E.Troche-Pesqueira, S. R. Woodruff, C.Gayathri, N. V. Tsarevsky and R. R. Gil, *Magn. Reson. Chem*. **2012**, 50, S89-S91.

Table S2: $^{2}J(HH)/\ ^{2}T(HH)$ values extracted from the PIP-HSQC spectra of strychnine recorded in isotropic and anisotropic conditions.

		^{1}H NMR	**CPMG-PROJECT**	**PIP-HSQC**				
		Isotropic[a]	**Anisotropic[a]**	**Isotropic[a]**	**Anisotropic[a]**		**Predicted[c]**	**Others** [ref.2]
H	δ (ppm)	$^{2}J_{HH}$ (Hz)	$^{2}T_{HH}$ (Hz)	$^{2}J_{HH}$ (Hz)	$^{2}T_{HH}$ (Hz)	$^{2}D_{HH}$ (Hz)	$^{2}D_{HH}$ (Hz)	$^{2}D_{HH}$ (Hz)
H_{11a}	3.12	-17.3	-30.1	-17.3	-29.9	-12.6	-9.9	-12.5
H_{11b}	2.66	-17.4	-30.0	-17.4	-29.8	-12.4		-12.6
H_{15a}	2.36	-14.4	-n.m	-14.5	n.m	--	+10.2	+13.2
H_{15b}	1.47	-14.4	-n.m	-14.6	n.m	--		+13.3
H_{18a}	3.25	n.m	-n.m	n.m	n.m	--	+7.1	+8.8
H_{18b}	2.88	-9.6	-n.m	-9.6	n.m	--		+8.9
H_{20a}	3.73	-14.8	-34.7	-15.0	-34.8	-19.8	-15.3	-20.1
H_{20b}	2.76	-14.8	-34.9	-14.9	-34.9	-20.0		-20.1
H_{23b}	4.15	-13.8	-30.1	-13.7	-29.7	-16.0	-12.7	-16.2
H_{23a}	4.05	-13.8	ov[b]	-13.8	-29.8	-16.0		-16.3

n.m: not measured due to signal widening caused by $^{n}J_{HH}/\ ^{n}T_{HH}$ splitting.

[a] The sign of the measure has been extrapolated from ω1-iINEPT experiments [2].

[b] Overlapped with H_{23a} and H_{16} signals.

[c] The predicted values have been calculated with MSpin program (MESTREALAB RESEARCH SL, Santiago de Compostela, Spain. http://www.mestrelab.com).

[2] Measuring from the ω1-iINEPT experiment in isotropic and anisotropic media: J. Saurí, L. Castañar, P. Nolis, A. Virgili, T. Parella, *J. Magn. Reson*. 242 (2014) 33–40.

Table S3: Comparison of $^{2}J(HH)$/ $^{2}T(HH)$ values extracted from the conventional HSQC, CLIP-HSQC and PIP-HSQC spectra of strychnine recorded in isotropic and anisotropic conditions.

		^{1}H NMR	CPMG-PROJECT	HSQC		CLIP-HSQC		PIP-HSQC	
		Isotropic	Anisotropic	Isotropic	Anisotropic	Isotropic	Anisotropic	Isotropic	Anisotropic
H	δ (ppm)	$^{2}J_{HH}$ (Hz)	$^{2}T_{HH}$ (Hz)	$^{2}J_{HH}$ (Hz)	$^{2}T_{HH}$ (Hz)	$^{2}J_{HH}$ (Hz)	$^{2}T_{HH}$ (Hz)	$^{2}J_{HH}$ (Hz)	$^{2}T_{HH}$ (Hz)
H_{11a}	3.12	-17.3	-30.1	-17.8	-31.8	-17.8	-31.7	-17.3	-29.9
H_{11b}	2.66	-17.4	-30.0	-17.9	-32.0	-17.9	-31.9	-17.4	-29.8
H_{15a}	2.36	-14.4	-n.m	-15.1	n.m	-15.1	n.m	-14.5	n.m
H_{15b}	1.47	-14.4	-n.m	-15.3	n.m	-15.4	n.m	-14.6	n.m
H_{18a}	3.25	-n.m	-n.m	n.m	n.m	n.m	n.m	n.m	n.m
H_{18b}	2.88	-9.6	-n.m	-9.9	n.m	-10.0	n.m	-9.6	n.m
H_{20a}	3.73	-14.8	-34.7	-15.6	-37.3	-15.7	-37.2	-15.0	-34.8
H_{20b}	2.76	-14.8	-34.9	-15.6	-37.2	-15.6	-37.4	-14.9	-34.9
H_{23b}	4.15	-13.8	-30.1	-13.6	-32.1	-13.6	-32.2	-13.7	-29.7
H_{23a}	4.05	-13.8	-ov[b]	-13.9	-32.2	-13.9	-32.2	-13.8	-29.8

n.m: not measured due to signal widening caused by $^{n}J_{HH}$/ $^{n}T_{HH}$ splitting.

[a] The sign of the measure has been extrapolated from ω1-iINEPT experiments [2].

[b] Overlapped with H_{23a} and H_1 signals.

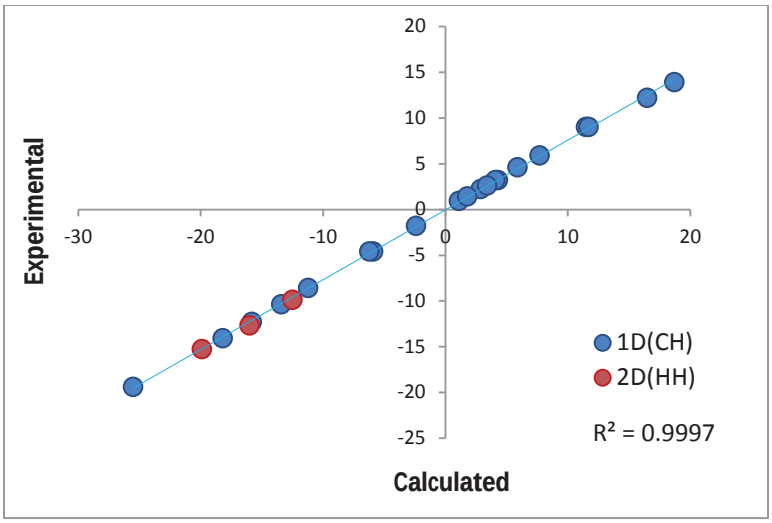

Figure S18: Plot showing the correlation between the experimental and calculated ^{1}D(CH) data for strychnine described in Table S1.

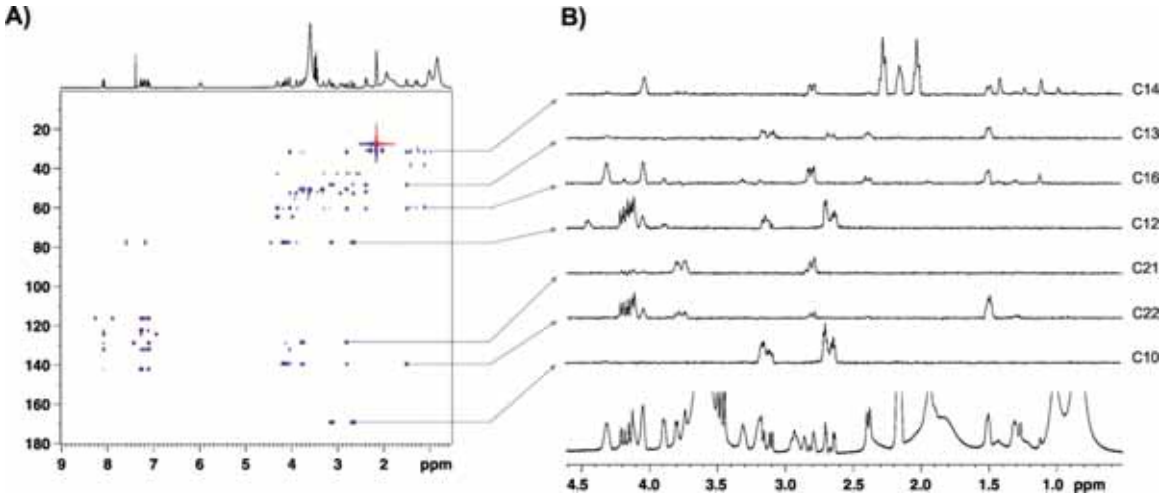

Figure S19: (A) 8-Hz optimized PIP-HSQMBC spectrum of (**1**) in anisotropic conditions; (B) 1D row slices taken at different ^{13}C frequencies showing in-phase multiplet patterns for all observed cross-peaks.

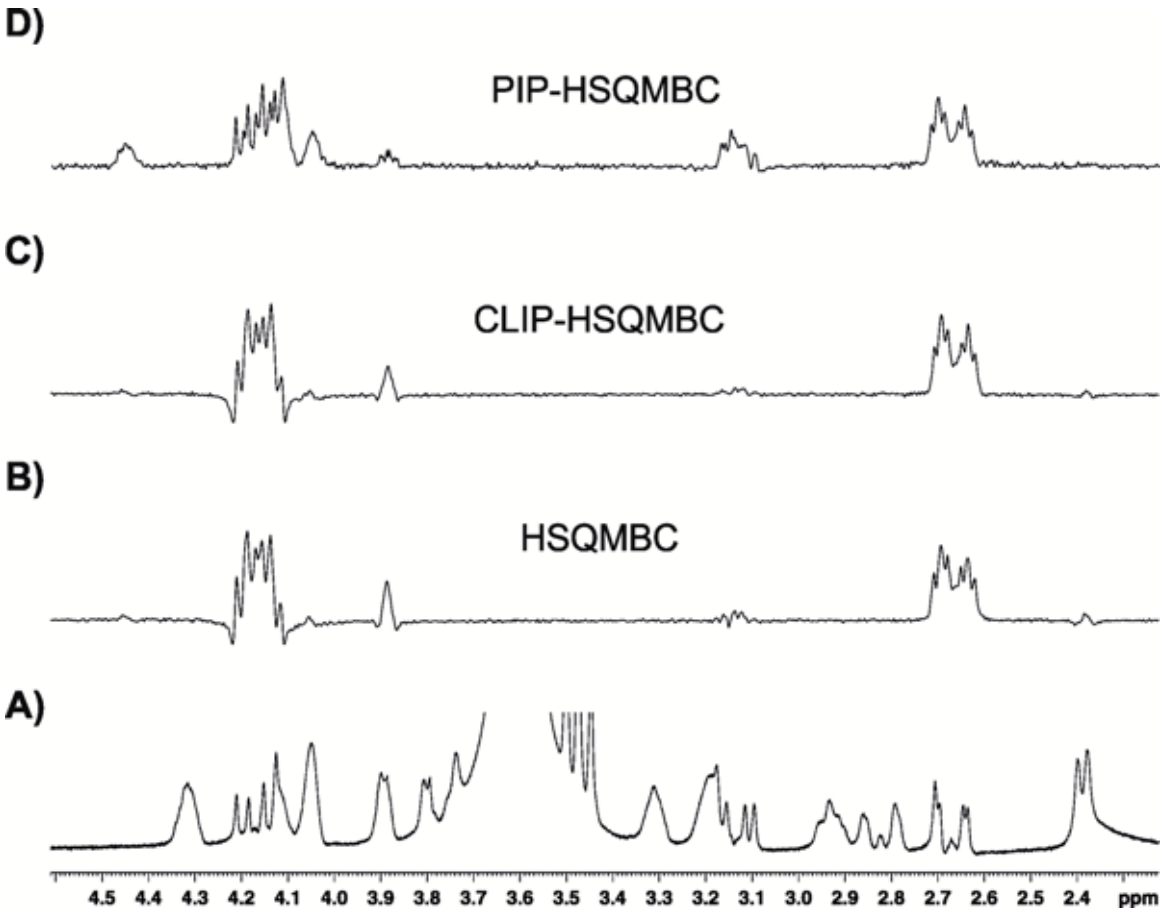

Figure S20: (A) ^{1}H-PROJECT spectrum of (**1**) in anisotropic conditions; (B-D) 1D traces extracted at the C12 chemical shift showing the signal distortions in (B) HSQMBC, (C) CLIP-HSQMBC and (D) PIP-HSQMBC spectra (all experiments were optimized to 8 Hz (Δ=62.5 ms)).

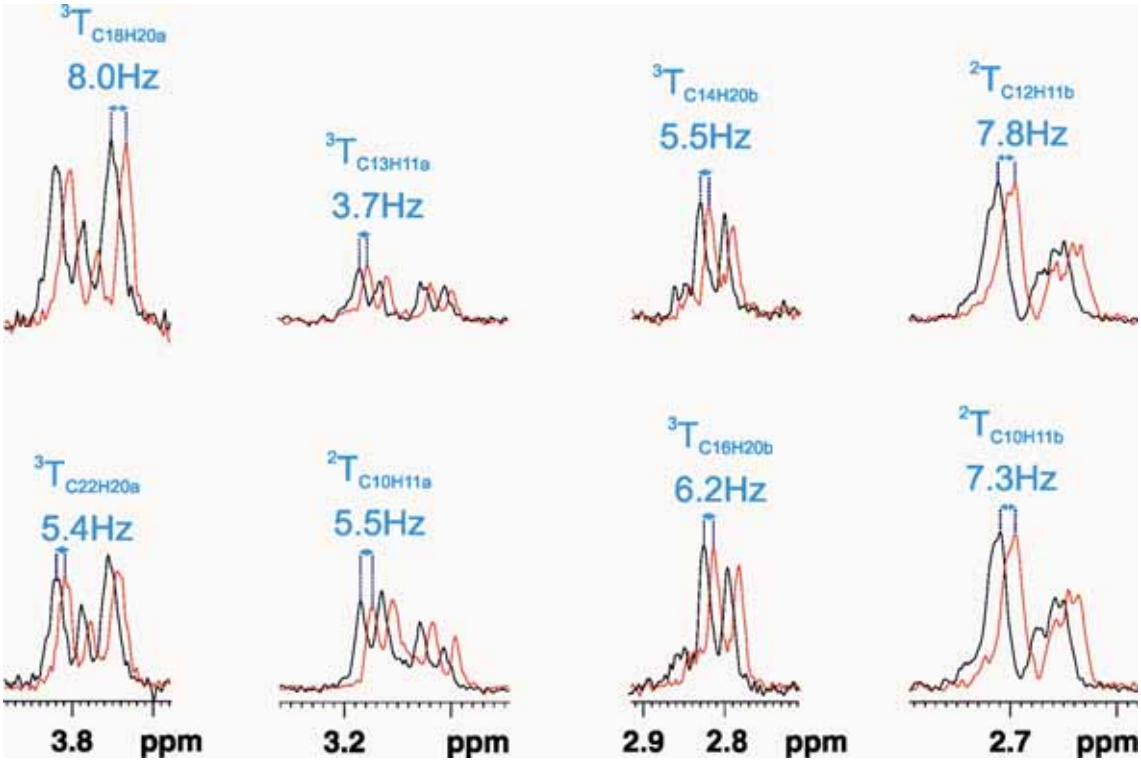

Figure S21: Measurement of $^{n}T_{CH}$ values of (**1**) in complex multiplets obtained under anisotropic conditions. 1D traces show overlaid α and β multiplets obtained in an IPAP PIP-HSQC experiment after IP±AP data combination.

Pulse Program code for Bruker spectrometers:

```
; PIPhsqmbc
;Pure In-Phase HSQMBC  with final adiabatic z-filter and perfect echo gradient
;optional IPAP using const25

#include <Avance.incl>
#include <Grad.incl>
#include <Delay.incl>

"p2=p1*2"
"d6=1s/(cnst2*4)"
"d0=3u"
"in0=inf1/2"

"DELTA2=d6-larger(p2,p14)/2"
"DELTA=p16+d16+p2+d0*2"
"DELTA4=p16+d16"

1 ze
2 d1 pl1:f1
3 (p1 ph1)

  DELTA2 pl0:f2
  (center (p2 ph1) (p14:sp3 ph6):f2 )
  DELTA2 pl2:f2 UNBLKGRAD

  (p1 ph2) (p3 ph3):f2
  d0
  (p2 ph5)
  d0
  p16:gp1*EA
  d16 pl0:f2
  (p24:sp7 ph4):f2
  DELTA pl2:f2
  (ralign (p1 ph1) (p3 ph4):f2 )

if "cnst25==0"
          {
          DELTA2 pl0:f2
          (center (p2 ph1) (p14:sp3 ph1):f2 )
          DELTA2 pl2:f2
          }
          else
          {
            d6
           (p2 ph2)
           d6
          }

  if "cnst25==0"
```

```
        {
        (p1 ph2):f1
        }
        else
        {
        (p1 ph1):f1
        }

 d12 pl0:f1
 300u gron0
 (p32:sp29 ph1):f1
 300u groff
 d12 pl1:f1
 p1 ph1

 DELTA4
 p2 ph1
 DELTA4
 p1 ph2
 DELTA4
 p2 ph1
 p16:gp2
 d16 BLKGRAD

 go=2 ph31
 d1 mc #0 to 2
   F1EA(calgrad(EA), caldel(d0, +in0) & calph(ph3, +180) & calph(ph6, +180) & calph(ph31, +180))
exit

ph1=0
ph2=1
ph3=0 2
ph4=0
ph5=0
ph6=0
ph31=0 2

;pl0 : 0W
;pl1 : f1 channel - power level for pulse (default)
;pl2 : f2 channel - power level for pulse (default)
;sp3: f2 channel - shaped pulse 180 degree
;sp7: f2 channel - shaped pulse 180 degree
;sp29: f2 channel - shaped adiabatic pulse 180 degree
;p1 : f1 channel -  90 degree high power pulse
;p2 : f1 channel - 180 degree high power pulse
;p3 : f2 channel -  90 degree high power pulse
;p4 : f2 channel - 180 degree high power pulse
;p14: f2 channel - 180 degree shaped pulse for inversion
;p24: f2 channel - 180 degree shaped pulse for refocusing
;p32: f2 channel - 180 degree shaped pulse for adiabatic z-filter
;p16: homospoil/gradient pulse
```

```
;d0 : incremented delay (2D)                    [3 usec]
;d1 : relaxation delay; 1-5 * T1
;cnst25=0 (IP) 1 (AP)
;cnst2= 8Hz
;d6 : 1/(4J)XH (long range coupling constant)
;d16: delay for homospoil/gradient recovery
;inf1: 1/SW(X) = 2 * DW(X)
;in0: 1/(2 * SW(X)) = DW(X)
;nd0: 2
;NS: 2 * n
;DS: >= 2
;td1: number of experiments
;FnMODE: echo-antiecho

;use gradient ratio:       gp 1 : gp 2
;                            80 : 20.1    for C-13
;                            80 :  8.1    for N-15

;for z-only gradients:
;gpz1: 80%
;gpz2: 20.1% for C-13, 8.1% for N-15
;gpz0: 3%

;use gradient files:
;gpnam1: SMSQ10.100
;gpnam2: SMSQ10.100
```

PUBLICATION 9

Suppression of phase and amplitude J_{HH} modulations in HSQC experiments

Laura Castañar, Eduard Sistaré, Albert Virgili, Robert Thomas Williamson and Teodor Parella.

Magn. Reson. Chem., **2014**, *53*, 115-119.

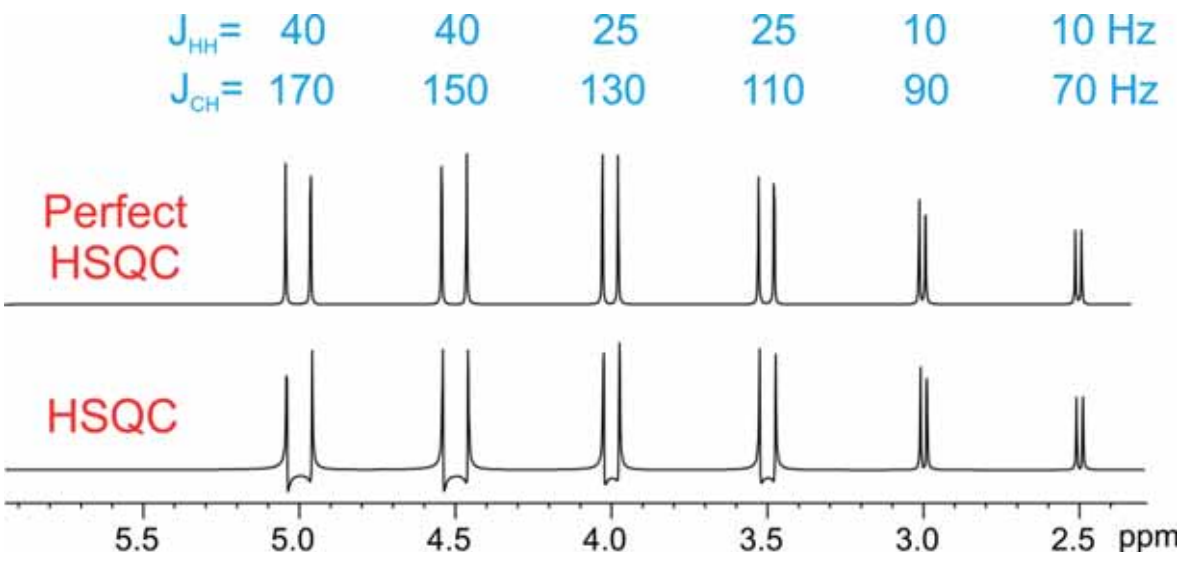

Introduction

There is an enormous interest in the use of the HSQC experiment as a quantitative NMR tool, as demonstrated for the many different approaches proposed in the last years.[95] In conventional HSQC and HSQMBC spectra, peak volumes of different protons are modulated according to each individual J_{HH} coupling pattern by the $\cos^2(\pi J_{H_1H_2}\Delta)$ function (see Eq.1.21 in section 1.2.1.1.). This non-uniform dependence causes a common source of error during volume integration and quantification.

In the previous publication has been demonstrated that the unwanted homo- and heteronuclear AP contributions in HSQC and HSQMBC experiments can be removed by applying an adiabatic *z*-filter, and the resulting PIP-HSQC and HSQCMBC spectra display undistorted in-phase cross-peaks. However, in these experiments the evolution under the J_{HH} takes place during the INEPT period and the final IP detected signal is still modulated by a $\cos^2(\pi J_{H_1H_2}\Delta)$ factor.

In this publication, it is shown experimentally and by simulation that the typical J_{HH} interferences present in conventional HSQC experiments can be efficiently suppressed using an improved perfect-HSQC pulse scheme. The proposal is based on the conventional HSQC pulse scheme where the standard INEPT block is replaced by a J_{HH}-compensated perfect-echo INEPT[96] module consisting of a double echo period in both defocusing/refocusing heteronuclear transfer periods. J_{HH} is refocused at the end of each double echo period, and therefore, the signal amplitude is only modulated by the effect of $^1J_{CH}$.

The resulting 2D perfect-HSQC spectra afford pure IP cross-peaks with respect to both $^1J_{CH}$ and J_{HH} rendering practical applications such as phase correction and multiplet analysis more convenient and accurate. There is a second and very significant positive consequence for removing J_{HH} interferences: signal intensity is amplitude modulated only by a $\sin^2(\pi J_{CH}\Delta)$ factor, and therefore the perfect-HSQC experiment is an excellent candidate to design future strategies for quantitative NMR studies. The proposed method is less aggressive than the use of CPMG-INEPT blocks where a train of simultaneous ^{1}H/^{13}C pulses are applied at high repetition rates, and where the resulting peaks can include

[95] a) H. Koskela, T. Väänänen, *Magn. Reson. Chem.,* **2002**, *40*, 705. b) S. Heikkinen, M. M. Toikka, P. T. Karhunen, A. Kilpeläinen, *J. Am. Chem. Soc.,* **2003**, *125*, 4362. c) H. Koskela, I. Kilpeläinen, S. Heikkinen, *J. Magn. Reson*., **2005**, *174*, 237. d) D. J. Peterson, N. M. Loening, *Magn. Reson. Chem.,* **2007**, *45*, 937. e) H. Koskela, O. Heikkilä, I. Kilpeläinen, S. Heikkinen, *J. Magn. Reson*., **2010**, *202*, 24.

[96] B. Baishya, C. L. Khetrapal. *J. Magn. Reson*., **2014**, *242*, 143.

unwanted dependences from offset effects or the presence of TOCSY contributions as well as deleterious effects on sample heating under extreme fast pulsing conditions.

The main disadvantage of the perfect-HSQC experiment arises from the longer duration of the perfect-echo INEPT versus the conventional INEPT (2Δ *vs.* Δ, respectively) that can lead to some signal loss due to additional T_2 relaxation. The overall duration of the sequence is extended about 3.6 ms for each perfect-echo INEPT period in a 140-Hz optimized experiment but this does not represent a serious issue for small molecules having reasonably long T_2 relaxation times (some hundreds of milliseconds).

Research article

MRC

Received: 10 May 2014 Revised: 11 July 2014 Accepted: 25 August 2014 Published online in Wiley Online Library: 3 October 2014

(wileyonlinelibrary.com) DOI 10.1002/mrc.4149

Suppression of phase and amplitude J(HH) modulations in HSQC experiments

Laura Castañar,[a,b] Eduard Sistaré,[a,b] Albert Virgili,[a,b] R. Thomas Williamson[c] and Teodor Parella[a,b]*

The amplitude and the phase of cross peaks in conventional 2D HSQC experiments are modulated by both proton–proton, J(HH), and proton–carbon, ^{1}J(CH), coupling constants. It is shown by spectral simulation and experimentally that J(HH) interferences are suppressed in a novel perfect-HSQC pulse scheme that incorporates perfect-echo INEPT periods. The improved 2D spectra afford pure in-phase cross peaks with respect to ^{1}J(CH) and J(HH), irrespective of the experiment delay optimization. In addition, peak volumes are not attenuated by the influence of J(HH), rendering practical issues such as phase correction, multiplet analysis, and signal integration more appropriate. Copyright © 2014 John Wiley & Sons, Ltd.

Keywords: NMR; HSQC; pure in-phase signals; perfect HSQC; J(HH) modulation

Introduction

Heteronuclear multiple-quantum correlation (HMQC)[1] and heteronuclear single-quantum correlation (HSQC)[2] experiments have become the most popular pulse schemes to obtain heteronuclear chemical-shift correlation NMR spectra. Both techniques use a similar logical concept based on a ^{1}H-to-^{13}C-to-^{1}H out-and-back magnetization transfer via the one-bond proton–carbon coupling constants, ^{1}J(CH).[3] The HMQC scheme is simpler in terms of the number of pulses, but its major complication relies on that proton magnetization is located in the transverse plane during the entire pulse sequence. Additionally, proton–proton coupling constants, J(HH), also evolve during the variable t_1 period. As a result, cross peaks present strongly distorted twist-phased patterns along the detected F2 dimension and a characteristic skew shape along the indirect F1 dimension of the two-dimensional (2D) map. On the other hand, the HSQC experiment uses INEPT blocks for heteronuclear magnetization transfer, and the evolution during the t_1 period is not affected by J(HH). However, J(HH) couplings evolve during the INEPT periods, and their influences on the phase and amplitude signal modulation must be considered when a detailed analysis is required. In practice, the magnitudes of ^{1}J(CH) (120–250 Hz) are generally more than one order of magnitude larger than J(HH) (0–15 Hz), and therefore, the prejudicial effects of J(HH) on the detected signal have usually been neglected.

On the other hand, the concept of perfect echo[4] has been successfully implemented in a series of NMR applications to solve some traditional issues, such as the elimination of peak distortion caused by homonuclear J-coupling in diffusion NMR experiments,[5] the determination of T_2 relaxation times from undistorted multiplets in 'perfect-echo Carr–Purcell–Meiboom–Gill (CPMG)' experiments,[6] the suppression of J(HH) evolution during the solvent-suppression period in a 'perfect water suppression by gradient tailored excitation' method,[7] or during the t_1 period in 'perfect-HMQC' experiments.[8] This concept has also been used in an effort to improve long-range heteronuclear transfers by means of a 'perfect-echo INEPT' element.[9]

Many chemists use the HSQC experiment in a qualitative way to correlate the chemical shifts of carbon and attached protons. For these applications, the issues with phase distortion caused by J(HH) are for the most part invisible and therefore irrelevant. However, these effects are present in the form of antiphase components and become highly relevant when trying quantitative measurements in terms of J or intensity measurements because they do not cancel out. It is shown here, experimentally and by simulation, that the typical J(HH) interferences present in conventional HSQC experiments can be efficiently suppressed in an improved perfect-HSQC pulse scheme (Fig. 1), which replaces the classical INEPT ($\Delta/2$-180$_x$(^{1}H,^{13}C)-$\Delta/2$) by a perfect-echo INEPT module consisting of a double echo period ($\Delta/2$-180$_x$(^{1}H)-$\Delta/2$-90$_y$(^{1}H)-$\Delta/2$-180$_x$(^{1}H,^{13}C)-$\Delta/2$) in both defocusing/refocusing heteronuclear transfer periods. The resulting 2D perfect-HSQC spectra afford pure in-phase cross peaks with respect to both ^{1}J(CH) and J(HH), and in addition, peak volumes are not influenced by J(HH), rendering practical applications such as phase correction, signal integration, and multiplet analysis more convenient and accurate.

Results and discussion

Figure 1 shows the pulse sequences of the F2-coupled and F2-heterodecoupled perfect-HSQC experiments. As a major novelty,

* Correspondence to: Teodor Parella, Servei de Ressonància Magnètica Nuclear, Universitat Autònoma de Barcelona, 08193 Bellaterra, Barcelona, Spain. E-mail: teodor.parella@uab.cat

a Servei de Ressonància Magnética Nuclear, Facultat de Ciències, Universitat Autònoma de Barcelona, 08193 Bellaterra, Barcelona, Catalonia, Spain

b Departament de Química, Facultat de Ciències, Universitat Autònoma de Barcelona, 08193 Bellaterra, Barcelona, Catalonia, Spain

c NMR Structure Elucidation, Process and Analytical Chemistry, Merck & Co. Inc., 126 E. Lincoln Avenue, Rahway, NJ, 07065, USA

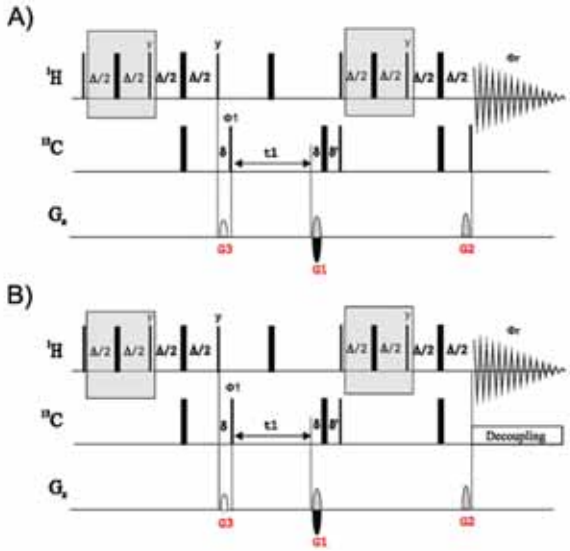

Figure 1. Pulse schemes of the (A) F2-coupled perfect-CLIP-HSQC and (B) broadband F2-heterodecoupled perfect-HSQC experiments designed to provide pure in-phase multiplet patterns with respect to ^{1}J(CH) and J(HH). Narrow and wide filled rectangles represent 90° and 180° pulses, respectively. Pulse phases are along the *x*-axis if not stated otherwise. Phase cycles were $\phi_1 = x, -x$ and $\phi_r = x, -x$. The interpulse delay Δ is set to 1/(2 * ^{1}J(CH)), and coherence selection is performed using the echo/antiecho protocol, with the G1 : G2 : G3 gradient ratio set to ±80:20.1:33. δ stands for the duration of the gradient and its recovery delay, and $\delta' = \delta + t_1 + p4$, where *p*4 is the duration of the 180° ^{1}H pulse. TPPI-like incrementation with the echo/antiecho recording scheme was achieved by simultaneous inversion of ^{13}C pulses applied prior to the variable t_1 period. Conventional HSQC experiments were recorded without the ^{1}H pulses and delays marked into the boxes.

the ^{1}H pulses and delays marked into the boxes represent the additional elements incorporated in the new perfect-HSQC schemes compared with conventional HSQC experiments. The F2-^{1}J(CH)-coupled version is obtained by inserting a 90° ^{13}C pulse just prior to acquisition and omitting the heteronuclear decoupling as described for the clean in-phase (CLIP)-HSQC experiment.[10]

First of all, spectral simulations have been performed to assess the signal amplitude and phase dependence with respect to both J(HH) and ^{1}J(CH) evolution in several 1D HSQC pulse schemes, neglecting relaxation effects (Fig. S1 in the Supporting information). To illustrate such effects for a wide range of coupling constant values, three independent diastereotopic CH_2 spin systems with J (HH) values of 10, 25, and 40 Hz, respectively, and ^{1}J(CH) magnitudes covering 70–150 Hz have been defined. The choice of this wide range of values has been made to demonstrate the features of the HSQC even under extreme conditions. Although organic compounds under isotropic conditions present a narrower range of J values, these intervals are commonly found when measuring J splittings in anisotropic conditions. For instance, it has been reported that experimental ^{2}T(HH) (^{2}J(HH) + ^{2}D(HH)) coupling values up to 30–40 Hz in magnitude and ^{1}T(CH) (^{1}J(CH) + ^{1}D(CH)) in the range of 100–180 Hz are measured in the case of strychnine dissolved in a $CDCl_3$/poly-methylmethacrylate gel.[11]

For the theoretical analysis using the product operator formalism,[12] an isolated heteronuclear three-spin system consisting of a directly attached C–H_1 pair with ^{1}J(CH_1) and a third H_2 proton nucleus with J(H_1H_2) is considered. The magnetization just prior to the acquisition period in a conventional HSQC can be described as a mixture of in-phase and antiphase homonuclear and heteronuclear components:

$$H_{1x}c^2s'^2\,(\text{term I}) - 2H_{1y}C_2c^2s's'c'\,(\text{term II}) + 2H_{1y}H_{2z}css'^2\,(\text{term III}) + 4H_{1x}H_{2z}C_2csc's's'\,(\text{term IV})$$

where c is cos(πJ(H_1H_2)Δ), s is sin(πJ(H_1H_2)Δ), c' is cos(π^{1}J(CH_1)Δ), s' is sin(π^{1}J(CH_1)Δ), and Δ is the echo period. Thus, the phase anomalies observed in F2-heterocoupled HSQC spectra (Fig. 2A) result from two independent effects: (i) the mismatch between the optimized Δ delay and the active ^{1}J(CH) value (terms II and IV) and (ii) the evolution of J(HH) during the echo INEPT periods (term III). Such anomalies prevent any attempt of accurate analysis in terms of quantification via integration or direct J measurement. A simple solution to partially solve these drawbacks was proposed with the CLIP-HSQC experiment,[10] which applies a 90° ^{13}C pulse just prior the acquisition. In this way, the antiphase contributions as a result of ^{1}J(CH) (terms II and IV) are converted to multiple-quantum coherence, and apparently, clean phase patterns are obtained although this is only true in the case of the presence of small J(HH) splittings (Fig. 2B). However, the effects of J(HH) evolution are still present (term III) although they have traditionally been omitted because of their relative low percentage compared with the desired response (term I). A simple calculation shows that these effects may become important. For instance, the relative percentage of the term III with respect term I in a 140-Hz optimized CLIP-HSQC experiment is of 5.6 and 17% for J(HH) values of 5 and 15 Hz, respectively. Such percentages can be more pronounced when measuring residual dipolar couplings in anisotropic media, where higher values can be involved.[13]

It has been shown that two major conclusions can be extracted from the analysis of the perfect-echo INEPT:[9] J(HH) is refocused at the end of the double-echo period, and the signal amplitude is only modulated by the effect of ^{1}J(CH), if relaxation is neglected. Thus, the magnetization just prior to acquisition in the perfect-HSQC experiment is defined exclusively by only two components:

$$H_{1x}s'^2 - 2H_{1y}C_2s's'c'$$

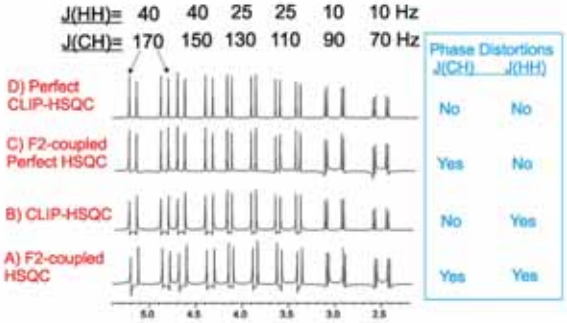

Figure 2. Simulated spectra showing the phase peak distortion effects in several 140-Hz optimized F2-heterocoupled HSQC experiments: (A) conventional HSQC, (B) CLIP-HSQC, (C) perfect-HSQC, and (D) perfect CLIP-HSQC. Six protons have been simulated with different J(HH) and ^{1}J(CH) values, as shown in the upper part.

MRC

Figure 2C shows that an F2-coupled perfect-HSQC spectrum without the CLIP pulse still shows phase distortions provided that Δ does not match the corresponding ^{1}J(CH) value. For instance, deviations of 10 and 20 Hz between ^{1}J(CH) and the Δ delay optimization generate antiphase contributions of about 11 and 23%, respectively, in a 140-Hz optimized experiment. Such distortions are efficiently suppressed using the perfect-CLIP-HSQC pulse scheme, affording perfect pure in-phase multiplet patterns for all peaks independent of their J(HH) and J(CH) values (Fig. 2D). Similar conclusions are also obtained from the analysis of broadband heterodecoupled HSQC and perfect-HSQC versions (Fig. 3). Note the perfect in-phase nature of all cross peaks in the perfect-HSQC spectra independent of experiment optimization.

A series of 2D F2-coupled and decoupled HSQC experiments have been experimentally recorded on a test sample of strychnine to verify the theoretical predictions. We have focused our attention on several diastereotopic CH_2 groups because the nonequivalent geminal protons present large mutual ^{2}J(HH) values (10–16 Hz). Figure 4 shows some multiplets extracted from equivalent 140-Hz optimized heteronuclear decoupled HSQC and perfect-HSQC spectra, and similar conclusions can be extracted analyzing the F2-coupled versions (Figs S2–S3 in the Supporting information). Significant antiphase contributions are clearly observed in some HSQC peaks that distort the signal phase and decrease their relative intensities. The H16 proton can be taken as a reference for a resonance that does not show large values, and therefore, a practically equal multiplet pattern and signal intensity are obtained in both spectra. However, differences up to 20% in signal intensity were observed for the diastereotopic H15a and H15b protons, and also, distortions can be observed for methine and methyl peaks, as shown for the H8 proton.

These distortions also introduce a source of error when an accurate measurement of J(HH) by direct peak maxima analysis is performed. In Fig. 5, it is shown that whereas the same J(HH) value is obtained from the conventional ^{1}H and the perfect-HSQC peak, considerable errors are made when direct peak picking on distorted HSQC and HSQC preservation of equivalent pathway (PEP) multiplets is applied. This perfect phase behavior is not achieved in the sensitivity-improved PEP version of the perfect-HSQC experiment,[14] where stronger phase distortions as a result of J(HH) are obtained (Figs S2–S4 in the Supporting information). In this case, two different magnetization components are involved, and the perfect INEPT block does not avoid the J(HH) modulation for both contributors. It is important to highlight that the perfect INEPT element could be implemented as a general building block in a large number of multidimensional NMR experiments that use the classical INEPT and HSQC pulse timings for the quantitative measurement of coupling constants.

In conventional HSQC spectra, peak volumes of different protons are variably modulated as a function of each individual J(HH)

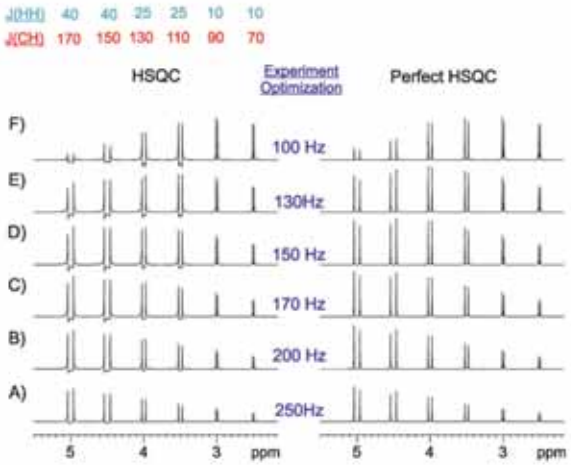

Figure 3. Simulated spectra showing the peak phase and intensity dependence in HSQC and perfect-HSQC experiments. Pure in-phase patterns are achieved for all signals in all perfect-HSQC spectra, independent to J(HH), ^{1}J(CH), and delay optimization (Δ = 1/(2 * ^{1}JCH)). From bottom to the top, (A) 250 Hz (Δ = 2.0 ms), (B) 200 Hz (Δ = 2.5 ms), (C) 170 Hz (Δ = 2.94 ms), (D) 150 Hz (Δ = 3.33 ms), (E) 130 Hz (Δ = 3.84 ms), and (F) 100 Hz (Δ = 5.0 ms).

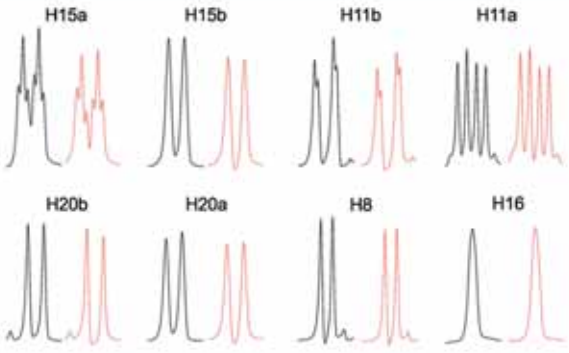

Figure 4. Comparison of some perfect-HSQC (left) and conventional HSQC (right) multiplets obtained from F2-heterodecoupled of strychnine. Note the evident phase distortions and decreased sensitivity in signals presenting large J(HH) values. The H16 proton can be taken as an undistorted reference signal not showing large J(HH) values.

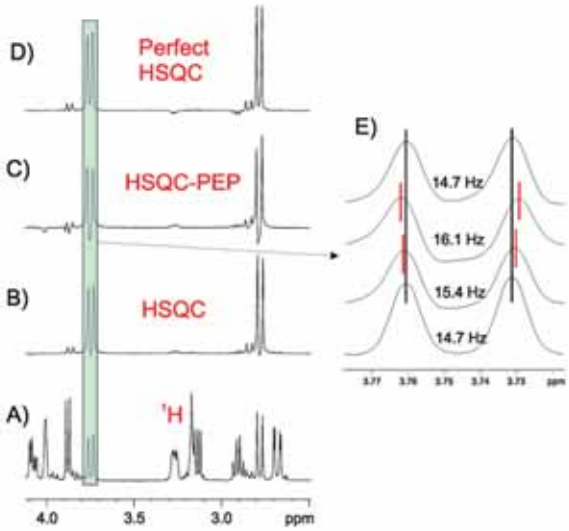

Figure 5. (A) Expanded area of the 500.13-MHz ^{1}H NMR spectrum of strychnine; (B–D) 1D traces extracted at the C20 carbon frequency of the following broadband F2-heterodecoupled 2D experiments: (B) conventional HSQC, (C) conventional HSQC-PEP, and (D) perfect-HSQC. (E) Experimental determination of J(HH) in H20a by using direct peak-maxima analysis.

coupling pattern. This nonuniform dependence causes a common source of error during integration and quantification of response intensities. In the perfect-HSQC experiment, there is a second and very significant positive consequence for removing J(HH) interferences: Signal intensity is amplitude modulated only by the $\sin^2(\pi J(CH)\Delta)$ factor (Fig. S4 in the Supporting information) and is therefore an excellent candidate to design future strategies for quantitative NMR studies.[15] The proposed method is less aggressive than the use of CPMG-INEPT blocks where a train of simultaneous $^1H/^{13}C$ pulses are applied at high repetition rates and where the resulting peaks can include unwanted dependence from offset effects or the presence of TOCSY contributions as well as deleterious effects on sample heating under extreme fast-pulsing conditions.[15c,15f]

To evaluate the $^1J(CH)$-compensated intensity strategy based on the proper selection of multiple polarization transfer values,[15b] we have simulated the perfect-HSQC spectrum of a spin system consisting of several protons having J(HH) in the extreme range between 10 and 30 Hz and $^1J(CH)$ ranging between 120 and 180 Hz. From a single-Δ 140-Hz perfect-HSQC experiment, a pure in-phase spectrum with peak volume differences up to 25% is obtained (Fig. 6A). On the other hand, Fig. 6B shows the $^1J(CH)$-compensated perfect-HSQC spectrum after combining four datasets acquired with Δ values of 2.94 ms (170 Hz), 2.86 ms (175 Hz), 2.86 ms (175 Hz), and 5.88 ms (85 Hz). Note that intensity differences below 2% are obtained in the complete $^1J(CH)$ range between 120 and 180 Hz. Of course, these simulations have been performed neglecting differential relaxation effects between different protons and carbons. A more exhaustive and detailed analysis is out of the scope of this communication but may be considered in the future.

The only apparent disadvantage of the perfect-HSQC experiment arises from the longer duration of the perfect-echo INEPT *versus* the conventional INEPT (2Δ vs Δ, respectively) that can lead to some signal loss as a result of relaxation losses. The duration of the sequence is extended about 3.6 ms for each perfect-echo INEPT period in a 140-Hz optimized experiment, but this is not a serious problem for small molecules having reasonably long T_2 relaxation times. For example, the experimental T_2 relaxation times for strychnine are about 0.35–0.50 s for aliphatic protons and around 0.6–0.7 s for aromatic protons as measured on a 20-mg sample in a 500-MHz spectrometer at 298 K (refer to Table S1 in the Supporting information). These values become larger in more dilute samples or at lower magnetic fields.[16]

In conclusion, a 2D perfect-HSQC experiment has been proposed that avoids any interference as a result of J(HH) coupling constants. The method is very simple to implement, and it can be recorded with and without broadband heteronuclear decoupling during acquisition. The resulting cross peaks exhibit pure in-phase multiplet patterns, irrespective of the experiment optimization. These uniform and predictable responses are more amenable to an accurate and quantitative analysis than what is encountered with the results of standard HSQC pulse sequences, with particular emphasis in the determination of $^1J(CH)$ and J(HH) coupling values. In addition, signal intensity is not modulated by J(HH), which opens the opportunity to design quantitative NMR applications based on perfect-HSQC datasets.

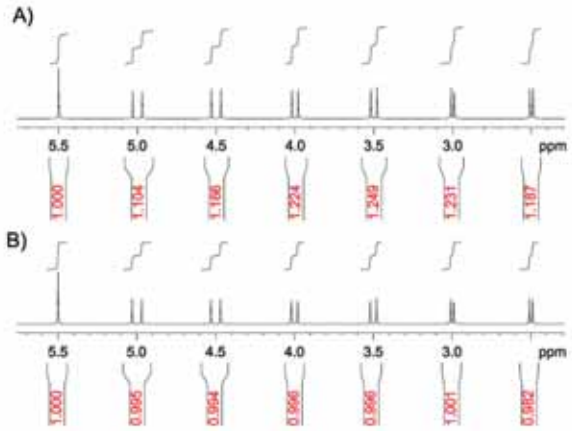

Figure 6. Spectral simulations showing integration ratios in heterodecoupled perfect-HSQC spectra: (A) optimized to a single Δ value of 3.6 ms, corresponding to 140 Hz; (B) average spectrum after combining four datasets acquired with Δ values of 2.94 ms (170 Hz), 2.86 ms (175 Hz), 2.86 ms (175 Hz), and 5.88 ms (85 Hz). The simulated protons have J(HH) and $^1J(CH)$ values in the range between 10-30 Hz and 120–180 Hz, respectively.

Methods and materials

NMR experiments were collected at 298 K on a Bruker AVANCE spectrometer (Bruker BioSpin, Rheinstetten, Germany) operating at 500.13-MHz proton frequency, equipped with a 5-mm TXI cryoprobe probe including a *z*-axis pulsed field gradient accessory (maximum strength of 53.5 G/cm). Experimental data were acquired with a sample of 20 mg of strychnine (Scheme 1) dissolved in 600 µl $CDCl_3$ and processed using the TOPSPIN v3.1 software package (Bruker BioSpin, Rheinstetten, Germany).

For the conventional HSQC and HSQC-PEP experiments, the standard hsqcetgpsp and hsqcetgpsisp2 pulse programs (Bruker library) were used. The corresponding F2-heterodecoupled and CLIP versions were created from these pulse programs, by adding a hard 90° ^{13}C pulse just before acquisition and omitting the decoupling during acquisition. For all conventional HSQC and perfect-HSQC experiments, ^1H and ^{13}C carrier frequencies were set at 4.5 and 90 ppm, respectively. Spectra were acquired with spectral windows of 8 (^1H dimension) and 160 (^{13}C dimension) ppm, using a prescan delay of 1 s and two scans per t_1 increment. Data were acquired with 2048 complex points in the ^1H dimension and 128 complex points in the ^{13}C dimension using the echo/antiecho detection mode. Zero filling up to 4 * 1 K was used prior to Fourier transformation using a 90° phase-shifted squared sine-bell apodization in both dimensions. Gradients G1 and G2 with a duration of 1 ms (δ) were used for echo–antiecho coherence selection. The proportionality between gradients G1 : G2 was set to ±80:20.1. ^{13}C 180° pulses are applied as CHIRP inversion and refocusing pulses of 500 µs and 2 ms of duration, respectively.

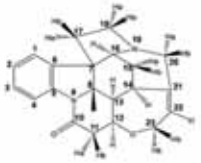

Scheme 1. Chemical structure and numbering of Strychnine

MRC

NMR simulations

Spectral simulations were performed using the NMRSIM v5.4 module included in the TOPSPIN (Bruker BioSpin, Rheinstetten, Germany). 1D pulse scheme equivalents to the first increment of the 2D pulse schemes shown in Figure 1 were used for simulations. The linewidth for all peaks used in the simulations is 0.2 Hz, and all 1D data were processed using an exponential function with a line broadening of 3 Hz prior to Fourier transformation.

For the spectral simulations of Figs 2, 3, S4, and S5, three independent diastereotopic CH_2 spin systems were defined, with different values of J(HH) and ^{1}J(CH), for studying the performance of the proposed perfect-HSQC experiment *versus* conventional HSQC and HSQC-PEP experiments. Spin system: $\delta(H_A) = 2.5$ ppm, $\delta(H_B) = 3.0$ ppm, $\delta(H_C) = 3.5$ ppm, $\delta(H_D) = 4.0$ ppm, $\delta(H_E) = 4.5$ ppm, $\delta(H_F) = 5$ ppm; $\delta(C_1) = 30$ ppm, $\delta(C_2) = 40$ ppm, and $\delta(C_3) = 50$ ppm; $^1J(C_1H_A) = 70$ Hz, $^1J(C_1H_B) = 90$ Hz, $^1J(C_2H_C) = 110$ Hz, $^1J(C_2H_D) = 130$ Hz, $^1J(C_3H_E) = 150$ Hz, and $^1(C_3H_F) = 170$ Hz; $^2J(H_AH_B) = 10$ Hz, $^2J(H_CH_D) = 25$ Hz, and $^2J(H_EH_F) = 40$ Hz.

Spectral simulations shown in Fig. 6 were performed on the following spin system: $\delta(H_A) = 2.5$ ppm, $\delta(H_B) = 3.0$ ppm, $\delta(H_C) = 3.5$ ppm, $\delta(H_D) = 4.0$ ppm, $\delta(H_E) = 4.5$ ppm, $\delta(H_F) = 5$ ppm, and $\delta(H_G) = 5.5$ ppm; $\delta(C_1) = 30$ ppm, $\delta(C_2) = 40$ ppm, $\delta(C_3) = 50$ ppm, and $\delta(C_4) = 35$ ppm; $^1J(C_1H_A) = 120$ Hz, $^1J(C_1H_B) = 130$ Hz, $^1J(C_2H_C) = 140$ Hz, $^1J(C_2H_D) = 150$ Hz, $^1J(C_3H_E) = 160$ Hz, $^1J(C_3H_F) = 170$, and $^1J(C_4H_G) = 180$ Hz; $^2J(H_AH_B) = 10$ Hz, $^2J(H_CH_D) = 20$ Hz, and $^2J(H_EH_F) = 30$ Hz.

Acknowledgements

Financial support for this research provided by Ministerio de Economía y Competitividad (project CTQ2012-32436) is gratefully acknowledged. We also thank the Servei de Ressonància Magnètica Nuclear, Universitat Autònoma de Barcelona, for allocating instrument time to this project.

References

[1] (a) L. Muller. *J. Am. Chem. Soc.* **1979**, *101*, 4481–4484;
(b) A. Bax, R. Griffey, B. Hawkins. *J. Magn. Reson.* **1983**, *55*, 301–315.
[2] G. Bodenhausen, D. J. Ruben. *Chem. Phys. Lett.* **1980**, *69*, 185–189.
[3] P. K. Mandal, A. Majumdar. *Conc. Magn. Reson. Part A* **2004**, *20A*, 1–23.
[4] K. Takegoshi, K. Ogura, K. Hikichi. *J. Magn. Reson.* **1989**, *84*, 611–615.
[5] A. M. Torres, G. Zheng, W. S. Price. *Magn. Reson. Chem.* **2010**, *48*, 129–133.
[6] J. A. Aguilar, M. Nilsson, G. Bodenhausen, G. A. Morris. *Chem. Commun.* **2012**, *48*, 811–813.
[7] R. W. Adams, C. M. Holroyd, J. A. Aguilar, M. Nilsson, G. A. Morris. *Chem. Commun.* **2013**, *49*, 358–360.
[8] B. Baishya, C. L. Khetrapal, K. K. Dey. *J. Magn. Reson.* **2013**, *234*, 67–74.
[9] B. Baishya, C. L. Khetrapal. *J. Magn. Reson.* **2014**, *242*, 143–154.
[10] A. Enthart, J. C. Freudenberger, J. Furrer, H. Kessler, B. Luy. *J. Magn. Reson.* **2008**, *192*, 314–322.
[11] J. D. Snider, E. Troche-Pesqueira, S. R. Woodruff, C. Gayathri, N. V. Tsarevsky, R. R. Gil. *Magn. Reson. Chem.* **2012**, *50*, S89–S91.
[12] O. W. Sørensen, G. W. Eich, M. H. Levitt, G. Bodenhausen, R. R. Ernst. *Prog. Nucl. Magn. Reson. Spectrosc.* **1983**, *16*, 163–192.
[13] (a) T. Carlomagno, W. Peti, C. Griesinger. *J. Biomol. NMR* **2000**, *17*, 99–109;
(b) P. Permi. *J. Magn. Reson.* **2001**, *153*, 267–272;
(c) P. Permi. *J. Biomol. NMR* **2002**, *22*, 27–35;
(d) E. Miclet, E. O'Neil-Cabello, E. P. Nikonowicz, D. Live, A. Bax. *J. Am. Chem. Soc.* **2003**, *125*, 15740–15741;
(e) C. M. Thiele. *J. Org. Chem.* **2004**, *69*, 7403–7413;
(f) P. Tzvetkova, S. Simova, B. Luy. *J. Magn. Reson.* **2007**, *186*, 193–200;
(g) J. Sauri, L. Castañar, P. Nolis, A. Virgili, T. Parella. *J. Magn. Reson.* **2014**, *242*, 33–40.
[14] L. E. Kay, P. Keifer, T. Saarinen. *J. Am. Chem. Soc.* **1992**, *114*, 10663–10665.
[15] (a) H. Koskela, T. Väänänen. *Magn. Reson. Chem.* **2002**, *40*, 705–715;
(b) S. Heikkinen, M. M. Toikka, P. T. Karhunen, A. Kilpeläinen. *J. Am. Chem. Soc.* **2003**, *125*, 4362–4367;
(c) H. Koskela, I. Kilpeläinen, S. Heikkinen. *J. Magn. Reson.* **2005**, *174*, 237–244;
(d) D. J. Peterson, N. M. Loening. *J. Magn. Reson.* **2007**, *45*, 937–941;
(e) A. Lewis, R. H. Karsten, M. E. Norton, M. Tonelli, W. M. Westler, J. L. Markley. *Anal. Chem.* **2010**, *82*, 4558–4563;
(f) H. Koskela, O. Heikkilä, I. Kilpeläinen, S. Heikkinen. *J. Magn. Reson.* **2010**, *202*, 24–33;
(g)P. Giraudeau. *Magn. Reson. Chem.* **2014**; In press. DOI 10.1002/mrc.4068.
[16] R. T. Williamson, G. E. Martin, A. Buevich, T. Parella. *J. Org. Chem.* **2014**, *79*, 3887–3894.

Supporting information

Additional supporting information may be found in the online version of this article at the publisher's website

Supporting Information

Suppression of phase and amplitude J(HH) modulations in HSQC experiments

Laura Castañar, Eduard Sistaré, Albert Virgili, R. Thomas Williamson and Teodor Parella*

Table of Contents

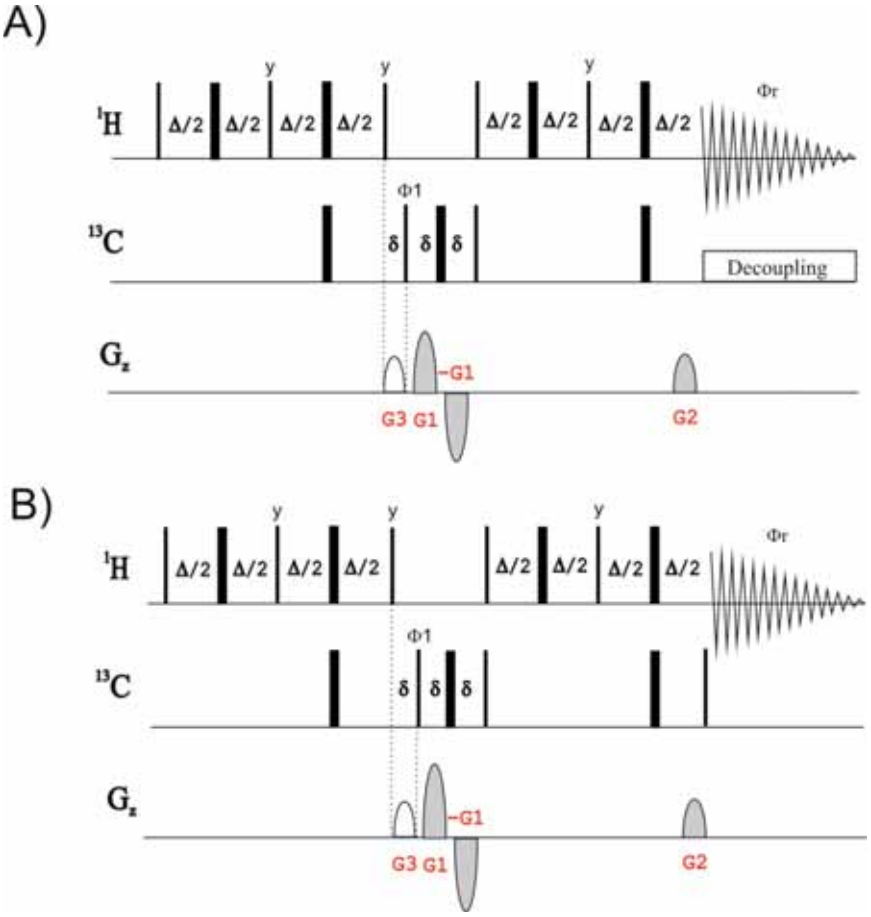

Figure S1: 1D Pulse schemes used in simulations. The recycle delay was set to 1s and the inter-pulse delay Δ was optimized to $1/(2*{}^{1}J(CH))$. Gradients G1:G2 with a duration of 1 ms followed by a recovery time the 100μs (δ=1.1ms) were set to a 80:20.1 ratio. The purge gradient G3 applied during the zz filter was set to 33%. 2 scans were recorded with ϕ_1=x,-x and ϕ_r=x,-x, using the spin systems defined in the experimental section. Data were processed by Fourier transformation without any window function.

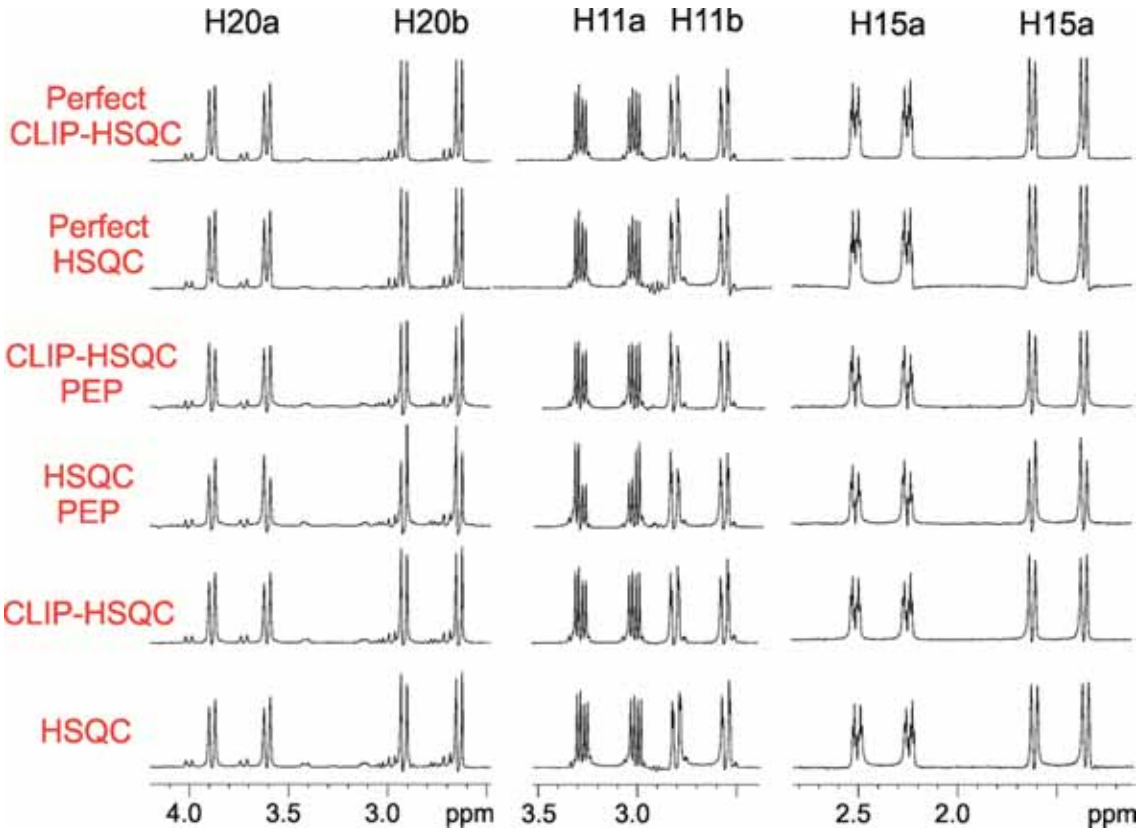

Figure S2: 1D traces extracted at C20, C11 and C15 carbon frequencies of several F2-coupled HSQC experiments. Note the perfect phase for all peaks in the perfect-CLIP-HSQC experiment when compared to all other experiments.

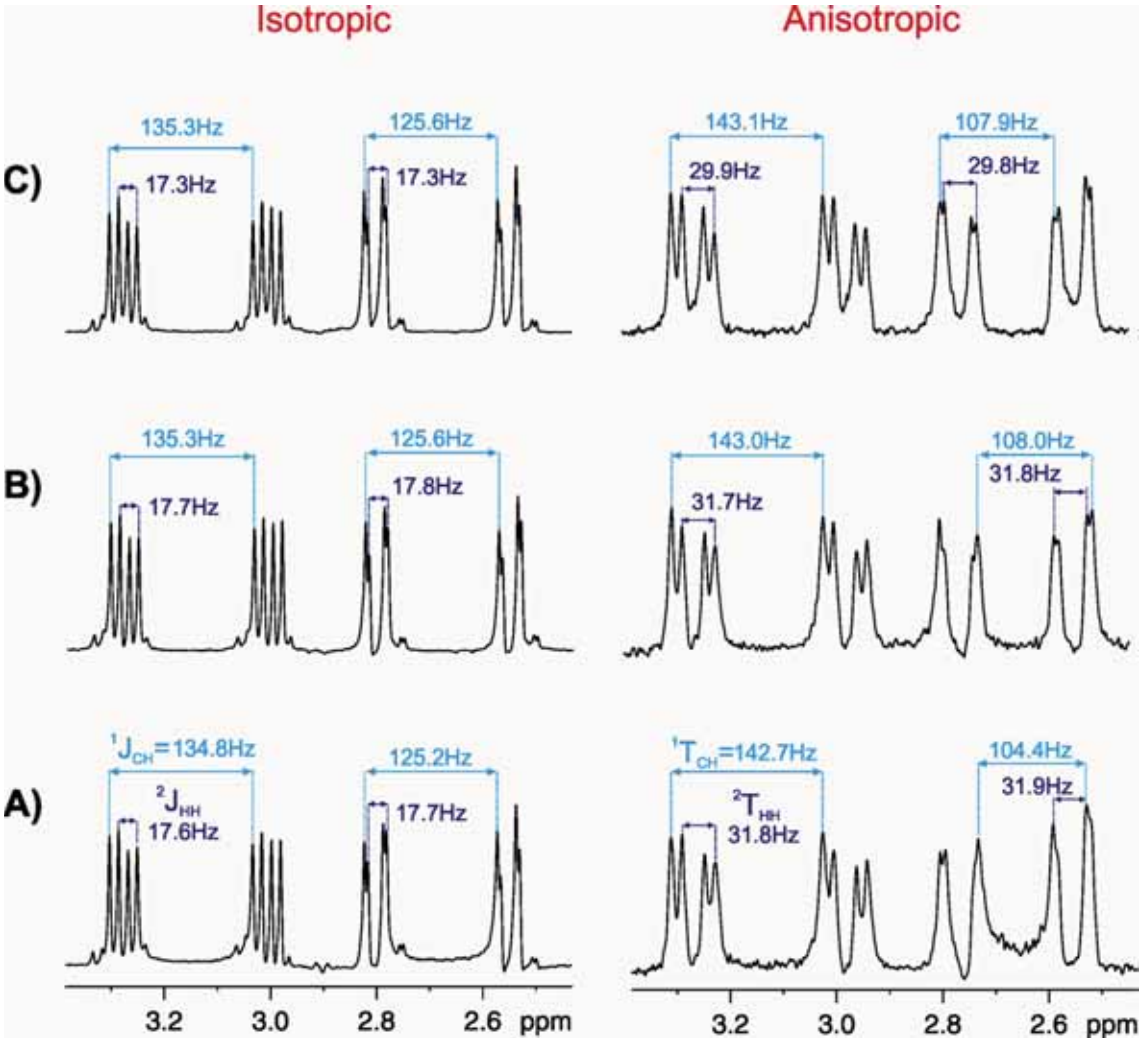

Figure S3: Comparison of the experimental measurement of J(HH)/T(HH) and ^{1}J(CH)/ ^{1}T(CH) from direct peak maxima analysis in A) HSQC, B) CLIP-HSQC, C) perfect CLIP-HSQC cross-peaks corresponding to the 11-CH_2 group of strychnine in both conventional isotropic and also non-isotropic conditions. For the measurement of RDCs in the anisotropic media, 4 mg of strychnine was weakly aligned in a poly(methylmethacrylate) (PMMA) gel swollen in 200µl of $CDCl_3$ using the reversible compression relaxation method. The ^{2}H quadrupolar splitting ($\Delta\upsilon_Q$) for the $CDCl_3$ signal was of 26 Hz.

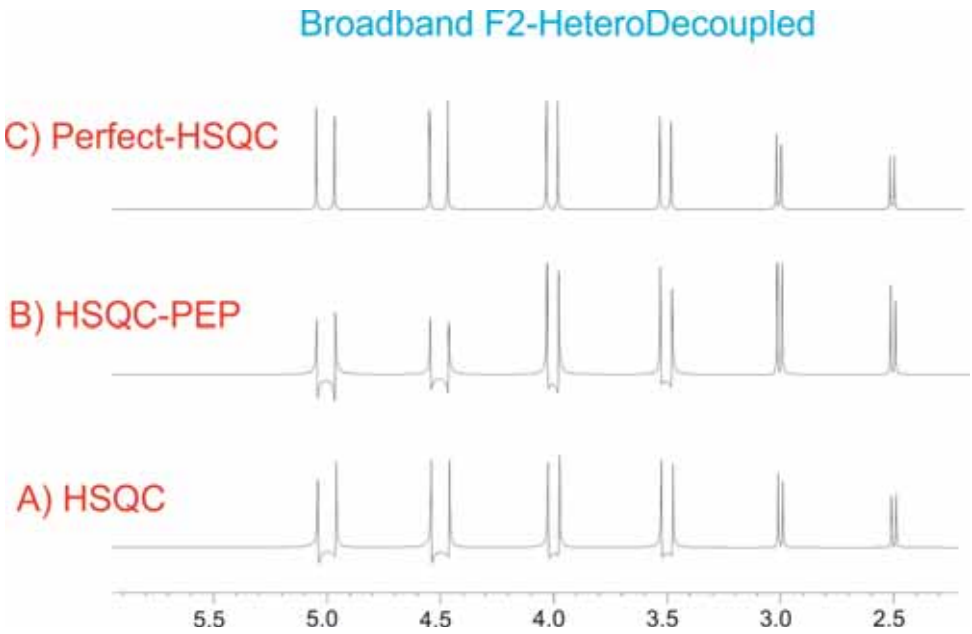

Figure S4: Spectral simulations showing the exclusive effects of J(HH) in several 140-Hz optimized broadband F2-heterodecoupled HSQC experiments: A) Conventional HSQC, B) HSQC-PEP and C) perfect-HSQC. Same conditions as Fig. 3 but using heteronuclear decoupling during acquisition.

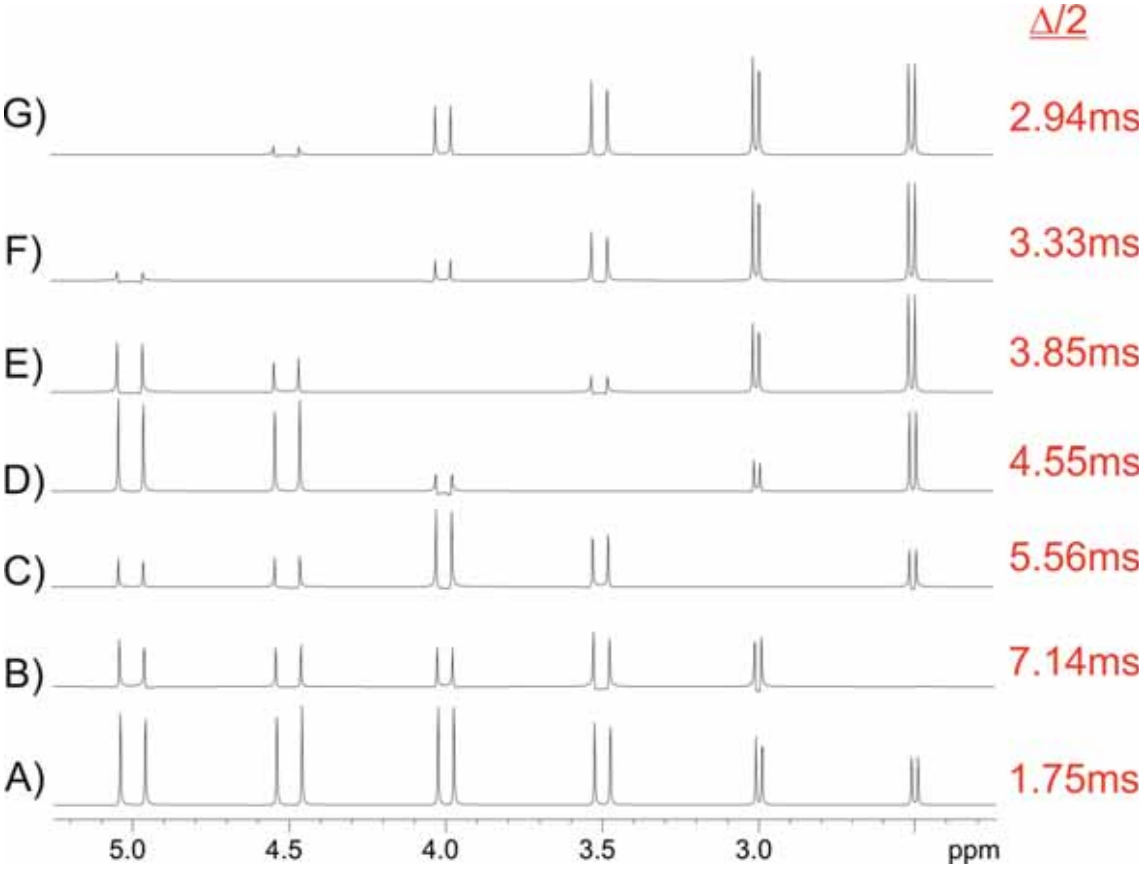

Figure S5: Spectral simulations showing the exclusive signal intensity dependence with respect to the $\sin^2(\pi J\Delta)$ function. A) is the regular experiment optimized to $\Delta/2=1/(4*{}^1J_{CH})=1.75$ ms. Spectra B-F) are delivery optimized to specific $\Delta/2=1/(2*{}^1J_{CH})$ values to demonstrate that null intensities are obtained when Δ exactly match ${}^1J_{CH}$, independent of the involved J(HH) values. For instance, B) is the 35-Hz optimized perfect-HSQC spectrum where the signal having ${}^1J(CH)=70$ Hz (2.5ppm) shows null intensity. In the same way, G) corresponds to the 75-Hz optimized perfect-HSQC spectrum and therefore signals with ${}^1J(CH)$ values of 70 and 90 Hz (2.5 and 3.0 ppm, respectively) shows maximum intensity whereas that with ${}^1J(CH)=150$ Hz (5.0 ppm) is perfectly nulled.

	T_2 (s)	r^2		T_2 (s)	r^2
H1	0.6268	0.9999	H15a	0.3699	0.9969
H2	0.6176	0.9992	H15b	0.3638	0.9944
H3	0.7161	0.9995	H17	0.3101	0.9981
H4	0.7321	0.9996	H18a	0.3295	0.9793
H8	0.5232	0.9981	H18b	0.3443	0.9588
H11a	0.4755	0.9889	H20a	0.3630	0.9877
H11b	0.4495	0.9991	H20b	0.3545	0.9797
H12	0.4865	0.9968	H22	0.4128	0.9983
H13	0.4986	0.9996	H23a	0.4006	0.9941
H14	0.4466	0.9972			

Table S1: Experimental T2 values measured for a sample of 20 mg strychnine in $CDCl_3$ in a 500 MHz spectrometer at 298K. Ten different CPMG-PROJECT spectra were recorded using an inter-pulse time of 1.5ms (n=4) and a different number of loops: 1, 10, 25, 50, 100, 150, 200, 250, 375 and 500, with a total echo time of 0.012 s, 0.066 s, 0.157 s, 0.306 s, 0.609 s, 0.911 s, 1.212 s, 1.514 s, 2.267 s and 3.021 s respectively.

PUBLICATION 10

Recent advances in small molecule NMR: Improved HSQC and HSQMBC experiments

Laura Castañar and Teodor Parella.
Annu. Rep. NMR Spectrosc., **2015**, *84*, 163-232.

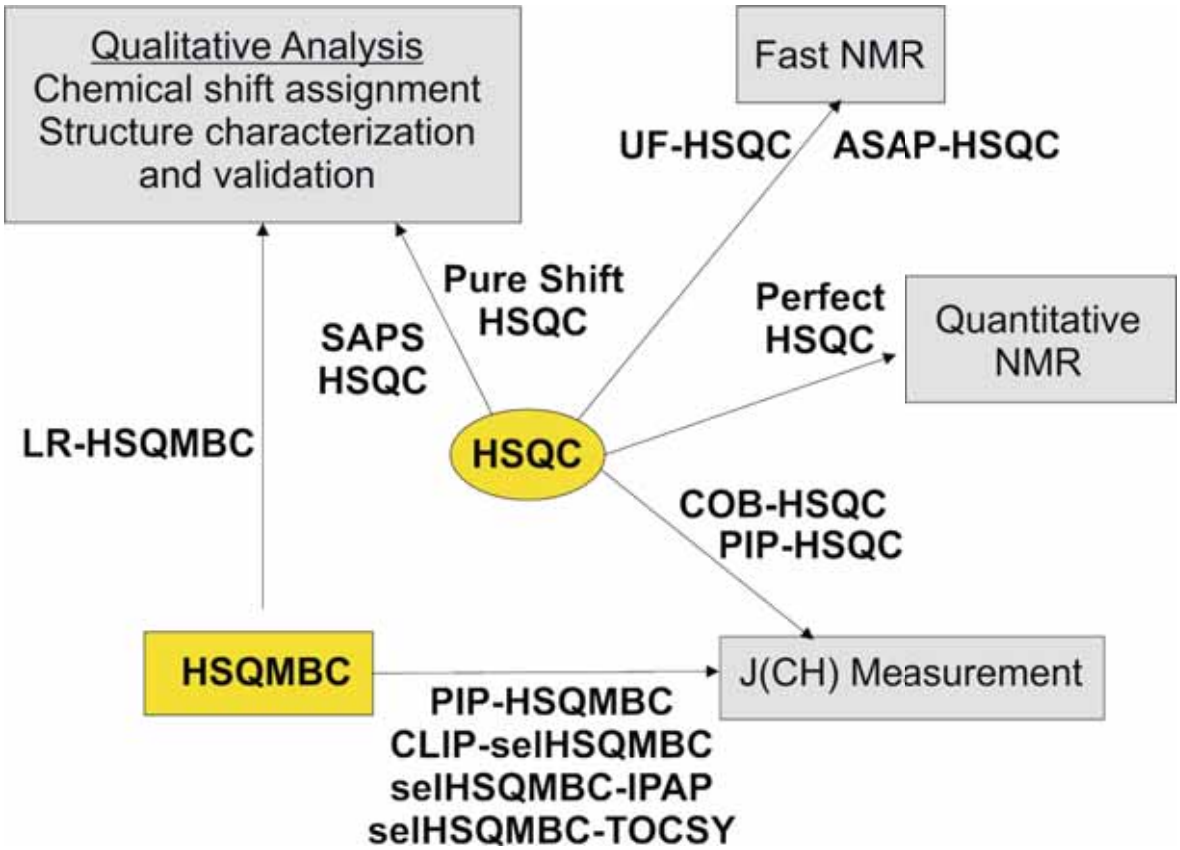

Introduction

This publication is a chapter of the book entitled “Annual Reports on NMR Spectroscopy”. It is a review work where a deeply discussion about the recent developments introduced into novel HSQC and HSQMBC pulse sequences (including all the publications related with HSQC/HSQMBC experiments with and without pure shift methodology discussed in this doctoral thesis). Special emphasis is made on modern concepts such as fast NMR, pure shift NMR, and also on robust techniques affording pure in-phase multiplet patterns, which are amenable for a simpler and a more accurate analysis.

This publication is also focused on the different practical applications of these modern HSQC and HSQMBC experiments, with special emphasis in the measurement of homo- and heteronuclear coupling constants. The suitability of some of these methods for the quantitative measurement of one-bond and long-range proton–carbon coupling values in molecules in isotropic and weakly aligned anisotropic conditions is ilustrated.

CHAPTER FOUR

Recent Advances in Small Molecule NMR: Improved HSQC and HSQMBC Experiments

Laura Castañar, Teodor Parella
Servei de Ressonància Magnètica Nuclear and Departament de Química, Universitat Autònoma de Barcelona, Bellaterra, Catalonia, Spain

Contents

Annual Reports on NMR Spectroscopy, Volume 84
ISSN 0066-4103
http://dx.doi.org/10.1016/bs.arnmr.2014.10.004

Abstract

A general description of the latest developments in heteronuclear single-quantum correlation and heteronuclear single-quantum multiple bond correlation experiments designed for small molecules at the natural isotopic abundance is reported. A discussion is made on the details introduced into novel NMR pulse sequences with special emphasis on modern concepts such as fast NMR or pure shift NMR and also on robust techniques affording pure in-phase multiplet patterns, which are amenable for a simpler and a more accurate analysis. The suitability of some of these methods for the quantitative measurement of one-bond and long-range proton–carbon coupling values in molecules in isotropic and weakly aligned anisotropic conditions is also reviewed.

Keywords: NMR, HSQC, HSQMBC, Proton–carbon coupling constants, Pure Shift NMR, Pulse sequence development

1. INTRODUCTION

Proton-detected two-dimensional (2D) NMR experiments, essentially based on two different pulse schemes referred to as heteronuclear single-quantum correlation (HSQC) [1] and heteronuclear multiple-quantum correlation (HMQC) [2], have been key NMR tools during many years for chemists and biochemists to provide valuable structural information on $^{1}H–^{13}C$ (and $^{1}H–^{15}N$) chemical bonds in a molecule. Nowadays, these experiments are usually performed in a complete automation mode in both data acquisition and processing steps, practically without any need for direct user intervention. The resulting 2D maps are very simple to analyze and to interpret, even for non-experienced NMR users, typically displaying well-dispersed cross-peaks that correlate ^{1}H (direct F2 dimension) and ^{13}C (indirect F1 dimension) chemical shifts between directly attached $^{1}H–^{13}C$ groups, through the one-bond proton–carbon coupling constant ($^{1}J(CH)$) transfer mechanism. Compared to HMQC, the standard HSQC presents a better defined pulse scheme with characteristic steps which can be individually analyzed and modified in a straightforward way. Thus, heteronuclear magnetization transfers performed by INEPT elements and the evolution of single-quantum ^{13}C coherences to generate the indirect F1 dimension are the two main features that define the HSQC experiment.

Since its introduction, the HSQC pulse scheme has been modified in so many different ways in order to improve important experimental aspects such as sensitivity, resolution, efficiency, robustness, and performance. A recommendable work to understand the fundamentals and the different features, options and practical details of both HMQC and HSQC experiments is available as a comprehensive reading and as a complementary

reference to this article [3]. Historically, a major development in pulse sequence design was the incorporation of pulsed field gradients (PFGs) for coherence pathway selection. In both HSQC and HMQC experiments, PFGs allow a clear distinction between $^{1}H–^{12}C$ versus $^{1}H–^{13}C$ magnetization, which results in the collection of high-quality free-artifacts NMR spectra under standard routine conditions [4,5]. In addition, the use of PFGs reduces the requirement for an extensive number of phase cycles to be executed, significantly reducing the overall experiment time when sensitivity is not the limiting factor. PFGs have also been used as purge zz and refocusing elements, and further combination with water suppression strategies extent its applicability for biomolecules working in H_2O solutions. Two additional enhancements of the basic HSQC pulse scheme involved the modification of the last retro-INEPT element: (i) the incorporation of the preservation of equivalent pathways (PEP) technique that afford an important sensitivity improvement for CH and NH spin systems [6] and (ii) the use of the transverse relaxation optimized spectroscopy (TROSY) strategy enables a better sensitivity and resolution for large biomolecules and complexes in high magnetic fields [7]. All these improvements have been successfully incorporated in a large number of multidimensional NMR experiments designed to detect NH groups on isotopically labeled proteins and nucleic acids [8].

Nowadays, clean $^{1}H–^{13}C$ HSQC spectra can be obtained in minutes using conventional hardware configurations and with only some milligrams of a sample at natural isotopic abundance. The availability of high magnetic fields, cryogenically cooled radiofrequency (rf) coils and preamplifier components, and low-volume tube and capillary probes has dramatically improved the detection limits of the NMR spectroscopy, allowing to obtain such 2D spectra even for very low concentrated samples. These innovations can lead to an approximate 20-fold increase in mass sensitivity compared with conventional NMR instrumentation at the same field, providing chemists with new capabilities for exploration of submilligram natural product samples [9]. For instance, it has been reported that a conventional $^{1}H–^{13}C$ HSQC spectrum of 7.5 μg of a natural product dissolved in 30 μl of solvent can be obtained in 15–30 min in a 1.7-mm microcryoprobe at 600 MHz [10] or the measurement of ^{1}J(CH) values from an F2-coupled $^{1}H–^{13}C$ HSQC spectrum has been accomplished with 90 μg of the natural product muironolide in an overnight acquisition [11]. Less-sensitive $^{1}H–^{15}N$ HSQC of natural products can be obtained from about 1 mg samples using a 1.7-mm microcryoprobe within 4 h.

Over the years, the original HSQC pulse scheme has also been largely modified to provide additional and complementary information from a

single NMR experiment. For instance, the multiplicity-edited HSQC (ME-HSQC) experiment [12] is a common and very useful technique used in routine NMR protocols to additionally obtain information about the carbon multiplicity (distinction of CH/CH_3 vs. CH_2 spin systems) as a function of the relative positive/negative phase of HSQC cross-peaks. The experiment uses an extended ^{13}C echo period during the evolution of ^{13}C single-quantum coherences (SQCs) that minimally affect the overall sensitivity and therefore, in practical terms, the ME-HSQC can be preferred to the standard HSQC to trace out connectivities and to obtain multiplicity information in an unique spectrum. The HSQC-TOCSY experiment [13] is another simple but complementary extension of the HSQC experiment which provides the simultaneous information of ^{1}H and ^{13}C chemical shifts into a complete *J*-coupled spin system, offering a relevant interest in the analysis and unambiguous assignments of complex spin systems. The experiment relies in a consecutive and sensitive $^{1}J(CH) + J(HH)$ transfer mechanism but, as a main drawback, only works for protonated carbons. On the other hand, and in analogy to the classical heteronuclear multiple bond connectivity (HMBC) experiment [14,15], the long-range optimized HSQC experiment (referred to as heteronuclear single-quantum multiple bond correlation or HSQMBC) [16] provides information about protons and carbons separated by more than one-bond, typically two- and three-bond connectivities. In its basic form, the regular HSQC pulse timing is executed with a different setting of the interpulse delay (typically 50–75 ms) to match the smallest long-range proton–carbon coupling constant ($^{n}J(CH)$; $n > 1$) values, typically in the range of 0–15 Hz. The less-sensitive ADEQUATE experiments [17] are based on extended $J(CH) + J(CC)$ transfer mechanisms, where the main features of the HSQC experiment are combined with an intermediate ^{13}C double-quantum mixing period. The basic 1,1-ADEQUATE experiment provides two-bond connectivities according to a $^{1}H–^{13}C–^{13}C$ spin system, and complementary 1,*n*-, *n*,1-, and *n*,*n*-ADEQUATE versions have been also useful to trace out longer $^{1}H/^{13}C$ correlations [18].

In addition to the tremendous potential of the HSQC experiment as an analytical method for unambiguous chemical shift assignment, structure characterization and validation, and mixture analysis, it has also demonstrated to be very efficient for other purposes, such as the quantitative measurement of $^{1}J(CH)$ couplings, the determination of T_1/T_2 relaxation times, or for quantitative studies by peak volume integration. For small molecules in isotropic conditions, $^{1}J(CH)$ values are large in magnitude (in the range of ~120–250 Hz) and positive in sign, and they can be quickly measured for

the large doublet observed in coupled HSQC spectra. ^{1}J(CH) has been found to have interesting applications in many constitutional, configurational, and conformational studies [19–22] and, in the last decade, a renewed interest for the measurement of one-bond proton–carbon residual dipolar coupling (RDC) constants (^{1}D(CH)) has appeared when working in weakly aligned anisotropic media [23–27]. The magnitude and the relative sign of ^{1}D(CH) are determined from the differences obtained from the experimental isotropic versus anisotropic values according to $^{1}D(\mathrm{CH}) = {}^{1}J(\mathrm{CH}) - {}^{1}T(\mathrm{CH})$, and they are strongly related to the CH bond orientation with respect to the molecular tensor and the permanent magnetic field. On the other hand, related NMR experiments based on the HSQC-TOCSY and HMBC/HSQMBC pulses schemes have been proposed for the quantitative measurement of smaller ^{n}J(CH) couplings.

The aim of this article is to compile all new HSQC-related NMR experiments published in the last years that have been specifically designed and applied to small molecules at natural abundance (Scheme 1). Special focus will be made on novel HSQC schemes including concepts such as fast NMR and pure shift NMR. In addition, reference to improved *J*-compensated HSQC sequences will be made, discussing the effects of the intensity and phase signal modulation dependence with respect to ^{1}J(CH) and/or J(HH) which are generated during INEPT periods. A particular analysis will be also made on modern NMR methods designed for the quantitative measurement of ^{1}J(CH) and/or ^{1}D(CH) and, by

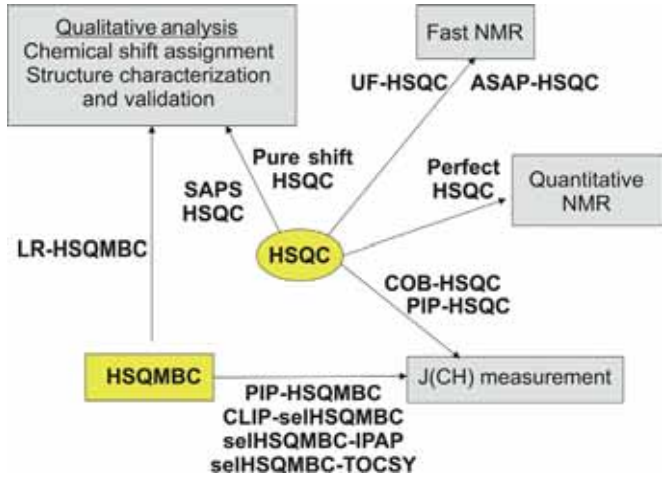

Scheme 1 Graphical representation of some recently reported HSQC/HSQMBC-related NMR methods.

extrapolation, for the determination of the magnitude and/or the sign of small ^{n}J(CH) coupling constants. Finally, miscellaneous HSQC/HSQMBC methods to obtain semiquantitative spectra suitables for a direct peak volume integration, to achieve optimum signal resolution in F1 and/or F2 dimensions, or to observe very long-range heteronuclear connectivities will be commented.

2. THE BASIC HSQC EXPERIMENT

Figure 1 shows the five basic independent steps that can be identified in a standard 2D gradient-selected HSQC pulse scheme. *Step 1*: The pre-scan period is usually defined by a long recycle delay (some seconds of duration, accordingly to the existing $T_1(^1H)$ relaxation times) to allow the recovery of the ^1H magnetization to a pre-equilibrium state just before to start the sequence. *Step 2*: After the initial ^1H excitation, heteronuclear transfer via J(CH) takes place using an INEPT element. *Step 3*: Antiphase (AP) ^{13}C SQC evolves during a variable t_1 period under the effect of ^{13}C chemical shift, whereas the evolution of heteronuclear J(CH) couplings is

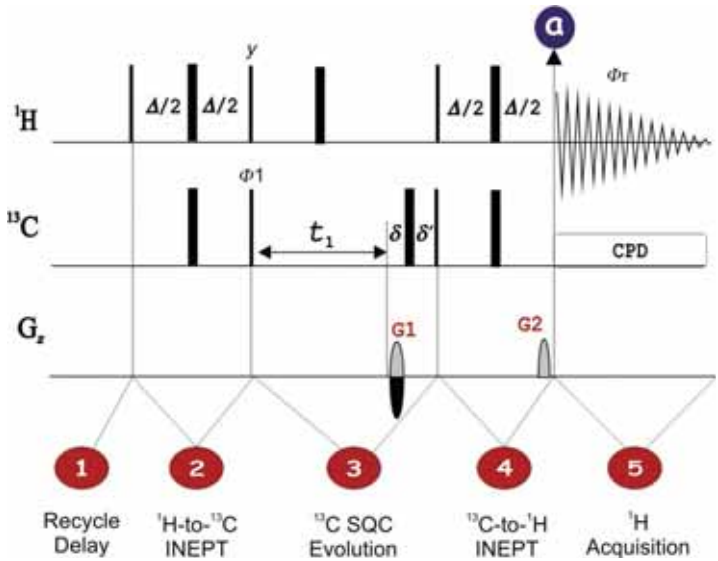

Figure 1 Schematic representation of the different steps involved in a standard 2D ^1H–^{13}C HSQC pulse sequence. Thin and thick vertical rectangles represent 90° and 180° hard pulses, respectively. The delay Δ should be set to $1/(2*^1J(CH))$, and δ represents the duration of the PFG and its recovery delay. In this scheme, coherence selection is performed by the gradient pair G1/G2 using the echo–antiecho protocol.

decoupled by the central 180° ^{1}H pulse. *Step 4*: During the retro-INEPT element, ^{13}C magnetization is initially reconverted to ^{1}H magnetization, whereas the subsequent J(CH) evolution generates in-phase (IP) magnetization prior to acquisition. *Step 5*: The sequence ends with a ^{1}H detection period under optional broadband heteronuclear composite pulse decoupling (CPD). This scheme deserves some additional comments because it is used as a pattern for most experiments described in this report. First, it uses coherence selection by PFGs using the echo–antiecho approach, where the encoding gradient G1 (of duration δ) is located into a ^{13}C spin-echo period to avoid any evolution during this application. The decoding gradient G2 applied during the last evolution period is optimized according to the refocusing gradient condition ($G1 = (\gamma_H/\gamma_C)$*G2).

The interpulse INEPT delay is optimized to a single J value, according to $\Delta = 1/(2*^{1}J(CH))$, and therefore, the cross-peak intensities do not show an uniform response owing to the variable and wide range of ^{1}J(CH) coupling values. The magnitude of ^{1}J(CH) is a direct measurement for the degree of hybridization of the involved carbon atom, presenting approximate values of ~120–140 Hz for aliphatic sp^3 carbons, ~150–170 Hz for olefinic systems or 240–270 Hz for acetylenic functional groups. The practical use of ^{1}J(CH) has found a wide interest for structural analysis of small molecules including, for instance, the distinction of axial and equatorial protons in cyclic systems, of anomeric protons in carbohydrates, or the use of RDCs as angular constraints, among other.

For a proper knowledge how the HSQC pulse scheme works, the signal intensity and phase dependences generated during the INEPT periods can be easily analyzed by the product operator formalism [28]. At the end of the refocusing ^{13}C-to-^{1}H INEPT period and just before acquisition (point **a** in Fig. 1), the observable ^{1}H magnetization for an isolated ^{1}H–^{13}C two-spin system, with a mutual coupling of ^{1}J(CH), can be described as a mixture of IP and AP components:

$$H_x s'^2 (\text{Term I}) - 2H_y C_z s' c' (\text{Term II}) \quad (1)$$

where c' is $\cos(\pi J(CH)\,\Delta)$, s' is $\sin(\pi J(CH)\,\Delta)$, and Δ is the J evolution INEPT period. The term II in Eq. (1) can be removed by heteronuclear CPD during acquisition. To understand the effects of J(HH) in an HSQC experiment, each INEPT block can be considered as an spin-echo period for protons and therefore, the undesired J(HH) evolution during the overall Δ period can be assessed by considering a heteronuclear three-spin H_1, H_2, and

C system, with active $J(H_1H_2)$ and $J(CH_1)$ couplings. In this case, the magnetization of spin H_1 at point **a** in Fig. 1 can be now described as:

$$H_{1x}c^2s'^2(\text{Term I}) - 2H_{1y}C_zc^2s'c'(\text{Term II}) + 2H_{1y}H_{2z}css'^2(\text{Term III}) + 4H_{1x}H_{2z}C_zcsc's'(\text{Term IV}) \quad (2)$$

where c' is $\cos(\pi J(CH_1)\,\Delta)$, s' is $\sin(\pi J(CH_1)\,\Delta)$, c is $\cos(\pi J(H_1H_2)\Delta)$, and s is $\sin(\pi J(H_1H_2)\,\Delta)$. Although that terms II and IV in Eq. (2) can be removed by heteronuclear CPD during acquisition, this more complex signal intensity dependence usually hinders any attempt for the quantitative use of standard HSQC data, requiring the design of more robust J(HH)- and J(CH)-compensated INEPT sequences to improve/avoid such anomalies (see Section 5.1.2).

3. SPEEDING-UP HSQC DATA ACQUISITION

There has always been a general interest to develop fast NMR methods to reduce the experimental time required for a complete 2D acquisition and to economize valuable spectrometer time. There are two main factors that determine the overall duration of a given 2D experiment: (i) the long recycle delay (typically in the order of some seconds) needed to achieve a preequilibrium proton polarization and (ii) the number of variable linearly sampled t_1 increments required for an optimum resolution in the indirect F1 dimension. Several approaches to accelerate data acquisition in HSQC experiments have been reported.

3.1. ASAP-HSQC Experiment

In conventional HSQC experiments, the preparatory recycle period is determined as a function of the $T_1(^1H)$ values, typically 1–2 s in routine analysis. Thus, a simple solution to speed up data acquisition should be the reduction of the recycle delay between scans to some milliseconds. However, fast pulsing generates partial signal saturation and the overall sensitivity can be significantly decreased.

Fast acquisition of ^1H–^{15}N HSQC spectra in proteins has been performed using the SOFAST or BEST approaches, which is based on the replacement of all hard ^1H pulses by region-selective 90° and 180° ^1H (^{15}N) pulses in order to reduce the longitudinal $T_1(^1HN)$ relaxation [29,30]. This allows the combined use of very short recycle delays with an optimized Ernst-angle excitation to achieve optimal sensitivity per time unit. However, this region-selective excitation strategy is not of general

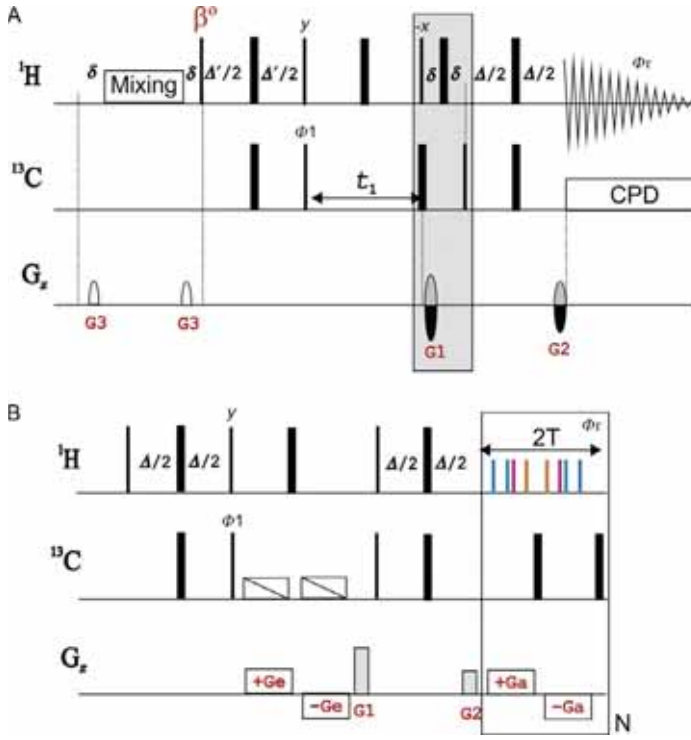

Figure 2 Two different approaches to achieve fast recording of HSQC spectra: (A) ASAP-HSQC experiment and (B) single-scan Ultrafast HSQC (UF-HSQC) experiment.

application to small molecules. Recently, a fast ASAP-HSQC experiment [31] (ASAP stands for Acceleration by Sharing Adjacent Polarization) (Fig. 2A) has been proposed to quickly obtain a 2D HSQC map in less than 30 s for relatively concentrated samples, and it has been demonstrated that better spectral and cross-peak quality is obtained than a previous ASAP-HMQC experiment [32]. The ASAP method [33] uses a short (40 ms) PFG-flanked isotropic mixing period instead of the conventional long recycle delay and it can be combined with the use of an optimized Ernst-angle pulse excitation (β) and shorter Δ' delays during the first defocusing INEPT periods. The main originality of the sequence relies in the management of ^{1}H magnetization just after the evolution of ^{13}C SQC during the variable t_1 period, which retains the polarization reservoir for all the passive spins not directly bound to the NMR-active heteronucleus. This modified experiment applies a 90°(^{1}H) pulse of the backtransfer step with $-x$ phase before the actual coherence order selection and echo–antiecho encoding. As described in the original publication, this

way the polarization reservoir is flipped along z, ensuring that it is not affected by the gradients. Coherence order selection is then achieved by dephasing either zero-quantum or double-quantum coherences with a proper setting of the involved gradient strengths. The fast acquisition of HSQC spectra allows the averaging over many more scans or to acquire a large number of t_1 increments for the same experiment time. Overall, the ASAP-HSQC shows a moderate gain in SNR per time unit when compared to the standard HSQC recorded into the same experimental time. It must be emphasized that for long acquisitions, precautions should be taken because rapid pulsing could generate sample heating and damage probe components.

The original ASAP-HMQC pulse sequence has been evaluated for rapid screening of natural products [34], and an ASAP version of the HMBC experiment (defined as IMPACT-HMBC) has been also reported and further tested for analyzing silylated derivatives [35] and for monitoring hydrogen bonding in peptides [36].

3.2. Non-uniform Sampling

It is recognized that one of the major inconveniences of any 2D experiment is the need to record a minimum number of t_1 increments, which determines the resolution achieved in the indirect dimension and also influences the overall experimental time. Several approaches have been proposed to improve the resolution along the indirect dimension of an HSQC experiment and to reduce spectrometer times: (i) the use of band selection in the indirect dimension that allows the use of a reduced ^{13}C spectral width [37,38]; (ii) the application of data processing techniques such as zero-filling or linear prediction; (iii) the use of a deliberate reduced ^{13}C spectral width to achieve spectral folding or spectral aliasing which depends on the acquisition mode [39–42]; or (iv) the use of non-uniform sampling (NUS) [43,44] techniques. For small molecules, NUS can facilitate significant reductions (~50%) in the time needed to collect 2D HSQC spectra by using ~50% of sampling density, or otherwise offering gains in spectral resolution along the indirect ^{13}C dimension by recording less number of t_1 increments. Some of these algorithms are already implemented in modern NMR software packages, and non-experienced users can use them in a fully transparent and automatic way without any further modification of the standard pulse programs or general setup parameters. The quality of the resulting spectra depends crucially on the sampling schedules and the algorithms for data reconstruction. However,

precaution should be taken for the presence of unwanted artifacts that can generate distorted or false cross-peaks.

An accelerated 3D HSQC-DOSY experiment has been proposed to obtain individual 2D HSQC maps of each component in a mixture by joint sparse sampling of the diffusion and time dimensions [45].

3.3. Ultrafast HSQC

The spatially encoded single-scan or Ultrafast (UF) NMR technique allows performing 2D experiments in a single scan, within a few seconds, provided that sensitivity and sample concentration are sufficient [46–49]. Since its earliest days, an important number of new developments and applications have converted UF-NMR as a powerful analytical tool for real-time monitoring of chemical and biochemical processes [50–52]. Several UF-HSQC pulse sequences have been proposed where the key elements are the use of spatially encoding gradients during Step 3 of the basic HSQC scheme (see Fig. 1) and an echo planar imaging acquisition mode as traditionally implemented in magnetic resonance imaging applications (Fig. 2B). In practice, a general applicability of the UF-HSQC experiment in routine protocols of small molecules is hampered because the UF dimension window is limited by the strength of the encoding/decoding gradients and also by the severe sensitivity losses due to slice selection. Experimentally, the spectral width observable in the ^{13}C dimension is limited to a few tens of ppm [53,54] although that an improved version has been reported that combines spatial encoding with iterative compressed-sensed reconstruction [55]. UF-HSQC has been successfully applied for the real-time mechanistic monitoring of chemical reactions [56], for the fast measurement of $^{1}J(CH)/^{1}D(CH)$ in oriented media [57] and combined with *ex situ* dynamic nuclear polarization (DNP) [58]. Although these experiments can be currently defined as non-routine techniques due to their apparent complexity, valuable documentation describing the experimental details (the step-by-step protocol, pulse sequences and processing programs) required to implement UF-HSQC experiments in modern spectrometers is available [59–61].

4. HIGH-RESOLVED HSQC USING PURE SHIFT NMR

4.1. PS-HSQC Experiments

In the last years, the old idea of broadband homodecoupling [62] has emerged in the field of small molecule ^{1}H NMR spectroscopy under the acronym of pure shift NMR. [63–66] A number of homodecoupled

versions of the most traditional 1D and 2D NMR experiments have been proposed providing the collapse of the typical *J*(HH) multiplet patterns to simplified singlet lines along the detected dimension. Among the different homodecoupling approaches developed over the years, the Zangger–Sterk (ZS) experiment has become one of the most powerful approaches to efficiently improve signal resolution. It is based on the combination of a hard 180° pulse and a selective inversion element applied in the center of an echo period to allow the exclusive evolution of ^{1}H chemical shifts of the active protons (those experiencing the selective inversion perturbation), whereas all their passive *J*(HH) couplings are refocused. The implementation of the ZS method involves a pseudo-2D acquisition scheme that usually requires the collection of 16–32 measurements and a special free induction decay (FID) reconstruction of an 1D homodecoupled FID from the concatenation of the initial chunk of each increment with a duration $1/SW_1$, where SW_1 is about twice the width of the widest multiplet to be decoupled (typically about 10 ms) [63,67]. Alternatively, a real-time 1D acquisition scheme that requires conventional data processing offers a considerable gain of sensitivity per time unit ratios but at some cost in spectral quality and resolution and limited to the use of short selective pulses [62,64,68]. In principle, the direct implementation of these ZS methods should be suitable for all known 1D and 2D experiments involving IP magnetization with respect to *J*(HH), such as TOCSY, NOESY, ROESY, and HSQC experiments, but would fail for those involving AP magnetization such as traditional COSY or HMBC/HSQMBC experiments. Thus, HSQC has been a good target to evaluate the performance, the advantages, and also the limitations of such implementations, and a number of different pure shift HSQC (PS-HSQC) experiments have been reported incorporating the pseudo-2D or real-time acquisition strategies, using either a BIRD element to invert selectively ^{1}H–^{12}C versus ^{1}H–^{13}C [62] or spatially encoded frequency-selective pulses.

The first proposal RESET-HSQC experiment [69] implemented the original pseudo-2D ZS element just prior to acquisition, using a BIRD element as selective inversion module to homodecouple ^{1}H–^{13}C protons from those belonging to ^{1}H–^{12}C. An improved version offering better suppression of strong coupling effects and better tolerance to the mismatch INEPT/BIRD delays optimization has been further proposed (Fig. 3A) [70]. As a main drawback, this approach uses a 3D acquisition scheme, and therefore, the gains associated with multiplet collapsing are strongly minimized by the need of extra spectrometer time to record

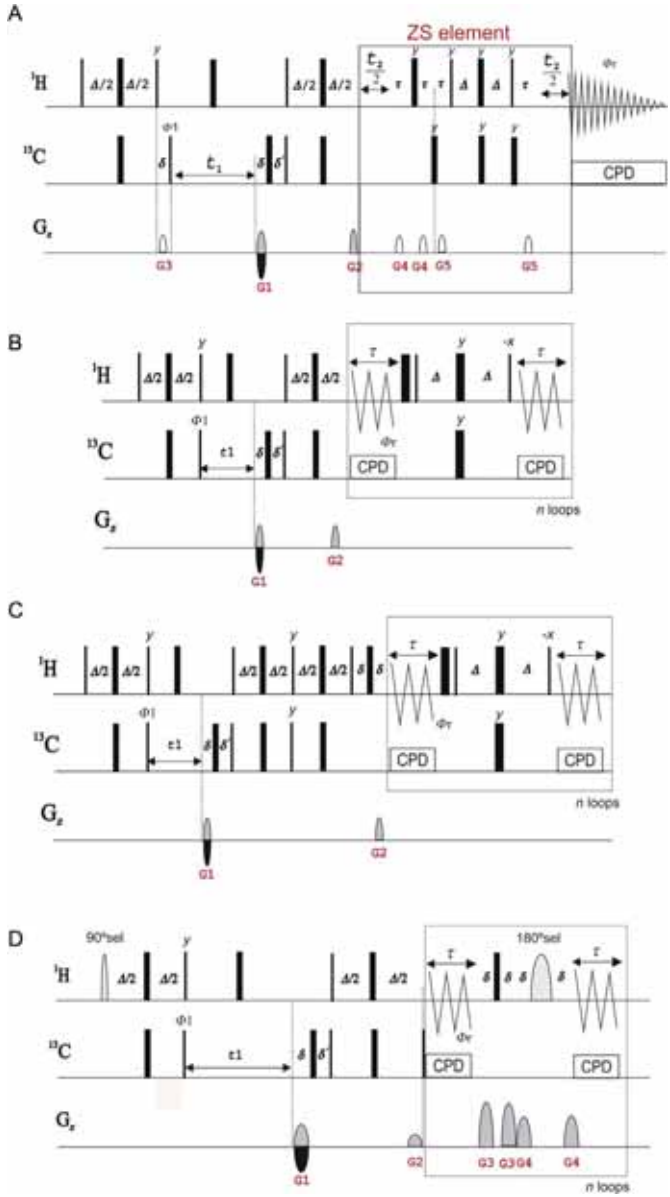

Figure 3 Pulse schemes to obtain pure shift HSQC spectra. (A) HSQC-RESET experiment which uses a pseudo-3D BIRD-based ZS acquisition scheme; (B) PS-HSQC experiment using real-time homodecoupling by the combination of a hard 180°(^{1}H)-BIRD element during data acquisition; (C) sensitivity-improved PS-HSQC; (D) HOBS-HSQC experiment using real-time homodecoupling during detection achieved by applying a pair of hard/band-selective 180° ^{1}H pulses (represented as solid and shaded shapes). In (B–D), the homodecoupling element is applied at the middle of $2\tau = AQ/n$ periods, where AQ is the acquisition time and n is the number of concatenated loops. See original publications for a more detailed description.

the homodecoupled ^{1}H dimension. F2-heterocoupled versions of the RESET-HSQC experiment have been also reported for the measurement of ^{1}J(CH) couplings (see Section 5.1.5).

An enhanced approach of the PS-HSQC experiment uses the real-time detection method where the homodecoupled BIRD-based inversion element is applied into short echo periods during the acquisition period (Fig. 3B) [71]. This real-time BIRD-based technique was initially proposed as a 1D method [62,68] to avoid the strong coupling effects associated with slice selection, but it also delivers two orders of magnitude of sensitivity lost when compared to a conventional ^{1}H spectrum due to the unavoidable editing of ^{1}H–^{13}C magnetization at natural abundance (1%). However, the incorporation of this module in a 2D HSQC scheme affords the maximum attainable sensitivity and improved resolution than the regular experiment because the HSQC pulse train by itself acts as a ^{1}H–^{13}C filter and the homodecoupled element applied during the acquisition period only decouples these selected protons from the passive ^{1}H–^{12}C. It is important to mention that real-time broadband homodecoupling is fully compatible with classical broadband heteronuclear decoupling which is applied during the FID periods.

Experimentally, it has been shown that pure-shift approach can afford a general sensitivity enhancement by 10–40% through collapse of the multiplet structure, and a substantial signal enhancement for CH cross-peaks can be achieved with the sensitivity-improved PS-HSQC experiment (Fig. 3C) [72]. However, the BIRD cluster is not able to suppress the effects of geminal homonuclear couplings and protons belonging to diastereotopic CH_2 groups appear partially homodecoupled with characteristic doublets due to the active ^{2}J(HH) splitting (Fig. 4). Broadband homodecoupling could be incorporated in any type of HSQC-like experiments as reported originally with the multiplicity-edited HSQC (PS-edHSQC) experiment [71].

4.2. HOBS-HSQC: Homodecoupled Band-Selective HSQC

Band-selective NMR spectroscopy experiments are really useful for peptides and proteins because a set of equivalent spins (amide NH, H_α, or aliphatic side-chain protons) appear in well-separated regions. Another alternative to obtain PS-HSQC spectra is by implementing the HOmodecoupled Band-Selective (HOBS) detection scheme [73,74]. This technique has been successfully implemented in a suite of NMR experiments involving IP ^{1}H magnetization, such as Inversion-Recovery and CPMG-Project experiments

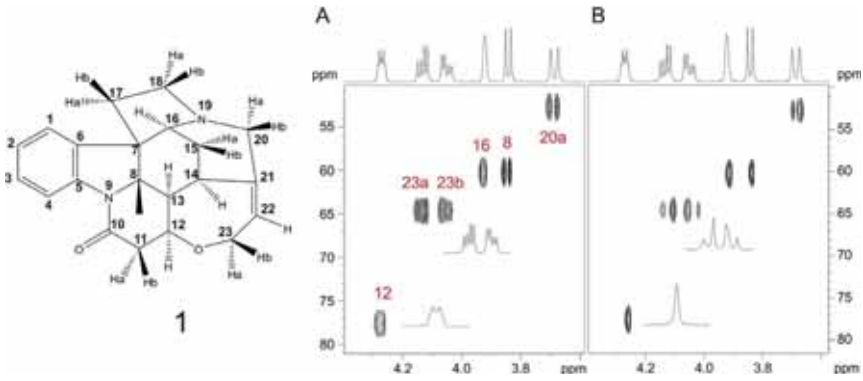

Figure 4 Selected areas corresponding to the (A) conventional HSQC and (B) pure-shift HSQC spectra of strychnine (**1**). One-dimensional traces are shown for selected CH and CH_2 spin systems. Data were acquired, processed, and displayed with the same conditions to allow a quantitative comparison.

to measure T_1 and T_2 relaxation times in overlapped signals [75] or in homonuclear 2D TOCSY [73], NOESY [74], and ROESY [76] experiments. Similarly, a band-selective version of the PS-HSQC experiment has been also reported, the so-called HOBS-HSQC experiment [73,74], where a region-selective 180° ^{1}H pulse is used instead of the BIRD element as a selective inversion element (Fig. 3D). The HOBS method is based on the real-time instant ZS experiment proposed by Meyer and Zangger [64] but yields full sensitivity because the original spatially encoding gradient applied simultaneously to the selective 180° ^{1}H pulse is omitted. Similarly as described above for the BIRD element, the homodecoupling scheme consists of n concatenated loops that include a pair of hard/region-selective 180° ^{1}H pulses (each one flanked by strong G1 and G2 gradients) applied at intervals of 2τ period (τ is set to AQ/2n).

The HOBS-HSQC experiment has demonstrated its usefulness for a natural-abundance sample of cyclosporine (**2**) (Fig. 5). The collected data allow conventional data processing and the best results in terms of selectivity and optimum relaxation were obtained using 180° REBURP semiselective ^{1}H pulses of 5–7.5 ms and decoupling intervals of $2\tau = 10$–15 ms. The method affords broadband homodecoupling for all protons into the selected region, except those that are mutually J coupled which will show their corresponding doublet pattern, as shown for the excitation of the H_α region in **2**. Note the improved sensitivity and signal resolution obtained from the selected 1D slice in Fig. 5. In a similar implementation, a ^{1}H–^{15}N HSQC technique for measuring ^1D(NH) RDCs in protonated ^{15}N/^{13}C-enriched ubiquitin weakly aligned in Pf1 has been reported [74]. A spatial-encoded

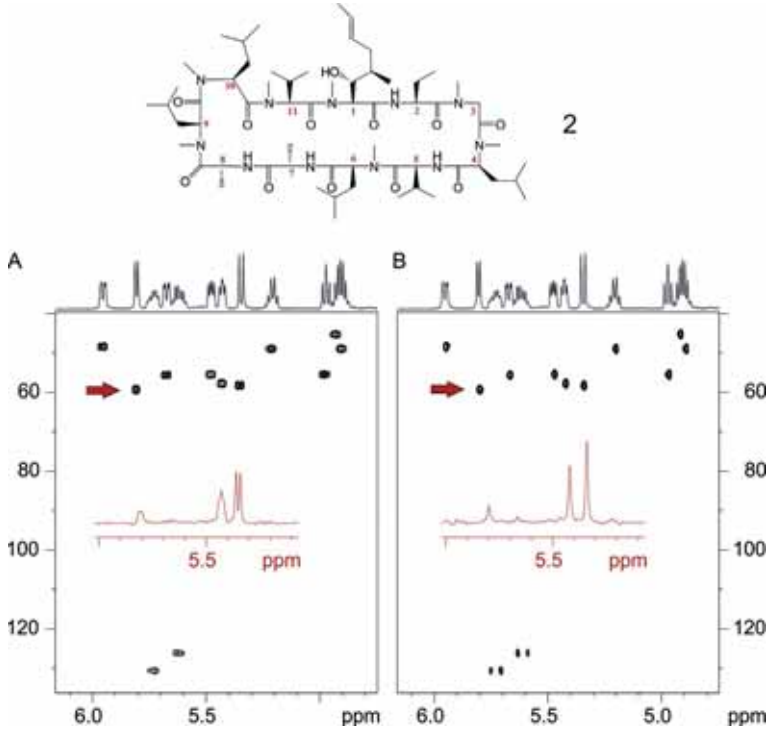

Figure 5 (A) Conventional and (B) fully homo- and heteronuclear decoupled HOBS-HSQC spectra of the peptide cyclosporine (**2**) after selection of the H_α region. Note the residual doublet splitting of the two mutually *J*(HH) coupled olefinic protons belonging to the residue 1 in (B). *Adapted from Ref. [73].*

homodecoupled version of a constant-time HSQC experiment has been also proposed using the instant detection technique and applied to a ^{13}C-labeled intrinsically disordered protein but this approach suffers from high levels of sensitivity losses due to slice selection [77].

4.3. SAPS-HSQC: Spectral Aliasing and Pure-Shift NMR

A very simple experimental trick based on the reduction of the ^{13}C spectral width in HSQC experiments (for instance, from the typical 160 to 5 ppm) is extremely useful to improve digital resolution and signal dispersion by one or two orders of magnitude (for a given number of t_1 increments) along the indirect dimension of an HSQC map, without a substantial modification of the total experimental time. Signals outside of the selected spectral width appear folded or aliased depending on the acquisition scheme [42,78–80]. Recently, a highly resolved Spectral Aliased Pure Shift

(SAPS-HSQC) [72] method has proved to be a fast and very efficient tool for the detection and accurate differentiation and quantification of very small $\Delta\Delta\delta$ values simultaneously for ^{1}H and ^{13}C (Fig. 6). The method combines the complementary features of the pure shift approach that enhances signal resolution in the alternate ^{1}H dimension with those related to spectral aliasing in the ^{13}C dimension. This approach has been successfully applied to enantiodifferentiation studies and it can found interest in the analysis of complex mixtures or the distinction of isomers with very similar NMR spectra.

Enantiodifferentiation analysis through the SAPS-HSQC spectrum has been shown to be superior than the conventional 1D ^{1}H, the conventional ^{13}C, or even the broadband homodecoupled 1D ^{1}H ZS spectra. SAPS-HSQC data allow the detection of enantiodifferentiated signals even in the case that $\Delta\Delta\delta(^{1}H)$ or $\Delta\Delta\delta(^{13}C)$ is close to 0, whenever one of these two values is sufficiently dispersed. In a previous work, 1D pure shift ^{1}H NMR already demonstrated its practical usefulness in enantiodifferentiation studies to distinct signals separated by more than

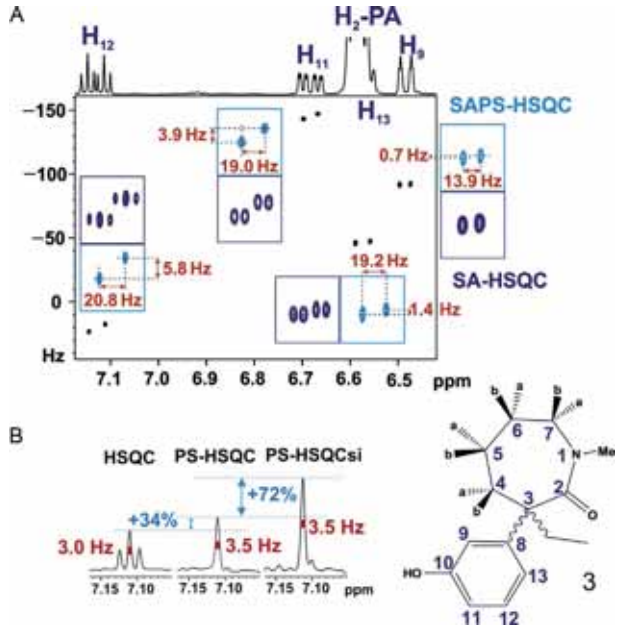

Figure 6 (A) Expanded areas comparing some cross-peaks in SA- and SAPS-HSQC spectra of the racemic compound (**3**)/*R*-PA (Pirkle Alcohol) mixture acquired with a reduced ^{13}C spectral width of 2.5 ppm. (B) Experimental line widths and relative sensitivities obtained in conventional HSQC, pure shift HSQC (PS-HSQC) and pure shift sensitivity-improved HSQC (PS-HSQCsi) experiments. One-dimensional traces correspond to the H12/C12 cross-peak. *Adapted from Ref. [72].*

2 Hz [81]. Similarly, a conventional fully decoupled 1D ^{13}C spectrum is one of the oldest pure shift experiment and it has been shown that enantiodifferentation can also be accomplished with signals above 2 Hz in a 600-MHz spectrometer [82]. To quantify the better enantiodifferentiation and signal dispersion achieved in a 2D HSQC cross-peak, a new parameter $\Delta\Delta\delta(CH)^2 = \Delta\Delta\delta(^1H)^2 + \Delta\Delta\delta(^{13}C)^2$ has been defined. It can be stated that both $\Delta\Delta\delta(^1H)$ and $\Delta\Delta\delta(^{13}C)$ values can be measured when $\Delta\Delta\delta(CH) > 5$ ppb, even in the case that signals are not differentiated in the conventional 1D ^{1}H or ^{13}C spectra. In terms of spectral quality, homodecoupling during acquisition in PS-HSQC experiments generates sidebands at specific frequencies around the main signal and a slight broadening of the signal (~3 vs. ~3.5 Hz) when compared to regular experiments (Fig. 6B). In practice, this does not affect the $\Delta\Delta\delta$ determination, and signal discrimination less than 1 Hz can be achieved in a 600-MHz spectrometer, even for those NMR signals with no apparent splitting in the ^{1}H and/or in the ^{13}C spectrum (<2 Hz). For instance, the H9/C9 and H13/C13 signals are two excellent examples showing how two carbon signals that do not appear split in the 1D ^{13}C spectrum can be clearly distinguished with $\Delta\Delta\delta(^{13}C)$ values of 0.7 and 1.4 Hz (4.6 and 9.2 ppb), respectively, from the 2D cross-peak analysis. In the example shown in Fig. 6A, only 5 of the 16 available proton signals were clearly enantiodifferentiated in the conventional ^{1}H spectrum, 10 in the 1D ZS spectrum, and 15 in the SAPS-HSQC spectrum. On the other hand, 6 of the 11 protonated carbons were enantiodifferentiated in the 1D ^{13}C spectrum acquired overnight, whereas 10 signals were distinguished in the SAPS-HSQC data collected in only 10 min.

The improved signal dispersion achieved due to the combined effects of ^{1}H and ^{13}C δ differentiation and the enhanced multiplet pattern simplification provided by both homo- and heteronuclear decoupling in both dimensions is also illustrated in Fig. 7. The H-15 methyl signal consists of two overlapped triplets where it is difficult to extract the exact chemical shift values in both ^{1}H and conventional HSQC spectra. Note the superior performance of the SAPS approach for an automated peak picking to determine a more accurate and simultaneous determination of $\delta(^{13}H)$, $\delta(^{13}C)$, $\Delta\Delta\delta(^1H)$, and $\Delta\Delta\delta(^{13}C)$ and to quantify each individual singlet signal by direct peak volume integration.

In analogy, small ^{13}C chemical shift differences for quaternary carbons can also be determined by implementing spectral aliasing in HSQMBC experiments. Unfortunately, a real-time broadband homodecoupling

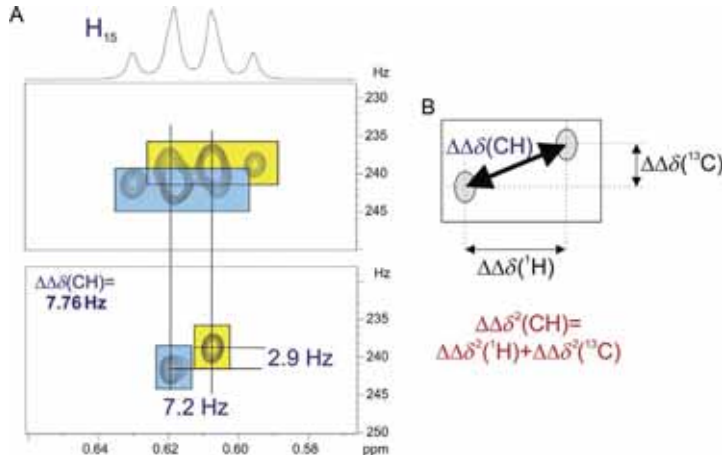

Figure 7 (A) Expanded area showing the C15/H15 cross-peak enantiodifferentiation of (**3**) by using in (top) SA-HSQC and (bottom) SAPS-HSQC spectra. (B) Definition of the new $\Delta\Delta\delta$(CH) enantiodifferentation parameter. *Adapted from Ref. [72].*

acquisition scheme as described previously for the HSQC scheme cannot be implemented in conventional HSQMBC sequences because the detected ^{1}H signals are directly attached to ^{12}C and the BIRD element is not able to distinguish between different *J*(HH)-coupled ^{1}H(^{12}C) protons. However, two different approaches have been reported to achieve pure shift long-range heteronuclear correlation experiments: (i) A band-selective version based on the HOBS technique (HOBS-HSQMBC), which is described in detail in Section 6.5 and (ii) a broadband homodecoupled HMBC spectrum based on a 3D *J*-resolved HMBC experiment [83]. In this latter case, a special data processing and the requirement for a longer 3D acquisition time can limit its practical use.

Finally, the incorporation of spectral aliasing in HSQC-TOCSY experiments also shows to be complementary to the HSQC counterparts for unambiguous chemical shift assignments of signals belonging to each enantiomer. As discussed before, it has not been reported any NMR method incorporating broadband homodecoupling in the HSQC-TOCSY experiment, mainly due to the same reasons as given for the long-range correlation experiments. However, broadband homodecoupled HSQMBC and HSQC-TOCSY experiments could be designed using the real-time instant or the pseudo-2D ZS strategy based on slice selection but they would become prohibitive in terms of sensitivity and overall experimental time.

5. HSQC METHODS FOR MEASURING ^1J(CH)

The HSQC experiment has been largely used for the sensitive measurement of ^1J(CH)/^1D(CH) coupling constants in solution and anisotropic media, respectively, of both small molecules at natural abundance and large labeled biomolecules [84–86]. A comparison of standard F1- and F2-coupled HSQC methods to measure ^1J(CH) and ^1T(CH) in diastereotopic protons of strychnine was reported some years ago [87], and more recently, the pros and cons of new HSQC methods have been evaluated, with special focusing on the design of robust NMR methods to perform such measurements in an easy, user-friendly, and accurate way, and considering some relevant aspects such as (i) the discussion about whether the ^1J(CH) splitting should be measured from the direct F2 (^{1}H) or the indirect F1 (^{13}C) dimension of a 2D HSQC spectrum, (ii) the optimum measurement when a large variation of ^1J(CH)/^1T(CH) values are present, (iii) the determination of ^1J(CH) for individual protons in diastereotopic CH_2 or NH_2 groups, (iv) the simultaneous determination of additional coupling constants from the analysis of the same cross-peak, being the maximum interest the sign-sensitive determination of geminal ^2J(HH) values, and (v) the detection and recognition of the presence of undesired strong coupling effects and evaluation of their influence on the accuracy of the measurement.

5.1. F2-Coupled HSQC Experiments

The easier method to measure ^1J(CH) is from the detected dimension of a conventional HSQC experiment recorded without heteronuclear decoupling during proton acquisition, referred here to as F2-HSQC experiment (Fig. 8A). The main advantages of such an approach are its easy and direct measurement due to the presence of large doublets (Fig. 9A), the high levels of digital resolution readily available in the proton dimension and different peaks belonging to diastereotopic CH_2 groups can be individually analyzed. The drawbacks are that signals exhibit the typical J(HH) multiplet pattern structure, and therefore, the lack of a well-defined multiplicity J substructure or undesired line broadening effects can preclude accurate determinations, factors that are emphasized in anisotropic media due to the important HH dipolar contribution. In addition, strong coupling effects can be quickly recognized by the distortions observed in one of the two components, as shown in Fig. 9B, hindering an accurate measurement.

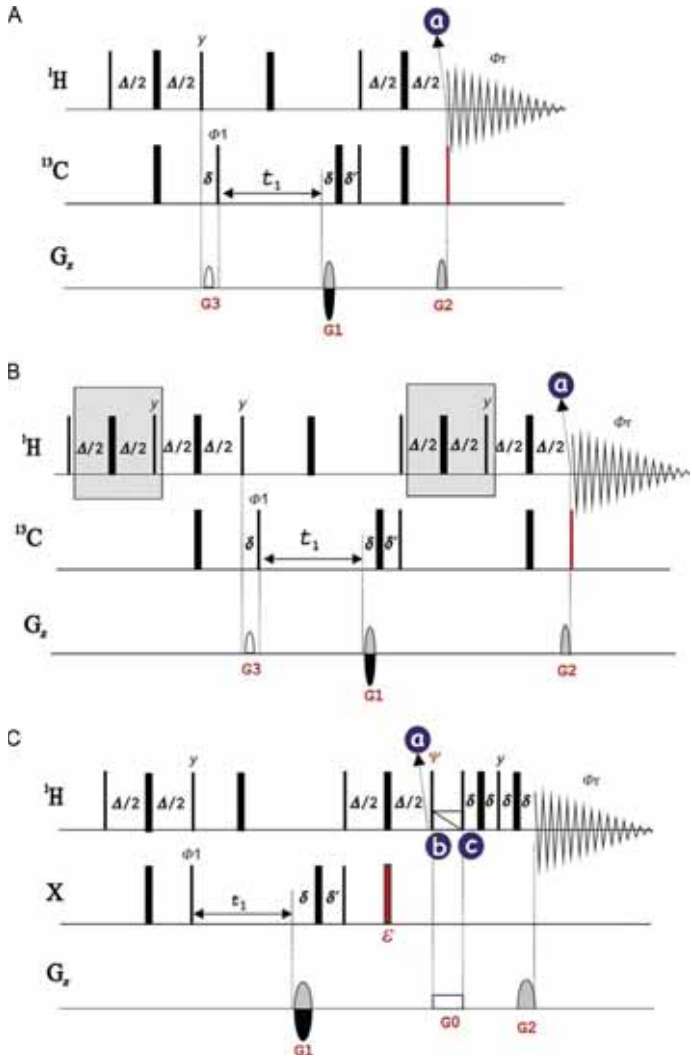

Figure 8 Basic pulse schemes to obtain F2-heterocoupled two-dimensional ^{1}H–^{13}C HSQC spectra: (A) CLIP-HSQC, (B) perfect-CLIP-HSQC, and (C) PIP-HSQC experiments. Narrow and broad pulses represent 90° and 180° pulses, respectively, with phase *x*, unless specified explicitly. The interpulse delay Δ is set to $1/(2^{*1}J(\mathrm{CH}))$ and a basic two-step phase cycling is executed with $\phi_1 = x,-x$ and receiver $\phi_r = x,-x$. Gradients for coherence selection using the echo–antiecho protocol are represented by G1 and G2 and δ stands for the duration and the gradient and its recovery delay. A purge gradient G3 is placed for zz-filtering whereas the final and optional 90°(^{13}C) stands for the so-called CLIP pulse to remove heteronuclear AP contributions. F2-heterodecoupled versions of all three HSQC schemes should be obtained by applying broadband heterodecoupling during the acquisition period. In such cases, the CLIP pulse in (A) and (B) is not required.

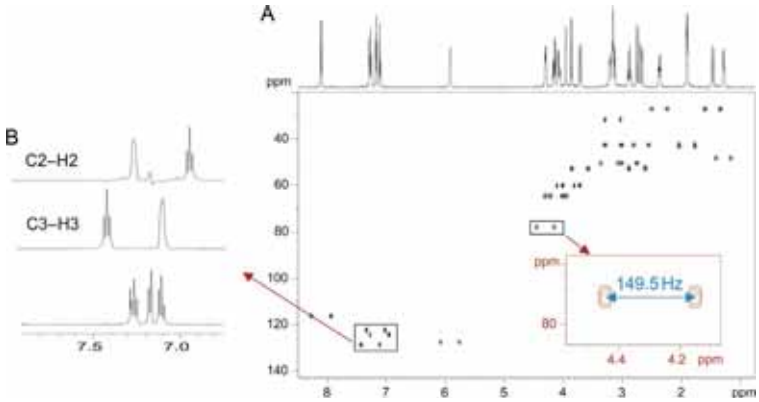

Figure 9 (A) Conventional F2-coupled CLIP-HSQC spectrum of (**1**) recorded in a 500-MHz spectrometer. ^{1}J(CH) can be easily measured from the large doublet along the detected dimension, as shown in the inset. (B) One-dimensional slices showing distorted signals due to the presence of strong-coupling effects.

The effects on the phase and the intensity observed in different HSQC cross-peaks as a function of the magnitudes of J(HH), ^{1}J(CH), and the delay Δ optimization for several F2-HSQC schemes have been studied by 1D spectral simulations (Fig. 10). Thus, the phase anomalies observed in conventional F2-HSQC cross-peaks (Fig. 10A) result from the mismatch between the optimized Δ delay and the active ^{1}J(CH) value (terms II and IV derived in Eq. 2), and from the evolution of J(HH) during the echo INEPT periods (term III in Eq. 2). Such distortions limit any attempt to realize an accurate analysis in terms of signal quantification via peak integration or direct ^{1}J(CH) and J(HH) measurements.

5.1.1 CLIP-HSQC

A simple solution to partially solve these phase distortions was proposed with the CLean IP HSQC (CLIP-HSQC) experiment [88], which applies a 90° ^{13}C pulse (from the x-axis) just prior the acquisition (Fig. 8A). In this way, the AP contributions due to ^{1}J(CH) are converted to multiple-quantum coherences (terms II and IV) and, apparently, clean IP patterns should be obtained in the absence of any J(HH) coupling.

$$\text{Eq. (2)} \xrightarrow{90°(x,^{13}\text{C})} \begin{aligned} &H_{1x}\, c^2 s'^2\,(\text{Term I}) + 2H_{1y}C_y c^2 s' c'\,(\text{Term II}) \\ &+ 2H_{1y}H_{2z} c s s'^2\,(\text{Term III}) - 4H_{1x}H_{2z}C_y c s c' s'\,(\text{Term IV}) \end{aligned} \tag{3}$$

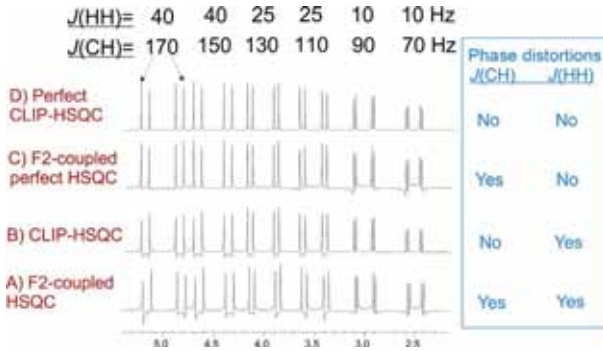

Figure 10 Simulated 1D spectra showing the phase peak distortion effects in several 140-Hz optimized F2-heterocoupled HSQC experiments: (A) Conventional HSQC, (B) CLIP-HSQC, (C) perfect-HSQC, and (D) perfect CLIP-HSQC. Six protons belonging to three different diastereotopic CH_2 groups have been simulated with a wide range of *J*(HH) and ^1J(CH) values, as shown in the upper part. *Adapted from Ref. [95].*

However, in the presence of *J*(HH), a mixture of observable IP and AP components ($H_{1x} + 2H_{1y}H_{2z}$) are still active, as shown in the simulated spectrum of Fig. 10B. In practice, due to the large difference of magnitudes between ^1J(CH) and *J*(HH), these unwanted contributions are small and they have been traditionally omitted in cross-peak analysis in CLIP-HSQC or in conventional decoupled HSQC experiments. A simple calculation shows that these effects may become important. For instance, the relative percentage of the term III with respect to term I in an 140-Hz optimized CLIP-HSQC experiment is of 5.6% and 17% for *J*(HH) values of 5 and 15 Hz, respectively. Such percentages can be more pronounced when measuring RDCs in anisotropic media, where higher values of HH couplings are usually involved.

Enthart *et al.* also introduced the IPAP technique into the F2-HSQC (CLIP/CLAP-HSQC experiment) [88] to edit the two components of the doublet in two separate spin-state selective α/β spectra in order to avoid accidental signal overlap. Similar IPAP techniques have been also implemented in broadband homodecoupled F2-HSQC (see Section 5.1.5) and selHSQMBC (see Section 6) experiments. The robustness of the CLIP/CLAP experiments has been also tested using optimized designed broadband 90° and 180° pulses.

5.1.2 J(HH)-Compensated INEPT: Perfect-HSQC

The evolution of *J*(HH) during homonuclear or heteronuclear echo periods also generates AP components that distort the phase of the signal. The

product operator analysis of a conventional echo element (Fig. 11A) for a weakly coupled AX H_1/H_2 two-spin system, with a mutual $J(H_1H_2)$ coupling, can be summarized as:

$$-H_{1y}-H_{2y}\xrightarrow{\Delta-180-\Delta}\begin{array}{l}-H_{1y}\cos(\pi J\Delta)+2H_{1x}H_{2z}\sin(\pi J\Delta)\\-H_{2y}\cos(\pi J\Delta)+2I_{2x}I_{1z}\sin(\pi J\Delta)\end{array} \quad (4)$$

An interesting general NMR building block, referred to as perfect echo, has shown a renewed interest in the last years because the J(HH) effects generated during a spin-echo period can be efficiently refocused for a spin AX system (Eq. 5). Basically, it is a double spin-echo scheme separated by an orthogonal J-refocusing 90° pulse, with the interpulse delay set to $\Delta \ll 1/J(\mathrm{HH})$ (Fig. 11B) [89].

$$\begin{aligned}\mathrm{Eq.}(4)&\xrightarrow{90(y)}-H_{1y}\cos(\pi J\Delta)-2H_{1z}H_{2x}\sin(\pi J\Delta)-H_{2y}\cos(\pi J\Delta)\\&\quad-2H_{2z}H_{1x}\sin(\pi J\Delta)\\&\xrightarrow{\Delta-180-\Delta}-H_{1y}\cos^2(\pi J\Delta)+2H_{1x}H_{2z}\cos(\pi J\Delta)\sin(\pi J\Delta)\\&\quad-2H_{1z}H_{2x}\sin(\pi J\Delta)\cos(\pi J\Delta)-H_{2y}\sin^2(\pi J\Delta)\\&\quad-H_{2y}\cos^2(\pi J\Delta)+2H_{2x}H_{1z}\cos(\pi J\Delta)\sin(\pi J\Delta)\\&\quad-2H_{2z}H_{1x}\sin(\pi J\Delta)\cos(\pi J\Delta)-H_{1y}\sin^2(\pi J\Delta)\\&=-H_{1y}-H_{2y}\end{aligned} \quad (5)$$

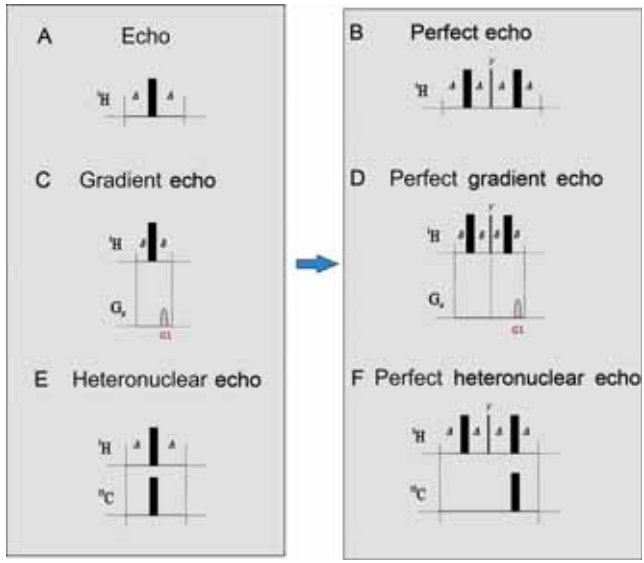

Figure 11 NMR building blocks comparing conventional versus J(HH)-compensated spin-echo elements.

The concept of perfect echo has been successfully implemented in a series of NMR applications to solve some traditional issues, such as the determination of T_2 relaxation times from undistorted multiplets in "perfect-echo CPMG" experiments [90], the elimination of peak distortion caused by J(HH) in diffusion NMR experiments [91], the suppression of J(HH) evolution during the solvent-suppression period in a "perfect WATERGATE" method [92], or during the variable t_1 period in "perfect-HMQC" experiments to remove the typical cross-peak tilting along the indirect dimension [93]. In the heteronuclear case, a J(HH)-compensated INEPT sequence called "perfect-echo INEPT" element (Fig. 11F) has been introduced to refocus J(HH) modulations appeared during INEPT elements and it has been applied to improve long-range heteronuclear transfers in conventional 1D refocused ^{13}C INEPT experiments [94].

The J(HH) interferences present in conventional HSQC experiments have been efficiently minimized in a perfect-HSQC pulse scheme (Fig. 8B) which replaces the classical INEPT by a J(HH)-compensated perfect-echo INEPT module consisting of a double echo period in both defocusing/refocusing heteronuclear transfer periods [95]. J(HH) is refocused at the end of each double echo period, and therefore, the signal amplitude is only modulated by the effect of ^1J(CH). Thus, in contrast to the conventional HSQC experiment (see Eq. 2), the magnetization just prior to acquisition in the perfect-HSQC experiment is defined exclusively by only two components, as similarly described in Eq. (1). The resulting 2D perfect-HSQC spectra afford pure IP cross-peaks with respect to both ^1J(CH) and J(HH) and, in addition, peak volumes are not influenced by J(HH), rendering practical applications such as phase correction, signal integration, and multiplet analysis more convenient and accurate.

Figure 10C shows that the simulated F2-coupled perfect-HSQC spectrum without the CLIP pulse still shows some phase distortions provided Δ does not match the corresponding ^1J(CH) value. For instance, deviations of 10 and 20 Hz between ^1J(CH) and the Δ delay optimization generate antiphase contributions of about 11% and 23%, respectively, in a 140-Hz optimized experiment. Such distortions can be efficiently suppressed using the perfect-CLIP-HSQC pulse scheme (Fig. 8B), affording perfect pure IP multiplet patterns for all peaks independent of their J(HH) and J(CH) values (Fig. 10D).

Figure 12 compares some experimental multiplets extracted from equivalent 140-Hz optimized heteronuclear decoupled HSQC and perfect-HSQC spectra. Significant AP J(HH) contributions are observed in those HSQC peaks presenting large J(HH) values that distort the signal phase

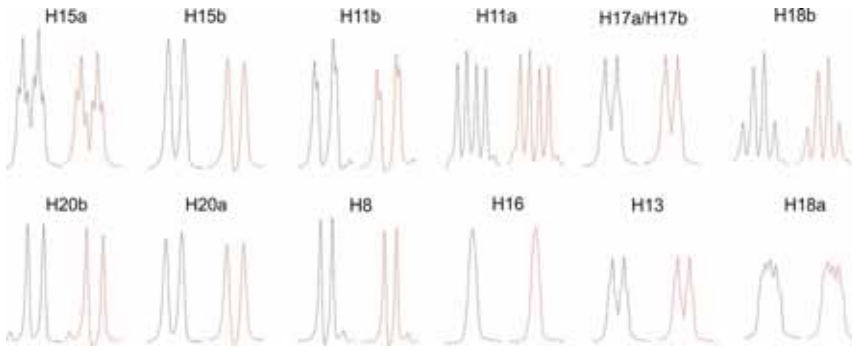

Figure 12 Comparison of perfect-HSQC (left) and HSQC (right) signals of (**1**), both acquired under the same experimental conditions. Phase distortions and decreased sensitivity in conventional HSQC multiplets are due to *J*(HH) modulation during the INEPT blocks. *Adapted from Ref. [95].*

and decrease their relative intensities. The H16 proton can be taken as a reference for a resonance which does not show large values, and therefore, a practically equal multiplet pattern and signal intensity are obtained in both spectra. For instance, differences up to 20% in signal intensity were observed for the diastereotopic H15a and H15b protons and distortions could be also observed for the methine H8 peak.

The main disadvantage of the perfect-HSQC experiment arises from the longer duration of the perfect-echo INEPT versus the conventional INEPT (2Δ vs. Δ, respectively) that can lead to some signal loss due to additional T_2 relaxation. The overall duration of the sequence is extended about 3.6 ms for each perfect-echo INEPT period in a 140-Hz optimized experiment but this does not represent a serious issue for small molecules having reasonably long T_2 relaxation times (some hundreds of milliseconds).

5.1.3 J(CH)-Compensated INEPT: COB-HSQC

Traditional HSQC experiments use a single heteronuclear echo element for both defocusing and refocusing magnetization transfer which are optimized for a single ^1J(CH) value. Thus, the efficiency of such transfer and therefore the observed signal intensities can vary considerably depending on the matching between the interpulse delay optimization and the active ^1J(CH). Several attempts have been made to compensate for variation of ^1J(CH) values in HSQC experiments: (i) by adding data acquired with different delays, (ii) by exploiting the time-dependent inversion that is characteristic of adiabatic inversion pulses to apply different refocusing delays to

different ^{13}C chemical shifts [96,97], or (iii) by designing alternative *J*-compensated INEPT sequences that usually require a much number of rf pulses and delays, increasing the overall duration of the element and making it more sensitivity to rf inhomogeneities (Fig. 13B) [98,99]. Signal intensity also depends on the imperfections due to carbon chemical shift offsets and B_1 field inhomogeneities, and all these can be improved by replacing the hard rectangular 180° ^{13}C pulse by adiabatic or broadband inversion pulses [100].

In order to improve the broadband response in HSQC experiments, several modified INEPT transfer elements that compensate for a wide range of couplings, offsets, and B_1-inhomogeneities (COB) have been reported [101]. The initial COB-INEPT element (Fig. 13C) takes profit on the availability of effective optimization of shaped broadband pulses and the compensation covers all the needs of HSQC-type experiments of small molecules with, e.g., scalar coupling constants in the range of 120–250 Hz [102]. The same authors have recently proposed improved COB3-INEPT elements that are able to cover a much wider range of ^1J(CH) couplings (120–750 Hz) for all different CH, CH_2, and CH_3 multiplicities (Fig. 13D) [103]. In general, it has been shown that these *J*(CH)-compensated sequences strongly require the use of broadband, specifically

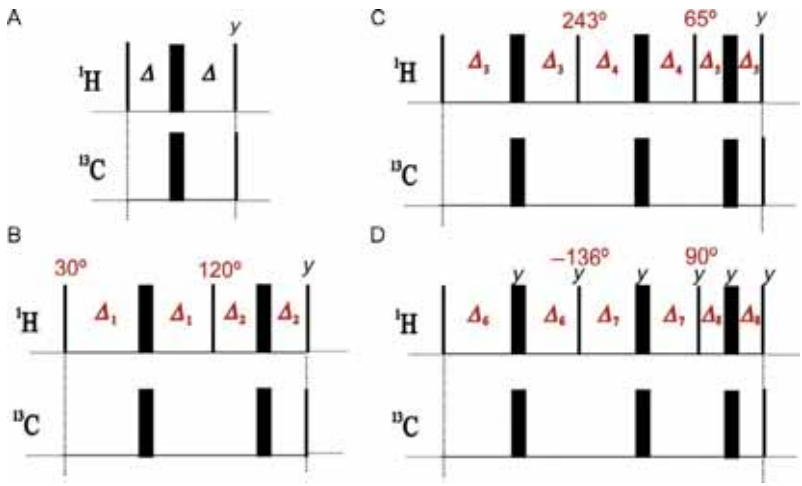

Figure 13 Basic ^1J(CH)-compensated INEPT elements using hard pulses: (A) conventional; (B) J45+90A INEPT; (C) COB-INEPT, and (D) COB3-INEPT. Delays: $\Delta = 1/(4*{}^1J(CH))$; $\Delta_1 = 2.68/{}^1J(CH)$; $\Delta_2 = 1.34/{}^1J(CH)$; $\Delta_3 = 1.469/{}^1J(CH)$; $\Delta_4 = 2.134/{}^1J(CH)$; $\Delta_5 = 0.394/{}^1J(CH)$; $\Delta_6 = 1.07$ ms; $\Delta_7 = 1.065$ ms; and $\Delta_8 = 0.54$ ms. All original COB-INEPT elements were described using shaped-optimized ^1H and ^{13}C pulses.

designed, and optimized broadband pulses for an optimum and uniform intensity response. These transfer elements are quite robust due to the application of offset and field B_1-compensated point-to-point (PP) pulses such as BEBOP [104–107] universal rotation (UR) pulses such as BURBOP [108,109], and broadband excitation (BEBE) and broadband UR and broadband inversion (BUBI) pulses [110]. Potential applications of such methods have been proposed for the measurement of any type of heteronuclear coupling constants with particular emphasis to the determination of ^1D(CH) RDCs of partially oriented molecules in anisotropic media. For instance, it has been shown that whereas in a 145-Hz optimized conventional HSQC experiment only cross-peaks corresponding to couplings up to 200 Hz are visible, signals corresponding to couplings up to 375–400 Hz are observed with optimum sensitivity in a COB3-HSQC spectrum of a partially aligned sample of a tetrasubstituted pyrrolidine dissolved in a liquid crystalline PBLG/$CDCl_3$ phase. However, all these approaches do not consider the effect of J(HH) modulation and they are not suitable as an accurate quantitative NMR method.

5.1.4 PIP-HSQC Experiment

Another simple and general solution to obtain heteronuclear correlation spectra that yield truly pure absorption line shapes and IP multiplet structures for all available cross-peaks with respect to both J(CH) and all passive J(HH) coupling constants along the detected dimension is the so-called Pure In-Phase HSQC (PIP-HSQC) experiment [111]. The key point is an appended adiabatic zero-quantum filter (ZQF) [112] applied just before a refocusing gradient perfect-echo element and the acquisition. Thus, after the $90°_y(^1\mathrm{H})$ pulse (point **b** in Fig. 8C) the above four components derived from Eq. (2) are converted to

$$\begin{aligned}\text{Eq. (2)} \rightarrow\ & -\mathrm{H}_{1z}c^2s'^2(\text{Term I}) - 2\mathrm{H}_{1y}\mathrm{C}_z c^2 s' c'(\text{Term II}) \\ & + 2\mathrm{H}_{1y}\mathrm{H}_{2x}css'^2(\text{Term III}) - 4\mathrm{H}_{1z}\mathrm{H}_{2x}\mathrm{C}_z csc's'(\text{Term IV})\end{aligned} \tag{6}$$

where the second and fourth terms represent transverse AP heteronuclear magnetization and the third element represents a mixture of homonuclear ZQ and DQ coherences, which are also eliminated by the effect of the simultaneous adiabatic 180° ^{1}H pulse and the purging G0 gradient pair. As a result, only the first term representing the desired IP magnetization remains detectable after the z-filter (point **c** in Fig. 8C). To maintain the pure IP character during detection, the classical gradient echo block has been

replaced by a perfect gradient echo element (see Fig. 11C vs. D) where J(HH) should be fully refocused. Such distortions could become critical when measuring J(CH) in the presence of large J(HH) values, as could be found in the measurement of RDCs, or in experiments involving longer Δ delays (see PIP-HSQMBC experiment in Section 6.6). Table 1 shows the experimental ^1J(CH)/^1D(CH) values obtained for a sample of strychnine weakly aligned in a poly(methyl methacrylate) (PMMA) gel swollen in $CDCl_3$ using the reversible compression relaxation method (Fig. 14). It has been shown that errors up to 10% Hz can be introduced from the analysis of distorted cross-peaks in conventional F2-coupled CLIP-HSQC and F2-decoupled HSQC spectra.

5.1.5 F2-Coupled Pure Shift HSQC Experiments

Several F2-coupled versions of the previously described PS-HSQC schemes (see Section 4) have also been proposed for the measurement of ^1J(CH) from simplified homodecoupled doublets (Fig. 15A–C). As discussed before, the use of a pseudo-3D acquisition mode produces long acquisition times when compared to 2D HSQC analogs but the obtention of simplified doublets can facilitate the semi-automated peak picking and the measurement from simple frequency differences between singlet peak maxima. Two very similar schemes of the real-time PS-HSQC experiment using a BIRD element with broadband pulses that is not compensated for ^1J(CH) variations have been simultaneously reported [70,113]. The CLIP/CLAP-RESET HSQC method (Fig. 15A) [113] leads to complete homonuclear decoupling for CH groups and CH_3 groups in isotropic samples but leaves residual splittings with AP contributions for CH_2 groups due to ^2J(HH) coupling evolution that is not decoupled by the BIRD element. In terms of experimental times, whereas a conventional HSQC was obtained in 6 min, the corresponding CLIP-RESET spectrum acquired with 16 increments of the homodecoupled dimension required 1 h and 25 min. Pure shift HSQC versions using the COB-INEPT element and broadband-shaped excitation, inversion and refocusing pulses were also introduced to provide a much better uniform response and to obtain a much cleaner IPAP editing (COB-CLIP-RESET experiment) [113]. Alternatively, a more sophisticated constant-time version (CT-CLIP-RESET experiment) was also proposed with full homonuclear decoupling for weakly coupled CH_2 spin systems, but sensitivity was further compromised. Unfortunately, J(CH)-compensated BIRD elements are not yet available. The authors make a comparative study between different CLIP methods to

Table 1 Experimental ^1J(CH)/^1T(CH) values extracted from the PIP-HSQC spectra of strychnine (**1**) recorded in isotropic and anisotropic conditions.

				Isotropic	Anisotropic		Predicted[a]
C	δ (ppm)	H	δ (ppm)	$^1J_{CH}$ (Hz)	$^1T_{CH}$ (Hz)	$^1D_{CH}$ (Hz)	$^1D_{CH}$ (Hz)
C1	122.3	H1	7.16	158.3	174.8	+16.5	+12.2
C2	124.2	H2	7.09	160.8[b]	163.7[b]	+2.9	+2.2
C3	128.6	H3	7.25	159.2[b]	163.5[b]	+4.3	+3.2
C4	116.2	H4	8.08	168.4	187.1	+18.7	+13.9
C8	60.1	H8	3.86	144.9	133.7	−11.2	−8.6
C11	42.5	H11a	3.12	135.4	143.1	+7.7	+5.9
		H11b	2.66	125.5	107.6	−18.2	−14.1
C12	77.6	H12	4.28	150.0	134.2	−15.8	−12.3
C13	48.2	H13	1.27	124.8	118.9	−5.9	−4.6
C14	31.6	H14	3.15	131.3	117.9	−13.4	−10.4
C15	26.8	H15a	2.36	130.9	135.0	+4.1	+3.2
		H15b	1.47	129.9	131.0	+1.1	+0.9
C16	60.2	H16	3.98	146.7	158.2	+11.5	+9.0
C17	42.8	H17a/b	1.90	133.2	139.1	+5.9	+4.6
C18	50.3	H18a	3.25	146.3	148.1	+1.8	+1.4
		H18b	2.88	131.7	143.4	+11.7	+9.0
C20	52.7	H20a	3.73	138.8	ov[c]		−7.7
		H20b	2.76	138.7	132.9	−6.2	−4.6
C22	127.6	H22	5.93	158.8	156.4	−2.4	−1.8
C23	64.6	H23b	4.15	145.5	148.9	+3.4	+2.6
		H23a	4.05	137.2	111.7	−25.5	−19.4

[a]The predicted values have been calculated with MSpin program (MESTREALAB RESEARCH SL, Santiago de Compostela, Spain. http://www.mestrelab.com).
[b]Strong coupling effect.
[c]Overlapped with PMMA signals.

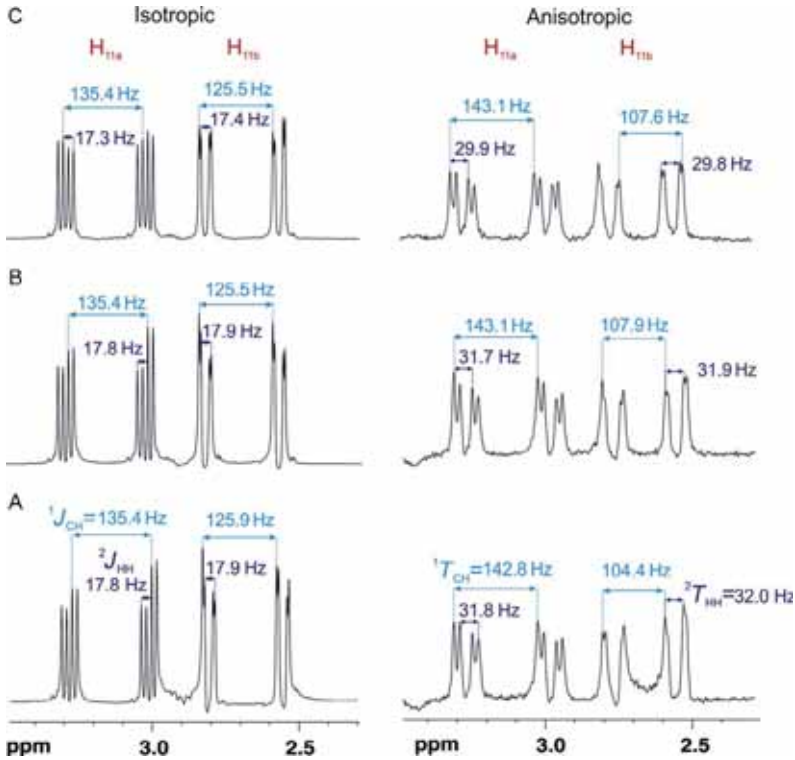

Figure 14 1D traces extracted at the C11 chemical shift of (**1**) in isotropic and anisotropic conditions showing the signal distortions originated in (A) conventional HSQC, (B) CLIP-HSQC, and (C) PIP-HSQC spectra recorded with Δ set to 3.6 ms ($^1J_{CH} = 140$ Hz). *Adapted from Ref. [111].*

measure ^1J(CH) on a sample of menthol, and some guidelines to identify the effects of strong coupling effects were presented and discussed.

Non-refocused and refocused versions of the F2-coupled HOBS-HSQC experiment described in Section 4.2 have also been reported (see pulse diagram in Fig. 15C), and the important sensitivity and resolution enhancements as well as the multiplet simplification can be quickly evidenced when comparing the selected 1D slices in Fig. 15D versus E. In addition, analogs counterparts of the previously described 2D perfect-HSQC (Section 5.1.2) and PIP-HSQC (Section 5.1.4) experiments could be easily designed by incorporating BIRD-based or HOBS broadband homodecoupling as outlined in Fig. 15B and C, respectively.

A modified version of the non-refocused HMQC pulse train has been proposed to measure ^1J(CH) from the direct dimension using a pseudo-homodecoupling approach based on the scaled evolution of J(HH) during

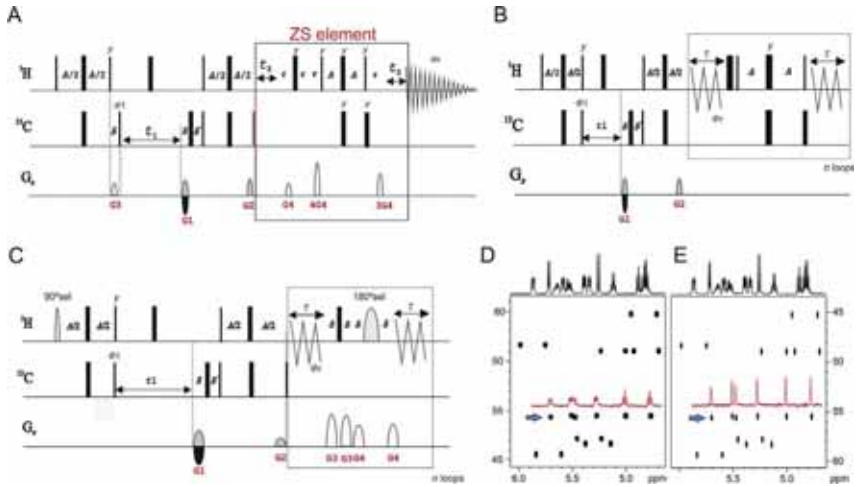

Figure 15 F2-heterecoupled PS-HSQC experiments: (A) pseudo 3D RESET-HSQC; (B) PS-HSQC using a BIRD inversion element during acquisition; (C) HOBS-HSQC using a band-selective pulse as the inversion element; (D,E) F2-coupled conventional HSQC and HOBS-HSQC spectra of (**2**). *Figure partially adapted from Ref. [73].*

the indirect t_1 period. In this HR-HSBC experiment [114], which is based on an early HR-HMBC experiment [115], the analysis of the resulting tilted cross-peaks in a specific row of the detected dimension avoids the complexity of the overall multiplet substructure.

5.2. F1-Coupled HSQC Experiments

The measurement of ^1J(CH) exclusively along the indirect F1 dimension of a HSQC spectrum is recommended to avoid the interferences of J(HH) splittings, but a major inconvenient arises for the need of a large number of t_1 increments, and therefore longer acquisition times. The successful use of NUS, J scaling factors or spectral folding/aliasing can speed up data acquisition and/or increase the digital resolution in the F1 dimension. Several F1-coupled HSQC pulse schemes have been compared and evaluated by Thiele and Bermel [116]. The most simple approach results from the removing of the central 180° ^{1}H pulse placed in the middle of the t_1 evolution period in the conventional HSQC experiment, referred to as F1-HSQC experiment (Fig. 16A). A more convenient method incorporates a G-BIRD^r module to allow the simultaneous evolution of both ^1J(CH) and ^{13}C chemical shift evolution while contributions from ^nJ(CH) are efficiently refocused [117]. The better line shapes along the indirect dimension allow

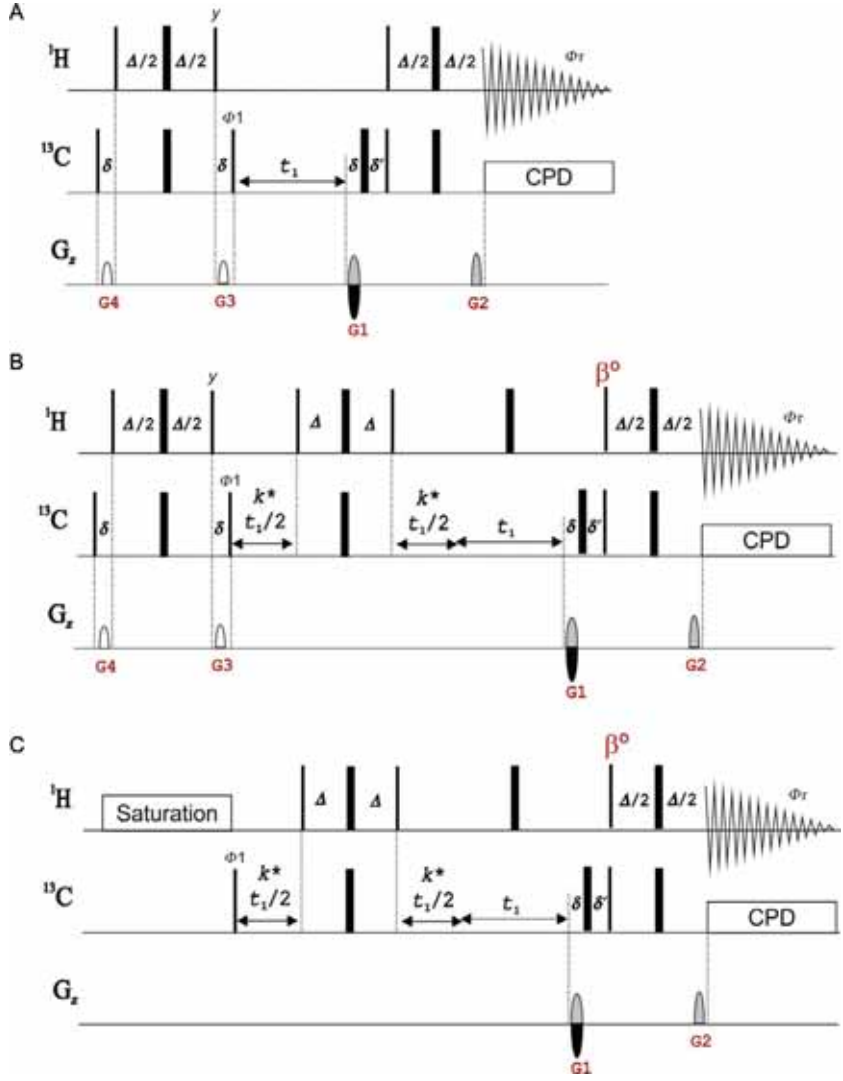

Figure 16 Several pulse schemes to achieve F1-heterocoupled HSQC spectra: (A) F1-HSQC, (B) BIRD-HSQC, and (C) F1-iINEPT experiments. Inversion and refocusing 180° ^{13}C pulses can be applied as adiabatic or BIP pulses and the $\delta(^{13}C)$ evolution period is optional. The interpulse delays in INEPT and BIRD elements are optimized according to $\Delta = 1/(2*^1J(CH))$ and a small flip angle ($\beta = 36^\circ$) generates E.COSY cross-peaks for $^2J(HH)$ couplings.

the determination of ^1J(CH) by simply measuring the frequency difference between the peak maxima of singlets instead of the centers of complex multiplets.

The accurate measurement of the two ^1J(CH) values and particularly the geminal ^2J(HH) coupling in diastereotopic CH_AH_B groups has always been a challenging task, particularly for F1-HSQC experiments. Several methods have been proposed for measuring them either from the F1 or from the F2 dimension, but they all present some drawbacks that have prevented their general use. For instance, the passive $^1J(C\text{-}H_B)$ value can be separately measured into the active H_A cross-peak, and vice versa, along the F1 dimension of a *J*-resolved HMQC experiment [118]. In addition, the large doublet is further split by the $^2J(H_AH_B)$ coupling yielding a doublet of doublet. The disadvantage is that additional experiments can be required to measure ^1J(CH) for CH or CH_3 spin systems, and significant distortions on the cross-peaks (banana shape peaks) are frequently observed in the spectra of complex small molecules. Another important group of NMR experiments are those based on spin-state selection specifically designed for methylene groups that yield simplified coupling patterns, and where the sign and the magnitude of the geminal ^2J(HH) can sometimes be additionally extracted [119–129].

5.2.1 BIRD-HSQC Experiment

The BIRD-HSQC approach uses two sequential blocks to separate the contributions from $\delta(^{13}C)$ and ^1J(CH) evolution during the heteronucleus frequency labeling period (Fig. 16B) [116,130]. This strategy presents several advantages: (i) the *J*(CH) evolution period can incorporate a BIRD element to remove long-range contributions; (ii) the *J*(CH) splitting in the indirect dimension can be scaled by a factor **k**; and (iii) the experiment can be optionally recorded with a very narrow spectral width in the indirect dimension (about 500 Hz) by omitting the $\delta(^{13}C)$ evolution period, affording a *J*-resolved HSQC format [131] with a considerable resolution gain by one of two orders of magnitude, whereas a reasonable number of t_1 increments can be collected in a shorter experimental time. A similar procedure has been reported where the ^1J(CH) evolution period is inserted in the initial INEPT period [130]. The utility of these *J*-resolved HSQC-BIRD spectra has been demonstrated by differentiating enantiomeric derivatives dissolved in anisotropic media from their different ^1J(CH) splitting sizes along the indirect dimension [132,133].

A major inconvenient in all F1-HSQC experiments is that the central lines of the F1−multiplet corresponding to a CH_2 group are not observed, and therefore, only the sum of the two ^1J(CH) can be determined from the indirect dimension. The BIRD-HSQC experiment can be analyzed considering an isolated diastereotopic CH_AH_B spin system defined with three different $^1J(CH_A)$, $^1J(CH_B)$, and $^2J(H_AH_B)$ coupling constants. The sequence starts with an initial 90°(^{13}C)-gradient element to remove any contribution coming from the ^{13}C Boltzmann polarization. After the ^{1}H-to-^{13}C INEPT transfer, AP ^{13}C magnetization is present as a mixture of $2H_{Az}C_y+2H_{Bz}C_y$, which evolve under the effects of ^1J(CH) and $\delta(^{13}C)$ in a sequential mode, by using separated and synchronously incremented time periods. Thus, the magnetization evolves first under the effect of a BIRD^{d,X} element [134] flanked by a variable *J*-scaled t_1 evolution period (defined by a scaling factor *k*) to allow the exclusive evolution of ^1J(CH), whereas ^{13}C chemical shift and long-range CH contributions are refocused, and then ^{13}C chemical shift can evolve from an optional t_1 evolution period as usual. In the subsequent analysis, the scaling factor, which is set arbitrarily within the limits set by relaxation and/or signal overlapping, the effects of the labeling G1 gradient and the optional ^{13}C chemical shift t_1 evolution period are neglected for the sake of clarity. Thus, for a single H_A spin, the evolution during the variable BIRD-based t_1 period ($k=1$) is described by $2H_{Az}C_y\cos(\pi(^1J(CH_A+^1J(CH_B))t_1)$, meaning that only the outer lines of the theoretical triplet or double–doublet coupling pattern of the methylene proton cross-peak would be observed and, therefore, only the sum of the both couplings ($^1J(CH_A+^1J(CH_B)$) will be observed as an IP doublet along the indirect dimension. This signal dependence with respect to the cosine function makes that multiplet patterns with relative intensities of 1:1 for CH, 1:0:1 for CH_2, and 3:1:1:3 for CH_3 will be displayed along the F1 dimension. The combined use of the *J*-scaled BIRD-HSQC and *J*-scaled BIRD-HSQC/HMQC experiments have been used to define a new strategy to assign unambiguously the diastereotopic CH_2 protons of strychnine from RDC data [135].

An optional but very useful feature in the BIRD-HSQC experiment is the use of a small flip ^{1}H pulse angle ($\beta=36°$) in the last retro-INEPT block which generates simplified E.COSY multiplet patterns for non-equivalent protons in CH_2 and CH_3 spin systems, allowing the determination of the sign and the magnitude of ^2J(HH) in these spin systems as a function of multiplet pattern slope. This idea comes from a time-optimized non-refocused version of an F1–F2 fully coupled HSQC experiment which has been proposed to measure ^1J(CH) and ^2J(HH) in diastereotopic CH_2 systems. The

major inconvenient of this simple Pure Exclusive HSQC (P.E.HSQC experiment) scheme is the number of multiple lines into a single cross-peak, requiring high levels of digitization in both dimensions and increasing the probability of accidental signal overlapping [136].

5.2.2 iINEPT Experiment

A simple modification of the small flip-angle BIRD-HSQC experiment has been reported for detecting the missing central lines in diastereotopic CH_2 cross-peaks. The resulting cross-peaks in this new 2D F1-coupled inverse INEPT experiment (referred to as F1-iINEPT) [137] present a characteristic E.COSY multiplet pattern that facilitates the straightforward measurement of both individual $^1J(CH_A)$ and $^1J(CH_B)$ values, as well as the sign and magnitude of the geminal $^2J(HH)$ coupling. Figure 17A summarizes the expected cross-peak pattern for a single diastereotopic CH_AH_B proton using the different F1-HSQC and F1-iINEPT approaches with $\beta = 90°$ and 36° (compare Fig. 17A vs. B). The sequence avoids the initial INEPT transfer, starting exclusively from the ^{13}C Boltzmann polarization (Fig. 16C). The experiment works for all multiplicities and it is easily adapted for a *J*-resolved presentation (referred to as F1-iINEPT-*J*) which allows to obtain higher levels of resolution within the same experimental time by the use of a reduced spectral width in the indirect dimension (Fig. 17F).

The initial 90° ^{13}C pulse generates IP $-C_y$ magnetization which evolves under the effect of $^1J(CH)$ during the variable t_1 BIRD-based period:

$$\begin{aligned} &2H_{Az}C_x\left[\sin\left(\pi^1J(CH_A)t_1\right)\cos\left(\pi^1J(CH_B)t_1\right)\right. \\ &\left.-2H_{Bz}C_x\cos\left(\pi^1J(CH_A)t_1\right)\sin\left(\pi^1J(CH_B)t_1\right)\right] \end{aligned} \tag{7}$$

The resulting pure absorptive 2D F1-iINEPT spectra display double–doublet coupling patterns along the F1 dimension for each individual H_A or H_B cross-peaks, which initially would consist of eight different components as shown in Fig. 17C. Analyzing only the H_A spin will show an anti-phase doublet pattern with respect to $^1J(CH_A)$ (sine modulated) and an additional IP doublet pattern with respect to $^1J(CH_B)$ (cosine modulated) along the F1 dimension. As discussed before, the effect to apply a small flip angle ($\beta = 36°$) will generate a simplified four-component cross-peak with a characteristic E.COSY multiplet pattern due to the mutual $^2J(H_AH_B)$ (Fig. 17D), which facilitates both the multiplet interpretation and analysis. Thus, the active $^1J(CH_A)$ coupling is directly extracted from the antiphase 1:−1 pattern along the same row in F1, whereas the passive $^1J(CH_B)$

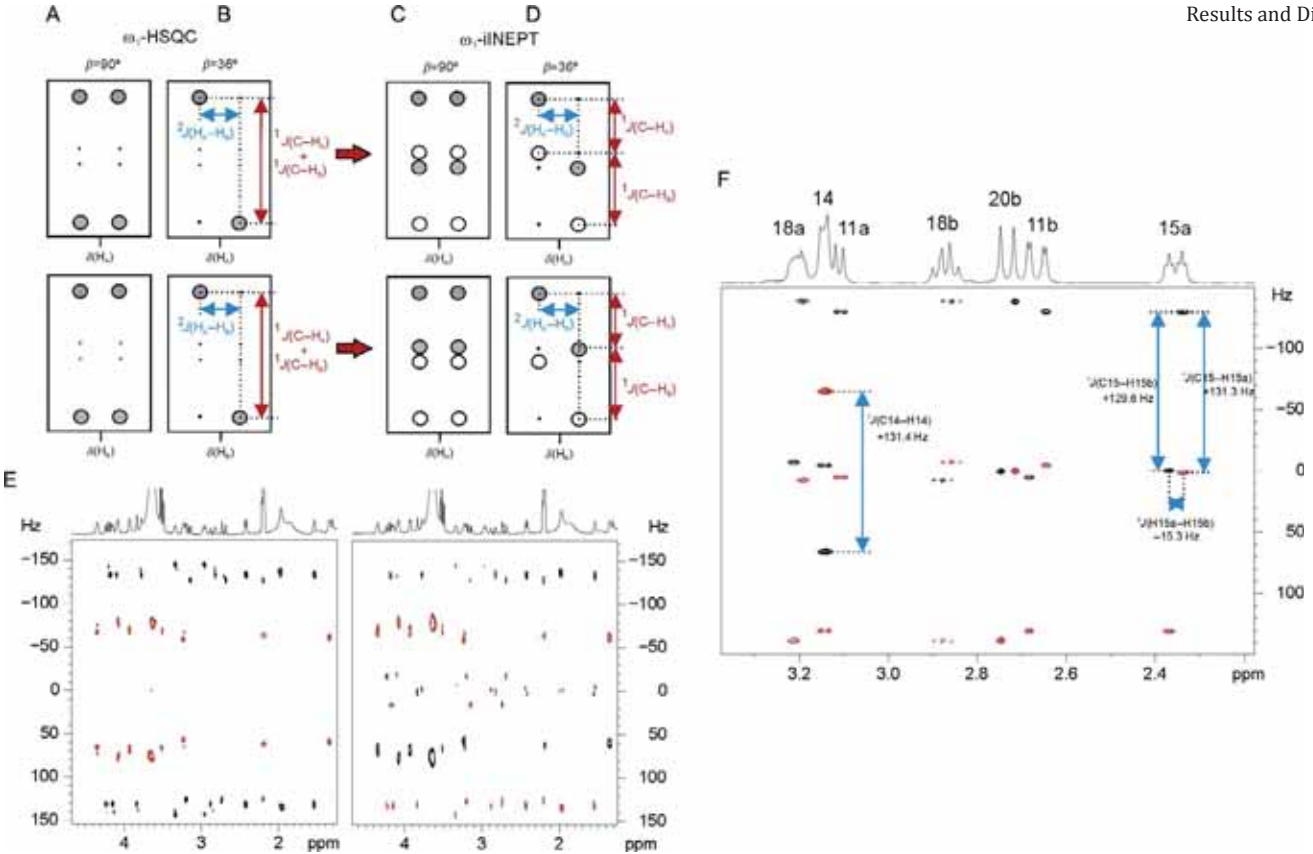

Figure 17 Schematic representation of the 2D multiplet pattern of each individual H_A and H_B proton belonging to a methylene CH_AH_B group. (A,B) ^{1}H-Boltzmann polarization driven (F1-HSQC) experiments using $\beta = 90°$ and 36°, respectively, and (C,D) ^{13}C-Boltzmann polarization driven experiments (F1-ilNEPT) using $\beta = 90°$ and 36°, respectively. In (D), the magnitude and the sign of all involved couplings (defined as $^2J(H_AH_B)$ and assuming that $^1J(CH_A) < {}^1J(CH_B)$) can be readily extracted. Open and dotted circles represent peaks with opposite phase. (E) Comparison between the BIRD-HSQC and ilNEPT *J*-resolved spectra of a sample of (**1**) in PMMA/$CDCl_3$. Note the appearance of the central lines for all diastereotopic CH_2 protons. (F) 2D ^{1}H–^{13}C F1-ilNEPT-*J* spectra of (**1**) in $CDCl_3$ (scaling factor $k = 1$ and omission of the ^{13}C chemical shift t_1 evolution period). *Adapted from Ref. [137].*

coupling can be also extracted directly by measuring the IP components in each part of the E.COSY pattern. Otherwise, the sign and the magnitude of ^{2}J(HH) are easily extracted from the frequency separation between tilted peaks along the F2 dimension (Fig. 17F). For CH groups, a doublet with relative 1:−1 intensities is obtained whereas a 1:1:−1:−1 coupling pattern is displayed for a CH_3 group. A related HSQC sequence using a refocused INEPT as a preparation period has been also published providing a 1:3:3:1 quartet for AX_3 spin system and a 1:2:1 triplet for AX_2. Experimental results are illustrated for NH_2 and NH_3^+ groups in ^{15}N-labeled proteins [138]. The success of the method has been demonstrated for the measurement of small ^{1}D(CH) and ^{2}D(HH) values of **1** in PMMA/$CDCl_3$ (Fig. 17E). Of the five diastereotopic CH_2 groups, three have negative ^{2}D(HH) values (^{2}D(H11a–H11b) = − 12.5 Hz, ^{2}D(H20a–H20b) = − 20.1 Hz, and ^{2}D(H23a–H23b) = − 16.2), whereas two are positive (^{2}D(H15a–H15b) = + 13.2 Hz and ^{2}D(H18a–H18b) = + 8.9 Hz), clearly evidencing their relative orientation with respect to the molecular tensor and the magnetic field. Similarly, ^{1}J(CH) provides distinctive results between diastereotopic protons (^{1}D(C11–H11a) = + 7.7 Hz vs. ^{1}D(C11–H11b) = − 18.2 Hz, and ^{1}D(C23–H23a) = + 3.4 Hz vs. ^{1}D(C23–H23b) = − 25.5 Hz).

Pure shift versions of the F1-HSQC and F1-iINEPT experiments have not been published but they are easy to design and implement with the aim to achieve automated peak picking and automated extraction of ^{1}J(CH) and ^{2}J(HH) coupling constants.

5.3. Strong Coupling Effects in HSQC Experiments

It has been recognized that strong J(HH) coupling effects can introduce severe systematic errors in the measurement of ^{1}J(CH) from F2-coupled HSQC spectra because a certain degree of asymmetry between the high- and low-field multiplet lines can be introduced. This is due to changes in the resonance frequency and relative intensities, line shapes, and/or phases of cross-peaks. Freedberg and coworkers have demonstrated by product operator formalism and spectral simulations that these effects can be present either in the direct or in the indirect dimension of an HSQC spectrum [139]. They reported errors by up to 4 Hz when comparing experimental ^{1}J(CH) measured from the F1 and F2 dimensions of HSQC spectra. In addition, strong discrepancies up to 7 Hz were found between values measured in the ^{1}H dimension versus those in the ^{13}C dimension. However, from an experimental point of view, the use of this strategy based on spectral

simulations and fitting can become time-consuming, and the requirement for individual simulations for each particular case severely limits its widespread use, particularly when applied to the measurement of RDCs.

To avoid a direct measurement by determining frequency differences, a ^1J(CH)-modulated constant-time INEPT CT-HSQC (CTi-CT-HSQC) method has been proposed to measure experimentally accurate ^1J(CH)/^1D(CH) in the presence of strong J(HH) coupling effects [140]. This method avoids the phase distortions of the signals of interest or the presence of spurious peaks due to strong coupling, and also improves the analysis of the multiplet structure in broad or complex signals or when large contributions of RDCs can generate poorly defined multiplets that difficult accurate measurements.

The originality of the method relies in a CT-INEPT transfer module with a constant duration of Δ, where the 180° ^{13}C pulse is moved away from the central 180° ^{1}H pulse for a period τ. Thus, ^1J(CH) evolves only during a $(\Delta - 2\tau)$ period. Signal intensity during the INEPT element depends on three variables: $T_2(^1\text{H})$ relaxation times, ^1J(CH), and J(HH) modulations. Thus, recording multiple datasets with different τ optimizations, a pure signal intensity dependence with respect to $\sin^2(\pi J(\text{CH})(\Delta - 2\tau))$ is obtained keeping the relaxation effects and the J(HH) modulation during the overall period Δ independent of τ for all data. It has been shown that the fitting of the J-modulation curve yields accurate ^1J(CH) values with minimum deviations due to strong J(HH) coupling interference. Experimentally, the major inconvenience is the requirement for a collection of multiple 2D J-modulated data that means large experimental times [114].

6. HSQMBC EXPERIMENTS FOR MEASURING ^nJ(CH)

The measurement of ^nJ(CH) in small molecules at the natural abundance has been another hot topic of interest in small molecule NMR. [141] A comprehensive overview on the different NMR methods and applications to structural, configurational, and conformational studies appeared in the last decade has been recently published [142]. Most of these available long-range methods rely on the basic HMQC and HSQC pulse schemes where the interpulse delay is optimized to a ^nJ(CH) value instead of the original ^1J(CH), or on related hybrid HSQC-TOCSY experiments with a limited application to protonated carbons. Figure 18 shows different spin topologies defining the transfer mechanism followed in HSQC/HSQMBC-based experiments designed to measure J(CH). The HMBC experiment

[143–145] usually gives better sensitivity ratios but, in many cases, the equivalent HSQMBC is the preferred technique because it generally affords a better performance in terms of simplicity, peak phase behavior, and pulse sequence analysis.

The basic HSQC pulse train can be easily tuned to detect and measure quantitatively long-range proton–carbon interactions, which typically are in the range of 0–15 Hz in magnitude. In its basic form, the only requirement is the re-optimization of the interpulse Δ delay to a small coupling value, about typically 6–10 Hz. Under these conditions, the undesired effects of J(HH) evolution during the long INEPT periods (typically about 50–80 ms) become very important because the magnitude of J(HH) and ^{n}J(CH) coupling values is similar in size. The HSQMBC experiment has been traditionally used in a non-refocused mode [16]. This minimizes losses by T_2 relaxation but multiplet patterns appear strongly phase distorted because of the AP character with respect to ^{n}J(CH) and the mixed phase due to the effects of J(HH) modulation during the long INEPT period. In addition, cross-peak intensities strongly depend on the mismatch between this Δ optimization and the corresponding ^{n}J(CH) values and also of the potential losses by relaxation. The experimental result is the obtention of highly distorted cross-peaks with complex phase and variable intensities, even for some of the expected cross-peaks that can be missing in the final spectrum. The hard analysis of these complex multiplets has prevented its general use in a routine and easy task.

With the main objective to develop simpler methods, a suite of new HSQMBC pulse schemes have been proposed to measure ^{n}J(CH) in a more straightforward way, without need of sophisticated and time-consuming post-processing tasks [146,147]. These new selHSQMBC methods (Fig. 19) avoid all typical problems associated with accidental line cancelation or complex analysis of AP multiplets, work for both protonated and non-protonated carbons, and the measurement is performed along the detected F2 dimension where resolution is not critical and therefore the number of required t_1 increments is only dependent on signal congestion in the ^{13}C dimension. The selHSQMBC experiment is basically a standard HSQC pulse train in which the central hard 180° ^{1}H pulse in the INEPT periods has been replaced by frequency-selective 180° ^{1}H pulses to prevent the undesired J(HH) coupling evolution, whereas selective heteronuclear polarization transfer for the selected protons is achieved. The main limitation of these experiments relies on the selective concept because not all the protons can be simultaneously excited/observed or decoupled/unmodulated at

the same time and several experiments may be needed to measure all the targeted couplings. However, multiple protons can be simultaneously studied in a single experiment using region-selective or multiple frequency-selective pulses, provided that all excited protons are not mutually *J*-coupled.

6.1. CLIP-HSQMBC

The basic selHSQMBC experiment is the 2D CLean In-Phase HSQMBC (CLIP-HSQMBC)] [148] (Fig. 19A) that yields undistorted IP ^{1}H multiplets with pure absorptive line shapes along the detected dimension from which the easy, direct, and accurate measurement of ^{n}J(CH) can be performed. The resulting cross-peaks show an additional splitting compared to the conventional ^{1}H multiplet arising from the active proton–carbon coupling because proton acquisition is performed without heteronuclear decoupling. As discussed before for other CLIP experiments, the key point of this sequence is the 90° ^{13}C pulse applied just prior to acquisition, which efficiently converts the existing dispersive AP contribution to non-observable multiple-quantum coherences. Figure 20 clearly shows that for simple and well-resolved multiplets, the magnitude of ^{n}J(CH) can be extracted directly by analyzing peak frequency separation as usually made for conventional ^{1}H multiplets. The phase properties of the multiplet and therefore the accurate extraction of ^{n}J(CH) are independent of experiment optimization, with a small uncertainty of 0.1–0.2 Hz, but important errors of 20–30% should be easily introduced when omitting the CLIP pulse. In practice, a perfect match between ^{n}J(CH) and the experiment optimization is not critical, cross-peaks show a clear dependence with the $\sin^2(\pi^{n}J(\mathrm{CH})\Delta)$ function, and ^{n}J(CH) values in the range 3–10 Hz can be measured in a 6–8 Hz optimized selHSQMBC experiment.

For more complex multiplets, the separation of the outer peaks of the multiplet can be compared to that in the ^{1}H spectrum to indirectly extract the additional splitting or, alternatively, a simple fitting procedure taking the internal satellite ^{1}J(CH) component as decoupled reference multiplet can be applied. On the other hand, a double-selective 1D version of a refocused HSQMBC experiment has been also proposed for the fast and accurate measurement of specific ^{n}J(CH) values from pure IP 1D multiplets [149].

6.2. selHSQMBC-IPAP

A powerful alternative for the simple and direct of ^{n}J(CH) in broad, unresolved, or highly selHSQMBC multiplets is based on the incorporation of

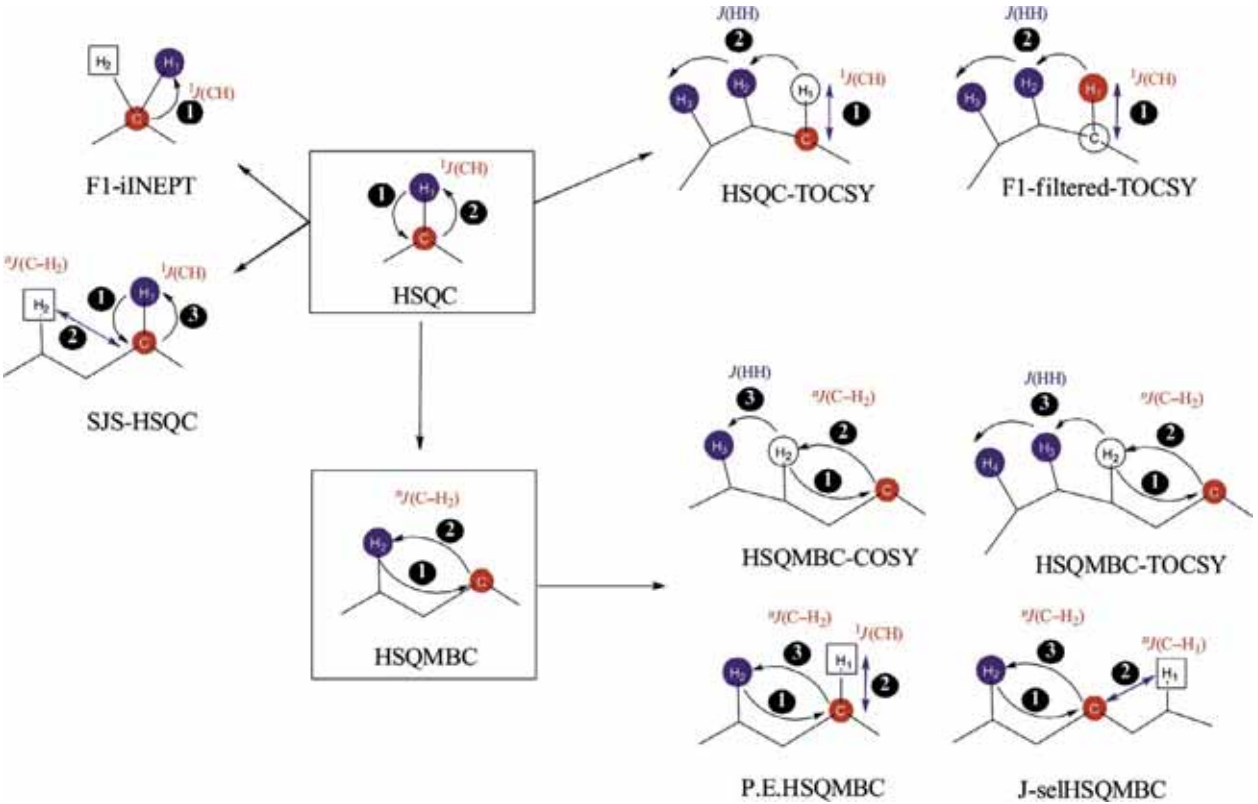

Figure 18 Schematic representation of several spin systems and NMR experiment names that can be studied by HSQC and HSQMBC type experiments.

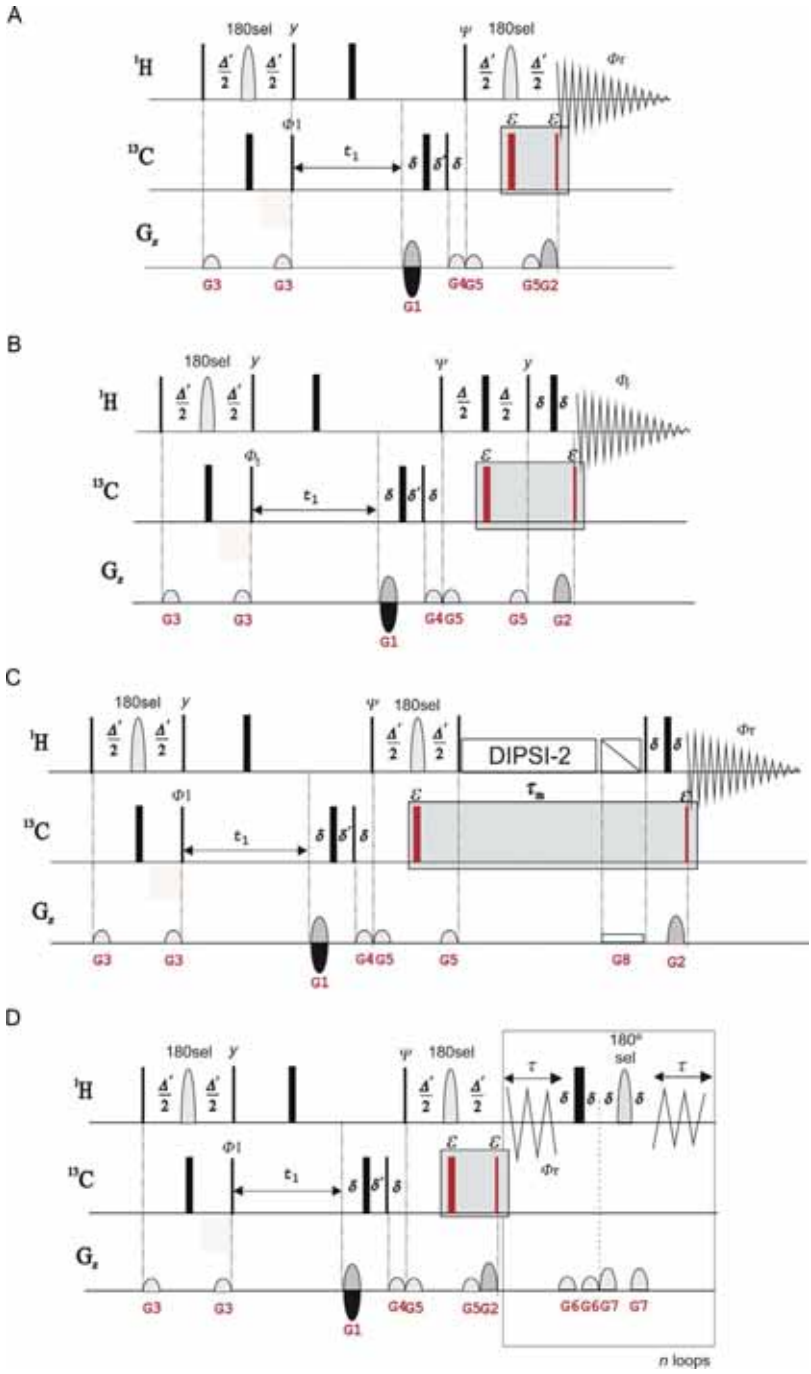

Figure 19 See legend on next page.

the IPAP principle (selHSQMBC-IPAP) that relies on the separate acquisition of complementary IP and AP datasets [150,151]. The IP data are generated as described for the CLIP-HSQMBC experiment ($\Psi = y$ and $\varepsilon =$ on), whereas the AP data (with a $\sin(\pi {}^{n}J(\mathrm{CH})\Delta)$ signal intensity dependence) are obtained using the same scheme with $\Psi = x$ and omitting the last 180° and 90° ^{13}C pulses to avoid ${}^{n}J(\mathrm{CH})$ refocusing ($\varepsilon =$ off). Time-domain data combination (IP ± AP) affords two separate pure-phase α− and β-selHSQMBC subspectra where the ${}^{n}J(\mathrm{CH})$ value can be extracted by direct analysis of the relative frequency displacement between these α/β cross-peaks along the highly resolved F2 dimension. Figure 21 summarizes this protocol for the broad pseudo-triple H22 proton of **1**. Accurate ${}^{n}J(\mathrm{CH})$ values can be easily extracted, irrespective of the multiplet complexity and avoiding the typical overestimation associated to the direct analysis of AP signals or the lack of multiplet definition in IP signals.

The success of the IPAP technique relies on the complementarity between the IP and AP data, and the percentage of undesired cross-talk generated during IP±AP data combination will be proportional to a $\sin^2(\pi {}^{n}J(\mathrm{CH})\Delta)$-$\sin(\pi {}^{n}J(\mathrm{CH})\Delta)$ factor. The use of individualized scaling factor (AP ± k*IP) factors can compensate unbalanced IPAP cross-peaks. As a

Figure 19—Cont'd Several ^{1}H-selective 2D HSQMBC schemes designed to measure long-range proton–carbon coupling constants: (A) selHSQMBC, (B) selHSQMBC-COSY, (C) selHSQMBC-TOCSY, and (D) HOBS-selHSQMBC experiments. Frequency-selective 180° ^{1}H pulses represented as shaped pulses are applied in the middle of the INEPT blocks ($\Delta = 1/(2*{}^{n}J(\mathrm{CH})) = \Delta'$+p180 where p180 is the duration of the selective 180° ^{1}H pulse that must be set accordingly to the required selectivity in each case). ^{1}H data are acquired without ^{13}C decoupling. CLIP versions of the experiments are obtained using ($\Psi = y$ and $\varepsilon =$ on). Alternatively, the IPAP methodology can be applied: Two independent IP and AP data are separately collected as a function of the pulses marked with ε: IP ($\Psi = y$ and $\varepsilon =$ on) and AP ($\Psi = x$ and $\varepsilon =$ off). α/β data are obtained after time-domain addition/subtraction data (AP ± IP). A minimum two-step phase cycle was applied: $\phi_1 = x,-x$ and $\phi_{rec} = x,-x$, all other unlabeled pulses are from the x-axis. In (A–C) gradients G1 and G2 are used for coherence selection using echo–antiecho, G4 acts as a zz-filter, G3 and G5 flank the inversion proton pulses to generate pure refocusing elements and G8 is simultaneously applied to a and adiabatic CHIRP pulse to remove undesired ZQ contributions. In (D), the selective 180° ^{1}H pulse applied at the middle of INEPT periods and during detection have the same shape and duration and we found that REBURP pulses in the order of 3–7.5 ms provides the best result as a function of the required selectivity. Homonuclear decoupling during the acquisition time (AQ) is performed using a refocusing blocks including a pair of hard/selective 180°^{1}H pulses flanked with gradient G6 and G7 and applied at intervals of $2\tau =$ AQ/n, where n is the number of loops.

bonus, the IPAP methodology offers additional controls to confirm the accuracy of the measurement or the presence of cross-talking. Three different multiplets (IP, AP, and α/β) are available for independent measurements and proper data comparison and validation.

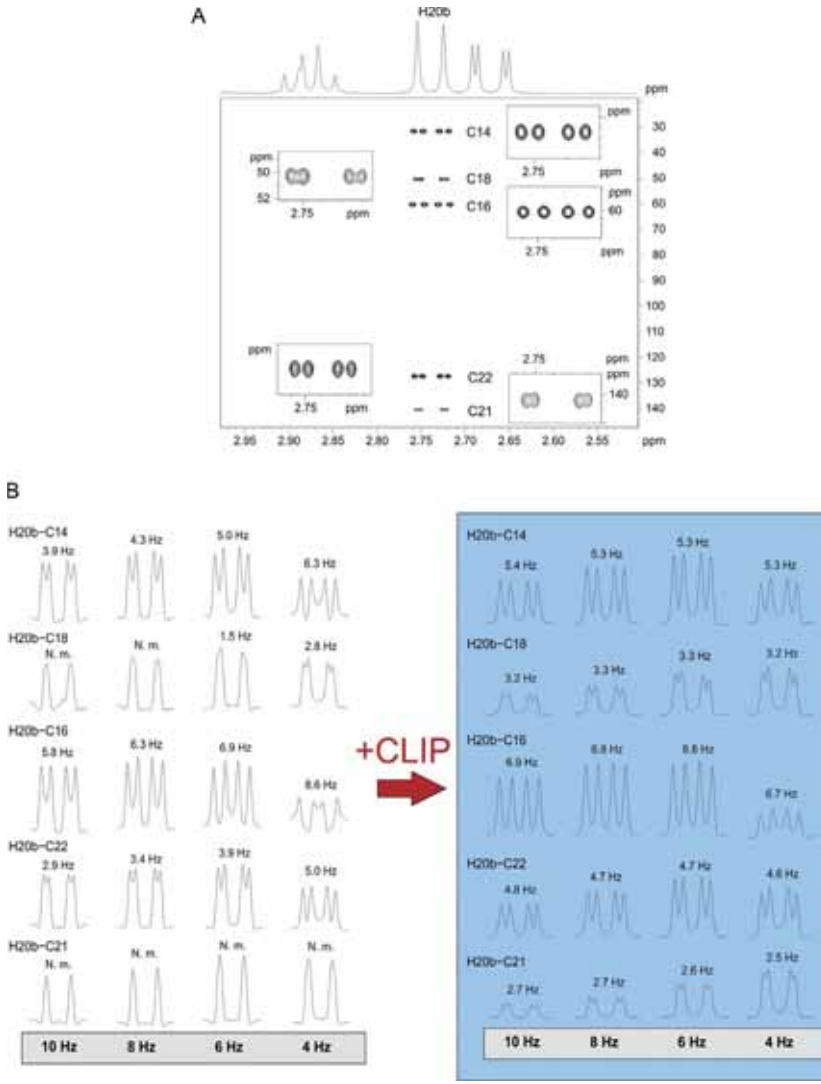

Figure 20 (A) 2D CLIP-selHSQMBC spectrum after selective excitation of the H-20b proton of (**1**). (B) Direct extraction ^{n}J(CH) can be made from pure in-phase cross-peaks, independent of experiment optimization (from 4 to 10 Hz). *Adapted from Ref. [148].*

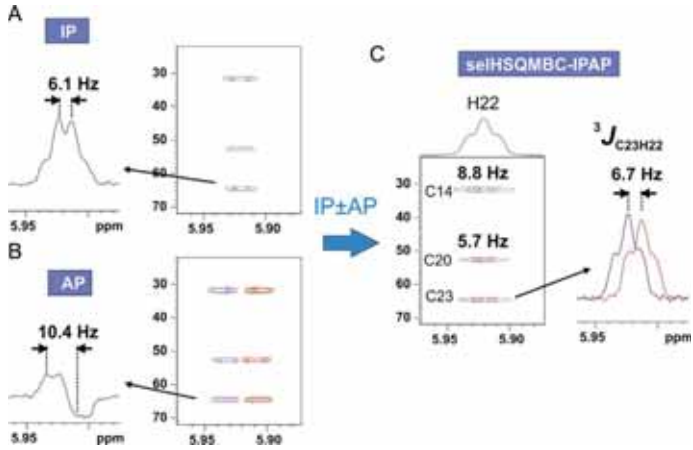

Figure 21 selHSQMBC-IPAP experiments after selective excitation of the olefinic H-22 proton in **1**: The acquired (A) IP and (B) AP datasets are added/subtracted to provide (C) separate α/β subspectra. The relative displacement between α/β cross-peaks along the F2 dimension provides a direct measurement of ^nJ(CH) without any posterior analysis. *Adapted from Ref. [142].*

6.3. selHSQMBC-TOCSY

An enhanced CLIP-selHSQMBC-TOCSY experiment [148] has been proposed where an appended TOCSY period consisting of a DIPSI mixing element included into a ZQF [112] is inserted just prior to acquisition (Fig. 19C). The method expands and improves the features of the original selHSQMBC experiment because it uses a sequential transfer mechanism based on a dual step via $^nJ(CH_1)+J(H_1H_2)$. Thus, starting from a selected H1 proton, a relayed C-H2 cross-peak can be observed with an intensity independent to its $^nJ(CH_2)$ coupling value. Due to the IP nature of the TOCSY transfer, the resulting cross-peaks will also show IP multiplet patterns from which small ^nJ(CH) values could be determined. A simple comparison between selHSQMBC and selHSQMBC-TOCSY spectra acquired under the same experimental conditions (Fig. 22) reveals a major number of cross-peaks to be analyzed from a single experiment, even for those signals appearing in overlapped regions where selective irradiation should not be feasible.

The IPAP technique can be also implemented to yield a robust selHSQMBC-TOCSY-IPAP experiment to determine coupling values smaller than the linewidth [152]. As a major enhancement, the method allows additionally the easy and direct determination of the relative sign

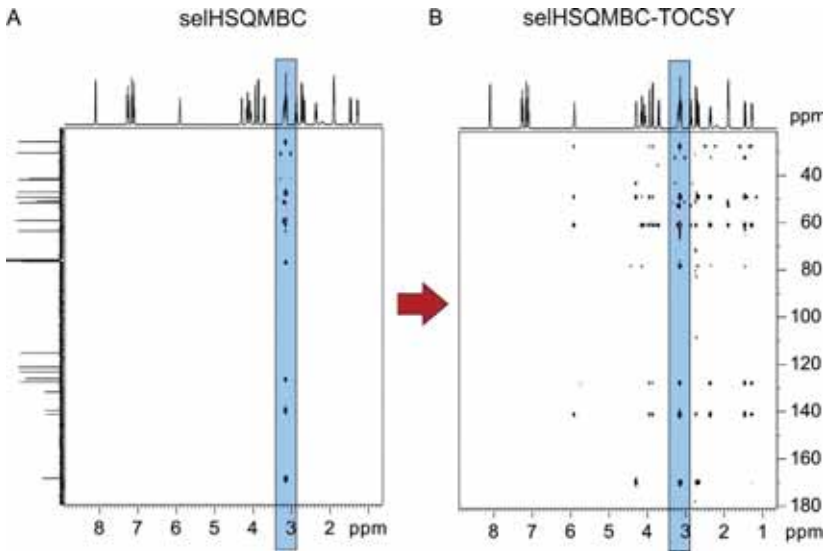

Figure 22 Comparison between a (A) 2D selHSQMBC and (B) selHSQMBC-TOCSY spectra of (**1**) after selective refocusing of the three overlapped protons (H14, H11a, and H18a) resonating at 3.15 ppm. The mixing time in TOCSY was of 60 ms. *Adapted from Ref. [142].*

of ^{n}J(CH) by analyzing the relative left–right or right–left displacement of α/β multiplets, avoiding any complex and time-consuming fitting procedure. The extraction of relative signs is only applicable when signals from the same row are compared (the same carbon) but not for peaks of the same column but different rows (different carbons). Figure 23 demonstrates the powerful of the selHSQMBC-TOCSY-IPAP experiment by analyzing the 1D traces from the carbonyl C10 carbon. Large negative values are revealed for H11a and H11b protons (−6.3 and −7.9 Hz, respectively) and a small positive value for H12 (+2.0 Hz). On the other hand, the olefinic C21 carbon at 140.5 ppm presents positive values for H13 (+7.6 Hz), H15b (+6.5 Hz) and H15a (+1.3 Hz) and negative values for the two-bond H14 (−5.8 Hz) and even for the tiny four-bond H16 (−1.0 Hz) correlations. In addition, the optimum performance to work with IP multiplets rather from AP multiplets is clearly evidenced by the better sensitivity of the IP multiplets and the important cancelation effects in AP multiplets, as shown for the H12 proton.

Related 1D versions of the selHSQMBC-TOCSY experiment have been published to measure the sign and the magnitude of heteronuclear coupling constants in other nuclei than ^{13}C in a very fast and efficient way [153].

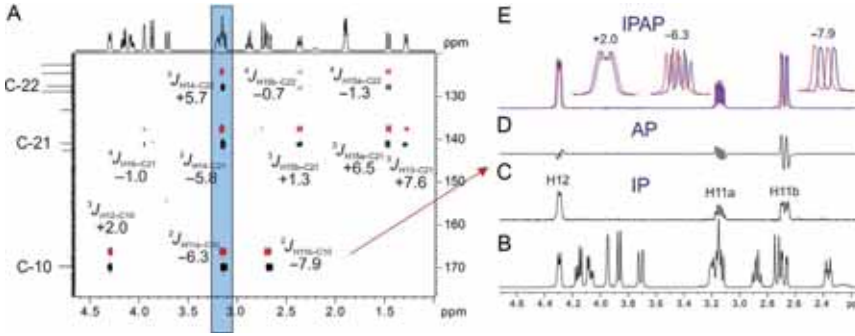

Figure 23 (A) Expanded area corresponding of the 2D selHSQMBC-TOCSY-IPAP spectra of (**1**). (B) Conventional 1D ^{1}H NMR spectrum and (C–E) 1D slices extracted at the C10 frequency showing the excellent pure-phase properties of (C) IP, (D) AP, and (E) overlayed α/β data. *Adapted from Ref. [152].*

Two different approaches have been reported: (i) the Up&Down technique relies on the direct analysis of antiphase multiplets whereas (ii) the Left&Right technique is based on the relative displacement between separate IPAP components. Examples are provided for high-abundant (^{19}F and ^{31}P) and low-abundant (^{77}Se, ^{29}Si, and ^{119}Sn) heteronuclei demonstrating that small *J*(XH) couplings and their corresponding signs can be determined between remote spins separated for more than the conventional two- and three-bond connectivities.

6.4. selHSQMBC-COSY-IPAP

The IPAP methodology also works when two mutually *J*-coupled protons are simultaneously excited in selHSQMBC experiments. IP and AP data only differ in the application of ^{13}C pulses, and therefore, the resulting α/β cross-peaks present the same relative phase distortion because *J*(HH) modulation does not affect the addition/subtraction procedure [154]. Based on this premise, a selHSQMBC-COSY-IPAP experiment has been derived by replacing the selective 180° ^{1}H pulse in the refocusing INEPT period by a hard 180° ^{1}H pulse (Fig. 19B) [155]. In this way, simultaneous *J*(HH) and ^{n}*J*(CH) evolution takes place during this period that generates COSY transfer when a last 90°(*y*) ^{1}H pulse is applied. The experiment retains the simplicity in both acquisition and processing steps and maintains the same overall duration of the original selHSQMBC experiment. Similarly as discussed by the TOCSY transfer, an increased number of coupling values with their corresponding signs can be measured. Although the mixed phases are present in the corresponding α- and β-COSY multiplets, this does not affect

the direct measurement because only the relative displacement between α/β signals is of interest. Very importantly, the sign of ^{n}J(CH) is also encoded as the relative left/right (negative) or right/left (positive) frequency peak displacement. Based on these fundamentals, broadband versions of the HMBC-IPAP and HSQMBC-IPAP experiments have been reported which do not require the use of selective pulses [156]. In addition, an excellent complementarity has been demonstrated between HMBC/HSQMBC and its counterparts HMBC-COSY/HSQMBC-COSY experiments which are designed by simply adding a 90° ^{1}H pulse at the end of the sequence. This complementarity can be an interesting alternative to other approaches to retrieve some missing cross-peaks, such as the use of different delay-optimized experiments or the use of accordion spectroscopy.

6.5. HOBS-selHSQMBC

The incorporation of broadband homodecoupling in experiments detecting antiphase HH magnetization components, like the regular COSY, HMBC, or HSQMBC experiments, fails because multiplet components should be partially or fully canceled. However, the excellent IP nature demonstrated for the selHSQMBC experiment allows that homonuclear and/or heteronuclear decoupling can be implemented along the detected dimension using the HOBS technique (see Section 4.2), obtaining simplified cross-peaks without their characteristic fine J multiplet structure. Figure 19D shows the ^{1}H-homodecoupled band-selective HSQMBC (HOBS-selHSQMBC) pulse scheme, which represents a new way to measure ^{n}J(CH) from the simplified IP doublets generated along the detected dimension [157]. The selective 180° pulses applied in the INEPT and during detection have the same shape and duration, minimizing the requirements for additional experimental setup. Thus, all protons selected by the region-selective 180° ^{1}H pulse appear homodecoupled from all other protons that do not experience this pulse, and the result is a band-selective homodecoupled observation of a specific region of the ^{1}H spectrum. Figure 24 compares the band-selective CLIP-HSQMBC versus CLIP-HOBS-selHSQMBC spectra of cyclosporine after applying a 5 ms REBURP 180° pulse on the H_α proton region. It can be observed how the ^{1}H–^{1}H J multiplet structures of all H_α resonances along the detected dimension are collapsed because of the effective homodecoupling of H_α–NH and H_α–H_β coupling constants, affording enhanced resolution and improved sensitivity as shown from the 1D slices.

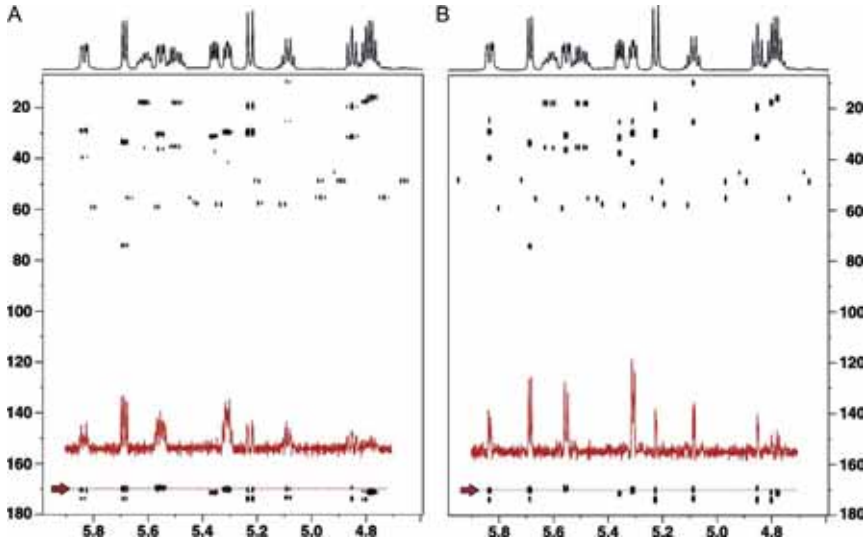

Figure 24 (A) Conventional band-selective HSQMBC and (B) HOBS-selHSQMBC spectra of (**2**) acquired under the same experimental conditions. A selected 1D slice is plotted for each spectrum at the same absolute scale to compare the relative sensitivity and resolution achieved in the 2D spectra. *Adapted from Ref. [157].*

A detailed inspection shows that HOBS-HSQMBC cross-peaks are simplified to IP doublets due to the active ^{n}J(CH) coupling (Fig. 25). The direct and semi-automated extraction of the ^{n}J(CH) can be made by direct analysis of cross-peaks if the multiplet is resolved enough. In cases of poor resolved multiplets or when the accuracy of the measurements may be doubtful, the application of the IPAP methodology described above can offer a better solution. A perfect agreement between the ^{n}J(CH) values measured directly from the proposed HOBS and HOBS-IPAP methods with those extracted from selHSQMBC-TOCSY spectra has been reported.

The HOBS-selHSQMBC experiment is also compatible for broadband heteronuclear decoupling during acquisition. Figure 26 shows the substantial sensitivity and resolution enhancements achieved by sequential implementation of hetero- and homodecoupling in a regular selHSQMBC experiment. An average enhancement by factors of 1.2 (with heteronuclear decoupling), 1.6 (with homonuclear decoupling), and 2.4 (with both homo- and heteronuclear decoupling) when compared with fully coupled data (normalized average factor of 1) has been reported.

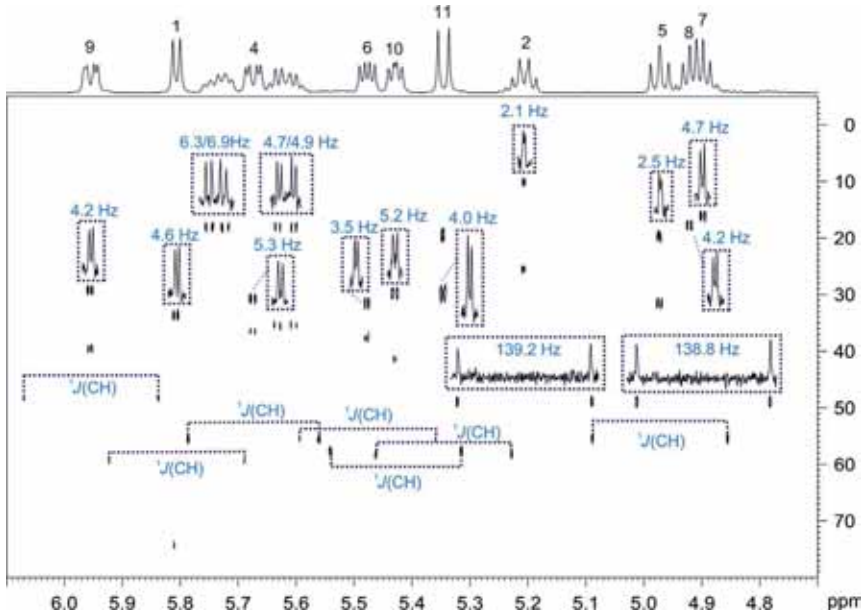

Figure 25 In-phase HOBS-selHSQMBC spectra of (**2**) showing how the value of *J*(CH) for all direct and long-range cross-peaks can be extracted directly from the analysis of the clean IP doublets along the detected dimension. *Adapted from Ref. [157].*

6.6. PIP-HSQMBC

A broadband Pure In-Phase HSQMBC (PIP-HSQMBC) experiment yielding pure IP multiplet patterns for all long-range cross-peaks has been recently reported (Fig. 27) [111]. It is an extension of the PIP-HSQC experiment described in Section 5.1.4, where the interference due to undesired *J*(HH) evolution during the longer heteronuclear transfer periods is more pronounced than the HSQC counterpart because the size of ^{n}J(CH) and *J*(HH) is of the same order. As largely reported for older HSQMBC experiments, the standard INEPT transfer can be replaced by other schemes such as INEPT-BIRD, CPMG, or CPMG-BIRD elements (Fig. 27B–D). In all these versions, pure IP multiplets would be obtained but with a different signal intensity dependence as a function of the chosen transfer element. As shown previously for PIP experiments, the key element is the adiabatic *z*-filter that removes any AP contribution due to *J*(HH) and unmatched ^{n}J(CH) couplings evolution. The importance of the adiabatic z-filter is illustrated with the superior performance of the 8-Hz PIP module over conventional, CLIP, and z-filtered HSQMBC experiments acquired under the

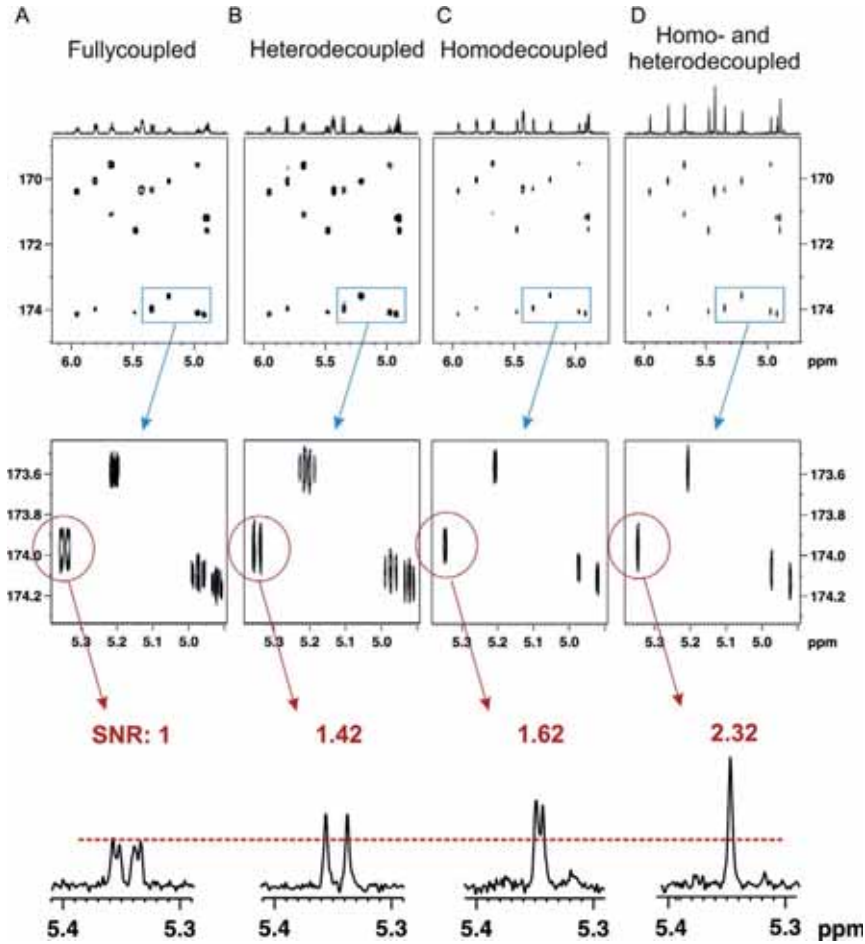

Figure 26 Resolution enhancement effects after incorporation of homo or/and heteronuclear decoupling in $^{1}H_{\alpha}$–^{13}CO HSQMBC spectra (2): (A) Conventional; (B) broadband ^{13}C-decoupled, (C) HOBS-selHSQMBC, and (D) broadband ^{13}C-decoupled HOBS-selHSQMBC. At the bottom, 1D slices showing the experimental SNR and multiplet simplification. *Adapted from Ref. [157].*

same conditions (Fig. 28). Note that dispersive components are observed in all cases rendering complicated the cross-peak analysis, except in the PIP-HSQMBC trace where pure IP pattern are observed for all signals.

Analysis of some selected 1D traces in the PIP-HSQMBC spectrum of strychnine reveals that all cross-peaks display a clean IP character (Fig. 29B). For instance, all PIP-HSQMBC cross-peaks belonging to the H8 and H20a protons show well-resolved multiplets (Fig. 29C) that allow direct and easy

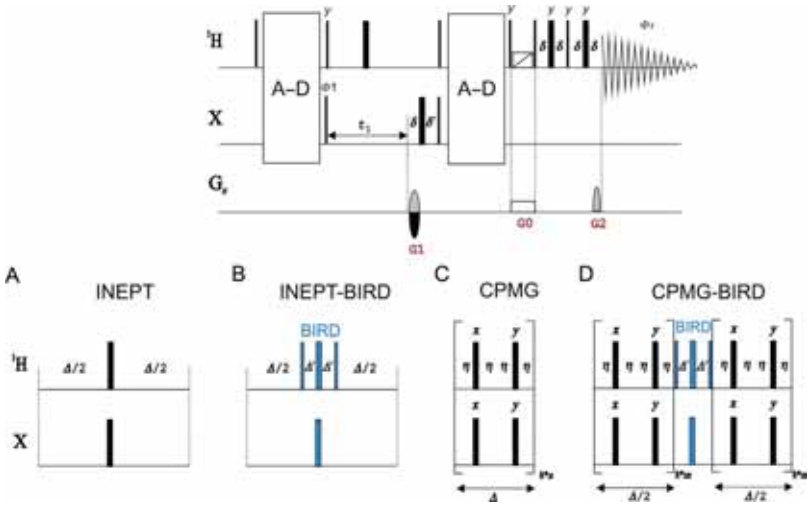

Figure 27 Basic pulse schemes to collect PIP-HSQMBC spectra. Several modules can be used for heteronuclear transfer elements ($\Delta = 1/[2*^{n}J(\mathrm{CH})]$): (A) the basic INEPT; (B) the INEPT-BIRD block ($\Delta' = 1/[2*^{1}J(\mathrm{CH})]$); (C) the CPMG XY-16 super cycle consisting of simultaneous ^{1}H and ^{13}C pulses applied at intervals 2η; and (D) the CPMG-BIRD element. All these variants use the same scheme with an adiabatic z-filter after the refocusing period and just before the refocusing gradient echo and the acquisition.

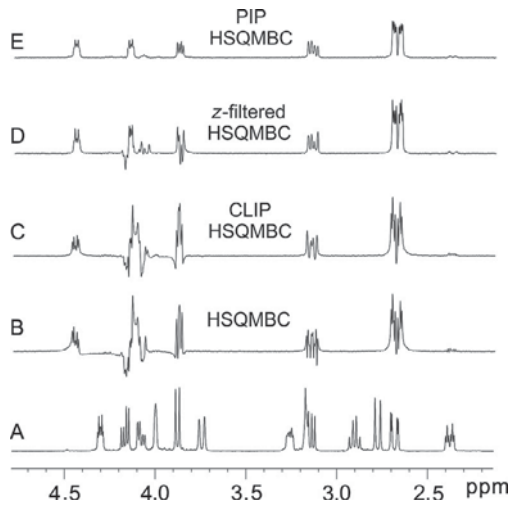

Figure 28 (A) ^{1}H NMR spectrum of (**1**); (B–E) 1D traces extracted at the C12 of (**1**) in 8-Hz optimized (B) HSQMBC, (C) CLIP-HSQMBC, (D) *z*-filtered HSQMBC, and (E) PIP-HSQMBC spectra. *Adapted from Ref. [111].*

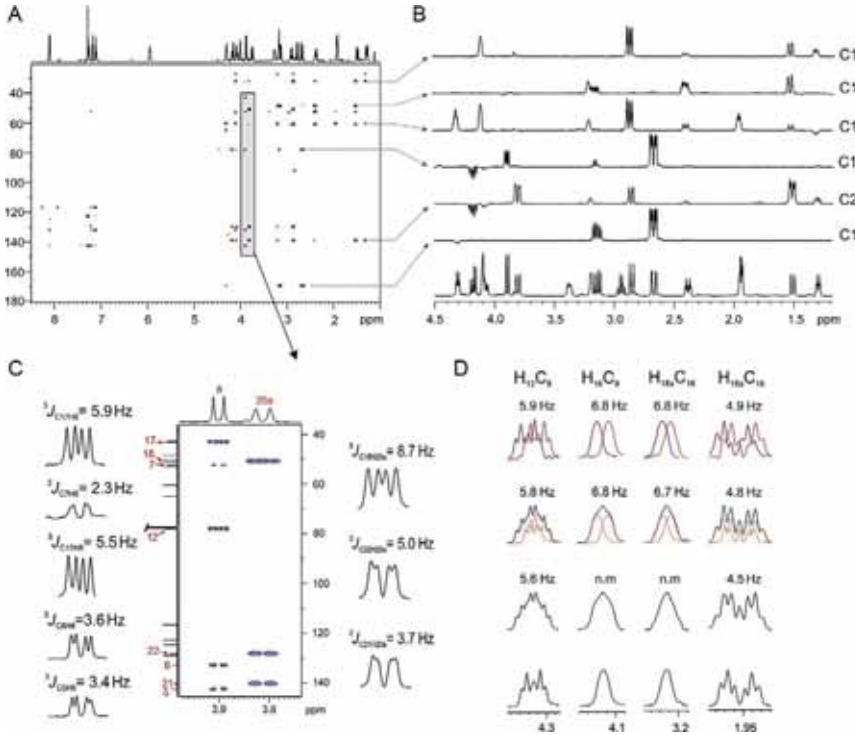

Figure 29 (A) 8-Hz optimized PIP-HSQMBC spectrum of (**1**); (B) 1D row slices taken at different ^{13}C frequencies showing in-phase multiplet patterns for all observed cross-peaks; (C) Expanded area showing how the magnitude of $^{n}J(CH)$ can be easily determined from direct analysis of undistorted and resolved IP peaks. (D) Comparison of several methods for the extraction of $^{n}J(CH)$ values in non-resolved or complex PIP-HSQMBC multiplets: (from bottom to top) multiplets obtained with and without ^{13}C decoupling during acquisition; fitting process performed from the decoupled multiplets in (A) to match the experimental coupled multiplets in (B); overlaid α and β multiplets obtained after IP ± AP data combination in a HSQMBC-IPAP experiment, respectively. *Adapted from Ref. [111].*

measurements of $^{n}J(CH)$ values up to 2–3 Hz. Doublets in the conventional ^{1}H spectrum for these protons are converted to IP double of doublets for the corresponding HSQMBC cross-peaks. As discussed previously, the extraction of $^{n}J(CH)$ in more complex or non-resolved multiplets becomes more complicated but it can be performed (i) by measuring overall multiplet widths, (ii) fitting/matching them to an external reference cross-peak obtained from the same sequence with broadband ^{13}C-decoupling during acquisition, (iii) from the internal satellite lines corresponding to the direct $^{1}J(CH)$ responses, if available, without need to acquire a second reference spectrum,

or (iv) by implementing the IPAP technique. Figure 29D shows some examples to measure ^{n}J(CH) by using the coupled/decoupled fitting or the IPAP approach. The performance of the PIP-HSQC and PIP-HSQMBC methods has been also verified for the efficient measurement of RDCs under anisotropic conditions.

6.7. Simultaneous Measurement of Multiple Coupling Constants

The selHSQMBC pulse scheme has also been modified to allow the simultaneous measurement of multiple homo- and heteronuclear coupling constants from a single 2D cross-peak, thanks to the complementarity between the E.COSY and the IPAP principles. In the P.E.HSQMBC experiment, the sign and the magnitude of J(HH) can be measured along the direct dimension from the relative E.COSY-type multiplet pattern displacement due to the passive ^{1}J(CH) splitting generated in the indirect dimension [158]. On the other hand, the corresponding ^{n}J(CH) is independently determined in the detected dimension from the IPAP multiplet displacement. The sequence combines in a single experiment (a) the accurate measurement of ^{1}J(CH) along the indirect dimension described for F1-coupled HSQC schemes; (b) the sign-sensitive measurement of ^{1}J(CH) and ^{2}J(HH) in E.COSY multiplets similarly as reported in the P.E.HSQC experiment, and (c) the precise measurement of ^{n}J(CH) using the IPAP methodology. The P.E.HSQMBC sequence (Fig. 30) is basically a selHSQMBC applied on an H_A proton and signal intensity will depend on the $\sin^2(\pi^{n}J(CH_A)\Delta')$ function. As an essential feature, a ^{n}J(CH)-scaling BIRD element is applied during the evolution of the transverse ^{13}C magnetization and the last step a selective 90° pulses on H_A proton is employed to provide a characteristic E.COSY-like transfer.

In a similar way, a new *J*-selHSQMBC-IPAP experiment has been proposed for the independent measurement of two different long-range $^{n}J(CH_A)$ and $^{n}J(CH_B)$ coupling constants from the same 2D cross-peak [159]. In addition, the E.COSY pattern provides additional information about the magnitude and relative sign between $J(H_AH_B)$ and $^{n}J(CH_B)$ coupling constants. The sequence is a selHSQMBC applied on an H_A proton, and a selective inversion element on a different H_B proton is applied during the evolution of the transverse ^{13}C magnetization (Fig. 31). Thus, whereas ^{13}C chemical shift is encoded in the usual way during the t_1 period, signal is also modulated by a $\cos((\pi^{n}J(CH_B)kt_1)$ factor that will cause an IP splitting due to $k^{*n}J(CH_B)$ in the F1 dimension. Each correlation can also show an additional doublet with an apparent $k^{*}J(CH_B)$ splitting in the F1 dimension.

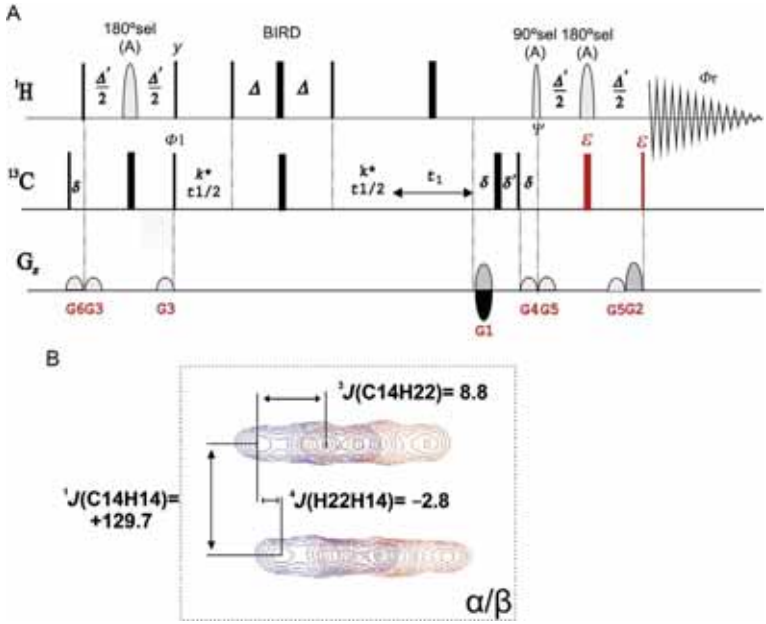

Figure 30 (A) Pulse scheme for the P.E.HSQMBC experiment. (B) Typical multiplet pattern of a P.E.HSQMBC cross-peak, where three couplings (^1J(CH), J(HH), and ^nJ(CH)) can be measured from a single cross-peak. General scheme of the IPAP procedure and the corresponding IP, AP, and α/β multiplet patterns obtained from this experiment. *Adapted from Ref. [158].*

Thus, two independent $^nJ(CH_A)$ and $^nJ(CH_B)$ coupling constants on the same carbon can be independently measured from the analysis of a single 2D cross-peak. Moreover, additional information about $J(H_AH_B)$ and the relative sign between $J(H_AH_B)$ and $^nJ(CH_B)$ can be also extracted from the E.COSY pattern generated by the passive H_B proton.

This same inversion element has also been implemented in a high-sensitive selective *J*-scaled sensitivity-improved HSQC (SJS-HSQC) experiment [160], which allows the simultaneous determination of the magnitude and sign of both $J(H_AH_B)$ and $^nJ(CH_B)$ in a CH_A HSQC cross-peak. The success of this experiment has been demonstrated by determining the relative configuration of the natural product 10-*epi*-8-deoxycumambrin B using long-range CH RDCs.

A suite of coupled/decoupled versions of fluorine-detected triple resonance $^{19}F–^{13}C\{^1H\}$ HSQMBC and HMBC spectra of fluorinated compounds to determine the size and the sign of J(CH), J(CF), and J(HF) coupling constants from E.COSY multiplet patterns has been also reported [161].

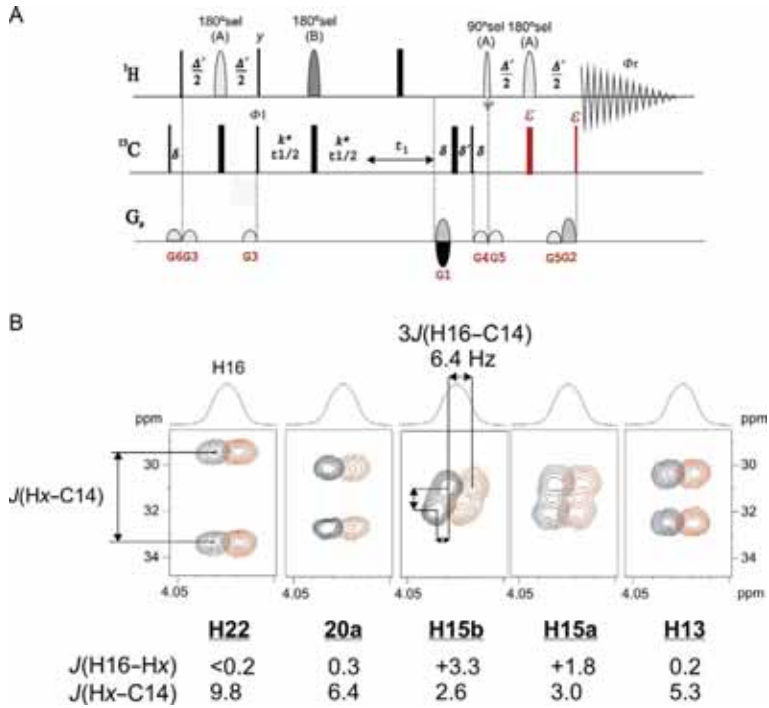

Figure 31 (A) Pulse scheme for the J-selHSQMBC-IPAP experiment. (B) Several multiplet patterns corresponding to the H16–C14 cross-peak of (**1**) after selective excitation of a second proton. *Adapted from Ref. [159]*.

7. OTHER METHODS

7.1. Quantitative HSQC

There is an enormous interest in the use of the HSQC experiment as a quantitative NMR tool and many different approaches have been proposed in the last years [162–169]. In conventional HSQC spectra, peak volumes of different protons are variably modulated as a function of each individual J(HH) coupling pattern. This non-uniform dependence causes a common source of error during integration and quantification of response intensities. In the perfect-HSQC experiment described in Section 5.1.2, there is a second and very significant positive consequence for removing J(HH) interferences: signal intensity is amplitude modulated only by the $\sin^2(\pi J(\mathrm{CH})\Delta)$ factor, and is therefore an excellent candidate to design future strategies for quantitative NMR studies. The proposed method is less aggressive than the use of

CPMG-INEPT blocks where a train of simultaneous $^{1}H/^{13}C$ pulses are applied at high repetition rates, and where the resulting peaks can include unwanted dependences from offset effects or the presence of TOCSY contributions as well as deleterious effects on sample heating under extreme fast-pulsing conditions.

To evaluate the ^{1}J(CH)-compensated intensity strategy based on the proper selection of multiple polarization transfer values, the perfect-HSQC spectrum of a spin system consisting of several protons having J(HH) in the extreme range between 10 and 30 Hz and ^{1}J(CH) ranging between 120 and 180 Hz has been simulated. From a single-Δ 140-Hz perfect-HSQC experiment, a pure IP spectrum with peak volume differences up to 25% is obtained (Fig. 32A). On the other hand, Fig. 32B shows the ^{1}J(CH)-compensated perfect-HSQC spectrum after combining four datasets acquired with Δ values of 2.94 ms (170 Hz), 2.86 ms (175 Hz), 2.86 ms (175 Hz), and 5.88 ms (85 Hz). Note that intensity differences below 2% are obtained in the complete ^{1}J(CH) range between 120 and 180 Hz.

7.2. LR-HSQMBC

HMBC and HSQMBC are traditionally used to trace out long-range proton–carbon correlations. Most of the observed cross-peaks correspond

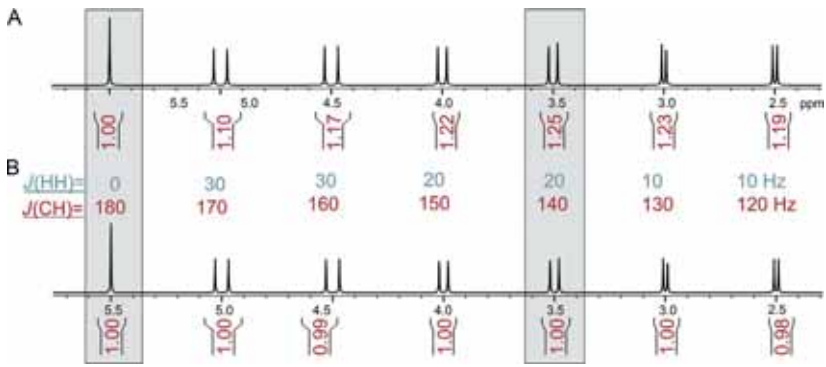

Figure 32 Spectral simulations showing integration ratios in heterodecoupled perfect-HSQC spectra: (A) optimized to a single Δ value of 3.6 ms, corresponding to 140 Hz; (B) average spectrum after combining four datasets acquired with Δ values of 2.94 ms (170 Hz), 2.86 ms (175 Hz), 2.86 ms (175 Hz), and 5.88 ms (85 Hz). The simulated protons have J(HH) and ^{1}J(CH) values in the range between 10–30 Hz and 120–180 Hz, respectively. Enhanced boxes compare signal intensity integration for two different protons. *Adapted from Ref. [95].*

to two- and three-bond away connectivities and attempt to use a 2- to 4-Hz optimized HMBC experiment to find longer correlations results in a considerable loss in sensitivity due to AP cancelation of responses. Classical alternatives such as HSQC-TOCSY or ADEQUATE experiments present some limitations for a widespread use. Thus, a long-range HSQMBC (LR-HSQMBC) experiment [170] has been proposed as a complement to the classical HMBC to overcome its typical $^{2,3}J$(CH) limitation, by extending the visualization of long-range correlation data to four-, five-, and even six-bond long-range ^{n}J(CH) heteronuclear couplings, in a similar way as achieved by 1,*n*-ADEQUATE experiments. This technique should prove to be an effective experiment to complement HMBC for testing the structure of proton-deficient molecules.

The pulse sequence itself is a refocused and heterodecoupled modification of the G-BIRD^{r,x}-HSQMBC pulse sequence optimized for the observation of very long-range correlations. Refocusing the desired ^{n}J(CH) magnetization after the t_1 evolution time provides two advantages. First, it generates IP ^{n}J(CH) correlations which avoid the AP cancelation of responses with very small coupling constants. Second, refocusing the heteronuclear coupling allows the application of ^{13}C decoupling during the acquisition time. This operation collapses the heteronuclear coupling of the response and partially recovers some of the SNR lost as a result of relaxation processes encountered during the long duration of the delays optimized for detection of very small ^{n}J(CH) couplings.

It has been reported that the 2-Hz optimized LR-HSQMBC experiment acquired a provided a major number of very long-range correlations than analogs HMBC and D-HMBC experiments. These data could be obtained in 2–3 h from a 4.9 mg sample of strychnine (10.5 μmol) dissolved in 40 μL of $CDCl_3$ in a 600-MHz spectrometer equipped with a 1.7-mm MicroCryoProbe. Data were also compared with an equivalent dual optimization inverted ^{1}J(CC) 1,*n*-ADEQUATE spectrum acquired in about 24 h [171]. In comparison, 29 of the ADEQUATE correlations were missing in the LR-HSQMBC data (23.6%), but additional 62 new correlations (50.4%) not observed in the inverted ^{1}J(CC) 1,*n*-ADEQUATE data were visualized in the LR-HSQMBC experiment. While drawing comparisons, the sole negative attribute of the LR-HSQMBC experiment relative to dual optimization inverted ^{1}J(CC) 1,*n*-ADEQUATE is that the former does not allow the unequivocal differentiation of ^{1}J(CC) from ^{n}J(CC) (^{2}J(CH) vs. ^{n}J(CH) where $n \geq 3$) afforded by the latter experiment [172–175].

The recently reported LR-HSQMBC experiment has been optimized for $^{1}H–^{15}N$ long-range heteronuclear couplings [176]. Several previously unreported four-bond correlations, consistent with the predicted by DFT calculations (0.2–0.3 Hz ^{4}J(NH) couplings), have been observed for strychnine using 2 Hz optimization of the LR-HSQMBC experiment. The $^{1}H–^{15}N$ LR-HSQMBC experiment affords a viable, high sensitivity alternative to HMBC and the accordion-optimized IMPEACH and CIGAR experiments when long-range correlations to nitrogen must be established for either small couplings or in proton-deficient molecules such as might be encountered in natural products or pharmaceuticals.

A triple-resonance 2D H(C)N experiment, referred to as HCNMBC [177], based on the sequential transfer mechanism via ^{1}J(CH)+J(NC) has been recently proposed as an alternative to $^{1}H–^{15}N$ HMBC or HSQMBC experiments to detect multiple-bond proton–nitrogen correlations. It has been shown that clean HCNMBC spectra despite the extremely low content of the isotopomers containing both ^{15}N and ^{13}C isotopes in the same molecule can be obtained if cryogenically cooled probes are available. Because of the similarity between ^{1}J(CN) and ^{2}J(CN) in a variety of nitrogen containing molecules, the experiment is not quite as straightforward to interpret as, for example, an 1,1-ADEQUATE.

8. CONCLUSION

Since its introduction 30 years ago, the HSQC pulse scheme has been modified in a large number of varieties and even now, the existing sequences can be improved in many different aspects. The last developments in HSQC and HSQMBC experiments have been described in this revision covering new NMR methodologies for a faster acquisition, more uniform response for a wide range of ^{1}J(CH) values, the obtention of pure IP undistorted multiplets or improved resolution and/or enhanced sensitivity achieved from broadband homodecoupled signals. It has also described a suite of robust NMR methods designed for the accurate quantitative determination of ^{1}J(CH) and small ^{n}J(CH) scalar and RDCs and also complementary tools to the current techniques that allow one to trace out ultralong range heteronuclear correlations among others. All these methods are a demonstration that the development of new pulse sequences is still a very active and attractive area of interest in the field of small molecule NMR.

ACKNOWLEDGMENTS

Financial support for this research provided by the Spanish MINECO (project CTQ2012-32436) is gratefully acknowledged. We also thank the Servei de Ressonància Magnètica Nuclear, Universitat Autònoma de Barcelona, for allocating instrument time to this project.

REFERENCES

[1] G. Bodenhausen, D.J. Ruben, Natural abundance nitrogen-15 NMR by enhanced heteronuclear spectroscopy, Chem. Phys. Lett. 69 (1980) 185–189.
[2] A. Bax, R. Griffey, B. Hawkins, Correlation of proton and nitrogen-15 chemical shifts by multiple quantum NMR, J. Magn. Reson. 55 (1983) 301–315.
[3] P.K. Mandal, A. Majumdar, A comprehensive discussion of HSQC and HMQC pulse sequences, Concepts Magn. Reson. 20A (2004) 1–23.
[4] T. Parella, Pulsed-field gradients: a new tool for routine NMR, Magn. Reson. Chem. 36 (1998) 467–495.
[5] W. Willker, D. Leibfritz, R. Kerssebaum, W. Bermel, Gradient selection in inverse heteronuclear correlation spectroscopy, Magn. Reson. Chem. 31 (1993) 287–292.
[6] L. Kay, P. Keifer, T. Saarinen, Pure absorption gradient enhanced heteronuclear single quantum correlation spectroscopy with improved sensitivity, J. Am. Chem. Soc. 114 (1992) 10663–10665.
[7] K. Pervushin, R. Riek, G. Wider, K. Wüthrich, Attenuated T_2 relaxation by mutual cancellation of dipole-dipole coupling and chemical shift anisotropy indicates an avenue to NMR structures of very large biological macromolecules in solution, Proc. Natl. Acad. Sci. U. S. A. 94 (1997) 12366–12371.
[8] I. Bertini, K.S. McGreevy, G. Parigi, NMR of Biomolecules: Towards Mechanistic Systems Biology, Wiley-VCH, Weinheim, 2012.
[9] T.F. Molinski, NMR of natural products at the nanomole-scale, Nat. Prod. Rep. 27 (2010) 321–329.
[10] Y. Liu, M.D. Green, R. Marques, T. Pereira, R. Helmy, R.T. Williamson, W. Bermel, G.E. Martin, Using pure shift HSQC to characterize microgram samples of drug Metabolites, Tetrahedron Lett. 55 (2014) 5450–5453.
[11] D.S. Dalisay, B.I. Morinaka, C.K. Skepper, T.F. Molinski, A tetrachloro polyketide hexahydro-^{1}H-isoindolone, muironolide A, from the marine sponge Phorbas sp. natural products at the nanomole scale, J. Am. Chem. Soc. 131 (2009) 7552–7553.
[12] R.D. Boyer, R. Johnson, K. Krishnamurthy, Compensation of refocusing inefficiency with synchronized inversion sweep (CRISIS) in multiplicity-edited HSQC, J. Magn. Reson. 165 (2003) 253–259.
[13] L. Lerner, A. Bax, Sensitivity-enhanced two-dimensional heteronuclear relayed coherence transfer NMR spectroscopy, J. Magn. Reson. 69 (1986) 375–380.
[14] J. Furrer, Recent developments in HMBC studies, Annu. Rep. NMR Spectrosc. 74 (2011) 293–354.
[15] W.F. Reynolds, D.C. Burns, Getting the most out of HSQC and HMBC spectra, Annu. Rep. NMR Spectrosc. 76 (2012) 1–21.
[16] R.T. Williamson, B.L. Márquez, W.H. Gerwick, K.E. Kövér, One- and two-dimensional gradient-selected HSQMBC NMR experiments for the efficient analysis of long-range heteronuclear coupling constants, Magn. Reson. Chem. 38 (2000) 265–273.
[17] B. Reif, M. Köck, R. Kerssebaum, J. Schleucher, C. Griesinger, Determination of ^{1}J, ^{2}J, and ^{3}J carbon–carbon coupling constants at natural abundance, J. Magn. Reson. B 112 (1996) 295–301.

[18] G.E. Martin, Using 1,1- and 1, n-ADEQUATE 2D NMR Data in structure elucidation protocols, Annu. Rep. NMR Spectrosc. 74 (2011) 215–291.
[19] I. Tvaroska, F.R. Taravel, One-bond carbon-proton coupling constants—angular-dependence in alpha-linked oligosaccharides, Carbohydr. Res. 221 (1991) 83–94.
[20] I. Tvaroska, F.R. Taravel, One-bond carbon-proton coupling constants—angular-dependence in beta-linked oligosaccharides, J. Biomol. NMR 2 (1992) 421–430.
[21] N.C. Maiti, Y.P. Zhu, I. Carmichael, V.E. Anderson, $^{1}J_{CH}$ correlates with alcohol hydrogen bond strength, J. Org. Chem. 71 (2006) 2878–2880.
[22] S. Uhrinova, D. Uhrin, T. Liptaj, J. Bella, J. Hirsch, Measurement of one-bond proton-carbon coupling constants of saccharides, Magn. Reson. Chem. 29 (1991) 912–922.
[23] C.M. Thiele, Use of RDCs in rigid organic compounds and some practical considerations concerning alignment media, Concepts Magn. Reson. Part A 30 (2007) 65–80.
[24] R.R. Gil, Constitutional, configurational, and conformational analysis of small organic molecules on the basis of NMR residual dipolar couplings, Angew. Chem. Int. Ed. 50 (2011) 7222–7224.
[25] C.M. Thiele, Residual dipolar couplings (RDCs) in organic structure determination, Eur. J. Org. Chem. 34 (2008) 5673–5685.
[26] G. Kummerlowe, B. Luy, Residual dipolar couplings as a tool in determining the structure of organic molecules, Trends Anal. Chem. 28 (2009) 483–493.
[27] G. Kummerlowe, B. Luy, Residual dipolar couplings for the configurational and conformational analysis of organic molecules, Annu. Rep. NMR Spectrosc. 68 (2009) 193–232.
[28] O.W. Sørensen, G.W. Eich, M.H. Levitt, G. Bodenhausen, R.R. Ernst, Product operator formalism for the description of NMR pulse experiments, Prog. NMR Spectrosc. 16 (1983) 163–192.
[29] P. Schanda, H. Van Melckebeke, B. Brutscher, Speeding up three-dimensional protein NMR experiments to a few minutes, J. Am. Chem. Soc. 128 (2006) 9042–9043.
[30] J. Farjon, J. Boisbouvier, P. Schanda, A. Pardi, J.P. Simorre, B. Brutscher, Longitudinal-relaxation-enhanced NMR experiments for the study of nucleic acids in solution, J. Am. Chem. Soc. 131 (2009) 8571–8577.
[31] D. Schulze-Sünninghausen, J. Becker, B. Luy, Rapid heteronuclear single quantum correlation NMR spectra at natural abundance, J. Am. Chem. Soc. 136 (2014) 1242–1244.
[32] J. Furrer, A robust, sensitive, and versatile HMBC experiment for rapid structure elucidation by NMR: IMPACT-HMBC, Chem. Commun. 46 (2010) 3396–3398.
[33] E. Kupce, R. Freeman, Fast multidimensional NMR by polarization sharing, Magn. Reson. Chem. 45 (2007) 2–4.
[34] W.F. Reynolds, R.C. Breton, D.C. Burns, Evaluating ASAP-HMQC and PS-HSQC NMR pulse sequences with non-uniform sampling for rapid screening of natural products, Planta Med. 80 (2014) IL26.
[35] J. Farjon, A. Giros, S. Deloisy, L. Blanco, J. Hannedouche, E. Schulz, D. Merlet, ^{29}Si-^{1}H IMPACT HMBC: a suitable tool for analyzing silylated derivatives, Magn. Reson. Chem. 51 (2013) 230–233.
[36] A. Altmayer-Henzien, V. Declerck, D.J. Aitken, E. Lescop, D. Merlet, J. Farjon, Fast-pulsing NMR techniques for the detection of weak interactions: successful natural abundance probe of hydrogen bonds in peptides, Org. Biomol. Chem. 11 (2013) 7611–7615.
[37] C. Gaillet, C. Lequart, P. Debeire, J.M. Nuzillard, Band-Selective HSQC and HMBC experiments using excitation sculpting and PFGSE, J. Magn. Reson. 139 (1999) 454–459.

[38] S.A. Bradley, K. Krishnamurthy, A modified CRISIS-HSQC for band-selective IMPRESS, Magn. Reson. Chem. 43 (2005) 117–123.
[39] D. Jeannerat, High resolution in heteronuclear ^{1}H-^{13}C NMR experiments by optimizing spectral aliasing with one-dimensional carbon data, Magn. Reson. Chem. 41 (2003) 3–7.
[40] M. Foroozandeh, D. Jeannerat, Deciphered chemical shifts in aliased spectra recorded with two slightly different narrow windows or differential chemical shift evolution, ChemPhysChem 12 (2011) 2409–2411.
[41] D. Jeannerat, Rapid multidimensional NMR: high resolution by spectral aliasing, in: R.K. Harris, R.E. Wasylishen (Eds.), Encyclopedia of Magnetic Resonance, John Wiley, Chichester, 2011.
[42] B. Vitorge, S. Bieri, M. Humam, P. Christen, K. Hostettmann, O. Muñoz, S. Loss, D. Jeannerat, High-precision heteronuclear 2D NMR experiments using 10-ppm spectral window to resolve carbon overlap, Chem. Commun. (2009) 950–952.
[43] K. Kazimierczuk, V.Y. Orekhov, Accelerated NMR spectroscopy by using compressed sensing, Angew. Chem. Int. Ed. 50 (2011) 5556–5559.
[44] K. Kazimierczuk, W. Koźmiński, I. Zhukov, Two-dimensional Fourier transform of arbitrarily sampled NMR data sets, J. Magn. Reson. 179 (2006) 323–328.
[45] M. Urbanczyk, W. Kozminski, K. Kazimierczuk, Accelerating diffusion-ordered NMR spectroscopy by joint sparse sampling of diffusion and time dimensions, Angew. Chem. Int. Ed. 53 (2014) 6464–6467.
[46] L. Frydman, T. Scherf, A. Lupulescu, The acquisition of multidimensional NMR spectra within a single scan, Proc. Natl. Acad. Sci. 99 (2002) 15858–15862.
[47] P. Pelupessy, Adiabatic single scan two-dimensional NMR spectrocopy, J. Am. Chem. Soc. 125 (2003) 12345–12350.
[48] A. Tal, L. Frydman, Single-scan multidimensional magnetic resonance, Prog. Nucl. Magn. Reson. Spectrosc. 57 (2010) 241–292.
[49] P. Giraudeau, L. Frydman, Ultrafast 2D NMR: an emerging tool in analytical spectroscopy, Annu. Rev. Anal. Chem. 7 (2014) 129–161.
[50] A. Herrera, E. Fernández-Valle, R. Martínez-Álvarez, D. Molero, Z.D. Pardo, E. Sáez, M. Gal, Real-time monitoring of organic reactions with two-dimensional Ultrafast TOCSY NMR Spectroscopy, Angew. Chem. Int. Ed. 48 (2009) 6274–6277.
[51] Z.D. Pardo, G.L. Olsen, M.E. Fernández-Valle, L. Frydman, R. Martínez-Álvarez, A. Herrera, Monitoring mechanistic details in the synthesis of pyrimidines via real-time, ultrafast multidimensional NMR spectroscopy, J. Am. Chem. Soc. 134 (2012) 2706.
[52] I. Fernández, M.E. Fernández-Valle, R. Martínez-Álvarez, D. Molero-Vílchez, Z.D. Pardo, E. Sáez-Barajas, E. Sánchez, A. Herrera, Discovering mechanistic insights by application of *tandem* ultrafast multidimensional NMR techniques, J. Org. Chem. 79 (2014) 8086–8093.
[53] P. Giraudeau, S. Akoka, A new gradient-controlled method for improving the spectral width of ultrafast 2D NMR experiments, J. Magn. Reson. 205 (2010) 171–176.
[54] Y. Shrot, B. Shapira, L. Frydman, Ultrafast 2D NMR spectroscopy using a continuous spatial encoding of the spin interactions, J. Magn. Reson. 171 (2004) 162–169.
[55] Y. Shrot, L. Frydman, Compressed sensing and the reconstruction of ultrafast 2D NMR data: principles and biomolecular applications, J. Magn. Reson. 209 (2011) 352–358.
[56] L.H.K. Queiroz, P. Giraudeau, F.A.B. dos Santos, K.T. Oliveira, A.G. Ferreira, Real-time mechanistic monitoring of an acetal hydrolysis using ultrafast 2D NMR, Magn. Reson. Chem. 50 (2012) 496–501.
[57] P. Giraudeau, T. Montag, B. Charrier, C.M. Thiele, Fast access to residual dipolar couplings by single-scan 2D NMR in oriented media, Magn. Reson. Chem. 50 (2012) S53–S57.

[58] L. Frydman, D. Blazina, Ultrafast two-dimensional nuclear magnetic resonance spectroscopy of hyperpolarized solutions, Nat. Phys. 3 (2007) 415–419.
[59] L.H.K. Queiroz, A.G. Ferreira, P. Giraudeau, Optimization and practical implementation of ultrafast 2D NMR experiments, Quim. Nova 4 (2013) 577–581.
[60] http://www.sciences.univ-nantes.fr/CEISAM/ebsi/ultrafast/uf_acq.html.
[61] M. Pathan, B. Charrier, I. Tea, S. Akoka, P. Giraudeau, New practical tools for the implementation and use of ultrafast 2D NMR experiments, Magn. Reson. Chem. 51 (2013) 168–175.
[62] J.R. Garbow, D.P. Weitekamp, A. Pines, Bilinear rotation decoupling of homonuclear scalar interactions, Chem. Phys. Lett. 93 (1982) 504–509.
[63] K. Zangger, H. Sterk, Homonuclear broadband-decoupled NMR spectra, J. Magn. Reson. 124 (1997) 486–489.
[64] N.H. Meyer, K. Zangger, Simplifying proton NMR spectra by instant homonuclear broadband decoupling, Angew. Chem. Int. Ed. Engl. 52 (2013) 7143–7146.
[65] J.A. Aguilar, S. Faulkner, M. Nilsson, G.A. Morris, Pure shift ^{1}H NMR: a resolution of the resolution problem? Angew. Chem. Int. Ed. Engl. 49 (2010) 3901–3903.
[66] G.A. Morris, J.A. Aguilar, R. Evans, S. Haiber, M. Nilsson, True chemical shift correlation maps: a TOCSY experiment with pure shifts in both dimensions, J. Am. Chem. Soc. 132 (2010) 12770–12772.
[67] J.A. Aguilar, M. Nilsson, G.A. Morris, Simple proton spectra from complex spin systems: pure shift NMR spectroscopy using BIRD, Angew. Chem. Int. Ed. 50 (2011) 9716–9717.
[68] A. Lupulescu, G. Olsen, L. Frydman, Toward single-shot pure-shift solution ^{1}H NMR by trains of BIRD-based homonuclear decoupling, J. Magn. Reson. 218 (2012) 141–146.
[69] P. Sakhaii, B. Haase, W. Bermel, Experimental access to HSQC spectra decoupled in all frequency dimensions, J. Magn. Reson. 199 (2009) 192–198.
[70] I. Timári, L. Kaltschnee, A. Kolmer, R.W. Adams, M. Nilsson, C.M. Thiele, G.A. Morris, K.E. Kövér, Accurate determination of one-bond heteronuclear coupling constants with pure shift broadband proton-decoupled CLIP/CLAP-HSQC experiments, J. Magn. Reson. 239 (2014) 130–138.
[71] L. Paudel, R.W. Adams, P. Király, J.A. Aguilar, M. Foroozandeh, M.J. Cliff, M. Nilsson, P. Sándor, J.P. Waltho, G.A. Morris, Simultaneously enhancing spectral resolution and sensitivity in heteronuclear correlation NMR spectroscopy, Angew. Chem. Int. Ed. 52 (2013) 11616–11619.
[72] M. Pérez-Trujillo, L. Castañar, E. Monteagudo, L.T. Kuhn, P. Nolis, A. Virgili, R.T. Williamson, T. Parella, Simultaneous ^{1}H and ^{13}C NMR enantiodifferentiation from highly-resolved pure shift HSQC spectra, Chem. Commun. 50 (2014) 10214–10217.
[73] L. Castañar, P. Nolis, A. Virgili, T. Parella, Full sensitivity and enhanced resolution in homodecoupled band-selective NMR experiments, Chem. Eur. J. 19 (2013) 17283–17286.
[74] J. Ying, J. Roche, A. Bax, Homonuclear decoupling for enhancing resolution and sensitivity in NOE and RDC measurements of peptides and proteins, J. Magn. Reson. 241 (2014) 97–102.
[75] L. Castañar, P. Nolis, A. Virgili, T. Parella, Measurement of T_1/T_2 relaxation times in overlapped regions from homodecoupled ^{1}H singlet signals, J. Magn. Reson. 244 (2014) 30–35.
[76] V.M.R. Kakita, J. Bharatam, Real-time homonuclear broadband and band-selective decoupled pure-shift ROESY, Magn. Reson. Chem. 52 (2014) 389–394.

[77] N.H. Meyer, K. Zangger, Enhancing the resolution of multi-dimensional heteronuclear NMR spectra of intrinsically disordered proteins by homonuclear broadband decoupling, Chem. Commun. 50 (2014) 1488–1490.
[78] B. Vitorge, D. Jeannerat, NMR diffusion measurements in complex mixtures using constant-time-HSQC-IDOSY and computer-optimized spectral aliasing for high resolution in the carbon dimension, Anal. Chem. 78 (2006) 5601–5606.
[79] D. Jeannerat, Computer optimized spectral aliasing in the indirect dimension of ^{1}H–^{13}C heteronuclear 2D NMR experiments. A new algorithm and examples of applications to small molecules, J. Magn. Reson. 186 (2007) 112–122.
[80] W.F. Reynolds, R.G. Enriquez, The advantages of forward linear prediction over multiple aliasing for obtaining high-resolution HSQC spectra in systems with extreme spectral crowding, Magn. Reson. Chem. 41 (2003) 927–932.
[81] L. Castañar, M. Pérez-Trujillo, P. Nolis, E. Monteagudo, A. Virgili, T. Parella, Enantiodifferentiation through frequency-selective pure-shift ^{1}H Nuclear Magnetic Resonance spectroscopy, ChemPhysChem 15 (2014) 854–857.
[82] M. Pérez-Trujillo, E. Monteagudo, T. Parella, Evaluation of ^{1}H and ^{13}C NMR spectroscopy for the differentiation of enantiomeric molecules by chiral solvating agents, Anal. Chem. 85 (2013) 10887–10894.
[83] P. Sakhaii, B. Haase, W. Bermel, Broadband homodecoupled heteronuclear multiple bond correlation spectroscopy, J. Magn. Reson. 228 (2013) 125–129.
[84] M.H. Lerche, A. Meissner, F.M. Poulsen, O.W. Sorensen, Pulse sequences for measurement of one-bond ^{15}N-^{1}H coupling constants in the protein backbone, J. Magn. Reson. 140 (1999) 259–263.
[85] M. Ottiger, F. Delaglio, A. Bax, Measurement of J and dipolar couplings from simplified two-dimensional NMR spectra, J. Magn. Reson. 131 (1998) 373–378.
[86] L.S. Yao, J.F. Ying, A. Bax, Improved accuracy of ^{15}N-^{1}H scalar and residual dipolar couplings from gradient-enhanced IPAP-HSQC experiments on protonated proteins, J. Biomol. NMR 43 (2009) 161–170.
[87] C.M. Thiele, Simultaneous assignment of all diastereotopic protons in strychnine using RDCs: PELG as alignment medium for organic molecules, J. Org. Chem. 69 (2004) 7403–7413.
[88] A. Enthart, J.C. Freudenberger, J. Furrer, H. Kessler, B. Luy, The CLIP/CLAP HSQC: pure absorptive spectra for the measurement of one-bond couplings, J. Magn. Reson. 192 (2008) 314–322.
[89] K. Takegoshi, K. Ogura, K. Hikichi, A perfect spin echo in a weakly homonuclear J-coupled spin=1/2 system, J. Magn. Reson. 84 (1989) 611–615.
[90] J.A. Aguilar, M. Nilsson, G. Bodenhausen, G.A. Morris, Spin echo NMR spectra without J modulation, Chem. Commun. 48 (2012) 811–813.
[91] A.M. Torres, G. Zheng, W.S. Price, J-compensated PGSE: an improved NMR diffusion experiment with fewer phase distortions, Magn. Reson. Chem. 48 (2010) 129–133.
[92] R.W. Adams, C.M. Holroyd, J.A. Aguilar, M. Nilsson, G.A. Morris, "Perfecting" WATERGATE: clean proton NMR spectra from aqueous solution, Chem. Commun. 49 (2013) 358–360.
[93] B. Baishya, C.L. Khetrapal, K.K. Dey, "Perfect Echo" HMQC: sensitivity and resolution enhancement by broadband homonuclear decoupling, J. Magn. Reson. 234 (2013) 67–74.
[94] B. Baishya, C.L. Khetrapal, "Perfect Echo" INEPT: more efficient heteronuclear polarization transfer by refocusing homonuclear J-coupling interaction, J. Magn. Reson. 242 (2014) 143–154.

[95] L. Castañar, E. Sistaré, A. Virgili, R.T. Williamson, T. Parella, Suppression of phase and amplitude in J(HH) modulations in HSQC experiments. Magn. Reson. Chem. (2014), http://dx.doi.org/10.1002/mrc.4149, in press.
[96] K. Hallenga, G.M. Lippens, A constant time ^{13}C,^{1}H HSQC with uniform excitation over the complete 13C chemical shift range, J. Biomol. NMR 5 (1995) 59–66.
[97] P.W.A. Howe, Compensating for variation in ^{1}JCH coupling constants in HSQC spectra acquired on small organic molecules, Magn. Reson. Chem. 48 (2010) 837–841.
[98] S. Wimperis, G. Bodenhausen, Heteronuclear coherence transfer over a range of coupling constants. A broadband-INEPT experiment, J. Magn. Reson. 69 (1986) 264–282.
[99] V.S. Manu, A. Kumar, Fast and accurate quantification using Genetic Algorithm optimized ^{1}H-^{13}C refocused constant-time INEPT, J. Magn. Reson. 234 (2013) 106–111.
[100] E. Kupce, R. Freeman, Compensated adiabatic inversion pulses: broadband INEPT and HSQC, J. Magn. Reson. 187 (2007) 258–265.
[101] S. Ehni, B. Luy, A systematic approach for optimizing the robustness of pulse sequence elements with respect to couplings, offsets, and B_1-field inhomogeneities (COB), Magn. Reson. Chem. 50 (2012) S63–S72.
[102] T.E. Skinner, T.O. Reiss, B. Luy, N. Khaneja, S.J. Glaser, Application of optimal control theory to the design of broadband excitation pulses for high resolution NMR, J. Magn. Reson. 163 (2003) 8–15.
[103] S. Ehni, B. Luy, Robust INEPT and refocused INEPT transfer with compensation of a wide range of couplings, offsets, and B_1-field inhomogeneities (COB3), J. Magn. Reson. 247 (2014) 111–117. http://dx.doi.org/10.1016/j.jmr.2014.07.01.
[104] K. Kobzar, T.E. Skinner, N. Khaneja, S.J. Glaser, B. Luy, Exploring the limits of broadband excitation and inversion pulses, J. Magn. Reson. 170 (2004) 236–243.
[105] K. Kobzar, T.E. Skinner, N. Khaneja, S.J. Glaser, B. Luy, Exploring the limits of broadband excitation and inversion pulses II: RF-power optimized pulses, J. Magn. Reson. 194 (2008) 58–66.
[106] N.I. Gershenzon, K. Kobzar, B. Luy, S.J. Glaser, T.E. Skinner, Optimal control design of excitation pulses that accomodate relaxation, J. Magn. Reson. 188 (2007) 330–336.
[107] K. Kobzar, B. Luy, N. Khaneja, S.J. Glaser, Pattern pulses: design of arbitrary excitation profiles as a function of pulse amplitude and offset, J. Magn. Reson. 173 (2005) 229–235.
[108] T.E. Skinner, N.I. Gershenzon, M. Nimbalkar, W. Bermel, B. Luy, S.J. Glaser, New strategies for designing robust universal rotation pulses: application to broadband refocussing at low power, J. Magn. Reson. 216 (2012) 78–87.
[109] K. Kobzar, S. Ehni, T.E. Skinner, S.J. Glaser, B. Luy, Exploring the limits of broadband 90° and 180° universal rotation pulses, J. Magn. Reson. 225 (2012) 142–160.
[110] S. Ehni, B. Luy, BEBE^{tr} and BUBI: J-compensated concurrent shaped pulses for ^{1}H-^{13}C experiments, J. Magn. Reson. 232 (2013) 7–17.
[111] L. Castañar, J. Saurí, R.T. Williamson, A. Virgili, T. Parella, Pure in-phase heteronuclear correlation NMR experiments, Angew. Chem. Int. Ed. 53 (2014) 8379–8382.
[112] M.J. Thrippleton, J. Keeler, Elimination of zero-quantum interference in two-dimensional NMR spectra, Angew. Chem. Int. Ed. 86 (2003) 3938–3941.
[113] T. Reinsperger, B. Luy, Homonuclear BIRD-decoupled spectra for measuring one-bond couplings with highest resolution: CLIP/CLAP-RESET and constant time-CLIP/CLAP-RESET, J. Magn. Reson. 239 (2014) 110–120.
[114] B. Görling, S. Bräse, B. Luy, HR-HSBC: measuring heteronuclear one-bond couplings with enhanced resolution, Magn. Reson. Chem. 50 (2012) S58–S62.

[115] K. Furihata, M. Tashiro, H. Seto, High resolution-HMBC (HR-HMBC), a new method for measuring heteronuclear long-range coupling constants, Magn. Reson. Chem. 48 (2010) 179–183.
[116] C.M. Thiele, W. Bermel, Speeding up the measurement of one-bond scalar (^{1}J) and residual dipolar couplings (1D) by using non-uniform sampling (NUS), J. Magn. Reson. 216 (2012) 134–143.
[117] K. Fehér, S. Berger, K.E. Kövér, Accurate determination of small one-bond heteronuclear residual dipolar couplings by F1 coupled HSQC modified with a G-BIRD^r module, J. Magn. Reson. 163 (2003) 340–346.
[118] K.E. Kövér, K. Fehér, Measurement of one-bond heteronuclear dipolar coupling contributions for amine and diastereotopic protons, J. Magn. Reson. 168 (2004) 307–313.
[119] M. Ottiger, F. Delaglio, J.L. Marquardt, N. Tjandra, A. Bax, Measurement of dipolar couplings for methylene and methyl sites in weakly oriented macromolecules and their use in structure determination, J. Magn. Reson. 124 (1998) 365–369.
[120] P. Nolis, T. Parella, Solution-state NMR experiments based on heteronuclear cross-polarization, Curr. Anal. Chem. 3 (2007) 47–68.
[121] T.N. Pham, T. Liptaj, K. Bromek, D. Uhrin, Measurement of small one-bond proton-carbon residual dipolar coupling constants in partially oriented ^{13}C natural abundance oligosaccharide samples. Analysis of heteronuclear $^1J_{CH}$-modulated spectra with the BIRD inversion pulse, J. Magn. Reson. 157 (2002) 200–209.
[122] T. Carlomagno, W. Peti, C. Griesinger, A new method for the simultaneous measurement of magnitude and sign of $^1D_{CH}$ and $^1D_{HH}$ dipolar couplings in methylene groups, J. Biomol. NMR 17 (2000) 99–109.
[123] P. Permi, A spin-state-selective experiment for measuring heteronuclear one-bond and homonuclear two-bond couplings from an HSQC-type spectrum, J. Biomol. NMR 22 (2002) 27–35.
[124] E. Miclet, D.C. Williams Jr., G.M. Clore, D.L. Bryce, J. Boisbouvier, A. Bax, Relaxation-optimized NMR spectroscopy of methylene groups in proteins and nucleic acids, J. Am. Chem. Soc. 126 (2004) 10560–10570.
[125] G. Guichard, A. Violette, G. Chassaing, E. Miclet, Solution structure determination of oligoureas using methylene spin state selective NMR at ^{13}C natural abundance, Magn. Reson. Chem. 46 (2008) 918–924.
[126] T. Parella, M. Gairí, Simultaneous recording of spin-state-selective NMR spectra for different InS spin systems, J. Am. Chem. Soc. 126 (2004) 9821–9826.
[127] P. Permi, Two simple NMR experiments for measuring dipolar couplings in asparagine and glutamine side chains, J. Magn. Reson. 153 (2001) 267–272.
[128] E. Miclet, E. O'Neil-Cabello, E.P. Nikonowicz, D. Live, A. Bax, ^{1}H-^{1}H dipolar couplings provide a unique probe of RNA backbone structure, J. Am. Chem. Soc. 125 (2003) 15740–15741.
[129] P. Nolis, J.F. Espinosa, T. Parella, Optimum spin-state-selection for all multiplicities in the acquisition dimension of the HSQC experiment, J. Magn. Reson. 180 (2006) 39–50.
[130] J. Furrer, M. John, H. Kessler, B. Luy, J-spectroscopy in the presence of residual dipolar couplings: determination of one-bond coupling constants and scalable resolution, J. Biomol. NMR 37 (2007) 231–243.
[131] M. Liu, R.D. Farrant, J.M. Gillam, J.K. Nicholson, J.C. Lindon, Selective inverse-detected long-range heteronuclear J-resolved NMR spectroscopy and its application to the measurement of $^3J_{CH}$, J. Magn. Reson. B 109 (1995) 275–283.
[132] L. Ziani, J. Courtieu, D. Merlet, Visualisation of enantiomers via insertion of a BIRD module in X-H correlation experiments in chiral liquid crystal solvent, J. Magn. Reson. 183 (2006) 60–67.

[133] K. Kobzar, H. Kessler, B. Luy, Stretched gelatin gels as chiral alignment media for the discrimination of enantiomers by NMR spectroscopy, Angew. Chem. Int. Ed. 44 (2005) 3145–3147.
[134] D. Uhrin, T. Liptaj, K.E. Kövér, Modified BIRD pulses and design of heteronuclear pulse sequences, J. Magn. Reson. A 101 (1993) 41–46.
[135] J.D. Snider, E. Troche-Pesqueira, S.R. Woodruff, C. Gayathri, N.V. Tsarevsky, R.R. Gil, New strategy for RDCs assisted diastereotopic protons assignment using a combination of J-scaled BIRD HSQC and J-scaled BIRD HMQC/HSQC, Magn. Reson. Chem. 50 (2012) S86–S91.
[136] P. Tzvetkova, S. Simova, B. Luy, P.E. HSQC: a simple experiment for the simultaneous and sign-sensitive measurement of ($^1J_{CH}$ + D_{CH}) and ($^2J_{HH}$ + D_{HH}) couplings, J. Magn. Reson. 186 (2007) 193–200.
[137] J. Saurí, L. Castañar, P. Nolis, A. Virgili, T. Parella, Straightforward measurement of individual ^{1}J(CH) and ^{2}J(HH) in diastereotopic CH2 groups, J. Magn. Reson. 232 (2014) 33–40.
[138] Y. Takayama, D. Sahu, J. Iwahara, Observing in-phase single-quantum ^{15}N multiplets for NH_2/NH_3^+ groups with two-dimensional heteronuclear correlation spectroscopy, J. Magn. Reson. 194 (2008) 313–316.
[139] B.W. Yu, H. van Ingen, S. Vivekanandan, C. Rademacher, S.E. Norris, D.I. Freedberg, More accurate $^1J_{CH}$ coupling measurement in the presence of $^3J_{HH}$ strong coupling in natural abundance, J. Magn. Reson. 215 (2012) 10–22.
[140] B.W. Yu, H. van Ingen, D.I. Freedberg, Constant time INEPT CT-HSQC (CTi-CT-HSQC)—a new NMR method to measure accurate one-bond J and RDCs with strong ^{1}H-^{1}H couplings in natural abundance, J. Magn. Reson. 228 (2013) 159–165.
[141] B.L. Márquez, W.H. Gerwick, R.T. Williamson, Survey of NMR experiments for the determination of nJ(C, H) heteronuclear coupling constants in small molecules, Magn. Reson. Chem. 39 (2001) 499–530.
[142] T. Parella, J.F. Espinosa, Long-range proton-carbon coupling constants: NMR methods and applications, Prog. NMR Spectrosc. 73 (2013) 17–55.
[143] A. Bax, M. Summers, Sensitivity-enhanced detection of heteronuclear multiple-bond connectivity by 2D multiple quantum NMR, J. Am. Chem. Soc. 108 (1986) 2093–2094.
[144] J. Furrer, A comprehensive discussion of HMBC pulse sequences, part 1: the classical HMBC, Concepts Magn. Reson. 40A (2012) 101–127.
[145] J. Furrer, A comprehensive discussion of HMBC pulse sequences, part 2: some useful variants, Concepts Magn. Reson. 40A (2012) 146–169.
[146] J.M. Richardson, J.J. Titman, J. Keeler, D. Neuhaus, Assessment of a method for the measurement of long-range heteronuclear coupling constants, J. Magn. Reson. 93 (1991) 533–553.
[147] R.A.E. Edden, J. Keeler, Development of a method for the measurement of long-range ^{13}C–^{1}H coupling constants from HMBC spectra, J. Magn. Reson. 166 (2004) 53–68.
[148] J. Saurí, T. Parella, J.F. Espinosa, CLIP-HSQMBC: easy measurement of small proton-carbon coupling constants in organic molecules, Org. Biomol. Chem. 11 (2013) 4473–4478.
[149] J.F. Espinosa, P. Vidal, T. Parella, S. Gil, Measurement of long-range proton–carbon coupling constants from pure in-phase 1D multiplets, Magn. Reson. Chem. 49 (2011) 502–507.
[150] S. Gil, J.F. Espinosa, T. Parella, Accurate measurement of small heteronuclear coupling constants from pure-phase α/β HSQMBC cross-peaks, J. Magn. Reson. 213 (2011) 145–150.

[151] D. Uhrín, V. Varma, J.R. Brisson, A Method for measurement of long-range heteronuclear coupling constants from 2D HMQC spectra, J. Magn. Reson. A 119 (1996) 120–124.
[152] J. Saurí, J.F. Espinosa, T. Parella, A definitive NMR solution for a simple and accurate measurement of the magnitude and the sign of small heteronuclear coupling constants on protonated and non-protonated carbon atoms, Angew. Chem. Int. Ed. 51 (2012) 3919–3922.
[153] J. Saurí, P. Nolis, T. Parella, Efficient and fast sign-sensitive determination of heteronuclear coupling constants, J. Magn. Reson. 236 (2013) 66–69.
[154] J. Saurí, T. Parella, On the interference of J_{HH} in HSQMBC-IPAP and HMBC-IPAP experiments, Magn. Reson. Chem. 51 (2013) 509–513.
[155] J. Saurí, T. Parella, Efficient measurement of the sign and the magnitude of long-range proton-carbon coupling constants from a spin-state-selective HSQMBC-COSY experiment, Magn. Reson. Chem. 50 (2012) 717–721.
[156] S. Gil, J.F. Espinosa, T. Parella, IPAP–HSQMBC: measurement of long-range heteronuclear coupling constants from spin-state selective multiplets, J. Magn. Reson. 207 (2010) 312–321.
[157] L. Castañar, J. Saurí, P. Nolis, A. Virgili, T. Parella, Implementing homo- and heterodecoupling in region-selective HSQMBC experiments, J. Magn. Reson. 238 (2014) 63–69.
[158] J. Saurí, L. Castañar, P. Nolis, A. Virgili, T. Parella, P.E. HSQMBC: simultaneous measurement of proton-proton and proton-carbon coupling constants, J. Magn. Reson. 224 (2012) 101–106.
[159] J. Saurí, T. Parella, Simultaneous measurement of J(HH) two different ^{n}J(CH) coupling constants from a single multiple-edited 2D cross-peak, Magn. Reson. Chem. 51 (2013) 397–402.
[160] P. Trigo-Mouriño, A. Navarro-Vázquez, J. Ying, R.R. Gil, A. Bax, Structural discrimination in small molecules by accurate measurement of long-range proton-carbon NMR residual dipolar couplings, Angew. Chem. Int. Ed. 50 (2011) 7576–7580.
[161] K.A.M. Ampt, R.L.E.G. Aspers, P. Dvortsak, R.M. van der Werf, S.S. Wijmenga, M. Jaeger, Determination of size and sign of hetero-nuclear coupling constants from 2D ^{19}F-^{13}C correlation spectra, J. Magn. Reson. 215 (2012) 27–33.
[162] H. Koskela, T. Väänänen, Quantitative determination of aliphatic hydrocarbon compounds by 2D NMR, Magn. Reson. Chem. 40 (2002) 705–715.
[163] S. Heikkinen, M.M. Toikka, P.T. Karhunen, A. Kilpeläinen, Quantitative 2D HSQC (Q-HSQC) via suppression of J-dependence of polarization transfer in NMR spectroscopy: application to wood lignin, J. Am. Chem. Soc. 125 (2003) 4362–4367.
[164] H. Koskela, I. Kilpeläinen, S. Heikkinen, Some aspects of quantitative 2D NMR, J. Magn. Reson. 174 (2005) 237–244.
[165] D.J. Peterson, N.M. Loening, QQ-HSQC: a quick, quantitative heteronuclear correlation experiment for NMR spectroscopy, Magn. Reson. Chem. 45 (2007) 937–941.
[166] H. Koskela, O. Heikkilä, I. Kilpeläinen, S. Heikkinen, Quantitative two-dimensional HSQC experiment for high magnetic field NMR spectrometers, J. Magn. Reson. 202 (2010) 24–33.
[167] P. Giraudeau, Quantitative 2D liquid-state NMR, Magn. Reson. Chem. 52 (2014) 259–272.
[168] E. Martineau, S. Akoka, R. Boisseau, B. Delanoue, P. Giraudeau, Fast quantitative ^{1}H-^{13}C two-dimensional NMR with very high precision, Anal. Chem. 85 (2013) 4777–4783.

[169] A. Mäkelä, I. Kilpeläinen, S. Heikkinen, Quantitative ^{13}C NMR spectroscopy using refocused constant-time INEPT, Q-INEPT-CT, J. Magn. Reson. 204 (2010) 124–130.
[170] R.T. Williamson, A.V. Buevich, G.E. Martin, T. Parella, LR-HSQMBC: a sensitive NMR technique to probe very long-range heteronuclear coupling pathways, J. Org. Chem. 79 (2014) 3887–3894.
[171] M. Reibarkh, R.T. Williamson, G.E. Martin, W. Bermel, Broadband inversion of 1J(CC) responses in 1, n-ADEQUATE spectra, J. Magn. Reson. 236 (2013) 126–133.
[172] G.E. Martin, R.T. Williamson, P.G. Dormer, W. Bermel, Inversion of 1J(CC) correlations in 1, n-ADEQUATE spectra, Magn. Reson. Chem. 50 (2012) 563–568.
[173] M.M. Senior, R.T. Williamson, G.E. Martin, Using HMBC and ADEQUATE NMR data to define and differentiate long-range coupling pathways: is the Crews rule obsolete? J. Nat. Prod. 76 (2013) 2088–2093.
[174] G.E. Martin, K.A. Blinov, M. Reibarkh, R.T. Williamson, 1JCC-edited HSQC-1, n-ADEQUATE: a new paradigm for simultaneous direct and long-range carbon–carbon correlation, Magn. Reson. Chem. 50 (2012) 722–728.
[175] G.E. Martin, B.D. Hilton, K.A. Blinov, HSQC-1,1-ADEQUATE and HSQC-1, n-ADEQUATE: new methods for establishing adjacent and long-range carbon-carbon networks, J. Nat. Prod. 74 (2011) 2400–2407.
[176] R.T. Williamson, A.V. Buevich, G.E. Martin, Using LR-HSQMBC to observe long-range $^{1}H–^{15}N$ correlations, Tetrahedron Lett. 55 (2014) 3365–3366.
[177] S. Cheatham, P. Gierth, W. Bermel, E. Kupče, HCNMBC—a pulse sequence for H-(C)-N multiple bond correlations at natural isotopic abundance, J. Magn. Reson. 247 (2014) 38–41.

4. Summary and Conclusions

In summary, a novel set of modern pure shift NMR and HSQC/HSQMBC experiments have been developed for helping chemists to solve common problems encountered in their daily NMR activities.

Bellow, a brief summary with the main conclusions extracted from the experimental results is exposed:

- A new data collection technique to improve the SNR by one order of magnitude in slice-selective NMR experiments has been presented (**Publication 1**). The method is based on multiple-slice selection into a NMR tube by applying a multiple-frequency pulse simultaneously with a spatial encoding gradient. The experimental procedure to fulfill the sampled frequency requirement is simple and the results can be immediately adapted to a wide range of applications, such as demonstrated for pure shift ZS experiments.

- A new band-selective detection scheme (HOBS) has been proposed to collect homodecoupled NMR spectra of specific regions without sacrificing sensitivity (**Publication 2**). HOBS is especially useful in spectra presenting a set of equivalent spin systems in well-separated and defined regions (for instance, peptides and proteins). The main advantages of HOBS method are:
    - It is a full sensitivity experiment. The sensitivity of standard 1D ^{1}H NMR experiments is retained and even improved because to the collapse of the multiplet pattern to simplified singlets.
    - HOBS spectra present an excellent spectral quality.
    - Data collection is carry out in real-time mode without need of additional reconstruction methods, allowing a conventional FID data processing.

- The implementation of the HOBS approach is easy and reliable for a large number of standard mono- and multidimensional NMR experiments, as reported for:
    - HOBS-TOCSY and HOBS-HSQC (**Publication 2**)
    - HOBS-IR and HOBS-CPMG-PROJECT (**Publication 3**)
    - HOBS-selTOCSY (**Publication 4**)

- HOBS-HSQMBC (**Publication 6**)
- HOBS-HSQC-TOCSY (**Publication 7**)

- The HOBS experiments developed during this work has been used for several practical applications, as for example:
  - The simple measurement of T_1 and T_2 NMR relaxation times in overlapped areas without need of multi-exponential decay analysis or deconvolution methods. (**Publication 3**)
  - To carry out fast enantiodifferentiation studies in presence of CSAs. (**Publication 4**)
  - The direct measurement of heteronuclear coupling constants from simplified in-phase doublets. (**Publication 6**)
  - To carry out the distinction and assignment of highly complex mixtures of similar compounds exhibiting near-identical ^{1}H and ^{13}C NMR spectra. (**Publication 7**)

- The combination of spectral aliasing and pure shift HSQC approaches in SAPS-HSQC experiments represents an excellent routine tool for NMR enantiodifferentiation studies. The enantiodifferentiated data is obtained in short acquisition times and high signal dispersion simultaneously for both ^{1}H and ^{13}C nuclei. Overlapping problems of common 1D ^{1}H experiments are overcome, and poor enantiodifferentiation in 1D experiments can now be detected, allowing the study of cases abandoned in the past for reasons of poor enantioresolution and/or long experimental times. (**Publication 7**)

- In **Publication 8**...
  - It has been demonstrated that the use of an adiabatic *z*-filter is an extremely useful NMR element to suppress unwanted homo- and heteronuclear anti-phase contributions in HSQC and HSQMBC experiments. The improvement achieved is more spectacular in the long-range heteronuclear correlation experiments where the effects of the J_{HH} evolution are more pronounced.

- The proposed broadband PIP-HSQC and PIP-HSQMBC experiments yield undistorted in-phase cross peaks, which improve spectral quality and facilitate spectral analysis.

- PIP-HSQC and PIP-HSQMBC experiments have been applied to the measurement of homonuclear (J_{HH}) and direct ($^{1}J_{CH}$) and long-range ($^{n}J_{CH}$; n>1) heteronuclear scalar and residual (D_{HH}; $^{1}D_{CH}$; $^{n}D_{CH}$) coupling constants in isotropic and/or anisotropic media. The clean in-phase character displayed by the cross-peaks allows a direct and easy determination of $^{1}J_{CH}$/$^{n}J_{CH}$ and $^{1}D_{CH}$/$^{n}D_{CH}$. The proposed experiments are fully compatible with the IPAP methodology allowing the measurement of small coupling heteronuclear constants even in complex or non-resolved multiplets.

- The proposed methods can be recorded in full automation mode without any prior calibration and they offer a general implementation on a large variety of isotropic and anisotropic sample conditions.

- In **Publication 9**...

  - A perfect-INEPT block has been implemented in HSQC experiments to avoid any interference as a result of J_{HH} coupling constant evolution. It has been shown theoretically and experimentally that during the perfect-INEPT element the magnetization evolution under the effect of the J_{HH} is refocused.

  - It has been show that the resulting cross-peaks of the perfect-HSQC spectra exhibit pure in-phase multiplet pattern, irrespective of the experiment optimization. These uniform and predictable responses are more amenable to an accurate and quantitative analysis than what is encountered with the results of standard HSQC pulse sequence.

  - Particular emphasis has been made in the application of the proposed perfect-HSQC experiment in the accurate determination of homonuclear (J_{HH}) and one-bond heteronuclear scalar ($^{1}J_{CH}$) and residual (D_{HH}; $^{1}D_{CH}$) coupling constants in isotropic and/or anisotropic media.

  - It has been demonstrated that in perfect-HSQC experiments the final in-phase detected signal is only modulated by $\sin^2(\pi^n J_{H_1C}\Delta)$, which opens the opportunity to design quantitative NMR application.

- In **Publication 10**...
  - A compilation of novel HSQC experiments have been made, including a discussion of the new family of HSQC experiments developed in this thesis: pure shift HSQC (ps-HSQC-PEP, HOBS-HSQC, SAPS-HSQC) as well as the perfect-HSQC and PIP-HSQC experiments.
  - Similarly, a comprehensive analysis of HSQMBC experiments has been also performed, with detailed discussion on the new HOBS-HSQMBC and PIP-HSQMBC experiments developed in this thesis.

5. APPENDIX

This section contains some work carried out along this doctoral thesis which cannot be included as Publications. The reasons for which have not been included are:

- **Publication 11** and **Publication 12** were part of the Ph.D. thesis of Dr. Josep Saurí entitled "*Modern NMR methodologies for the measurement of homo- and heteronuclear coupling constants in small molecules*" which was presented in May 2014.

- **Publication 13** is a complete revision work about the recent developments and application of modern pure shift NMR experiments.

PUBLICATION 11

P.E.HSQMBC: Simultaneous measurement of proton-proton and proton-carbon coupling constants

Josep Saurí, Pau Nolis, Laura Castañar, Albert Virgili and Teodor Parella.
J. Magn. Reson., **2012**, *224*, 101-16.
DOI: 10.1016/j.jmr.2012.09.007

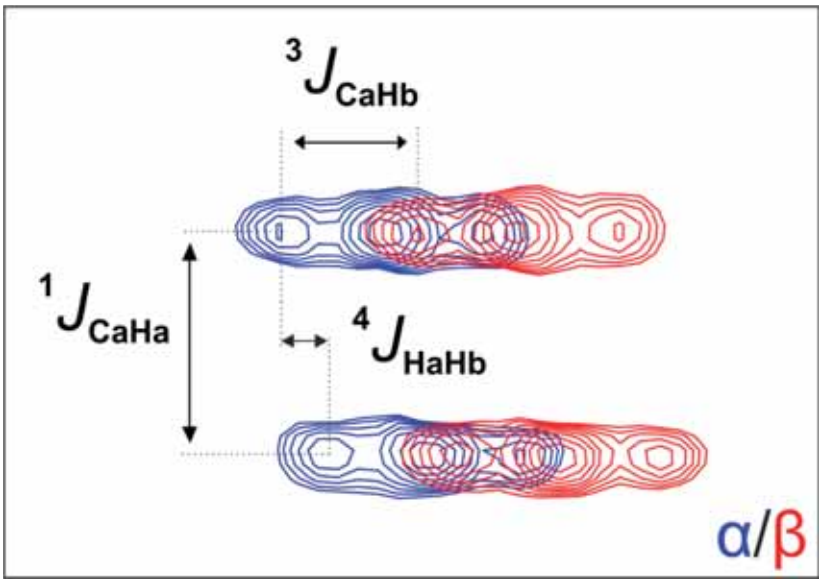

Introduction

In this publication, a new proton-selective NMR experiment, denoted as *Pure Exclusive* HSQMBC (P.E.HSQMBC), is presented to measure simultaneously $^{n}J_{HH}$, $^{1}J_{CH}$ and $^{n}J_{CH}$ coupling constants in a three $^{1}H_a$-$^{1}H_b$-^{13}C spin system. In addition, the experiment is also able to extract the relative sign of the $^{n}J_{HH}$ coupling constants.

The pulse scheme is based on the existing P.E.HSQC experiment,[67d] but optimized to long-range proton-carbon correlations instead of one-bond correlations. The experiment uses selective proton pulses to avoid any unwanted J_{HH} modulation during the INEPT periods. Additionally, it is shown how the concepts of *J*-resolved spectroscopy and the *Exclusive COrrelation SpectroscopY* (E.COSY) principle[97] can be fully complementary to the IPAP technique and they all can be incorporated into the same NMR experiment. In this way, several coupling constants can be simultaneous measured from a single 2D cross-peak.

The main goal of the P.E.HSQMBC experiment is to take profit of the large $^{1}J_{CH}$ value, which is used as a passive coupling constant, to generate a large splitting in the indirect dimension of 2D cross-peaks. The E.COSY pattern, which is generated by a small-flip (36^{o}) ^{1}H pulse, allows extract the magnitude and the sign of J_{HH}. The method also uses the IPAP technique along the detected dimension to get an accurate measurement of $^{n}J_{CH}$, as described in the original selHSQMBC experiment.[78]

[97] a) C. Griesinger, O. W. Sorensen, R. R. Ernst. *J. Am. Chem. Soc.*, **1985**, *107*, 6394. b) C. Griesinger, O. W. Sorensen, R. R. Ernst. *J.Chem. Phys.*, **1986**, *852*, 6837.

Journal of Magnetic Resonance 224 (2012) 101–106

Contents lists available at SciVerse ScienceDirect

Journal of Magnetic Resonance

journal homepage: www.elsevier.com/locate/jmr

P.E.HSQMBC: Simultaneous measurement of proton–proton and proton–carbon coupling constants

Josep Saurí [a], Pau Nolis [a], Laura Castañar [a,b], Albert Virgili [b], Teodor Parella [a,b,*]

[a] Servei de Ressonància Magnètica Nuclear, Universitat Autònoma de Barcelona, E-08193 Bellaterra, Barcelona, Spain
[b] Departament de Química, Universitat Autònoma de Barcelona, E-08193 Bellaterra, Barcelona, Spain

ARTICLE INFO

Article history:
Received 12 July 2012
Revised 10 September 2012
Available online 25 September 2012

Keywords:
HSQMBC
E.COSY
Proton–proton coupling constants
Long-range proton–carbon coupling constants
IPAP

ABSTRACT

A long-range optimized P.E.HSQC experiment, named P.E.HSQMBC, is proposed for the simultaneous measurement of a complete set of homonuclear and heteronuclear coupling constants from a single 2D cross-peak. The sign and the magnitude of proton–proton coupling constants are measured along the direct dimension from the relative E.COSY-type multiplet pattern displacement due to the passive one-bond coupling constant splitting generated in the indirect dimension. On the other hand, long-range proton–carbon coupling constants are independently determined in the detected dimension from a traditional fitting analysis of antiphase multiplet patterns or, more conveniently, from the IPAP multiplet displacement obtained from extended HSQMBC experiments.

1. Introduction

The determination of homonuclear and heteronuclear coupling constants is of prime importance in the structural and conformational studies of molecules in solution. Not only do *J*-couplings contain information about chemical connectivity, they also contain structural information as known for the typical Karplus-like dependence that exhibits ^3J vs dihedral angles. In addition, it has well been recognized during the last years that residual dipolar couplings (RDCs), as measured by solution state NMR, carry important structural information regarding internuclear vector orientation relative to the principal axis system of the molecule's alignment tensor [1].

Homonuclear proton–proton coupling constants, J(HH), can usually be determined by a variety of simple NMR methods, but the precise measurement of heteronuclear small long-range (^nJ(CH); $n > 1$) has not been so evident [2,3]. HSQC-TOCSY experiments becomes a sensitive and accurate approach to provide both the sign and the magnitude of ^nJ(CH) for protonated carbons [4–6]. On the other hand, NMR pulse schemes mainly based on the HMBC and HSQMBC experiments have been widely accepted to determine them on quaternary carbons [6–8]. However, the major inconvenient of this latter approach is the need for a post-processing fitting procedure by using the shape and intensity of signals simultaneously [6,9] to analyze the anti-phase nature of each multiplet pattern and the accuracy of the measurement is often questioned. Recently, IPAP versions have been suggested to avoid this fitting analysis by recording a series of refocused HSQMBC experiments to obtain complementary In-Phase (IP) and Anti-Phase (AP) data that are suitable to provide simplified spin-state selective multiplets after data addition/subtraction [10–13]. In this way, accurate and direct measurement of ^nJ(CH) can be made with simplicity even for complex multiplets. This IPAP approach has been also proposed to measure carbon–carbon coupling constants [14,15].

In addition to the IPAP technique, other different NMR approaches have been proposed to extract homo- and heteronuclear coupling constants from heteronuclear correlations experiments as, for instance, the elegant E.COSY (Exclusive Correlation Spectroscopy) principle [16]. The major advantages to analyze E.COSY-type multiplets are: (i) very easy interpretation; (ii) are suited equally well for the measurement of small and large coupling values, (iii) it provides information about the sign analyzing the relative slope of cross peaks components, (iv) works well even for coupling constants smaller than the NMR line width, (v) J values are measured from the direct dimension where good resolution requirements are more easily reached. Several E.COSY-type methods have been proposed for the simultaneous measurement of different scalar and residual dipolar couplings in small molecules. For instance, a simple and sensitive P.E.HSQC experiment, closely related to a fully coupled non-refocused HSQC pulse scheme, has been proposed to determine the sign and the magnitude of one-bond proton–carbon

* Corresponding author at: Servei de Ressonància Magnètica Nuclear, Universitat Autònoma de Barcelona, E-08193 Bellaterra, Barcelona, Spain.
E-mail address: teodor.parella@uab.cat (T. Parella).

1090-7807/$ - see front matter © 2012 Elsevier Inc. All rights reserved.
http://dx.doi.org/10.1016/j.jmr.2012.09.007

(^1J(CH) and ^1D(CH)) and two-bond proton–proton (^2J(HH) and ^2D(HH)) coupling constants from a single 2D spectrum [17]. Recently a spin-flip HSQC experiment has also been proposed for the simultaneous measurement of J(HH) and ^nJ(CH) [18]. Although this later technique is a proton-selective method that only works for protonated carbons, it has been proved that the addition of accurate long-range CH RDCs can significantly improve the structural discrimination power in complex small molecules with multiple stereogenic centers.

In what follows, we show a variant of the mentioned P.E.HSQC experiment, referred here as P.E.HSQMBC, for the simultaneous and accurate measurement of multiple J(HH), ^1J(CH) and ^nJ(CH) coupling constants. In this long-range ^1H–^{13}C correlation experiment, the large heteronuclear ^1J(CH) coupling constant is employed for separating two multiplet patterns along the indirect F_1 dimension while homonuclear HH couplings can be accurately measured from their relative E.COSY-type displacements in the detected F_2 dimension. The experiment closely relates to the XLOC experiment, a long-range correlation experiment designed to measure J(HH) in a similar E.COSY way [19–21]. Furthermore, we also present and discuss several options to extract ^nJ(CH) values at the same time and it will be shown that both E.COSY and IPAP principles can be implemented into the same pulse scheme to simultaneous measure different coupling constants from the same 2D multiplet with an extreme simplicity.

2. Results and discussion

Three different NMR pulse sequences suitable for an E.COSY version of the HSQMBC experiment are presented in Fig. 1. They combine the main features of three different older methods in a single experiment: (a) the accurate measurement of ^1J(CH) along the indirect dimension from F1-coupled HSQC schemes [22–25]; (b) the sign-sensitive measurement of ^1J(CH) and ^2J(HH) in E.COSY multiplets as reported in the P.E.HSQC experiment [17], and (c) the precise measurement of ^nJ(CH) using the IPAP technology in selHSQMBC experiments [11]. For the present work, we have chosen the general application of selective 180° ^1H pulses as a refocusing element in the INEPT block because this affords pure-phase multiplets and completely avoids any signal modulation due to J(HH).

The simplest pulse sequence is essentially a small-flip-angle non-refocused HSQC experiment where all CH coupling constants evolve freely during the entire t_1 period and the read ^1H pulse before acquisition is set to $\beta = 36°$ to achieve simplified multiplet structure. As described in the original P.E.HSQC experiment [17], instead of the long phase cycling schemes used in classical experiments, a simple small-angle pulse is used to generate the E.COSY-like pattern (Fig. 1A). In order to explain how pulse sequences work and describe the nature of multiplets generated in the proposed P.E.HSQMBC experiment, we concentrate the description on a heteronuclear three-spin system involving two active (H2 and C1) and a single passive (H1) spins (Scheme 1). These active spins having a long-range ^nJ(H2–C1) coupling determine the position of the cross-peak multiplet at (δ(H2), δ(C1)) which consists of two different components separated by the large ^1J(H1–C1) splitting along the F1 dimension. The magnitude and the sign of the J(H2–H1) coupling constant can be easily extracted comparing the relative displacement and the slope, respectively, between these two different rows in the detected F2 dimension (Fig. 2A). On the other hand, each row component of these E.COSY multiplets will present the characteristic antiphase pattern with respect to ^nJ(H2–C1) and pure in-phase character with respect all passive J(HH) couplings. The magnitude of ^nJ(H2–C1) must be extracted using well-established fitting algorithms that will not be discussed in detail here [6–9].

A modified P.E.HSQMBC version in where a BIRD^r cluster is incorporated into the carbon evolution period to suppress unwanted ^nJ(CH) contributions in the indirect dimension is shown in Fig. 1B. This option also offers the possibility to scale the ^1J(CH) splitting by a scaling factor k that strongly minimizes the resolution requirements and the number of t_1 increments to be acquired. This approach becomes particularly useful to obtain well defined multiplets in the indirect dimension that lead to precise measurement of scalar ^1J(CH) and/or dipolar ^1D(CH) values for weakly aligned samples. In analogy to the above description, this version also provides two separate cross peaks separated by $k * {}^1J$(CH) in the F1 dimension whereas ^nJ(CH) present the same AP features described above (Fig. 2B).

Finally, a refocused P.E.HSQMBC version has been developed to facilitate the measurement of ^nJ(CH) using the IPAP technique (Fig. 1C). Filtering the downfield and upfield doublet components into separate spectra is a successful concept to avoid the tedious analysis of anti-phase multiplets. This version can be understood as a F1-coupled analog of the recently proposed selHSQMBC experiment and although it suffers of a worse sensitivity due to the additional refocusing period, the magnitude of ^nJ(CH) can be extracted more accurately by the analysis of relative displacement of α/β cross-peaks in the detected dimension (see Fig. 2C). This more user-friendly method combines the principles of E.COSY and IPAP methodologies into a single NMR experiment whereas retains all the benefits described for the original selHSQMBC experiment [11].

Several details about sensitivity, multiplet patterns and relative pulse phases must be highlighted in order to explain the observed experimental data. Very importantly, two different mechanisms are present in the basic pulse scheme of Fig. 1A. First, the traditional pathway generated from the initial ^1H Boltzmann magnetization through the initial proton-selective INEPT transfer leads to two observable terms at the end of the t_1 period:

$$2H_{2y}C_{1z}\sin(\pi J_{H2-C1}\Delta)\cos(\pi J_{H2-C1}t_1)\cos(\pi J_{H1-C1}t_1) \quad (1a)$$

$$2H_{1y}C_{1z}\sin(\pi J_{H2-C1}\Delta)\sin(\pi J_{H2-C1}t_1)\sin(\pi J_{H1-C1}t_1) \quad (1b)$$

Thus, two different cross-peaks at δ(C1) appear showing pure anti-phase character with respect to J(H2–C1) in the F2 dimension: (i) a long-range H2–C1 correlation showing in-phase ^1J(CH) pattern and (ii) a direct H1–C1 cross-peak showing anti-phase ^1J(CH) pattern in the F1 dimension. The number of lines in the indirect dimension will depend on carbon multiplicity: CH appears as doublets, CH_2 as triplets and CH_3 as quartets with their intensities as described previously whereas quaternary carbons will not show splitting.

On the other hand, the original magnetization belonging to ^{13}C Boltzmann distribution also contributes to the final spectrum independently of the Δ delay and the selective proton pulse, in the form of the following term:

$$2H_{1y}C_{1z}\sin(\pi J_{H1-C1}t_1) \quad (2)$$

This pathway provides all direct correlations showing anti-phase pattern with respect to ^1J(CH) in both dimensions independently of the selective nature of the INEPT block and therefore, the measurement of the sign and the magnitude of all ^1J(CH) and ^2J(HH) couplings can be performed as exactly described for the regular P.E.HSQC experiment [17].

These two different pathways can be separately obtained by a proper phase cycling of the 90° proton pulse labeled with ϕ_2 phase. Thus, the separate acquisition of two complementary data acquired with the pulse scheme of Fig 1A and with $\phi_2 = y$ and $\phi_2 = -y$ afford the same spectrum but with inverted phase for components coming from INEPT transfer (Fig. 3A and B, respectively). Conventional data addition/subtraction affords independent

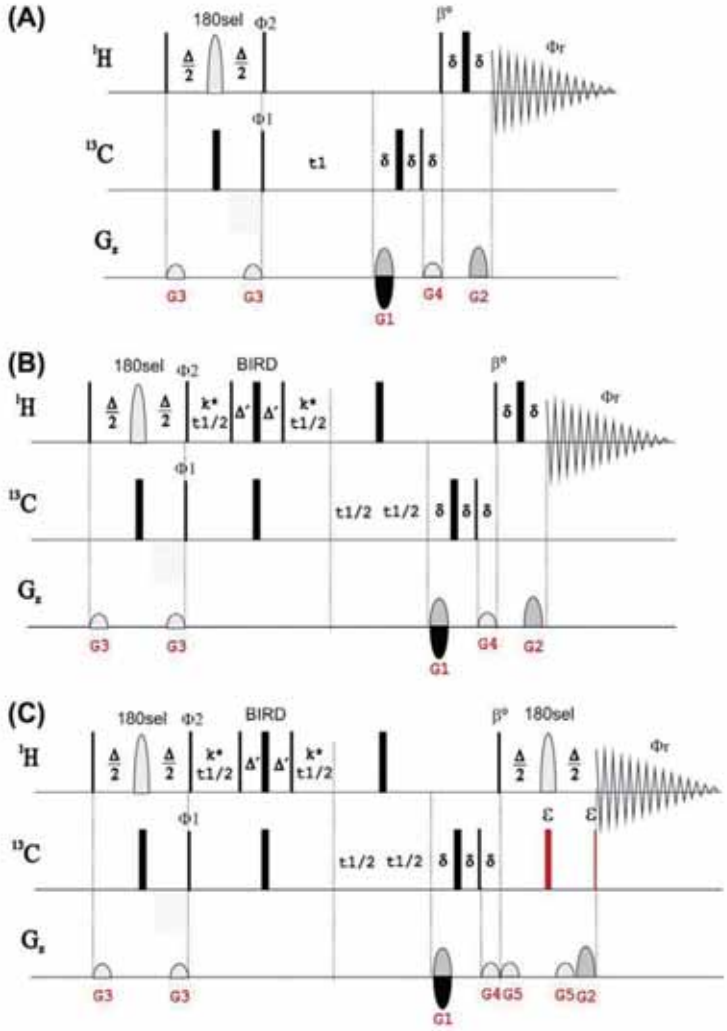

Fig. 1. Pulse sequences for the simultaneous determination of J(HH) and ^nJ(CH). Narrow and wide filled bars represent 90° and 180° pulses (unless the flip angle β = 36° is indicated), respectively, while half-ellipsoids denote ^{1}H-selective 180° pulses (p_{180}): (a) non-refocused fully-coupled P.E.HSQMBC sequence; (b) non-refocused fully-coupled P.E.HSQMBC sequence incorporating an ^1J(CH)-scalable BIRD^r module (scaling factor k) that allows the selective evolution of ^1J(CH) whereas refocuses all ^nJ(CH) components during the variable evolution t_1 period; (c) refocused IPAP version based on the separate acquisition of In-Phase (IP:ε = on) and Anti-Phase (AP:ε = off) data that are further combined to provide separate α- and β-P.E.HSQMBC spectra. The interpulse delays are optimized to $\Delta + p_{180} = 1/(2 \cdot {}^nJ(\mathrm{CH}))$ and $\Delta' = 1/(2 \cdot {}^1J(\mathrm{CH}))$. δ stands for the duration of each gradient and the recovery delay. The minimum phase cycle is $\phi_1 = x,-x$ and $\phi_r = x,-x$. See text for the importance of the phase ϕ_2: it is set to $\phi_2 = y$ for non-editing and $\phi_2 = y,y,-y,-y$ for editing of P.E.HSQC and P.E.HSQMBC data. Gradients G1 and G2 are used for coherence selection using echo-antiecho protocol, G3 and G5 are used for proper refocusing and G4 for zz-selection.

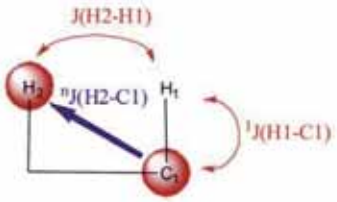

Scheme 1. Schematic representation of the spin-coupling networks involved in the simultaneous determination of ^1J(CH), J(HH) and ^nJ(CH). The blue arrow indicates the active H2–C1 coupling which is essential for coherence transfer. The desired E.COSY multiplet structure is caused by the large splitting of ^1J(H1C1) due to the spin passive H1 along the indirect dimension. Fig. 2 summaries the multiplet patterns obtained from each proposed experiment and how couplings can be measured. (For interpretation of the references to color in this figure legend, the reader is referred to the web version of this article.)

P.E.HSQC (Fig. 3C) and P.E.HSQMBC (Fig. 3D) spectra. Otherwise, the corresponding P.E.HSQMBC spectra could also be obtained directly by performing the subtraction during acquisition by applying a four-step phase cycling with $\phi_2 = y,y,-y,-y$. In this case, a 90°(^{13}C)-gradient element just before the initial 90° ^{1}H pulse helps to efficiently remove unwanted ^{13}C Boltzmann contribution.

P.E.HSQC data are analyzed exactly as described in the original experiment and no more details will be given here. On the other hand, Fig. 4 shows an expansion of the column corresponding to the H15b proton in the P.E.HSQMBC spectrum. The direct correlation, that is visible because the selective pulse also excites the satellite lines, shows pure in-phase character in the indirect F1 dimension. It is clearly shown that is possible to differentiate the corresponding active ^1J(H15b–C15) and the passive ^1J(H15a–C15)

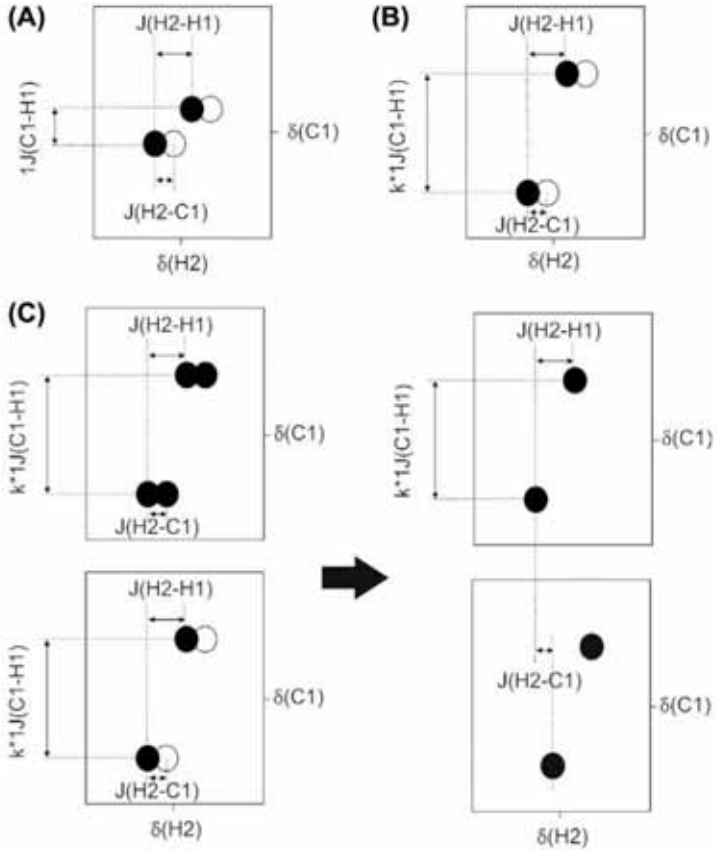

Fig. 2. (A–C) Schematics representing the expected multiplet patterns obtained from sequences of Fig. 1A, B and C, respectively. Filled and open circles represent multiplet components with opposite phase. In all cases, J(HH) is measured from the E.COSY pattern. On the other hand, ^nJ(CH) must be extracted from the analysis of anti-phase multiplet patterns in the same row (in A and B), or from the relative displacement between two components that are separated in two separate spin-state selected spectra (see C).

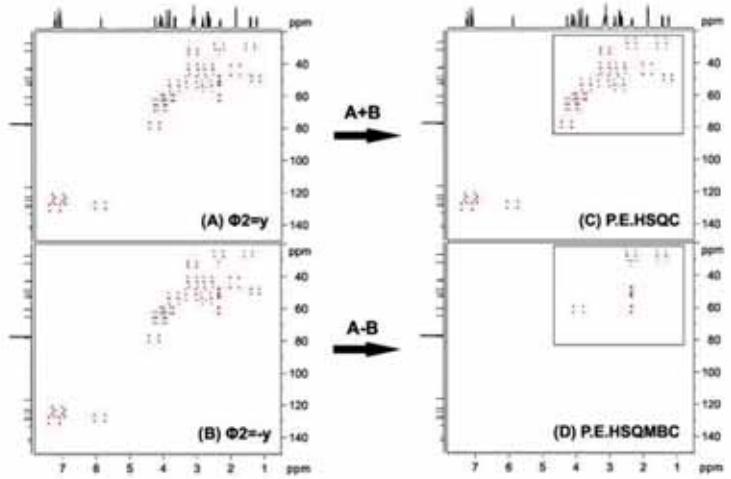

Fig. 3. General scheme to obtain separate P.E.HSQC and P.E.HSMBC spectra after selective refocusing of H15b proton (resonating at 2.35 ppm) of strychnine using the scheme of Fig. 1B. Two different data are independently acquired only changing the phase of the 90° proton pulse just applied after the t_1 period (A) using $\Phi_2 = y$ and (B) $\Phi_2 = -y$ whereas other relevant phase remain unchanged ($\Phi_1 = x,-x$ and $\Phi_r = x,-x$). After addition and subtraction of these data, two separate (C) P.E.HSQC and (D) P.E.HSQMBC spectra are obtained to determine ^1J(CH), J(HH) and ^nJ(CH). The scaling factor was set to $k = 3$ and the experiment optimized to 8 Hz.

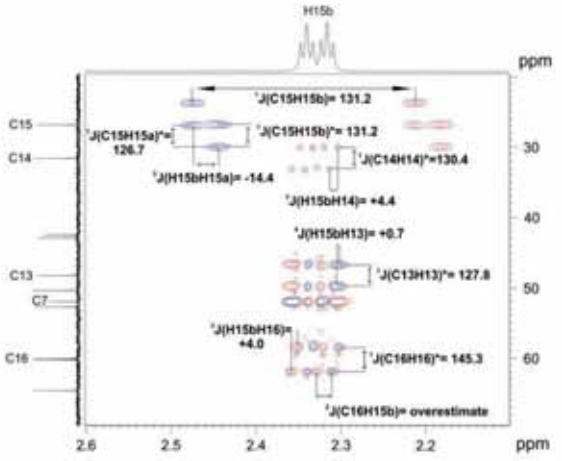

Fig. 4. Expanded region of the P.E.HSQMBC spectrum showing the column corresponding to the H15b proton (see Fig. 3D). Note that from the direct correlation, the relative sign between ^2J(HH) and ^1J(CH) can be obtained. From the other cross-peaks the sign and magnitude of ^3J(HH) can be extracted. The analysis of an specific row for the direct determination of ^nJ(CH) is not advisable due to an overestimation and a conventional fitting procedure is required.

in diastereotopic CH_2 spin systems as well as to the sign and magnitude of the geminal and passive J(H15b–H15a) coupling value. Additional H15b cross-peaks are also observed for the methines C14, C13 and C16 carbons and for the quaternary C7 carbon. The well-resolved doublets in F1 for each CH cross-peak evidences the relative displacement between them along the F2 dimension, allowing the measurement of both magnitude and sign of the corresponding J(HH) as a function of the observed signal tilting. On the other hand, each individual row displays a pure anti-phase pattern with respect to the active ^nJ(CH) that can be analyzed accordingly. The anti-phase nature structure of cross-peaks can cause partial intensity losses when the active scalar coupling is within the line width.

For this reason, a refocused version that uses the IPAP principle is proposed (Fig. 1C) for a much better and more user-friendly measurement on ^nJ(CH). Fig. 5 illustrates the experimental protocol to acquire, to process and to analyze these P.E.HSQMBC data taking the H15b–C16 cross-peak as an example. Two complementary IP and AP data are separately acquired as shown in Fig. 5A and B, respectively. Although J(HH) could already be measured in any of these spectra from the E.COSY pattern, the extraction of ^nJ(CH) would usually require an individual fitting analysis for each cross-peak. Sum and difference data (Fig. 5C and D) contain only the upfield and downfield components of the active doublet which makes it possible the straightforward measurement of ^nJ(CH) by analyzing the relative displacement between them. However, in analogy to the regular selHSQMBC experiment the sign information of ^nJ(CH) is not available from this analysis. In our hands, the use of a scaling factor of $k = 3$ is a good compromise to clearly resolve ^1J(CH) multiplet components in the indirect dimension using 256 t_1 increments. On the other hand, the non-equivalence between IP and AP data can afford undesired J-cross talk contributions that can introduce some error in the measurement. The use of an individualized scaling k' factor in the form of AP ± k' * IP can be used to correct them. The tolerance on these cross-talk effects has already been discussed previously [10,11].

A limitation of the proposed experiments is its ^{1}H-selective nature and therefore multiple experiments should be needed for a global determination of coupling values in a molecule. However, the extraction of ^nJ(CH) from multiple protons can be simultaneously obtained by applying the principles of multiple-site or band-selective excitation. Fig. 6 shows an example after selective refocusing of several protons that are not mutually coupled and acquired under the same experimental conditions as described in Fig. 3.

In summary, it has been shown that the concepts of J-resolved, E.COSY and IPAP principles can be mixed all together into the same pulse scheme in order to measure multiple coupling constants from a single 2D cross-peak analysis. We have developed a method that leads to the accurate measurement of both J(HH) and ^nJ(CH)

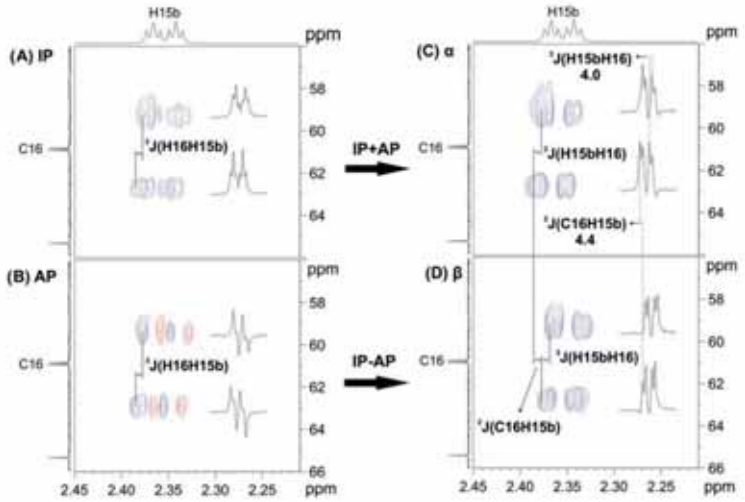

Fig. 5. Expanded areas corresponding to the H15b–C16 cross peak in the IPAP-selHSQMBC-E.COSY experiment acquired with the same experimental conditions as discussed in Fig. 3 and using pulse scheme of Fig. 1C. Two different data are acquired using the IPAP principle: (A) IP with the phase of β° pulse set to y and applying the pulses labeled with ε (on); (B) AP with the phase of β° pulse set to x and omitting the pulses ε (off). Time-domain data addition/subtraction followed by conventional processing afford complementary (C) α- and (D) β-selHSQMBC-E.COSY spectra from which the ^nJ(CH) value can be directly extracted in a simple way by analyzing the relative left/right displacement of signals in the F2 dimension.

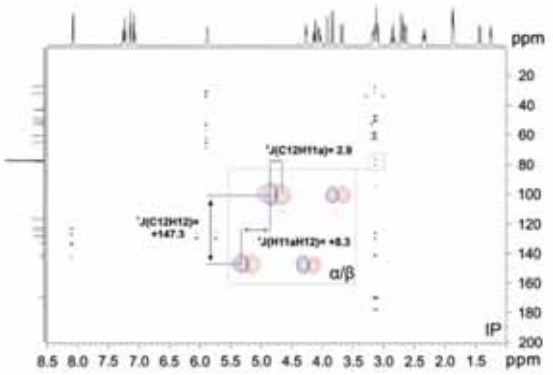

Fig. 6. Example showing the advantage to use multiple-site selective excitation in the P.E.HSQMBC experiment using shifted laminar pulses of non-mutually coupled protons. Different protons (H4 (8.15 ppm), H22 (5.9 ppm) and H11a/H18a/H14 (all three resonating near to 3.15 ppm)) were simultaneously refocused using a 40 ms Gaussian-shaped 180° proton pulse. The 2D spectrum corresponds to the In-Phase (IP) data and the inset shows the separate α/β data corresponding to the H11a–C12 cross peak.

from the high resolution obtained in the detected dimension whereas ^1J(CH) is precisely resolved in the indirect dimension. The proper combination of multiple proton excitation and non-uniform sampling can allow a faster measurement of all these couplings in small and medium size molecules. Alternatively, the experiment could be also implemented in a broadband mode, using for instance a CPMG-BIRD element instead of the selective INEPT block [26–28]. However, complete suppression of proton–proton coupling evolution and undesired sample heating remains to be solved. Much work is in progress to extrapolate all these concepts to the simultaneous measurement of the sign and magnitude of different types of heteronuclear coupling constants.

3. Methods and materials

All NMR experiments have been recorded on a BRUKER DRX-500 spectrometer equiped with a 3-channel 5-mm cryoprobe incorporating a *z*-gradient coil on a sample of 25 mg of strychnine, **1**, dissolved in 0.6 ml of $CDCl_3$. All experiments were optimized to 8 Hz, that means that ^nJ(CH) evolves during a period of $\Delta + p_{180} = 1/(2 * {}^nJ_{CH})$; where p_{180} is a selective 180° ^{1}H pulse. A Gaussian-shaped 180° pulse of duration of 20 ms (p_{180}) was used as a selective refocusing. The recycle and the interpulse BIRD^r ($\Delta' = 1/(2 * {}^1J(CH))$ delays were set to 1 s and 3.6 ms, respectively. An scaling factor $k = 3$ were used. Sine bell shaped gradients of 1 ms duration (δ) were used, followed by a recovery delay of 100 μs. Gradient ratios for G1:G2:G3:G4:G5:G6 were 80:20.1:33:50:11:17, measured as percentage of the absolute gradient strength of 5.35 G/cm.

All experiments were acquired and processed using the echo/anti-echo protocol. Quadrature detection is achieved inverting the G1and G2 gradient pulses for every second FID. Four scans were accumulated for each one of the 256 t_1 increments and the number of data points in t_2 was set to 4096. Spectral windows in both dimensions were 22500 (F1) and 4500 (F2) Hz, respectively. Prior to Fourier-transformation of each data, zero filling to 1024 in F1, 8192 points in F2 and a sine squared function in both dimensions were applied.

2D ^{1}H–^{13}C IP and AP-HSQMBC experiments of Fig. 5 were separately recorded using the same experimental conditions described in Fig. 4. The overall acquisition time for each individual IP and AP data was about 26 min which were added/subtracted in the time-domain without any scaling factor to provide spin-state selective data. Finally, the same conditions were applied for the spectra shown in Fig. 6 except for the selective refocusing. A 40 ms multiple-site pulse applied to three different frequencies was automatically generated using the shape tool package included into Tospin software (see captions for more details).

Acknowledgments

Financial support for this research provided by MICINN (Projects CTQ2009-08328 and Consolider Ingenio-2010 CSD2007-00006) and Bruker Española S.A. is gratefully acknowledged. We also thank to the Servei de Ressonància Magnètica Nuclear, Universitat Autònoma de Barcelona, for allocating instrument time to this project.

References

[1] C. Thiele, Eur. J. Org. Chem. (2008) 5673–5685.
[2] B.L. Márquez, W.H. Gerwick, R.T. Williamson, Magn. Reson. Chem. 39 (2001) 499–530.
[3] T. Parella, 2D methods for the measurement of long-range proton–carbon coupling constants, in: G.A. Morris, J.W. Emsley (Eds.), Multidimensional NMR Methods for the Solution State, vol. 305, John Wiley & Sons Ltd., Chichester, UK, 2010.
[4] P. Nolis, J.F. Espinosa, T. Parella, J. Magn. Reson. 180 (2006) 39–50.
[5] W. Koźmiński, J. Magn. Reson. 137 (1999) 408–412.
[6] K. Kobzar, B. Luy, J. Magn. Reson. 186 (2007) 131–141.
[7] M.J. Thrippleton, J. Keeler, Angew. Chem., Int. Ed. 42 (2003) 3938–3941.
[8] R.T. Williamson, B.L. Márquez, W.H. Gerwick, K.E. Kövér, Magn. Reson. Chem. 38 (2000) 265–273.
[9] L. Verdier, P. Sakhaii, M. Zweckstetter, C. Griesinger, J. Magn. Reson. 163 (2003) 353–359.
[10] S. Gil, J.F. Espinosa, T. Parella, J. Magn. Reson. 207 (2010) 312–321.
[11] S. Gil, J.F. Espinosa, T. Parella, J. Magn. Reson. 213 (2011) 145–150.
[12] J. Saurí, J.F. Espinosa, T. Parella, Angew. Chem., Int. Ed. 51 (2012) 3919–3922.
[13] D. Uhrín, V. Varma, J.R. Brisson, J. Magn. Reson. A 119 (1996) 120–124.
[14] K.E. Kövér, M. Lenoir, D. Uhrín, J. Magn. Reson. 190 (2008) 171–182.
[15] L. Jin, D. Uhrín, Magn. Reson. Chem. 45 (2007) 628–633.
[16] C. Griesinger, O.W. Sørensen, R.R. Ernst, J. Am. Chem. Soc. 107 (1985) 6394–6396.
[17] P. Tzvetkova, S. Simova, B. Luy, J. Magn. Reson. 186 (2007) 193–200.
[18] P. Trigo-Mouriño, A. Navarro-Vázquez, J. Ying, R.R. Gil, A. Bax, Angew. Chem., Int. Ed. 50 (2011) 7576–7580.
[19] M.D. Sørensen, J.J. Led, O.W. Sørensen, J. Biomol. NMR 4 (1994) 135–141.
[20] A. Meissner, O.W. Sørensen, Magn. Reson. Chem. 39 (2001) 49–52.
[21] A. Meissner, J.ø Duus, O.W. Sørensen, J. Magn. Reson. 128 (1997) 92–97.
[22] C. Thiele, W. Bermel, J. Magn. Reson. 216 (2012) 134–143.
[23] J. Furrer, M. John, H. Kessler, B. Luy, J. Biomol. NMR 37 (2007) 231–243.
[24] K. Fehér, S. Berger, K.E. Kövér, J. Magn. Reson. 163 (2003) 340–346.
[25] K.E. Kövér, K. Fehér, J. Magn. Reson. 168 (2004) 307–313.
[26] H. Koskela, I. Kilpeläinen, S. Heikkinen, J. Magn. Reson. 164 (2003) 228–232.
[27] K.E. Kövér, G. Batta, K. Fehér, J. Magn. Reson. 181 (2006) 89–97.
[28] S. Boros, K.E. Kövér, Magn. Reson. Chem. 49 (2011) 106–110.

PUBLICATION 12

Straightforward measurement of individual $^1J_{CH}$ and $^2J_{HH}$ in diastereotopic CH_2 groups

Josep Saurí, Laura Castañar, Pau Nolis, Albert Virgili and Teodor Parella.
J. Magn. Reson. ,**2014**, *242*, 33-40.
DOI: 10.1016/j.jmr.2014.02.003

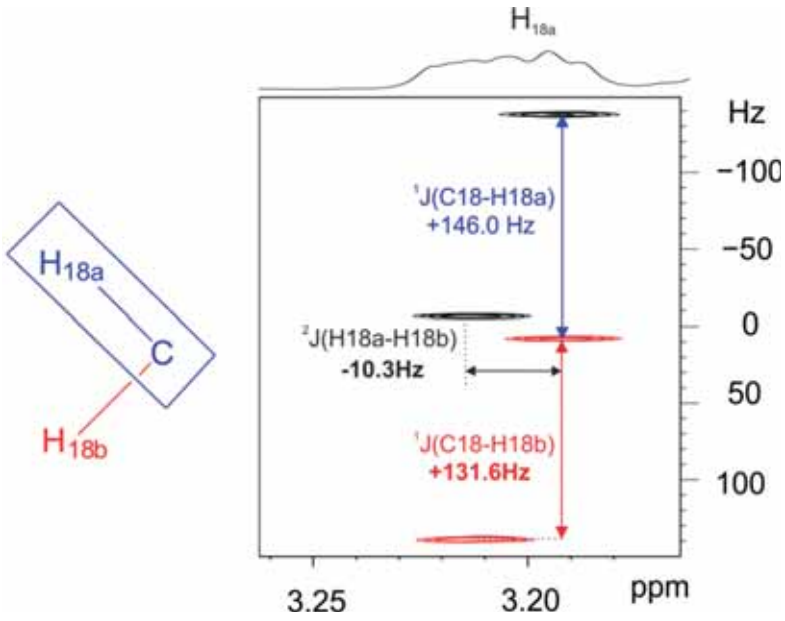

Introduction

The accurate measurement of $^{1}J_{CH}/^{1}T_{CH}$ for individual protons in diastereotopic CH_AH_B groups has been a challenging task. Several NMR methods has been proposed to measure them from the F1 or F2 dimension of HSQC spectra, but they all present some drawback that can prevent their general use.

In this publication, a new 2D ω_1-coupled inverse INEPT experiment (referred to as ω_1-iINEPT) is proposed for the simultaneous measurement of individual $^{1}J_{CH}/^{1}T_{CH}$ as well as the magnitude and the sign of geminal proton-proton coupling constants ($^{2}J_{HH}/^{2}T_{HH}$) in diastereotopic methylene groups in isotropic and anisotropic conditions. The method is based on a F1-coupled HSQC spectra that uses the initial ^{13}C Boltzmann polarization instead of the conventional INEPT transfer. The experiment is easily adapted for a *J*-resolved presentation (referred to as ω_1-iINEPT-*J*) which allows obtain higher levels of resolution within the same experimental time by the use of a reduced spectral width in the indirect dimension. The success of the method is illustrated for several samples in isotropic conditions and also for the accurate measurement of $^{1}D_{CH}$ and $^{2}D_{HH}$ RDCs in diastereotopic CH_2 groups for samples aligned in anisotropic media. These measurements are also feasible for CH and CH_3 multiplicities.

Journal of Magnetic Resonance 242 (2014) 33–40

Contents lists available at ScienceDirect

Journal of Magnetic Resonance

journal homepage: www.elsevier.com/locate/jmr

Straightforward measurement of individual $^1J(CH)$ and $^2J(HH)$ in diastereotopic CH_2 groups

Josep Saurí, Laura Castañar, Pau Nolis, Albert Virgili, Teodor Parella *

Servei de Ressonància Magnètica Nuclear and Departament de Química, Universitat Autònoma de Barcelona, E-08193 Bellaterra, Catalonia, Spain

ARTICLE INFO

Article history:
Received 17 December 2013
Revised 31 January 2014
Available online 12 February 2014

Keywords:
E.COSY
One-bond proton–carbon coupling constants
Two-bond proton–proton coupling constants
Methylene spin systems
Inverse INEPT
Residual dipolar couplings

ABSTRACT

The C–H_A cross-peak corresponding to a diastereotopic CH_AH_B methylene spin system exhibits a characteristic 1:0:1 multiplet pattern along the indirect dimension of a ω_1-coupled HSQC spectrum. It is shown here that the use of the initial ^{13}C Boltzmann polarization instead of the regular INEPT-based ^1H Boltzmann polarization makes visible the central lines of this multiplet pattern. A spin-state-selective method is proposed for the efficient measurement of both $^1J(CH_A)$ and $^1J(CH_B)$ along the indirect dimension of a 2D spectrum as well as to the magnitude and the sign of the geminal $^2J(H_AH_B)$ coupling constant from the straightforward analysis of a single four-component E.COSY cross-peak. Additionally, the extraction of $^1J(CH)$ values for CH and CH_3 multiplicities can be also performed from the same spectrum. The success of the method is also illustrated for the determination of residual dipolar $^1D(CH)$ and $^2D(HH)$ coupling constants in a small molecule weakly aligned in a PMMA swollen gel.

1. Introduction

In recent years, it has appeared an enormous interest for the measurement of scalar and residual dipolar (RDC) one-bond proton–carbon coupling constants ($^1J(CH)$ and $^1D(CH)$, respectively) in small molecules dissolved in weakly aligned anisotropic media [1–3]. HSQC-based pulse schemes have been generally chosen for this purpose and the accuracy and the simplicity on the experimental measurement of $^1J(CH)$ are subjects of discussion. Some topics of recent interest have been (i) the design of general and robust NMR methods that works efficiently for all multiplicities, (ii) the discussion about whether the $^1J(CH)$ splitting should be measured from the direct ω_2 (^1H) or the indirect ω_1 (^{13}C) dimension, (iii) the accurate measurement of $^1J(CH)$ for individual protons in diastereotopic CH_2 or NH_2 groups, or (iv) the simultaneous determination of additional coupling constants from the analysis of the same cross-peak, being the maximum interest the sign-sensitive determination of geminal $^2J(HH)$ values.

The measurement of $^1J(CH)$ from the detected dimension is relatively easy and high levels of digital resolution are readily available. For instance, the CLIP-HSQC experiment prove to be an efficient tool to determine the $^1J(CH)$ value from the resulting clean in-phase doublets [4]. However, strong J(HH) coupling effects can generate a high degree of asymmetry between the high- and low-field multiplet lines in ω_2-coupled HSQC spectra, which can preclude reliable determination of $^1J(CH)$ coupling constants values. In addition, broad signals and/or the large contributions of RDCs can generate poorly defined multiplets that make difficult accurate measurements. These drawbacks have already been described, particularly for CH spin systems in carbohydrates or on the typical strong geminal interaction found in diastereotopic CH_2 spin systems, and some practical solutions have been proposed [5–9]. To avoid such inconveniences, the measurement of $^1J(CH)$ along the ω_1 dimension have been advisable [9,10] although this requires the need for a large number of t_1 increments, and therefore longer acquisition times. The successful use of non-linear uniform sampling, J scaling factors or spectral folding can speed up data acquisition and/or increase the digital resolution in the ω_1 dimension [10].

The accurate measurement of $^1J(CH)$ for individual protons in diastereotopic CH_AH_B (or NH_AH_B) groups is one of the most challenging tasks in this field. Several methods have been proposed that measure them from the ω_1 or ω_2 dimension, but they all present some drawback that can prevent their general use [11–25]. For instance, the passive $^1J(C–H_B)$ value can be separately measured into the active H_A cross-peak, and vice versa, along the ω_1 dimension of a J-resolved HMQC experiment [11]. In addition, the large doublet is further split by the $^2J(H_AH_B)$ coupling yielding a double-doublet. The disadvantage is that additional experiments can

* Corresponding author.
E-mail address: teodor.parella@uab.cat (T. Parella).

http://dx.doi.org/10.1016/j.jmr.2014.02.003
1090-7807/

be needed to measure $^1J(CH)$ for CH or CH_3 spin systems. ^{13}C-edited versions of the 2D ^1H J-resolved experiment have been proposed to resolve enantiomeric derivatives dissolved in anisotropic media by visualizing their different $^1J(CH)$ splitting sizes along the indirect dimension [12,13]. Other related J-resolved HSQC experiments have been also described but they can require time-consuming 3D data acquisition [14] or the collection of multiple 2D J-modulated data [15,16]. An important group of NMR experiments are those based on spin-state selection specifically designed for methylene groups [8,17–25]. Some reported examples should be the P.E.HSQC [8] SPITZE [17] or CH_2-TROSY [19,20] experiments that yield simplified coupling patterns, and where the sign and the magnitude of the geminal $^2J(HH)$ can be additionally extracted. In all these cases, the central lines of the ω_1-multiplet corresponding to a CH_2 group are not observed, and therefore only the sum of the two $^1J(CH)$ can be determined from the indirect dimension.

In the present study, a new 2D ω_1-coupled inverse INEPT experiment (referred to as ω_1-iINEPT) is proposed for the observation of the missing central lines in diastereotopic CH_2 cross-peaks. The resulting cross-peak present a characteristic E.COSY multiplet pattern that facilitates the straightforward measurement of both individual $^1J(CH_A)$ and $^1J(CH_B)$ values, as well as the sign and magnitude of the geminal $^2J(HH)$ coupling. The method starts exclusively from ^{13}C Boltzmann polarization, it is driven with broadband ^{13}C decoupling during ^1H acquisition and, very importantly, also works for CH and CH_3 multiplicities. The experiment is easily adapted for a J-resolved presentation (referred to as ω_1-iINEPT-J) which allows obtain higher levels of resolution within the same experimental time by the use of a reduced spectral width in the indirect dimension [11–13,26,27]. The success of the method is illustrated for several samples and particular cases and as well as for the measurement of small residual coupling constants in small molecules dissolved in a weakly aligned media.

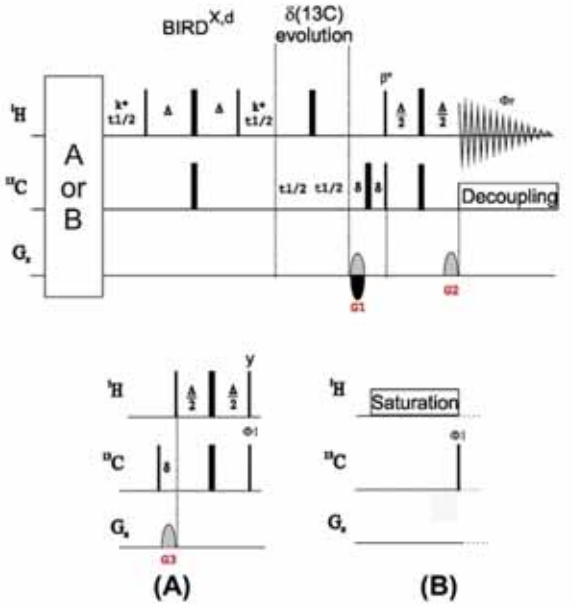

Fig. 1. Pulse sequences for the (A) ω_1-HSQC and (B) ω_1-iINEPT experiments. Thin and thick rectangles represent 90° and 180° rectangular pulses, respectively, applied along the *x* axis unless indicated differently. A basic two-step phase cycling is applied: $\varphi_1 = x,-x$; $\varphi_{rec} = x,-x$. A small flip angle ($\beta = 36°$) generates E.COSY cross-peaks. Inversion and refocusing 180° ^{13}C pulses can be applied as adiabatic pulses and the element labeled as $\delta(^{13}C)$ evolution period is optional. The inter-pulse delays in INEPT and BIRD elements are optimized according to $\Delta = 1/(2 * {}^1J(CH))$. The echo/anti-echo encoding of ω_1 frequencies was achieved by changing the sign of G1 between successive t_1 increments. The ratio between G1:G2:G3 were 80:20.1:13. The duration of a pulse-field gradient (PFG) and of the subsequent recovery delay amounts to δ.

2. Results and discussion

The idea to develop the ω_1-iINEPT experiment was born from the recent P.E.HSQMBC experiment, which was devised to measure three different $^1J(CH)$, $^2J(HH)$ and a $^nJ(CH)$ coupling constants from a single 2D cross-peak [28]. Other related works that have inspired us were the P.E.HSQC [8] and the BIRD-HSQC [9] experiments, this latter being further refined and evaluated by Thiele and Bermel (see Fig. 1c in Ref. [10]). The basic pulse scheme of the reference ω_1-coupled HSQC (ω_1-HSQC) experiment uses the traditional ^1H Boltzmann polarization as a starting point (Fig. 1A). In the following, we consider an isolated diastereotopic CH_AH_B spin system defined with three different $^1J(CH_A)$, $^1J(CH_B)$ and $^2J(H_AH_B)$ coupling constants. The sequence starts with an initial 90° (^{13}C)-gradient element to remove any contribution coming from the ^{13}C Boltzmann polarization. After the ^1H-to-^{13}C INEPT transfer, anti-phase ^{13}C magnetization is present as a mixture of $2H_{Az}C_y + 2H_{Bz}C_y$, which evolve under the effects of $^1J(CH)$ and $\delta(^{13}C)$ in a sequential mode, by using separated and synchronously incremented time periods. Thus, the magnetization evolves first under the effect of a $BIRD^{d,X}$ element [29,30] flanked by a variable J-scaled t_1 evolution period (defined by a scaling factor k) to allow the exclusive evolution of $^1J(CH)$ whereas ^{13}C chemical shift and long-range CH contributions are refocused, and then ^{13}C chemical shift can evolve from an optional t_1 evolution period as usual. In the subsequent analysis, the scaling factor, which is set arbitrarily within the limits set by relaxation and/or signal overlapping, the effects of the labeling G1 gradient and the optional ^{13}C chemical shift t_1 evolution period are neglected for the sake of clarity. Thus, for a single H_A spin, the evolution during the variable t_1 BIRD-based period ($k = 1$) is described as:

$$2H_{Az}C_y[\cos(\pi^1J(CH_A)t_1)\cos(\pi^1J(CH_B)t_1) - \sin(\pi^1J(CH_A)t_1) \times \sin(\pi^1J(CH_B)t_1)] \quad (1)$$

Applying the trigonometric relationship $\cos A\cos B - \sin A\sin B = \cos(A + B)$, we obtain

$$2H_{Az}C_y\cos(\pi^1J(CH_A + {}^1J(CH_B))t_1) \quad (2)$$

meaning that only the outer lines of the theoretical triplet or double-doublet coupling pattern of the methylene proton cross-peak would be observed and, therefore, only the sum of the both couplings ($^1J(CH_A + {}^1J(CH_B))$) will be observed as an in-phase doublet along the indirect dimension (Fig. 2A) [15]. This dependence with respect to the cosine function makes that multiplet patterns with relative intensities of 1:1 for CH, 1:0:1 for CH_2, and 3:1:1:3 for CH_3 will be displayed along the ω_1 dimension [8,34]. A key feature introduced in the last refocusing INEPT block is the small-flip ^1H pulse angle ($\beta = 36°$) which generates simplified E.COSY multiplet patterns for non-equivalent protons in CH_2 and CH_3 spin systems (Fig. 2B) [8,31–33].

To improve the appearance and usefulness of cross-peaks obtained from ω_1-iINEPT experiments, we propose to start the experiment with the initial ^{13}C Boltzmann polarization instead of the INEPT-based ^1H Boltzmann polarization because this leads to interesting changes in the central lines of methylene cross-peaks, as known for the analogous old ^{13}C-detected heteronuclear J-resolved 2D experiment [35]. The initial 90° ^{13}C pulse, applied after an

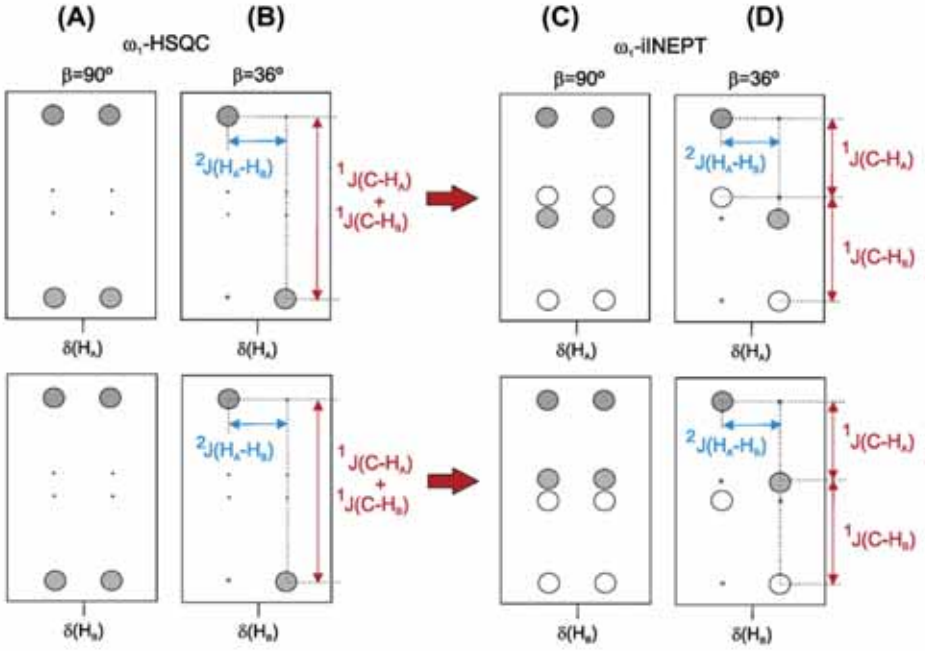

Fig. 2. Schematic representation of the 2D multiplet pattern of each individual H_A and H_B proton belonging to a methylene CH_AH_B group. (A and B) ^{1}H-Boltzmann polarization driven (ω_1-HSQC) experiments using $\beta = 90°$ and 36°, respectively, and (C and D) ^{13}C-Boltzmann polarization driven experiments (ω_1-iINEPT) using $\beta = 90°$ and 36°, respectively. In (D), the magnitude and the sign of all involved couplings (defined as $^2J(H_AH_B)$ and assuming $^1J(CH_A) < {}^1J(CH_B)$) can be readily extracted. Open and dotted circles represent peaks with opposite phase.

heteronuclear NOE enhanced pre-scan period by means of a ^{1}H WALTZ-16 pulse train saturation, generates in-phase $-C_y$ magnetization (Fig. 1B) which evolves under the effect of $^1J(CH)$ during the variable t_1 BIRD-based period:

$$-2H_{Az}C_x[\sin(\pi^1J(CH_A)t_1)\cos(\pi^1J(CH_B)t_1)] - 2H_{Bz}C_x[\cos(\pi^1J(CH_A)t_1)\sin(\pi^1J(CH_B)t_1)] \quad (3)$$

The result is a pure absorptive 2D ω_1-iINEPT spectra displaying double-doublet coupling patterns along the ω_1 dimension for each individual H_A or H_B cross-peaks, that initially would consist of eight different components as shown in Fig. 2C. Analyzing only the H_A spin, it will show an anti-phase doublet pattern with respect to $^1J(CH_A)$ (sine modulated) and an additional in-phase doublet pattern with respect to $^1J(CH_B)$ (cosine modulated) along the ω_1 dimension. As discussed before, the effect to apply a small flip angle ($\beta = 36°$) will generate a simplified four-component cross-peak with a characteristic E.COSY multiplet pattern due to the mutual $^2J(H_AH_B)$ (Fig. 2D), which facilites both the multiplet interpretation and analysis (see Fig. S1; supporting information). Thus, the active $^1J(CH_A)$ coupling is directly extracted from the anti-phase 1:−1 pattern along the same column in ω_1, whereas the passive $^1J(CH_B)$ coupling can be also extracted directly by measuring the in-phase components in each part of the E.COSY pattern. Otherwhise, the sign and the magnitude of $^2J(HH)$ is easily extracted from the frequency separation between tilted peaks along the w2 dimension. Fig. 2 summarizes the expected cross-peak pattern for a single diastereotopic CH_AH_B proton using the different ω_1-HSQC and ω_1-iINEPT approaches with $\beta = 90°$ and 36°. For CH groups, a doublet with relative 1:−1 intensities is obtained whereas a 1:1:−1:−1 coupling pattern will be displayed for a CH_3 group.

As a first example, Fig. 3A and B shows the equivalent ω_1-HSQC and ω_1-iINEPT correlation spectra, respectively, of strychnine (**1** in Scheme 1) acquired with the pulse schemes of Fig. 1, under the same experimental conditions and using a scaling factor of $k = 8$. The general coupling pattern for individual CH and CH_2 groups are marked with highlighted boxes. CH cross-peaks present the same doublet structure in both approaches. On the other hand, whereas the central lines for each individual CH_2 cross-peak are absent in the ω_1-HSQC spectrum, they are clearly distinguished in the ω_1-iINEPT version. A close inspection of the multiplet patterns for CH_2 cross-peaks in both spectra reveals the simplified E.COSY multiplet structure as described in other related experiments [8,19]. Also note the different in-phase *vs* anti-phase pattern behavior along the indirect dimension, although this is not relevant for the measurement. In cases where chemical shift assignment is already known and/or signal overlapping is not severe, the proposed method can be recorded in a J-resolved mode by simple omission of the ^{13}C chemical shift evolution period ($t_{1/2} - 180°(^1H) - t_{1/2}$). In this way the spectral width in the indirect dimension could be reduced by a factor of about 40, from 20,000 Hz (160 ppm at 500 MHz) to 500 Hz, and therefore the spectral resolution in ω_1 should be improved by a similar factor if all other experimental conditions remain the same. Fig. 3C and D shows the equivalent ω_1-HSQC-J and ω_1-iINEPT-J spectra, respectively, acquired with the same number of t_1 increments and using an scaling factor of $k = 1$. It can be observed that the absence of ^{13}C chemical shift signal dispersion does not introduce a serious problem on severe signal overlapping in a small molecule like **1**, where all cross-peaks can be succesfully analyzed. All the discussion and conclusions described in Ref. [10] about the application of non-linear sampling to accelerate data acquisition and/or to increase digital resolution in the indirect dimension could

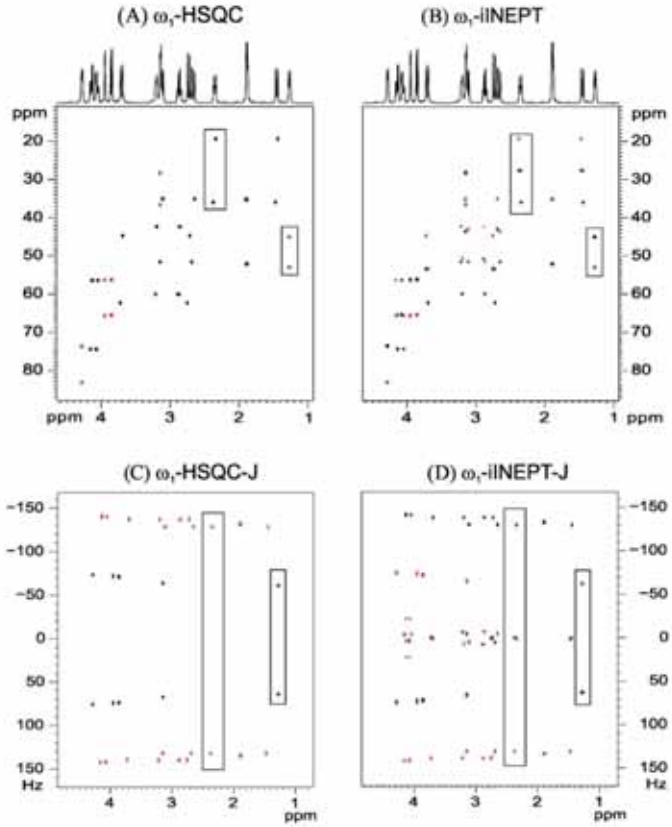

Fig. 3. 2D ^{1}H–^{13}C spectra of **1** acquired with the pulse sequences of Fig. 1. (A) ω_1-HSQC and (C) ω_1-HSQC-J spectra were obtained starting from ^{1}H Boltzmann magnetization, and (B) ω_1-ilNEPT and (D) ω_1-ilNEPT-J spectra were achieved starting from ^{13}C Boltzmann magnetization. (A) and (B) are heteronuclear correlation maps (acquired with an scaling factor of $k = 8$) whereas (C) and (D) are the corresponding J-resolved versions (scaling factor $k = 1$ and omission of the ^{13}C chemical shift t_1 evolution period). All spectra were acquired and processed under the same experimental conditions. 2 scans were collected for each one of the 256 t_1 increments using a pre-scan delay of 3 s. Squared boxes mark specific CH and diastereotopic CH_2 cross-peak as examples in each spectrum.

be extrapolated here for the proposed methods. Further increase of resolution by a factor of 3 can be additionally achieved by allowing signal folding in the indirect dimension (see Fig. S2 in the supporting information for an example provided using a reduced spectral width of 180 Hz).

Fig. 4 shows an expanded area of the 2D ω_1-ilNEPT-J spectrum, where the clean tilt, the straightforward analysis and the excellent resolution of the resulting peak patterns can be quickly observed. Note the perfect equivalence between the cross peaks of diastereotopic protons (for instance H-18a *vs* H-18b or H-11a *vs* H-11b) which permit the easy and direct measurement of the same three different involved couplings ($^{1}J(CH_A)$ and $^{1}J(CH_B)$ as well as the geminal $^{2}J(HH)$) from two independent cross-peaks. The comparison of the experimental J values extracted from these two different measurements evaluates the accuracy of the measurement, and also ensures the measurement of all couplings even in the case of accidental signal overlapping of one of the two diastereotopic proton prevents its analysis. For well resolved $^{2}J(HH)$ values, the difference between diastereotopic $^{1}J(CH)$ values is quickly ascertained from the relative displacement between the two central lines and accurate $^{1}J(CH)$ values can be easily measured even in the case of minor differences between $^{1}J(CH_A)$ and $^{1}J(CH_B)$. For instance, whereas a small difference smaller than 2 Hz is measured for the H-15a/H-15b pair, a big difference about 14.5 Hz is found for H-18a/H-18b. Experimental $^{1}J(CH)$ and $^{2}J(HH)$ data extracted from these spectra for compound **1** are in agreement with those reported previously in other works (see Table S1 in the supporting information) [5,36–39]. Even in the case of signal overlapping, CH cross-peaks can be easily distinguished from those of CH_2 groups by their different doublet or double-doublet coupling patterns and also from the relative opposite phase of the anti-phase components for CH/CH_3 and CH_2 groups because the BIRD element acts as a multiplicity-editing element. For instance, note the clear distinction and straightforward measurement that can be performed for the three different protons resonating close to 3.1–3.2 ppm.

When two diastereotopic protons have similar chemical shift and $^{1}J(CH)$ values, the central lines can be partially or completely cancelled, as shown for the H-17a/H-17b protons resonating at 1.9 ppm in Fig. 3D. Another special case is when the geminal $^{2}J(HH)$ is near to 0 Hz, where the distinction of the four E.COSY components will depend of the different $^{1}J(CH)$ sizes. One illustrative example is the H-8a and H-8b olefinic protons belonging to the exocyclic CH_2 group in 5-methylene-2-norbornene (**2**) (Fig. 5A) which present unresolved signals in the conventional ^{1}H spectrum, and where the mutual $^{2}J(H8a–H8b)$ coupling can not be directly measured. The well differentiated four components observed in the ω_1-ilNEPT-J spectra allow a measurement of $^{2}J(HH) = +1.1$ Hz,

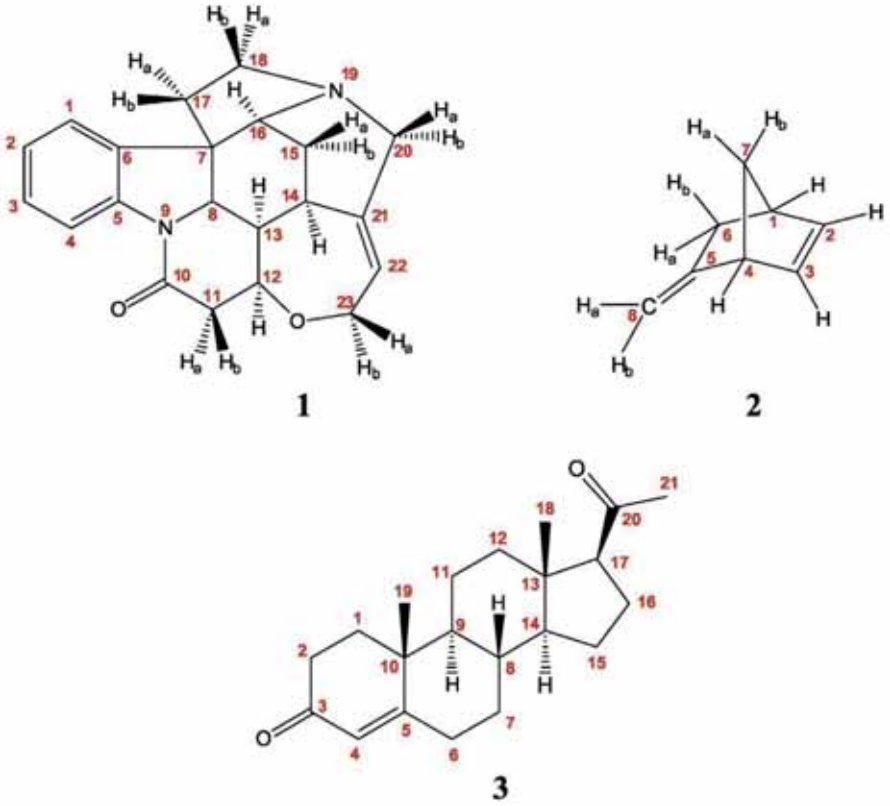

Scheme 1. Molecules used in this work.

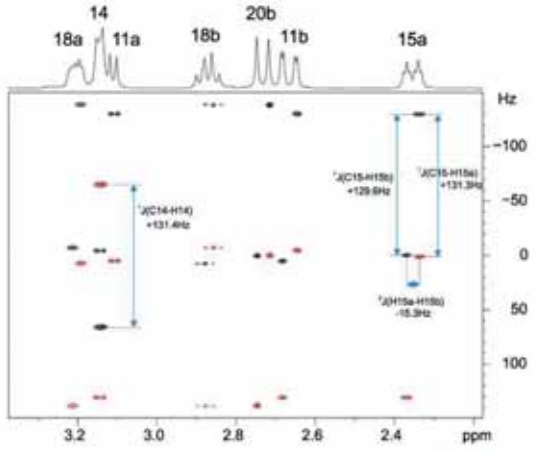

Fig. 4. Expanded area corresponding to the ω_1-ilNEPT-J spectrum of Fig. 3D, where the different multiplet patterns for a CH group and several diastereotopic CH_2 spin systems can be clearly visualized and analyzed, and all $^1J(CH)$ and $^2J(HH)$ can be measured with simplicity and accuracy.

where the positive sign can be determined by comparison with the opposite E.COSY tilt presented by other diastereotopic H-6 and H-7 methylene protons, which have large negative $^2J(HH)$ values of −15.3 Hz and −8.1 Hz, respectively. Although there are small differences between the two central lines, the measurement of each individual $^1J(CH)$ (155.1 *vs* 157.1 Hz) can be performed twice, independently from each cross-peak and with a minimal deviation of ±0.1 Hz (Table S2; supporting information).

The simplicity of the proposed ω_1-ilNEPT methods make them highly interesting for the measurement of small $^1D(CH)$ and $^2D(HH)$ RDCs, by comparison the difference between experimental measurements performed in isotropic *vs* anisotropic conditions ($D = T_{(aniso)} - J_{(is)}$). Compound **2** was weakly aligned in a poly(-methyl methacrylate) (PMMA) gel swollen in $CDCl_3$ using the reversible compression/relaxation method [40] , and $^1D(CH)$ and $^2D(HH)$ RDCs magnitudes and signs could be easily determined for all signals (see Fig. S3C; supporting information). Fig. 5 compares some cross-peaks obtained in both isotropic and anisotropic conditions. It can be seen how the relative orientation of each diastereotopic HH pair is clearly differentiated from their $^2D(HH)$ values: −0.2 Hz for H-8a/H-8b protons, −4.1 Hz for H-6a/H-6b protons and +3.1 Hz for H-7a/H-7b protons. A list of all measured scalar and residual dipolar coupling constants can be found in Table S2 of the supporting information.

The last example corresponds to a molecule having a more complex ^1H spectrum, progesterone (**3**), with high levels of signal overlapping in its aliphatic region. Fig. 6 shows an expanded area of the ω_1-ilNEPT spectrum, where cross-peaks for all multiplicites can be distinguished and the corresponding $^1J(CH)$ and $^2J(HH)$ values conveniently measured (see Table S3 in the supporting information). For instance, note the excellent signal dispersion and multiplet editing for the five resonances fully overlapped in the 1.5–1.65 ppm area. Accidental overlapping of multiplet components

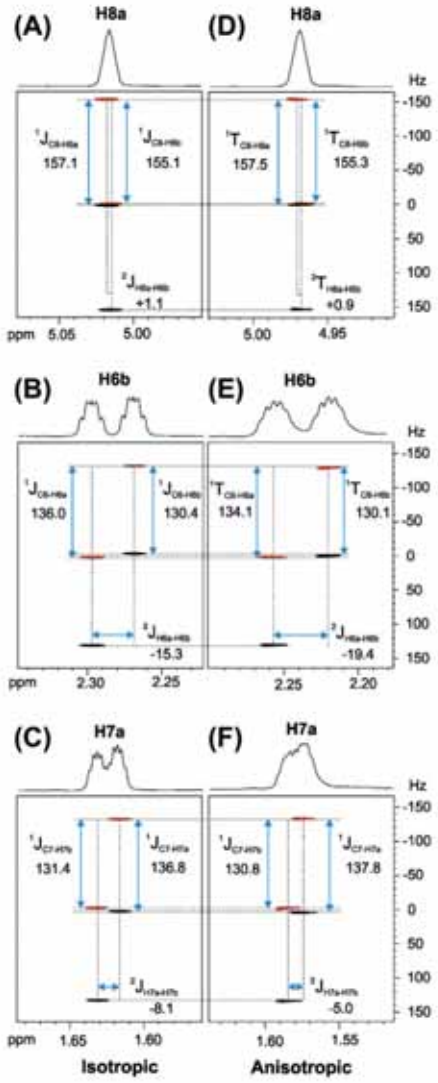

Fig. 5. Some illustrative 2D cross-peaks extracted from the ω_1-iINEPT-J spectra of **2** showing the easy measurement of the experimental $^1J(CH)/^1T(CH)$ and $^2J(HH)/^2T(HH)$ values measured in (A–C) isotropic ($CDCl_3$) and (D–F) anisotropic (weakly aligned in PMMA gel swollen in $CDCl_3$) conditions. Similar values for the same couplings are also measured from the cross-peaks of the other diastereotopic protons (see a complete set of coupling values in Table S2 in the Supporting information).

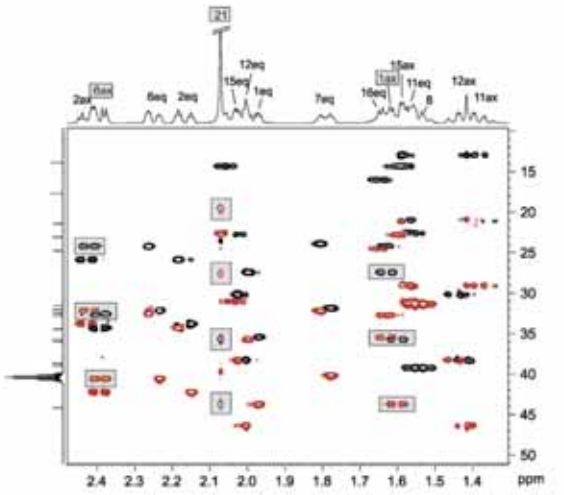

Fig. 6. Expanded area of the 2D ω_1-iINEPT spectrum of **3** acquired with 4 scans for each one of the 256 t_1 increments, and using a pre-scan delay of 3 s. Boxes enhance the different components corresponding to the H-6ax and H-1ax protons. In addition, the 1:1:−1:−1 multiplet corresponding to the methyl group 21 (at 2.08 ppm) is also highlighted.

can be overcomed by using the J-resolved version or by changing the scaling factor. The diastereotopicity in the three protons belonging to a methyl groups is not observed and they usually appear as a singlet due to their free rotation under isotropic conditions. However, in analogy with the discussion presented here for diastereotopic CH_2 spin systems, the same conclusions could be extracted from the analysis of a hypothetical non-equivalent protons in a CH_3 group [8,41]. Whereas isotropic CH_3 cross-peaks with no distinction between equivalent protons present a typical 3:1:1:3 multiplet pattern in ω_1-HSQC experiments [34], they display a symmetrical 1:1:−1:−1 coupling pattern in the ω_1-iINEPT, as seen for the Me-21 in Fig. 6. A modified HSQC experiment has been reported to recover the 1:2:1 and 1:3:3:1 pattern in NH_2 and NH_3^+ groups, respectively, and spin-state selected methods to study analysis have been used to study differential relaxation of the different line multiplets of methyl cross-peaks in proteins [41].

In terms of sensitivity, the ω_1-iINEPT experiment present a sensitivity decrease when compared to the analog ω_1-HSQC experiment, because of the differential signal enhancement achieved by heteronuclear polarization transfer via INEPT or by heteronuclear NOE effects. In addition, the pre-scan delay must be optimized as a function to the longer ^{13}C T_1 values, although that protonated carbons relax relatively fast. Our experimental data confirms such theoretical prediction and signal-to-noise enhancements by a factor of about 3 and 4 can be achieved for ω_1-iINEPT and ω_1-HSQC experiments, respectively, when compared with a reference non signal-enhanced ω_1-iINEPT experiment acquired without proton saturation and a pre-scan delay of 3 s (see Fig. S4 in the supporting information). Although the proposed methodology could distinguish diastereotopic protons in NH_2 groups, the large difference in sensitivity enhancement achieved by polarization transfer when compared with those obtained by direct ^{15}N Boltzmann magnetization without NOE enhancement (a theoretical factor about 10) makes the experiment of limited practical use due to its very low sensitivity. In addition, the two central lines are likely to be quite broad for large molecules.

In summary, a general and simple NMR method to obtain a characteristic spin-state-selected multiplet pattern for diastereotopic CH_AH_B methylene systems has been described. The magnitude and the sign of the three involved coupling values ($^1J(CH_A)$, $^1J(CH_B)$ and $^2J(H_AH_B)$) can be measured simultaneously from the analysis of a single and clean four-component E.COSY cross-peak. The method also measures $^1J(CH)$ for all other carbon multiplicities, and it is easily adapted for a J-resolved representation that allows the use of a more reduced spectral width in the carbon dimension, obtaining higher levels of resolution within the same experimental time. We have also shown that small $^1D(CH)$ and $^2D(HH)$ RDCs can be measured for small molecules weakly aligned in anisotropic media. The proposed techniques are appropriate for routine use because require minimum set-up and afford simple data analysis and interpretation.

3. Methods and materials

The isotropic samples used in this work were 0.12 M strychnine dissolved in $CDCl_3$ (**1**), 0.14 M 5-methylene-2-norbornene dissolved in $CDCl_3$ (**2**) and 0.13 M progesterone dissolved in DMSO (**3**) (see chemical structures in Scheme 1). For the measurement of RDCs, 10 mg of **2** was aligned in a poly(methyl methacrylate) (PMMA) gel swollen in $CDCl_3$ using the reversible compression/relaxation method [40]. The ^2H quadrupolar splitting ($\Delta\nu Q$) for the $CDCl_3$ signal was of 24 Hz. NMR experiments on **1** and **3** were recorded on a BRUKER DRX-500 spectrometer equipped with a 3-channel 5-mm cryoprobe incorporating a z-gradient coil. NMR experiments on **2** were carried out in a Bruker Avance 600 spectrometer equipped with a TXI HCN z-grad probe. The temperature for all measurements was set to 298 K.

In all experiments, the inter-pulse Δ ($=1/(2*{}^1J(CH))$ delays were set to 3.5 ms (optimized to $^1J(CH)=145$ Hz). Gradient ratios for G1:G2:G3 were set to 80:20.1:13, measured as percentage of the absolute gradient strength of 53.5 G/cm. Sine bell shaped gradients of 1 ms of duration and followed by a recovery delay of 100 μs were used. ^1H saturation during the entire pre-scan delay was accomplished applying a 2.5 kHz WALTZ-16 modulated pulse train. Broadband ^{13}C decoupling during acquisition was achieved applying a 8 kHz GARP modulated pulse train. All experiments were acquired and processed using the echo/anti-echo protocol where the gradient G1 was inverted for every second FID. An scaling factor $k = 8$ were used for the correlation experiments for all compounds. The J-resolved spectra were acquired omitting the $t_{1/2} - 180(^1H) - t_{1/2}$ element in the pulse sequence of Fig. 1 and reducing the spectral width in the indirect ω_1 dimension to 500 Hz.

For spectra of Figs. 3, 2 scans were accumulated for each one of the 256 t_1 increments and the number of data points in t_2 was set to 2048. The recycle delay was set to 1 s for ω_1-HSQC type experiments (Fig. 3A and C) and 3 s for ω_1-ilNEPT type experiments (Fig. 3B and D). Spectra 3A and 3B were acquired with an spectral window of 5000 Hz (in ω_2) and 20,000 Hz (in ω_1) giving a FID resolution of 2.4 and 9.8 Hz, respectively. Prior to Fourier-transformation of each data, zero filling to 4096 in ω_2, 1024 in ω_1 and a $\pi/2$-shifted sine-squared window function in both dimensions were applied. After applying zero filling the digital resolution was 1.2 and 2.4 Hz, respectively. In spectra of Figs. 3C and 3D, the spectral window in ω_1 dimension was reduced to 500 Hz giving a FID resolution of 2.4 Hz (in ω_2) and 1.9 Hz (in ω_1). After applying zero filling the digital resolution was 1.2 and 0.5 Hz, respectively.

In the ω_1-ilNEPT-J experiments recorded on **2** in isotropic and anisotropic media (Fig. 5), a recycle delay of 3 s was used, 4 scans were accumulated for each one of the 256 t_1 increments and the number of data points in t_2 was set to 2048. Both of them were acquired with an spectral window of 3600 Hz (in ω_2) and 500 Hz (in ω_1) giving a FID resolution of 1.8 and 1.9 Hz, respectively. Prior to Fourier-transformation of each data, zero filling to 4096 in ω_2, 1024 in ω_1 and a $\pi/2$-shifted sine-squared window function in both dimensions were applied. After applying zero filling the digital resolution was 0.9 and 0.5 Hz, respectively. In the ω_1-ilNEPT experiment recorded on **3** (Fig. 6), a recycle delay of 3 s was used, 4 scans were recorded for each one of the 256 t_1 increments and the number of data points in t_2 was set to 2048 in all the experiments. Data were acquired with an spectral window of 2000 Hz (in ω_2) and 12,500 Hz (in ω_1) giving a FID resolution of 1.0 and 6.1 Hz, respectively. Prior to Fourier-transformation of each data, zero filling to 4096 in ω_2, 1024 in ω_1 and a $\pi/2$-shifted sine-squared window function in both dimensions were applied. After applying zero filling the digital resolution was 0.5 and 1.5 Hz, respectively.

Acknowledgments

Financial support for this research provided by MINECO (project CTQ2012-32436) is gratefully acknowledged. Authors thanks to R.R. Gil and A. Navarro-Vázquez for a sample of PMMA gel. We also thank the Servei de Ressonància Magnètica Nuclear, Universitat Autònoma de Barcelona, for allocating instrument time to this project.

Appendix A. Supplementary material

Supplementary data associated with this article can be found, in the online version, at http://dx.doi.org/10.1016/j.jmr.2014.02.003.

References

[1] C.M. Thiele, Residual dipolar couplings (RDCs) in organic structure determination, Eur. J. Org. Chem. (2008) 5673–5685.
[2] G. Kummerlowe, B. Luy, Residual dipolar couplings for the configurational and conformational analysis of organic molecules, Annu. Rep. NMR Spectrosc. 68 (2009) 193–230.
[3] G. Kummerlowe, B. Luy, Residual dipolar couplings as a tool in determining the structure of organic molecules, Trend Anal. Chem. 28 (2009) 483–493.
[4] A. Enthart, J.C. Freudenberger, J. Furrer, H. Kessler, B. Luy, The CLIP/CLAP HSQC: pure absorptive spectra for the measurement of one-bond couplings, J. Magn. Reson. 192 (2008) 314–322.
[5] C.M. Thiele, Simultaneous assignment of all diastereotopic protons in strychnine using RDCs: PELG as alignment medium for organic molecules, J. Org. Chem. 69 (2004) 7403–7413.
[6] B.W. Yu, H. van Ingen, S. Vivekanandan, C. Rademacher, S.E. Norris, D.I. Freedberg, More accurate ^{1}JCH coupling measurement in the presence of ^{3}JHH strong coupling in natural abundance, J. Magn. Reson. 215 (2012) 10–22.
[7] B.W. Yu, H. van Ingen, D.I. Freedberg, Constant time INEPT CT-HSQC (CTI-CT-HSQC) – a new NMR method to measure accurate one-bond J and RDCs with strong 1H–1H couplings in natural abundance, J. Magn. Reson. 228 (2013) 159–165.
[8] P. Tzvetkova, S. Simova, B. Luy, P.E. HSQC: a simple experiment for the simultaneous and sign-sensitive measurement of (^{1}JCH + DCH) and (^{2}JHH + DHH) couplings, J. Magn. Reson. 186 (2007) 193–200.
[9] K. Fehér, S. Berger, K.E. Kövér, Accurate determination of small one-bond heteronuclear residual dipolar couplings by F1 coupled HSQC modified with a G-BIRD(r) module, J. Magn. Reson. 163 (2003) 340–346.
[10] C.M. Thiele, W. Bermel, Speeding up the measurement of one-bond scalar (1J) and residual dipolar couplings (1D) by using non-uniform sampling (NUS), J. Magn. Reson. 216 (2012) 134–143.
[11] K.E. Kövér, K. Fehér, Measurement of one-bond heteronuclear dipolar coupling contributions for amine and diastereotopic protons, J. Magn. Reson. 168 (2004) 307–313.
[12] L. Ziani, J. Courtieu, D. Merlet, Visualisation of enantiomers via insertion of a BIRD module in X-H correlation experiments in chiral liquid crystal solvent, J. Magn. Reson. 183 (2006) 60–67.
[13] U.R. Prabhu, S.R. Chaudhari, N. Suryaprakash, Visualization of enantiomers and determination of homo- and hetero-nuclear residual dipolar and scalar couplings: the natural abundant ^{13}C edited J/D-resolved NMR techniques, Chem. Phys. Lett. (2010) 334–341.
[14] J. Furrer, M. John, H. Kessler, B. Luy, J-spectroscopy in the presence of residual dipolar couplings: determination of one-bond coupling constants and scalable resolution, J. Biomol. NMR 37 (2007) 231–243.
[15] M. Ottiger, F. Delaglio, J.L. Marquardt, N. Tjandra, A. Bax, Measurement of Dipolar Couplings for methylene and methyl sites in weakly oriented macromolecules and their use in structure determination, J. Magn. Reson. 124 (1998) 365–369.
[16] T.N. Pham, T. Liptaj, K. Bronek, D. Uhrin, Measurement of small one-bond proton-carbon residual dipolar coupling constants in partially oriented ^{13}C natural abundance oligosaccharide samples. Analysis of heteronuclear ^{1}JCH-modulated spectra with the BIRD inversion pulse, J. Magn. Reson. 157 (2002) 200–209.
[17] T. Carlomagno, W. Peti, C. Griesinger, A new method for the simultaneous measurement of magnitude and sign of ^{1}DCH and ^{1}DHH dipolar couplings in methylene groups, J. Biomol. NMR 17 (2000) 99–109.
[18] P. Permi, A spin-state-selective experiment for measuring heteronuclear one-bond and homonuclear two-bond couplings from an HSQC-type spectrum, J. Biomol. NMR 22 (2002) 27–35.
[19] E. Miclet, D.C. Williams Jr., G.M. Clore, D.L. Bryce, J. Boisbouvier, A. Bax, Relaxation-optimized NMR spectroscopy of methylene groups in proteins and nucleic acids, J. Am. Chem. Soc. 126 (2004) 10560–10570.
[20] G. Guichard, A. Violette, G. Chassaing, E. Miclet, Solution structure determination of oligoureas using methylene spin state selective NMR at ^{13}C natural abundance, Magn. Reson. Chem. 46 (2008) 918–924.

[21] T. Parella, M. Gairí, Simultaneous recording of spin-state-selective NMR spectra for different I_nS spin systems, J. Am. Chem. Soc. 126 (2004) 9821–9826.
[22] P. Permi, Two simple NMR experiments for measuring dipolar couplings in asparagine and glutamine side chains, J. Magn. Reson. 153 (2001) 267–272.
[23] E. Miclet, E. O'Neil-Cabello, E.P. Nikonowicz, D. Live, A. Bax, ^1H–^1H dipolar couplings provide a unique probe of RNA backbone structure, J. Am. Chem. Soc. 125 (2003) 15740–15741.
[24] P. Nolis, J.F. Espinosa, T. Parella, Optimum spin-state-selection for all multiplicities in the acquisition dimension of the HSQC experiment, J. Magn. Reson. 180 (2006) 39–50.
[25] P. Nolis, T. Parella, Solution-state NMR experiments based on heteronuclear cross-polarization, Curr. Anal. Chem. 3 (2007) 47–68.
[26] M. Liu, R.D. Farrant, J.M. Gillam, J.K. Nicholson, J.C. Lindon, Selective inverse-detected long-range heteronuclear J-resolved NMR spectroscopy and its application to the measurement of ^3JCH, J. Magn. Reson. B 109 (1995) 275–283.
[27] K. Kobzar, H. Kessler, B. Luy, Stretched gelatin gels as chiral alignment media for the discrimination of enantiomers by NMR spectroscopy, Angew. Chem. Int. Ed. 44 (2005) 3145–3147.
[28] J. Saurí, L. Castañar, P. Nolis, A. Virgili, T. Parella, P.E. HSQMBC: simultaneous measurement of proton–proton and proton–carbon coupling constants, J. Magn. Reson. 224 (2012) 101–106.
[29] J.R. Garbow, D.P. Weitekamp, A. Pines, Bilinear rotation decoupling of homonuclear scalar interactions, Chem. Phys. Lett. 93 (1982) 504–509.
[30] D. Uhrín, T. Liptaj, K.E. Kövér, Modified BIRD pulses and design of heteronuclear pulse sequences, J. Magn. Reson. A 101 (1993) 41–46.
[31] C. Griesinger, O.W. Sørensen, R.R. Ernst, Two-dimensional correlation of connected NMR transitions, J. Am. Chem. Soc. 107 (1985) 6394–6396.
[32] L. Mueller, P.E-COSY, a simple alternative to E.COSY, J. Magn. Reson. 72 (1986) 191–196.
[33] C. Griesinger, O.W. Sørensen, R.R. Ernst, Practical aspects of the E.COSY technique. Measurement of scalar spin-spin coupling constants in peptides, J. Magn. Reson. 75 (1987) 474–492.
[34] Y. Takayama, D. Sahu, J. Iwahara, Observing in-phase single-quantum ^{15}N multiplets for NH_3/NH_3^+ groups with two-dimensional heteronuclear correlation spectroscopy, J. Magn. Reson. 194 (2008) 313–316.
[35] W.P. Aue, L. Muller, R.R. Ernst, Phase separation in two-dimensional spectroscopy, J. Magn. Reson. 28 (1977) 29–39.
[36] B. Luy, K. Kobzar, H. Kessler, An easy and scalable method for the partial alignment of organic molecules for measuring residual dipolar couplings, Angew. Chem. Int. Ed. 43 (2004) 1092–1094.
[37] A. Bagno, F. Rastrelli, G. Saielli, Toward the complete prediction of the ^1H and ^{13}C NMR spectra of complex organic molecules by DFT methods: application to natural substances, Chem. Eur. J. 12 (2006) 5514–5525.
[38] M. Misiak, W. Koźmiński, Determination of heteronuclear coupling constants from 3D HSQC-TOCSY experiment with optimized random sampling of evolution time space, Magn. Reson. Chem. 47 (2009) 205–209.
[39] J.C. Cobas, V. Constantino-Castillo, M. Martín-Pastor, F. del Río Portilla, A two-stage approach to automatic determination of 1H NMR coupling constants, Magn. Reson. Chem. 43 (2005) 843–848.
[40] C. Gayathri, N.V. Tsarevsky, R.R. Gil, RDCs analysis of small molecules made easy: fast and tuneable alignment by reversible compression/relaxation of reusable PMMA gels, Chem. Eur. J. 16 (2010) 3622–3626.
[41] G. Kontaxis, A. Bax, Multiplet component separation for measurement of methyl ^{13}C–^1H dipolar couplings in weakly aligned proteins, J. Biomol. NMR 20 (2001) 77–82.

Straightforward measurement of individual $^{1}J(CH)$ and $^{2}J(HH)$ in diastereotopic CH_2 groups.

Josep Saurí, Laura Castañar, Pau Nolis, Albert Virgili and Teodor Parella*

Supporting Information

Figure S1: Effect of the β angle in ω_1-iINEPT-J experiments.

Figure S2: Spectral Folding in ω_1-iINEPT-J experiment.

Figure S3: ω_1-iINEPT and ω_1-iINEPT-J spectra of 5–methylene-2-norbornene in isotropic and anisotropic media.

Figure S4: Intensity signal dependence with respect the pre-scan delay in ω_1-iINEPT and ω_1-HSQC experiments

Table S1: ^{1}J(CH) and ^{2}J(HH) coupling constants of strychnine measured from ω_1-iINEPT-J spectra and other published methods.

Table S2: ^{1}J(CH)/^{1}T(CH) and ^{2}J(HH)/^{2}T(HH) coupling constants of 5-methylene-2-norbornene measured from ω_1-iINEPT-J spectra.

Table S3: ^{1}J(CH) and ^{2}J(HH) coupling constants of progesterone measured from ω_1-iINEPT and ω1-HSQC spectra.

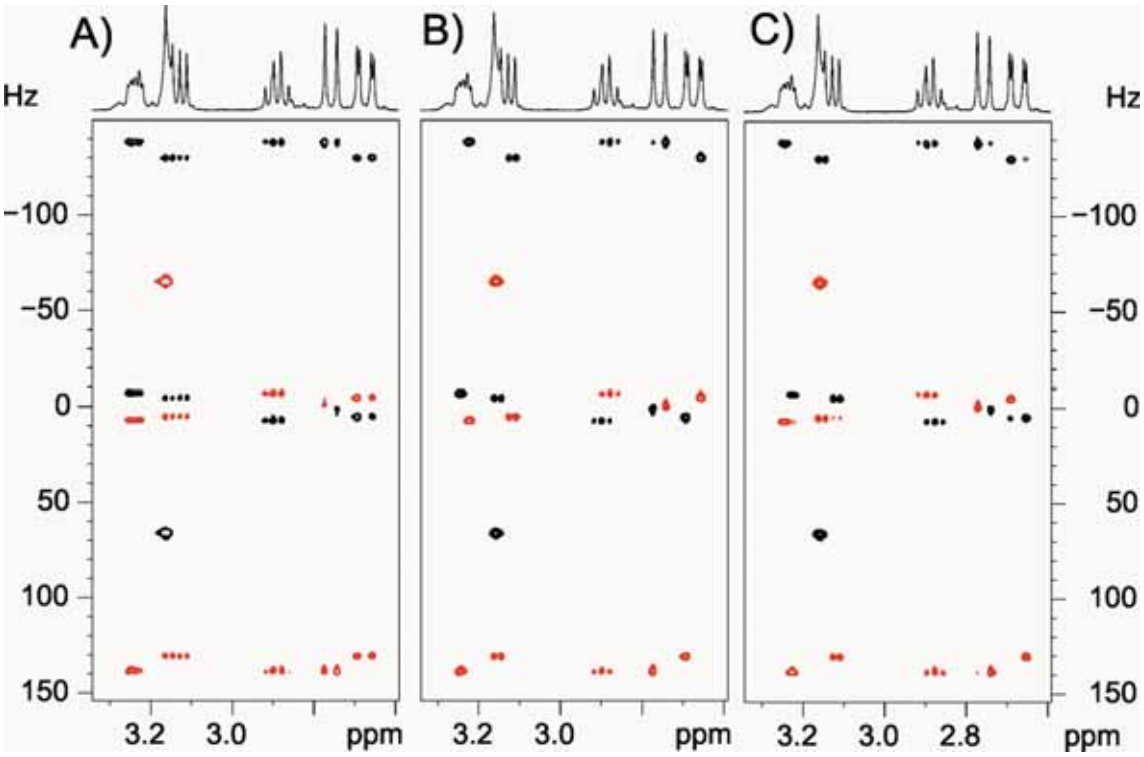

Figure S1: Effect of the β angle in ω_1-iINEPT-J experiments of **1**: A) β=90º, B) β=36º, and C) β=126º. Note the complementary spin-state selection in B *vs* C. Experimental conditions as described for Fig. 3D.

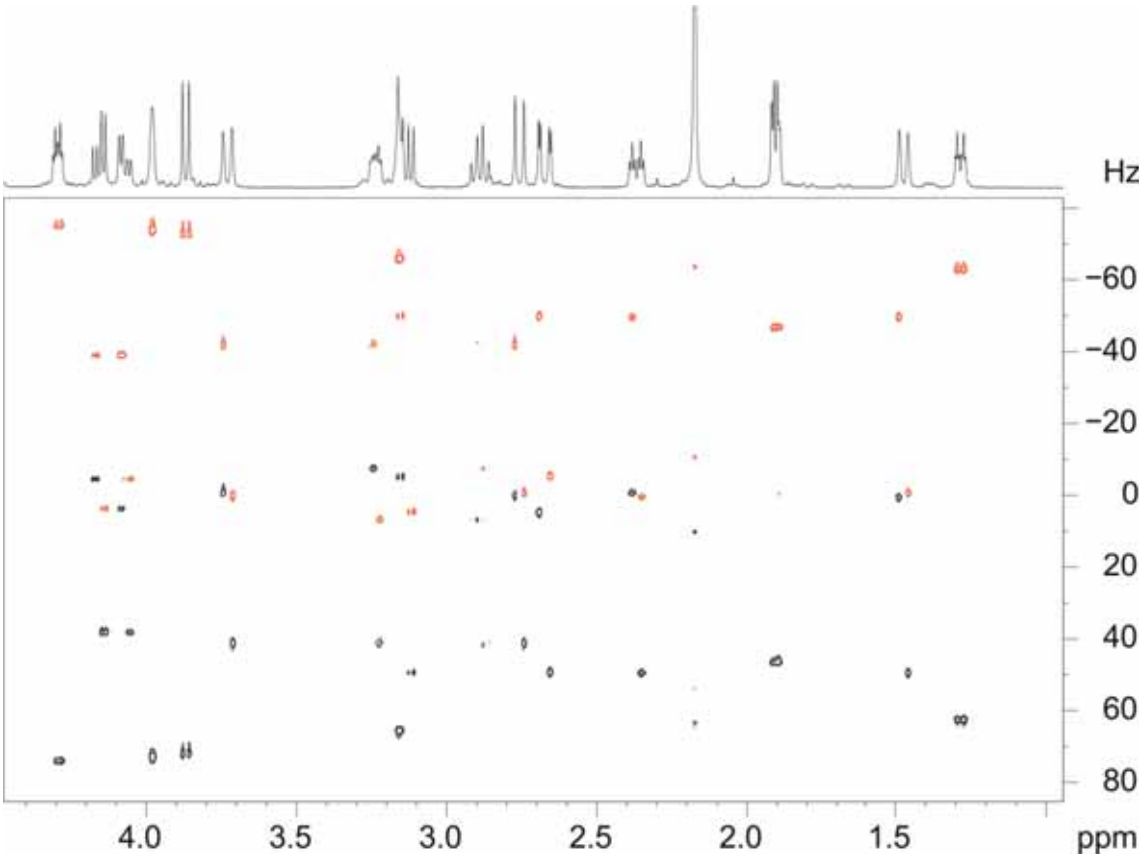

Figure S2: Spectral folding in the ω_1-iINEPT-J spectrum of **1**. 2 scans were collected for each one of the 256 t_1 increments using a spectral width (SW(F1)) of 180Hz in the indirect dimension. The digital resolution was of 0.18 Hz in the indirect dimension. All other experimental conditions as described in the Fig. 3D. ^{1}J(CH) coupling values are extracted from the relationship SW(F1)-$\Delta\nu(\omega_1)$, where $\Delta\nu(\omega_1)$ is the distance measured between individual components of a given cross-peak along the indirect dimension. Similarly, the distance between outer components allows to obtain the sum of the two coupling values, according to $^1J(CH_A)+ {}^1J(CH_B)=2*SW(F1)-\Delta\nu(F1)$.

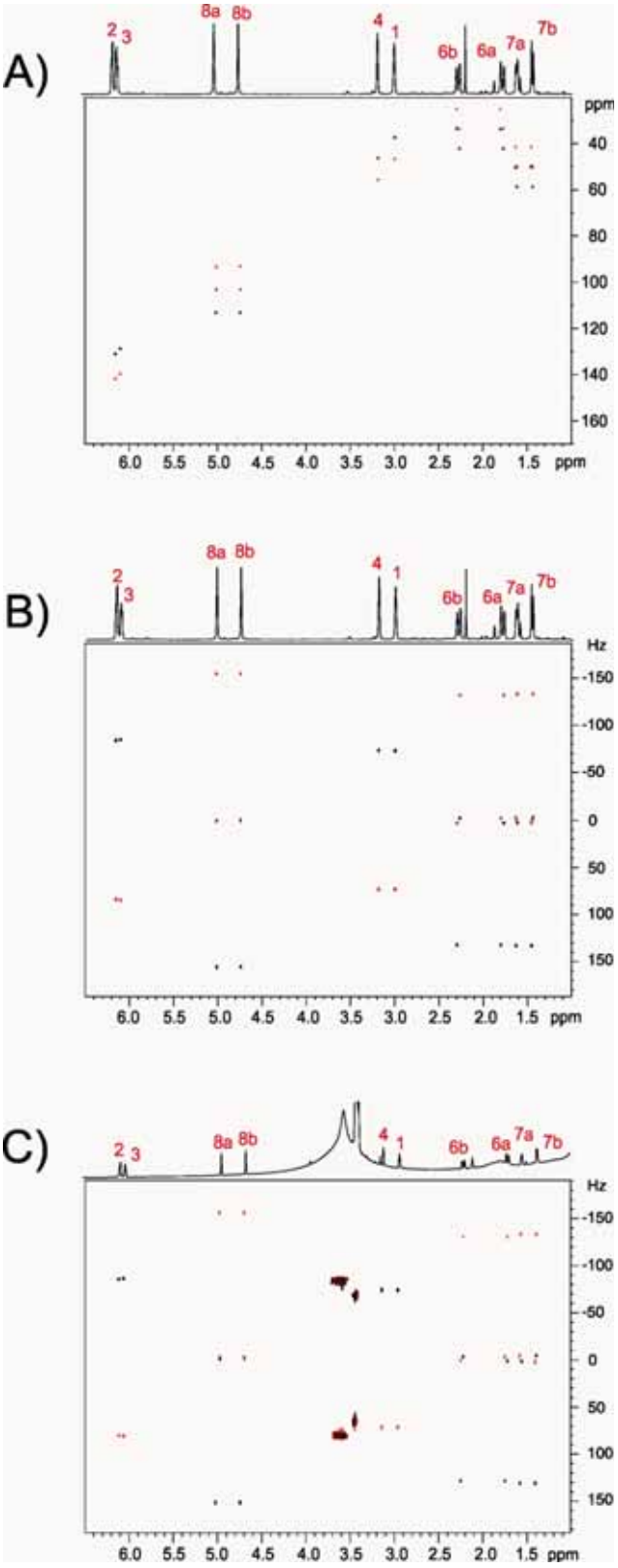

Figure S3: A) ω_1-iINEPT and B) ω_1-iINEPT-J spectra of **2** in isotropic $CDCl_3$ solution; C) ω_1-iINEPT spectra of **2** in anisotropic conditions (PMMA gel swollen in $CDCl_3$). ω_1-iINEPT experiment (A) was acquired with an scaling factor of k=8 whereas B) and C) used K=1. Other experimental conditions as described for Fig. 5.

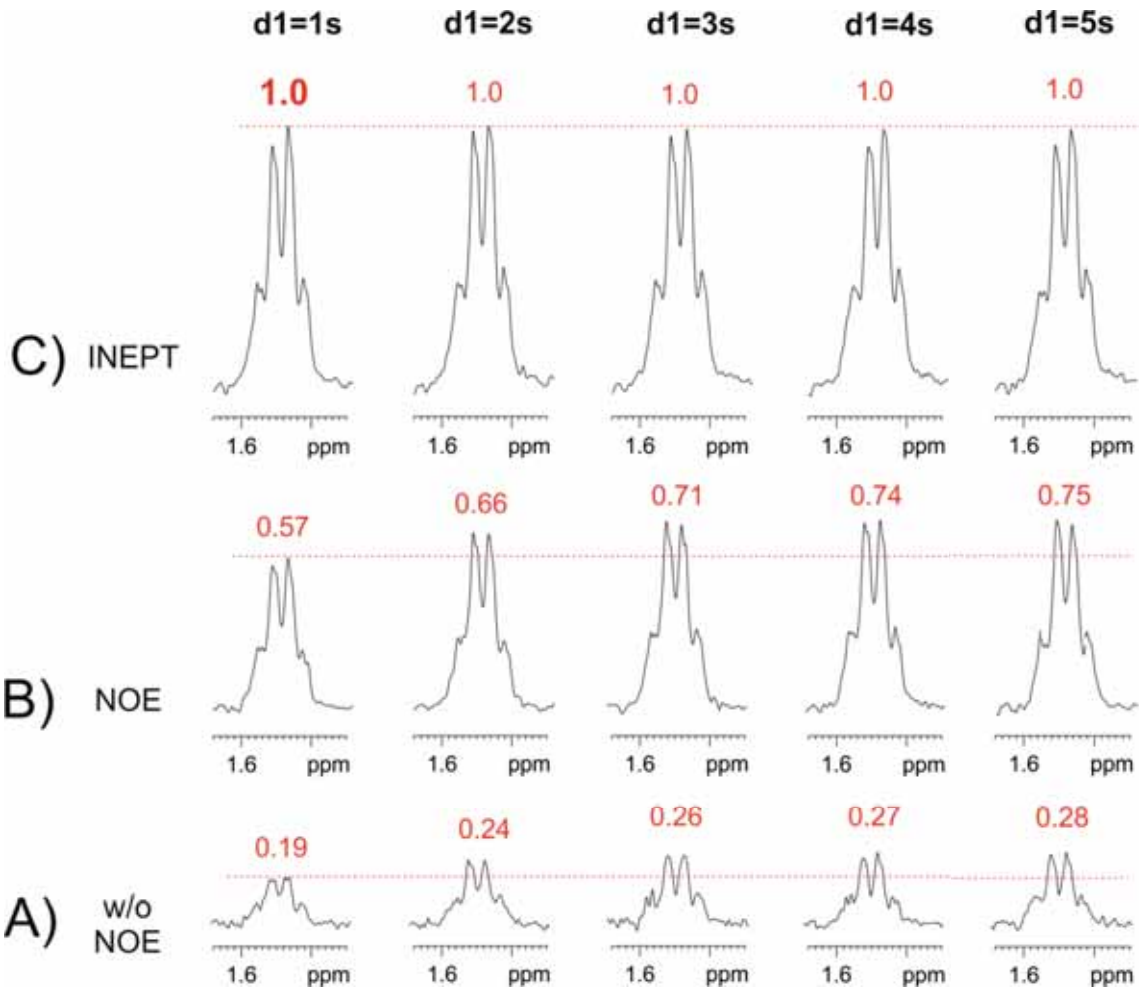

Figure S4: Signal intensity dependence of the H-8 proton in **3** as a function of the duration of the pre-scan delay: ω_1-iINEPT experiments A) without and B) with ^{1}H-saturation during the pre-scan delay, and c) ω_1-HSQC experiment using an initial INEPT transfer. As a reference, the intensity of the HSQC experiment using a recycle delay of 1 second has been normalized to 1.

Table S1: ^{1}J(CH) and ^{2}J(HH) coupling constants (in Hz) of strychnine (**1**) extracted from the ω_1-iINEPT-J spectrum.

		ω_1-iINEPT-J (This work)		**ref. [37]**	**ref. [36]**	**ref. [38]**	**ref. [5]**	**ref. [37]**	**ref. [39]**
		^{1}J(CH)	**^{2}J(HH)**	**^{1}J(CH)**				**^{2}J(HH)**	
C1	H1	158.9	-	158.0	158.8	159.0	159.0	-	-
C2	H2	161.7	-	162.0	160.7	161,3	161.56	-	-
C3	H3	160.3	-	159.0	-	159,4	159.85	-	-
C4	H4	169.1	-	168.2	168.7	168,6	168.4	-	-
C8	H8	144.9	-	145.1	144.7	144,9	144.89	-	-
C11 (from H11a)	H11a H11b	135.6 125.9	-18,1	133.8	134.9	135,3	135.06	-17,4	-17.38
C11 (from H11b)	H11a H11b	135.7 126.1	-18.3	125.2	125.8	125,5	126.08		
C12	H12	149.2	-	147.6	148.3	149,3	149.17	-	-
C13	H13	124.8	-	123.6	123.7	125,2	124.38	-	-
C14	H14	131.4	-	131.4	130.3	131,9	130.36	-	-
C15 (from H15a)	H15a H15b	131.3 129.6	-15.3	132.1	130.0	131,5	130.36	-14,5	-14.31
C15 (from H15b)	H15a H15b	130.7 129.6	-15.4	132.2	129.4	130,4	129.93		
C16	H16	146.8	-	146.9	145.9	146,3	146.6	-	-
C17	H17	133.1	-	134.0	134.2	133,1	132.93	-	-
C18 (from H18a)	H18a H18b	146.0 131.6	-10.3	139.7	147.1	147,6	146.17	-10,1	-
C18 (from H18b)	H18a H18b	146.1 131.3	-10.3	131.5	131.0	133,5	131.2		
C20 (from H20a)	H20a H20b	139.0 138.5	-15.6	137.7	138.4	139,7	138.91	-14,3	-14.74
C20 (from H20b)	H20a H20b	138.9 138.9	-15.5	137.7	138.7	139,9	138.91		
C22	H22	158.7	-	158.1	159.1	159,3	159.43	-	-
C23 (from H23a)	H23a H23b	145.1 137.3	-13.7	144.7	145.5	145,9	145.74	-13,7	-13.44
C23 (from H23b)	H23a H23b	145.6 137.2	-13.8	136.8	136.0	137,2	137.2		
Digital Resolution (Hz)		0.5	1.1	1.0	-	0.4	0.2	1.0	-

Table S2: $^{1}J(CH)$/ $^{1}T(CH)$ and $^{2}J(HH)$/$^{2}T(HH)$ coupling constants (in Hz) of 5–methylene-2-norbornene (**2**) measured from ω_1-iINEPT-J experiments in isotropic and anisotropic weakly aligned media.

		Isotropic		Anisotropic			
		$^{1}J_{CH}$	$^{2}J_{HH}$	$^{1}T_{CH}$	$^{2}T_{HH}$	$^{1}D_{CH}$[a]	$^{2}D_{HH}$[b]
C_1	H_1	147.2	-	147.9	-	0.7	-
C_2	H_2	168.9	-	168.2	-	-0.7	-
C_3	H_3	170.8	-	170.2	-	-0.6	-
C_4	H_4	148.3	-	148.8	-	0.5	-
C_6 (from H_{6a})	H_{6a}	136.0	-15.1	134.4	-18.9	-1.6	-3.8
	H_{6b}	130.7		130.1		-0.6	
C_6(from H_{6b})	H_{6a}	136.0	-15.3	134.1	-19.4	-1.9	-4.1
	H_{6b}	130.4		130.1		-0.3	
C_7 (from H_{7a})	H_{7a}	136.8	-8.1	137.8	-5.0	1.0	3.1
	H_{7b}	131.4		130.8		-0.6	
C_7 (from H_{7b})	H_{7a}	136.8	-8.1	137.9	-5.1	1.1	3.0
	H_{7b}	131.5		130.9		-0.6	
C_8 (from H_{8a})	H_{8a}	157.0	1.1	157.5	0.9	0.5	-0.2
	H_{8b}	155.1		155.3		0.2	
C_8 (from H_{8b})	H_{8a}	157.1	1.0	157.6	0.8	0.5	-0.2
	H_{8b}	155.1		155.4		0.3	
Digital Resolution (Hz)		0.5	0.9	0.5	0.9		

[a] RDCs ($^{1}D_{CH}$) values calculated from the different between the $^{1}T_{CH}$ values and the corresponding isotropic $^{1}J_{CH}$ values.

[b] RDCs ($^{2}D_{HH}$) values calculated from the different between the $^{2}T_{HH}$ values and the corresponding isotropic $^{2}J_{HH}$ values.

Table S3: $^{1}J(CH)$ and $^{2}J(HH)$ coupling constants of progesterone (**3**) measured from ω_1-iINEPT and ω_1-HSQC experiments.

		ω_1-iINEPT		**ω_1-HSQC**	
		$^{1}J(CH)$	**$^{2}J(HH)$**	**$^{1}J(CH)$ [a]**	**$^{2}J(HH)$**
C1 (from H1ax)	H1ax H1eq	126.8 129.9	-13.5	256.7	-13.8
C1 (from H1eq)	H1ax H1eq	126.5 127.7	-13.6	256.2	-13.3
C2 (from H2ax)	H2ax H2eq	123.9 132.1	-16.7	255.7	-16.6
C2 (from H2eq)	H2ax H2eq	124.3 132.3	-16.9	255.9	-16.9
C4	H4	158.8	-	158.7	-
C6 (from H6ax)	H6ax H6eq	124.8 130.6	-14.3	255.3	-14.5
C6(from H6eq)	H6ax H6eq	125.1 130.7	-14.4	255.1	-14.2
C7 (from H7ax)	H7ax H7eq	124.7 130.4	-13.2	254.5	-13.4
C7 (from H7eq)	H7ax H7eq	124.6 130.2	-13.3	254.5	-13.0
C8	H8	124.4	-	123.7	-
C9	H9	122.9	-	123.6	-
C11 (from H11ax)	H11ax H11eq	125.3 127.8	-9.5	253.7	-9.7
C11 (from H11eq)	H11ax H11eq	126.2 128.3	-10.8	253.8	-10.6
C12 (from H12ax)	H12ax H12eq	127.3 126.4	-13.7	256.2	-13.7
C12 (from H12eq)	H12ax H12eq	127.2 126.9	-13.5	256.1	-13.7
C14	H14	124.0	-	124.1	
C15 (from H15ax)	H15ax H15eq	130.7 132.4	-12.6	262.2	-12.9
C15 (from H15eq)	H15ax H15eq	ov 132.9	-13.7	262.1	-12.9
C16 (from H16ax)	H16ax H16eq	128.2 133.6	*	260.5	*
C16 (from H16eq)	H16ax H16eq	127.1 133.5	*	261.1	*
C17	H17	127.5	-	127.9	-
C18	H18	125.6	-	125.5	-
C19	H18	127.4	-	127.0	-
C21	H19	126.8	-	127.2	-
Digital Resolution (Hz)		1.5	0.5	1.5	0.5

[a] For diastereotopic CH_2 protons

PUBLICATION 13

Broadband ^{1}H homodecoupled NMR experiments: recent developments, methods and applications

Laura Castañar and Teodor Parella.
Mag. Reson. Chem., **2015**, *53*, 399-426.
DOI: 10.1002/mrc.4238

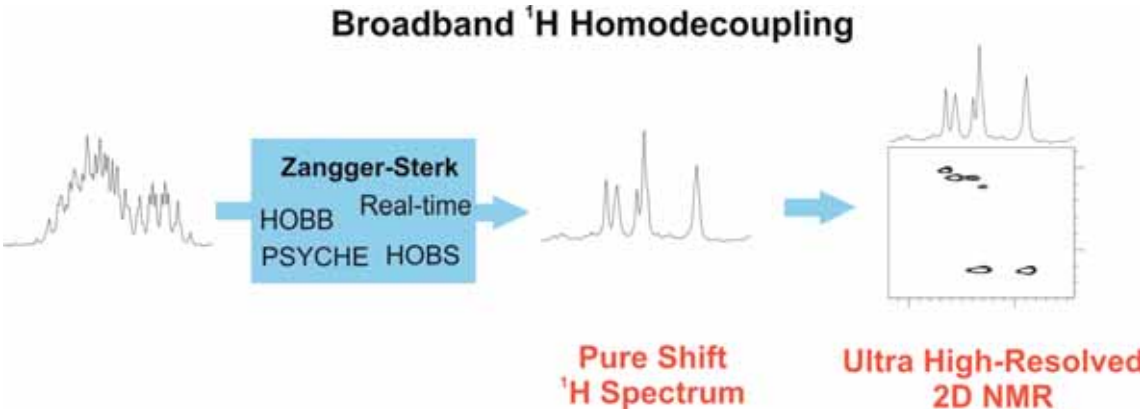

Introduction

In recent years, a great interest in the development of new broadband ^{1}H homonuclear decoupled techniques providing simplified J_{HH} multiplet patterns has emerged again in the field of small molecule NMR. The resulting highly resolved ^{1}H NMR spectra display resonances as collapsed singlets, therefore minimizing signal overlap and expediting spectral analysis. This publication is a complete revision work about modern pure shift NMR methodologies, with a particular emphasis to the Zangger–Sterk experiment. A description of the most important broadband homodecoupling building blocks and their implementation on different versions of the ZS experiment is made. A detailed discussion about the most relevant practical aspects in terms of pulse sequence design, selectivity, sensitivity, spectral resolution and performance is provided. Finally, the implementation of the different reported strategies into traditional 1D and 2D NMR experiments is described while several practical applications are also reviewed, including (i) the measurement of homo- and heteronuclear coupling constants from simplified multiplets, (ii) analysis of diffusion and relaxation data in overelapped regions, (iii) pure shift versions of standard 2D experiments, and (iv) the combined use of different but complementary resolution-enhanced techniques into a single NMR experiment in order to have ultra-high-resolved spectra with standard hardware configurations and conventional acquisition times.

Feature article: review

MRC

Received: 21 January 2015 Revised: 23 February 2015 Accepted: 25 February 2015 Published online in Wiley Online Library: 21 April 2015

(wileyonlinelibrary.com) DOI 10.1002/mrc.4238

Broadband ^{1}H homodecoupled NMR experiments: recent developments, methods and applications

Laura Castañar and Teodor Parella*

In recent years, a great interest in the development of new broadband ^{1}H homonuclear decoupled techniques providing simplified J_{HH} multiplet patterns has emerged again in the field of small molecule NMR. The resulting highly resolved ^{1}H NMR spectra display resonances as collapsed singlets, therefore minimizing signal overlap and expediting spectral analysis. This review aims at presenting the most recent advances in pure shift NMR spectroscopy, with a particular emphasis to the Zangger–Sterk experiment. A detailed discussion about the most relevant practical aspects in terms of pulse sequence design, selectivity, sensitivity, spectral resolution and performance is provided. Finally, the implementation of the different reported strategies into traditional 1D and 2D NMR experiments is described while several practical applications are also reviewed. Copyright © 2015 John Wiley & Sons, Ltd.

Keywords: NMR spectroscopy; pure shift NMR; homonuclear decoupling; Zangger–Sterk; BIRD; HOBB; HOBS; PSYCHE

Introduction

NMR spectroscopy is one of the most powerful tools for determining structural, dynamic, chemical and physical properties of molecules under a great variety of sample conditions. The most significant aspects in NMR are sensitivity and spectral resolution. Advances in sensitivity have been occurring over the years by a multitude of different techniques intended to improve NMR data acquisition and processing. The development and the improvements in NMR instrumentation have also played a key role to enhance sensitivity, with a particular emphasis in the technical design of cryogenically cooled probes or higher magnetic fields. On the other hand, spectral resolution is also improved inherently in higher magnetic fields, which disperse the chemical shifts over a wider frequency range, although the effects of signal overlap can still be a limiting factor when analyzing complex NMR spectra. The continuous development of new pulse sequences and the improvement of the existing ones have been another very important factor to understand the enormous potential of the NMR spectroscopy, and the incorporation of multiple-frequency dimensions achieves a tremendous qualitative and quantitative leap, particularly when it comes to improving signal dispersion.

The associated benefits of decoupling through-bond interactions for the apparent simplification of scalar coupling constant splittings are easily understood when analyzing a typical ^{13}C spectrum, which is routinely recorded under broadband heteronuclear ^{1}H decoupling during data acquisition.[1–5] In a standard 1D ^{13}C{^{1}H} spectrum, all signals appear as single lines providing excellent signal dispersion, allowing the knowledge of the number of signals that are present and also measuring accurate chemical shift values in a very straightforward way. In contrast, despite using high magnetic fields, 1D ^{1}H NMR spectra often suffer of low signal resolution and severe signal overlap due to the limited range of ^{1}H chemical shifts and also to the additional J_{HH} splittings observed in each proton resonance. The analysis of the fine multiplet structure contains valuable structural information such as the number and knowledge of neighboring spins or dihedral angle constraints, but, in many cases, signal overlap hampers a definitive multiplet analysis or the accurate extraction of chemical shifts, which are also fundamental in the analysis and interpretation of NMR spectra. On the other hand, *J* information can become redundant when multidimensional NMR spectra are analyzed, because only the correlation between chemical shifts is usually of interest for assignment purposes. Complex multiplet structures also negatively impact the usage of Computer-Assited Structure Elucidation (CASE) programs for automated structure elucidation, a problem that can be largely ameliorated with pure shift experiments.

The advantages of obtaining homonuclear decoupled ^{1}H NMR spectra have been extensively recognized, although there is not an easy and general solution to achieve this. Only as an example, Fig. 1 shows how the simplified *J* multiplet structure achieved in a small molecule like progesterone is a clear proof of the excellent complementarity between the homodecoupled and the standard 1D ^{1}H spectra. The absence of scalar coupling splittings improves signal dispersion, facilitates and accelerates chemical shift recognition and simplifies the analysis and assignment of complex regions, as illustrated for the overlap signals resonating around 1.6 and 2 ppm. Several homonuclear decoupling strategies have been suggested to improve signal resolution in ^{1}H NMR spectra, which are briefly commented in Section on Classical Homodecoupling Techniques. In the last few years, there has been a revival in the development of the so-called pure shift NMR techniques based

* *Correspondence to: Teodor Parella, Servei de Ressonància Magnètica Nuclear, Universitat Autònoma de Barcelona, E-08193, Bellaterra, Barcelona, Catalonia, Spain. E-mail: teodor.parella@uab.cat*

Servei de Ressonància Magnètica Nuclear and Departament de Química, Facultat de Ciències, Universitat Autònoma de Barcelona, E-08193, Bellaterra, Barcelona, Catalonia, Spain

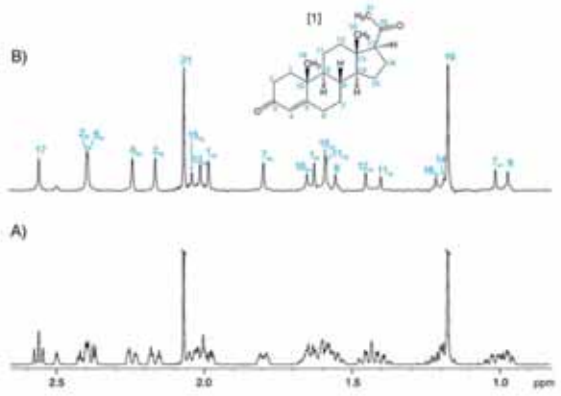

Figure 1. (A) 600-MHz conventional and (B) broadband homodecoupled 1D ^{1}H NMR spectra of the steroid progesterone [1] in dimethyl sulfoxide-d_6. Note how all simplified singlet resonances at their chemical shift frequencies can be distinguished in the pure shift spectrum, which was acquired in about 5 min using the PSYCHE experiment.

on the original *Zangger–Sterk* (ZS) experiment.[6] For this reason, we aim at presenting here the fundamentals and the recent progress in the design of new NMR pulse sequence elements to afford broadband homodecoupled ^{1}H NMR spectra. First, we describe some basic NMR building blocks designed to achieve broadband homodecoupling, discussing the pros and cons of each approach and introducing the most important practical aspects for a better performance. Then, the general strategies to implement these basic elements into standard 1D and 2D NMR experiments are introduced. Several recent applications are also highlighted showing the impact of these novel methodologies in the field of the small molecule NMR. At the time of writing this review, other excellent and complementary reviews about broadband homodecoupling NMR methods have also been published.[7–9] It is important to comment that the concept of homonuclear decoupling is also of high interest in other areas of the NMR spectroscopy, such as ^{13}C homodecoupling in experiments involving ^{13}C-labeled natural products,[10] proteins or nucleic acids,[11,12] or homonuclear decoupling of ^{1}H–^{1}H dipolar interactions when working in anisotropic media[13] or in solid-state NMR conditions,[14] but these descriptions are out of the scope of this review.

Broadband homodecoupling building blocks

The development and implementation of new homodecoupling building blocks into specific pulse schemes are nowadays an expanding area of research. Efforts are mainly concentrated in the design of methodologies that guarantee a routine use involving a simple and nonextended acquisition set-up, a standard and nonsophisticated data-processing procedure and general applicability in a wide range of NMR experiments.

Figure 2 illustrates a general building block to achieve broadband homodecoupling by combining the effects of a pair of NMR elements: a nonselective 180° pulse and a selective inversion element that affects only the so-called active spins. Some basic selective elements that perform such specific perturbation have been proposed: (i) a ^{12}C/^{13}C isotopic BIRD module (Fig. 2A),[15,16] (ii) frequency-selective 180° pulses (Fig. 2B–D), and (iii) spatially resolved elements consisting of a selective or adiabatic 180° pulse applied simultaneously to a weak *pulsed field gradient* (PFG) (Fig. 2E–H). In all these cases, the passive spins (decoupled spins) experience a 180° pulse whereas the active spins (detected spins) are unperturbed because they undergo an overall rotation of 360°. In practical terms, this means that chemical shift of active nuclei will not be affected and, therefore, it will evolve, while the homonuclear $J_{\text{Hpassive-Hactive}}$ coupling will be efficiently refocused. The amount of active spins being inverted is typically much smaller

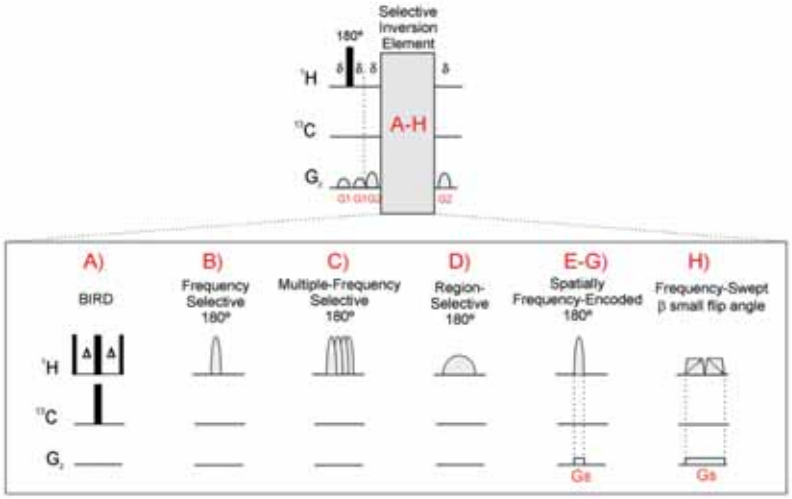

Figure 2. Basic NMR building blocks to perform broadband homonuclear decoupling, consisting of a nonselective 180° pulse and a selective inversion element: (A) BIRD cluster to selectively invert ^{1}H–^{13}C *versus* ^{1}H–^{12}C protons, or vice versa; (B–D) frequency-selective 180° pulses designed to invert/refocus a single or specific groups of signals; (E–G) slice-selective element to achieve spatially frequency-encoded perturbation along the *z*-axis, thanks to the simultaneously application of an encoding G_z gradient and a single-selective, multiple-selective or region-selective 180° pulse; (H) spatially selective element using a pair of small flip angle frequency-swept adiabatic pulses jointly with an encoding G_z gradient. The use of gradients (G1 and G2) flanking each inversion element can be optionally applied to remove improper refocusing/inversion. δ is the duration of the gradient and its recovery delay.

than the passive spins, entailing some cost in sensitivity that must be carefully evaluated in each case.

BIRD-based elements

A simple way to perform homonuclear decoupling is using the BIRD module, which is based on a different isotopic $^{12}C/^{13}C$ behavior. BIRD-based homodecoupling, introduced by Garbow and coworkers more than 30 years ago,[15] selectively inverts or refocuses all proton spins bounded to ^{13}C (active spins) while leaving ^{12}C bound protons (passive spins) unaffected ($BIRD^a$ element), or vice versa ($BIRD^r$ element), depending on the phases of BIRD pulses.[16] The basic homodecoupling block consists of the combination of a hard 180° ^1H pulse followed by a BIRD element (Fig. 2A), and the net effect is therefore a 360° rotation of protons directly bound to ^{12}C and a 180° rotation of the protons attached to ^{13}C. The main features of the success use of BIRD are as follows:

(i) Problems associated to strong J_{HH} coupling effects are minimized.
(ii) The geminal $^2J_{HH}$ interaction between diastereotopic protons is retained because the BIRD element cannot distinguish between protons directly bound to the same ^{13}C nucleus. As a practical consequence, BIRD-based pure shift spectra will show doublets for nonequivalent methylene protons. Recently, novel concepts based on constant-time BIRD[17] or perfect BIRD[18] elements have been proposed to refocus such $^2J_{HH}$ effects.
(iii) The ideal behavior expected for spins during the BIRD block can be compromised in real situations because of the single delay Δ (optimized to $1/2^*{}^1J_{CH}$) that may not simultaneously satisfy the heteronuclear couplings arising for different spins of the molecules and because of imperfect inversions for ^{13}C sites spanning up to 200 ppm in their chemical shift range. Either of these two deviations can affect the behavior expected for the ^{13}C-bonded protons, leading to artifacts. In practice, a suitable compromise value of Δ can be found to minimize the J_{CH}-derived artifacts whereas the use of adiabatic-shaped 180° ^{13}C pulses eliminates off-resonance effects.[19]
(iv) The price to pay for applying BIRD-based homodecoupling is sensitivity. Natural abundance of ^{13}C is approximately 1.1%, and therefore, an unavoidable sensitivity loss of ~99% is obtained after using a BIRD filter. This sensitivity penalty is avoided in experiments that preselect ^1H–^{13}C magnetization, as carried out in pure shift HSQC experiments.[20]
(v) BIRD fails for fully ^{13}C-labeled compounds because of J_{CC} evolution.

The BIRD-based homodecoupling method has been further refined and adapted for pure shift 1D[19,21] and 2D HSQC experiments[20,22] and applied in a variety of structural problems.[17,23–27]

Use of frequency-selective pulses

The use of a frequency-selective 180° pulse is a simple option to achieve selective inversion on a single or multiple ^1H signals (Fig. 2B–D). The performance is under the control of the NMR user by an appropriate choice of the duration and shape of the selected 180° pulse that defines the effective bandwidth of the selective excitation. Several options are feasible, including single-frequency, multiple-frequency or band-selective excitation covering a specific region of the proton spectrum. The only requirement is that this selective pulse must not affect to mutually J coupled protons to avoid the evolution of this mutual coupling.

These building blocks were initially used to significantly increase the spectral resolution in the indirect F1 dimension of 2D experiments, by collapsing J_{HH} multiplets to singlets by *band-selective homonuclear decoupling* (BASHD) techniques,[28,29] as reported for BASHD-COSY,[30] BASHD-TOCSY,[29,31–35] BASHD-ROESY[32,33,35,36] and BASHD-HMBC[37] experiments. This strategy can be combined with other homodecoupling techniques along the detected F2 dimension in order to obtain ultra high resolution in both dimensions of fully homodecoupled 2D spectra.

Spatial encoding

Conventional NMR experiments involve the nonspecific excitation and detection of the NMR signal in the entire detector coil (Fig. 3A). The incorporation of the spatial encoding concept, traditionally used in magnetic resonance imaging applications, into high-resolution NMR spectroscopic techniques is attracting an increasingly larger interest. Several strategies have been developed to perform spatial encoding into an NMR tube (Fig. 3B–D):

(i) Data collection is focused on a specific z-slice along the NMR sample (Fig. 3B). Spatially resolved NMR applications have been reported for the analysis and characterization of heterogeneous samples, for instance, to study biphasic systems,[38–40] to detect and quantify sample inhomogeneities and spatial distribution in different alignment media such as gels or liquid crystals,[41,42] to investigate solvation and diffusion of CO_2 in ionic liquids,[43] to perform fast titrations and *in situ* reaction monitoring for obtaining information about reaction mechanisms and detecting intermediates[44] or to avoid z-gradient imperfections in diffusion NMR experiments.[45,46]
(ii) Signal excitation of different slices is executed in a sequential mode with the aim of reducing the long recycle delay and therefore shortening the overall acquisition time in 1D and 2D experiments (Fig. 3C). Examples have been reported to speed up data acquisition in 1D broadband homodecoupled,[47] 2D COSY[48] and 2D HMQC[49] experiments or to monitor fast reactions by sampling different parts of the NMR tube.[50]
(iii) Achievement of a selective and simultaneous signal perturbation, where each proton frequency is excited at different z-positions (Fig. 3D). This is the basis of the original ZS experiment,[6] and it has also been applied in single-scan T_1 relaxation time measurements,[51] to measure coupling constants,[52,53] or for the efficient diagonal peak suppression in 2D experiments.[54]
(iv) Use of selective multiple-frequency pulses in order to excite simultaneously a specific signal in different parts of the NMR tube (multislice selection) (Fig. 3E).[55,56]
(v) Simultaneous selection of multiple z-slices by using a concerted signal excitation and acquisition scheme (Fig. 3F), as traditionally performed in single-scan ultra-fast 2D NMR techniques where the t_1 increments sequentially recorded in a standard 2D experiment are simultaneously carried out along the length of the sample.[57]

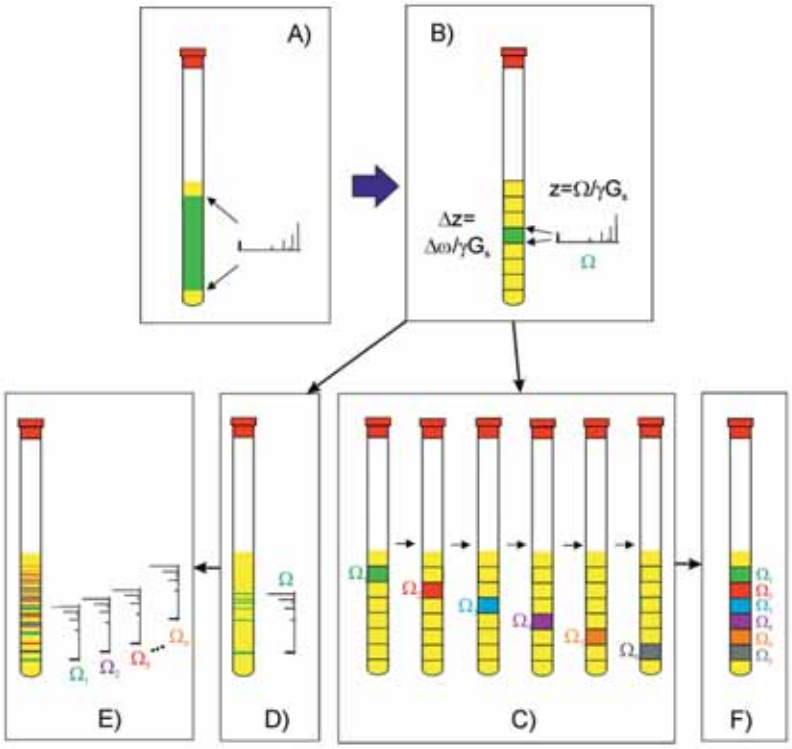

Figure 3. Different strategies to induce spatial selection along the *z*-axis of an NMR tube: (A) standard excitation/detection over the entire coil; (B) single-slice selection; (C) sequential spatial selection; (D) frequency-selective spatial selection; (E) simultaneous multiple frequency-selective spatial selection; (F) simultaneous multiple-slice excitation/detection.

Most of the reported slice-selective applications have been implemented in conventional liquid-state NMR spectrometers equipped with a basic hardware configuration; this is a direct or indirect detection probe incorporating a gradient coil that can deliver maximum gradient strengths around 50–60 G/cm along the *z*-axis. Experimentally, spatial frequency encoding is achieved by simultaneous application of a frequency-selective 90° or 180° pulses and a weak spatial-encoding PFG, G_z, both with the same duration (Fig. 2E–G).[6]

When a PFG is applied along the *z*-axis, the B_0 field is made spatially inhomogeneous by varying linearly along the applied dimension. Thus, during the application of a PFG, different parts of the sample experience a different magnetic field strength depending of its *z*-position, leading to a spatial-dependent frequency shift across the sample volume. Figure 4 compares the effects to apply a hard 90°, a frequency-selective 90° and a simultaneous selective 90°/gradient element. In the conventional ^{1}H spectrum, all signals from any part of the NMR tube into the active detector coil contribute to the observed signal (Fig. 4A). In the selective experiment, only those signals experiencing the selective pulse contribute to the detected data, although the maximum sensitivity for these signals is retained (Fig. 4B). In the slice-selective experiment, a complete ^{1}H spectrum can be obtained using optimized pulses and gradients, but each individual signal exclusively comes from a different part of the tube along the *z*-dimension (Fig. 4C). As an obvious consequence, a decrease of overall sensitivity is always associated with any slice-selective experiment, which is proportional to the number of generated *z*-slices.

Experimentally, the range of sampled frequencies or spectral width (SW_G) is defined by the strength of G_S according to

$$SW_G = \gamma . L . G_S \quad (1)$$

where γ is the gyromagnetic ratio of the spatially encoded nucleus and L is the active volume coil length. On the other hand, the carrier frequency (Ω) and the selective pulse bandwidth ($\Delta\omega$) determine the *z*-position of each nuclear spin (z) and the slice thickness (Δz) according to these two expressions, respectively:

$$z = \Omega / \gamma . G_S \quad (2)$$

$$\Delta z = \Delta\omega / \gamma . G_S \quad (3)$$

The SNR of slice-selective experiments depends on the active slice thickness because detected signal only comes from a selected *z*-slice. As shown, Δz depends both on the strength of G_S (which is proportional to the SW_G) and on the selectivity of the pulse (which should not exceed the smallest chemical shift difference expected between any coupled proton pairs). For instance, a typical 20-ms Gaussian-shaped 180° pulse (bandwidth of 60.7 Hz) applied simultaneously with a gradient G_S of 0.74 G/cm splits the sample height (L = 1.8 cm) into around 94 slices along the *z*-axis, defining a Δz of about 0.019 cm and covering an SW_G

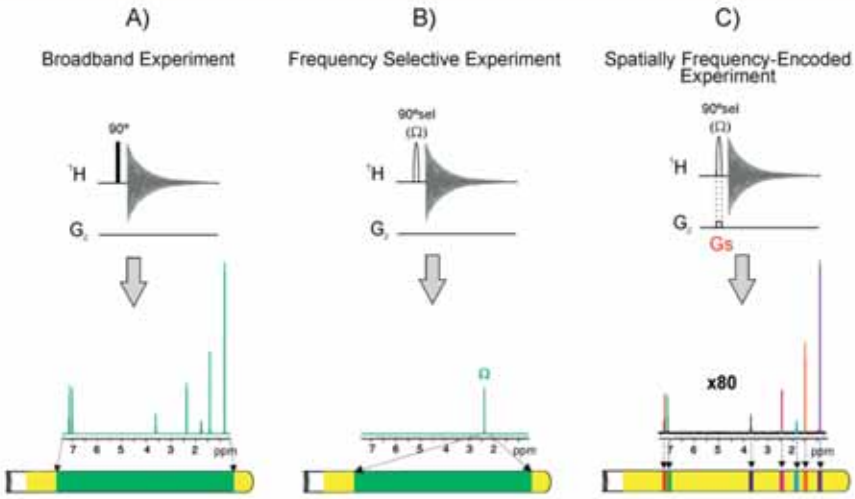

Figure 4. General illustration to understand slice-selective excitation: (A) conventional acquisition scheme to obtain an ^{1}H spectrum; (B) selective excitation using a 90° frequency-selective pulse; (C) slice selection consisting of the simultaneous application of a selective 90° pulse and a weak encoding gradient. In the latter case, the full spectrum is obtained, thanks to the spatial-dependent *z*-position of each individual resonance along the NMR tube.

of 5694 Hz (9.5 ppm in a 600-MHz spectrometer). Thus, under these general conditions, the single-slice selection procedure would afford only about 1% of the sensitivity of a conventional ^{1}H spectrum.

Several approaches have been reported to enhance SNR per time unit in slice-selective experiments:

(i) Sequential slice excitation (Fig. 3C) with the aim of reducing the long recycle delay and shortening the overall acquisition time in 1D and 2D experiments[47–49] or performing continuous data acquisition, as described in fast reaction monitoring studies.[50] This strategy uses a fast pulsing approach with around 100 ms of recycle delay, and after each scan, the offset of the selective shaped pulse is changed to access fresh equilibrium magnetization from adjacent frequency/spatial regions. Sakhaii *et al.* reported how an optimized division of the NMR tube in eight slices by changing the offset accordingly affords an experiment increment by a √8 factor in the original ZS experiment.[47] Similarly, spatially selective HMQC spectra have been rapidly recorded within 45–90 s dividing the NMR tube of protein samples in four *z*-slices.[49]

(ii) Use of multiple-frequency modulated pulses to simultaneously excite different slices in a single-NMR experiment (Fig. 5A).[55,56] This proposal is based on the careful setting of multiple offsets to avoid the excitation of mutually *J*-coupled protons within the same slice. Figure 5B shows different 1D *z*-profile images for a test sample of the anti-inflammatory drug ibuprofen acquired with a single scan, demonstrating that the user can have a full control on which signal and which *z*-position the excitation is performed. It can be shown how each individual signal in the conventional ^{1}H spectrum is excited in a particular *z*-position of the NMR tube. As predicted theoretically, an improved SNR by a factor of 4 is experimentally achieved using a four-site excitation (Fig. 5C).

(iii) It has been reported that the use of the so-called through-polarization sharing can afford an average enhancement by a factor of 2.[58] This approach is based on the original *acceleration by sharing adjacent polarization* (ASAP) technique that uses a short recycle delay consisting of a 40-ms isotropic DIPSI-2 (Decoupling In the Presence of Scalar Interactions) pulse train flanked by two gradients.[59] The method presents some limitations because sensitivity enhancement is not uniform for all signals and strongly dependent of the different relaxation properties of the excited protons while other spins remain unperturbed, preventing any attempt of quantification.

Slice selection works well for weakly coupled spin systems, but it can fail for strongly coupled signals. If the chemical shift difference ($\Delta\delta$) of coupled spins is less than the selective pulse bandwidth ($\Delta\omega$) but they are not very strongly coupled ($\Delta\omega > \Delta\delta > J$), couplings within $\Delta\omega$ become active, but the effects of couplings to other spins remain suppressed, retaining much of the resolution advantage. Where spins are fairly strongly coupled ($\Delta\omega > \Delta\delta \approx J$), weak extra signals appear at intermediate frequencies, and if they are very strongly coupled ($\Delta\omega > J > \Delta\delta$), it will typically yields distorted signals. The optimum selective 180° pulse and the encoding G_z gradient strength are quickly calibrated using a *slice-selective single-PFG echo* (ss-SPFGE) experiment. The excitation of two *J*-coupled protons into the same slice is observed as distorted multiplets in the corresponding 1D ss-SPFGE spectrum (Fig. 5C).[55]

Homodecoupling acquisition modes

Classical homodecoupling techniques

Each signal in an ^{1}H NMR spectrum exhibits a particular multiplet J_{HH} pattern as a result of its through-bond interactions with their neighboring protons. Thus, experimental issues such as signal dispersion, spectral resolution or signal overlap become very relevant to identify and assign each individual signal, in particular when a large number of resonances are present in a narrow range of frequencies. The use of NMR methods affording simplified multiplet structures are of interest because they can facilitate the

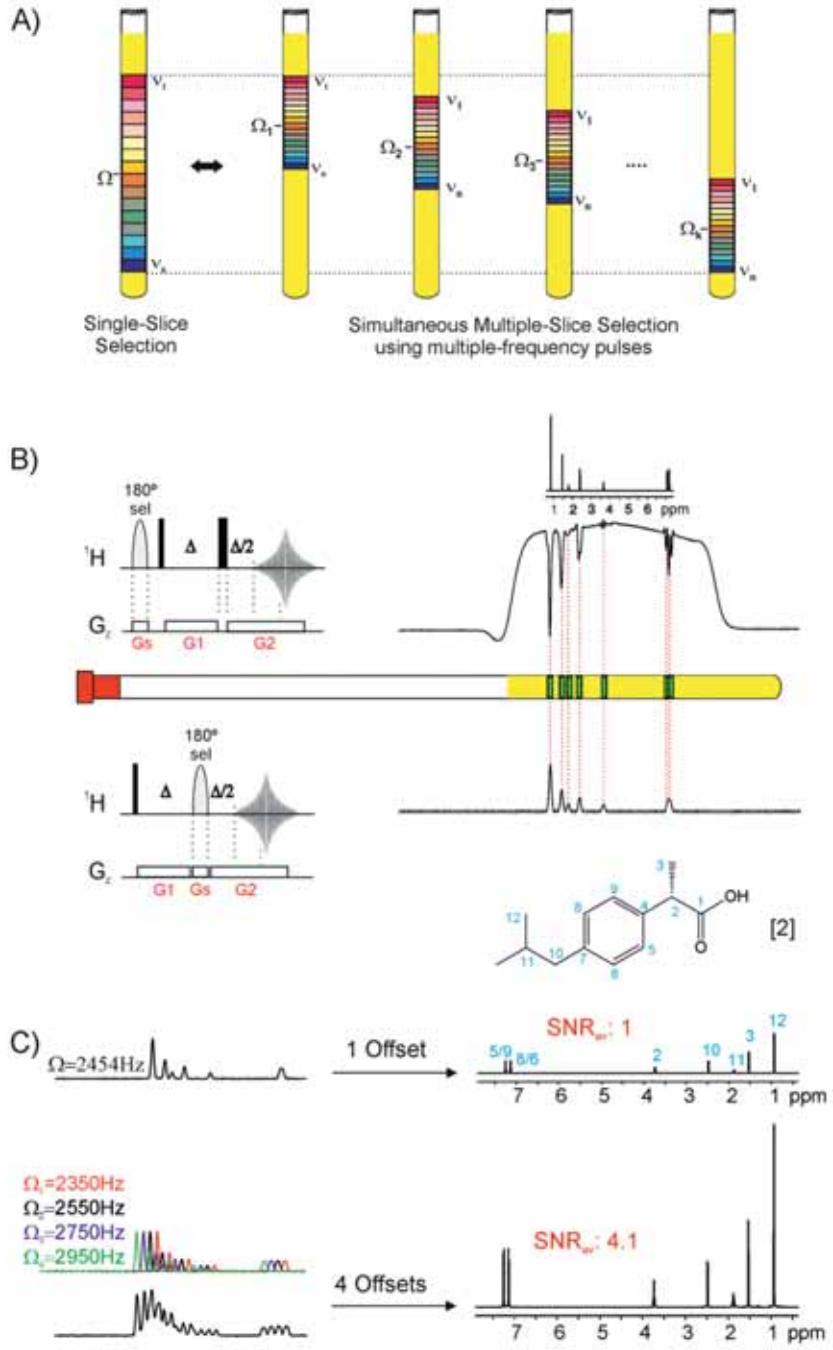

Figure 5. (A) Schematic illustration of the single *versus* multiple offset slice selection. (B) Pulse schemes to obtain 1D *z*-profile images of ibuprofen [2] along the NMR tube. (C) Experimental sensitivity enhancement obtained by a simultaneous four-site excitation. In (B) and (C), a selective 20-ms Gaussian-shaped 180° pulse was applied simultaneously with a square-shaped encoding gradient (G_S) of 0.742 G/cm. Figure adapted from reference.[55]

analysis and the interpretation of the corresponding spectra. The traditional way to achieve such simplification is by frequency-selective continuous-wave irradiation on a single-target signal during the acquisition period.[60] The method has been improved by multiple irradiation of different signals using multiple-frequency homodecoupling,[61] polychromatic pulses[62] or irradiating a group of signals resonating into the same region,[63–67] among others,[68] being the band-selective homodecoupling of the well-defined NH

or H_α regions in peptides and proteins one of the most reported applications.[69–72] All these approaches do not provide broadband homodecoupling in the entire spectrum, so only multiplet patterns of some signals are partially simplified according to the irradiated signals, and therefore, success is limited to specific and well-isolated spin systems.

A simple and classical approach to achieve a broadband homodecoupled ^{1}H spectrum is the 1D projection obtained along the detected dimension in a tilted homonuclear *J*-resolved experiment.[73–87] The standard experiment suffers of poor phase-twist lineshapes, and alternatives to obtain absorptive spectra such as the incorporation of spatial-selective encoding at expense of important sensitivity losses[83] or using a *z*-filter combined with a post-processing pattern recognition algorithm[84] have been proposed. Another drawback that has been recognized and evaluated in detail is the presence of extra peak artifacts due to strong coupling effects.[82] The use of appropriate data processing in *J*-resolved experiments has also been an interesting area to enhance sensitivity.[88] The *J*-resolved module has been appended as an NMR building block to standard 2D experiments, such as reported for homodecoupled versions of DOSY[89,90] and HMBC experiments,[87] although the resulting 3D experiments become more time consuming than the original ones. The *J*-resolved experiment has been successfully used in the determination of small chemical shift differences in complex mixtures, such as metabonomics[91] or enantiodifferentiation[86] studies, among others.

Separation of chemical shifts and *J* couplings while retaining absorption-mode lineshapes can also be obtained from the diagonal projected spectrum of a modified anti *z*-COSY experiment.[92] Another group of NMR experiments performs broadband homonuclear decoupling in the indirectly detected dimension of multidimensional experiments using time reversal,[93] constant-time evolution[94–102] or BIRD editing in the case of heteronuclear experiments.[103]

Pseudo-2D ZS experiment

Two different acquisition schemes are available to achieve broadband homodecoupling in the acquisition dimension: (i) a pseudo-2D acquisition mode where a homodecoupled FID is reconstructed by concatenating data chunks extracted from individual time domain datasets of a 2D experiment[6] (Fig. 6A) and (ii) a real-time acquisition mode that provides directly the homodecoupled FID (Fig. 6B).[19,104]

The original ZS experiment, reported in 1997,[6] uses a slice-selective 2D pulse timing where a variable delay is incremented stepwise as usual (Fig. 6A). The homodecoupling block (see several options in Fig. 2) is applied in the middle of this incremented delay to refocus any J_{HH} evolution. A special post-processing is needed, where the first data chunks of each FID are assembling to create a new reconstructed 1D FID that is processed and transformed by ordinary procedures to lead a homodecoupled ^{1}H NMR spectrum. A more robust ZS scheme has been proposed where the timing of the decoupling element was carefully designed to provide homodecoupling in the middle of each data chunk, where PFGs were also applied to suppress strong signals from passive spins.[105]

Experimentally, the evolution time (t_1) is incremented according to $1/SW_1$, where SW_1 is the defined spectral width in the indirect dimension (typically $SW_1 = 50–100$ Hz), and the first 10–20 ms of each individual FID are selected for a further FID reconstruction. In case of large scalar coupling constants, the increments must be set to smaller values ($SW_1 < J_{HH}$) in order to avoid scalar coupling evolution. This method produces small artifacts, typically in the form of weak sidebands at multiples of SW_1. The resolution of the signals is directly related with the number of increments in the indirect dimension. Normally, 16–32 increments are enough to obtain a high-quality 1D homodecoupled spectrum with optimum resolution and narrow line widths. Only as a reference, typical standard parameters to afford a nice 1D homodecoupled spectrum in ~5–10 min for a sample concentration about 10 mM would involve Gaussian or rSNOB shaped 180° ^{1}H pulses with a duration of 40–60 ms and an encoding G_z gradient around 0.5–1 G/cm. Under these general conditions, the pseudo-2D ZS method would afford only ~1–5% of the sensitivity of a conventional ^{1}H spectrum. SNR could be improved by using shorter and less selective pulses and/or less intense encoding gradients but always with an increased probability of accidental excitation of two coupled protons within the same slice. As discussed previously for slice-selective experiments, several ZS enhancements have been reported to improve this low SNR, including sequential slice selection,[47] multiple-slice selection[55,56] or ASAP enhancement[58] and to make these ZS experiments of practical use for moderately concentrated samples. For instance, Fig. 7 shows an example of multiple-slice

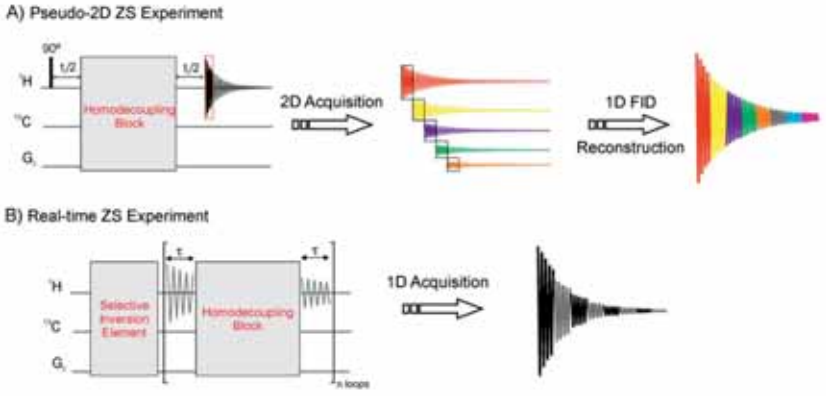

Figure 6. General schemes leading to 1D broadband homodecoupled ^{1}H NMR spectra: (A) The original ZS method is based on a 2D acquisition mode followed by an FID reconstruction from the initial data chunks of each increment; (B) the real-time ZS experiment incorporates periodically the homodecoupling block in the middle of the FID acquisition. The homodecoupling block can be any option described in Fig. 2.

selection where an experimental SNR enhancement by a factor of 7 achieved for the immunosuppressant drug cyclosporine by using a multiple frequency-modulated pulse at eight different offsets.[55]

The original ZS experiment was based on slice selection, and a BIRD-based ZS experiment has also been reported.[21] In a recent improvement, referred to as *pure shift yielded by chirp excitation* (PSYCHE) experiment (Fig. 8A),[106] a pair of low flip angle swept-frequency pulses and a weak PFG are used as a selective inversion element (Fig. 2H). By adjusting the pulse flip angle, it is possible to balance optimum sensitivity and full broadband homodecoupling for all signals in a given sample. PSYCHE can offer a sensitivity improvement of almost one order of magnitude in performance over conventional ZS methods performed by slice-selection or BIRD pulses (Fig. 8C–E).

The pseudo-2D ZS experiment has been applied to measure homonuclear[107] and heteronuclear[26,108,109] coupling constants, to detect small chemical shit differences in enantiodifferentiation studies,[24] and it has been implemented into 2D experiments, as reported for pure shift DOSY,[105,110,111] TOCSY,[112–114] NOESY,[102] HSQC[17,22,23] and Heteronuclear Single Quantum Multiple-Bond Correlation (HSQMBC).[109] The main drawback of these resulting pseudo-3D experiments is that their overall acquisition times can become extremely long for routine use.

Real-time ZS experiment

HOBB experiments

Real-time broadband homodecoupling was initially proposed using the BIRD element as homodecoupling block during data acquisition,[19] and shortly after, a slice selective version was also reported[104] using the general scheme of Fig. 6B. This new acquisition technique, referred to here as real-time ZS or *homodecoupled broadband* (HOBB) experiment, directly generates a single 1D FID that after standard processing leads to a broadband homodecoupled 1D ^{1}H NMR spectrum. This method offers instant and sped-up data acquisition and an improved SNR per time unit compared with the original ZS experiment, although the attainable sensitivity is still far from a regular ^{1}H spectrum because of the involved ^{13}C editing or slice selection procedures.

In the real-time ZS method, instead of recording each fraction of the FID in a series of individual experiments, a single FID is collected in each scan. The acquisition is interrupted after every τ period to perform either slice-selective or BIRD-based homodecoupling, as shown in Fig. 9A. Note that the first fraction of acquisition is only half as long as the subsequent ones. Thereby, full scalar decoupling is achieved in the middle of each fraction of the FID. These acquisition segments are assembled consecutively in a conventional FID, which can be treated like a regular 1D NMR experiment. The τ period is defined as $AQ/2n$ where AQ is the acquisition time and n the number of loops. As long as $\tau << 1/J_{HH}$, homonuclear J modulations occurring during these acquisition segments can be disregarded with no compromise in the final spectral resolution, leading to the potential collapse of all J_{HH} splittings. Deviations from this condition lead to incomplete homodecoupling and the appearance of distinct decoupling sidebands flanking each purely shifted resonance at spacing multiples of $2n/AQ$. On the other hand, while the acquisition is interrupted for decoupling, the magnetization is relaxing, and therefore, it is critical to keep the interruptions as short as possible, especially for larger molecules that have shorter T_2 relaxation times. Moreover, it is also important

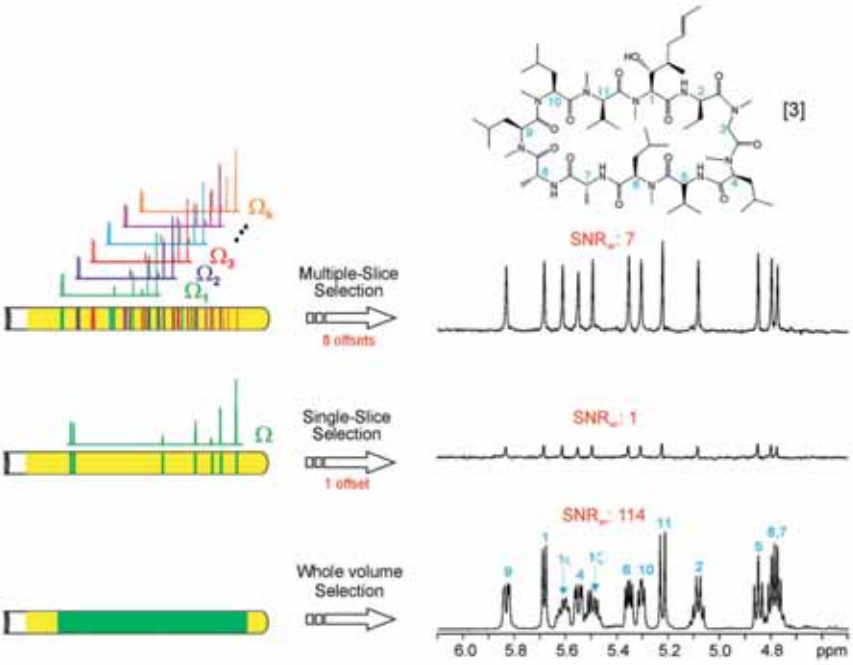

Figure 7. Comparison of the real SNR achieved in the pseudo-2D ZS experiment of cyclosporine [3], taking the standard ^{1}H spectrum as a reference. The pseudo-2D ZS experiment acquired with an rSNOB shaped pulse of 80 ms and a weak gradient of 1.13 G/cm affords an SNR factor of 1/114 whereas the use of an eight-site excitation improves SNR by an experimental factor of ~7. Figure reproduced with permission of reference.[55]

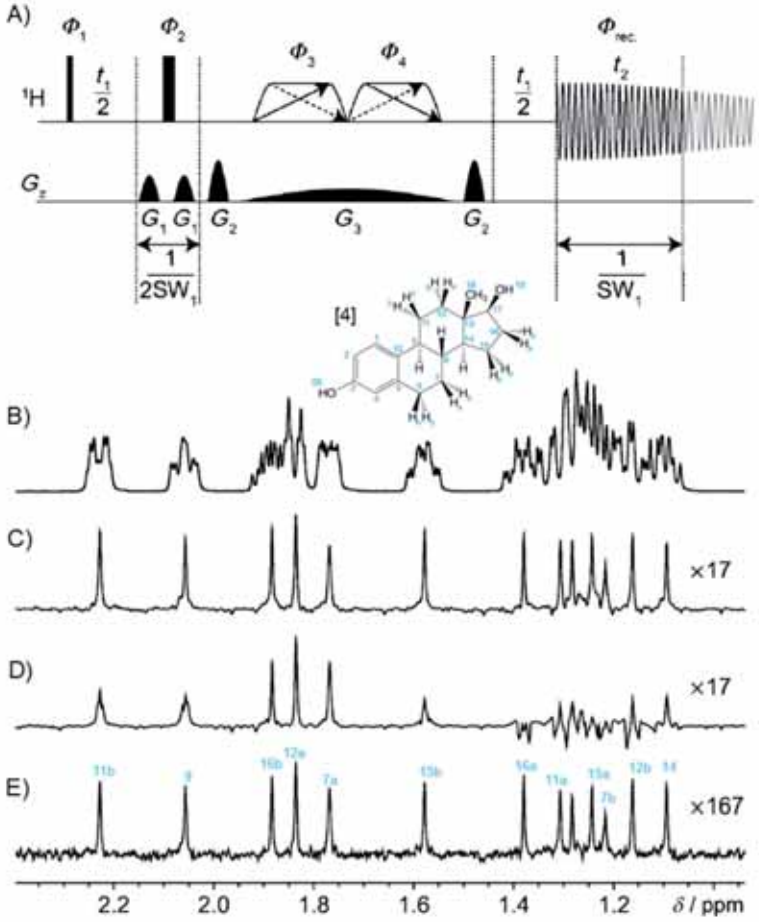

Figure 8. (A) Pulse scheme of the ZS-based PSYCHE experiment that uses a pair of low-power frequency-swept chirp pulses and a weak gradient as a selective inversion element. (B) 600-MHz ^{1}H NMR spectrum of the sex hormone estradiol [4] in $CDCl_3$; (C and D) original ZS spectra using 12- and 100-ms rSNOB 180° ^{1}H pulses, respectively; (E) PSYCHE spectrum obtained with two chirp pulses of 15 ms ($\beta = 20°$) and G3 = 0.75 G/cm. Each ZS spectrum in (C–E) was obtained in ~6 min. Adapted from reference.[106]

to minimize pronounced discontinuities during the FID that can lead to considerable sideband artifacts. If a BIRD-based homodecoupling block is used, the FID is interrupted about 6–8 ms (to $^1J_{CH}$ between 120 and 160 Hz). In the case of using a selective 180° pulse, a compromise duration of 5–10 ms balances between an optimum slice selection and an effective homodecoupling of nearby signals, while it minimizes the T_2 relaxation effects. In practice, real-time ZS acquisition reduces the overall experimental time and improves SNR per time unit but at some cost in spectral quality and the achievement of wider line widths. As an example, the HOBB spectrum of cyclosporine, quickly acquired in a single scan, shows full homodecoupling for most of the signals (except in some aliphatic CH_2 resonances), thanks to the well-dispersed spin systems (Fig. 9C). Importantly, the SNR of the HOBB experiment also suffers of the unavoidable losses due to slice selection (~8% of the maximum theoretical signal).

The real-time ZS acquisition mode becomes an attractive NMR building block for the design of pure shift methods, and, as a major advantage, it can be incorporated as a detection scheme in standard multidimensional experiments without increasing their original dimensionalities and continuing to use the same data-processing protocols. This represents a boost in SNR per time unit when compared with the pseudo-2D ZS experiment, as reported for HOBB-DOSY,[115] HOBB-TOCSY,[104] HOBB-ROESY[116] and HOBB-HSQC[20,24,25,117] experiments. From a strategic point of view, it is advisable to optimize first a 1D HOBB experiment in order to determine the best homodecoupling conditions for the sample under study. The signal simplification observed in 2D HOBB spectra will be the same obtained in a 1D HOBB spectrum recorded under the same conditions.

Recently, the sensitivity enhancement properties to the dissolution *dynamic nuclear polarization* combined with broadband homodecoupling techniques have been proposed to collect homonuclear decoupled proton NMR spectra with optimum sensitivity. This HyperBIRD experiment[27] is based on an initial ^{13}C *ex situ* hyperpolarization process, followed by a spontaneous ^{13}C-to-^{1}H polarization transfer via cross-correlation. Then, a rapid ^{1}H data collection using a 1D real-time BIRD-based ZS experiment exclusively detects ^{1}H directly attached to ^{13}C, whereas ^{1}H-^{12}C

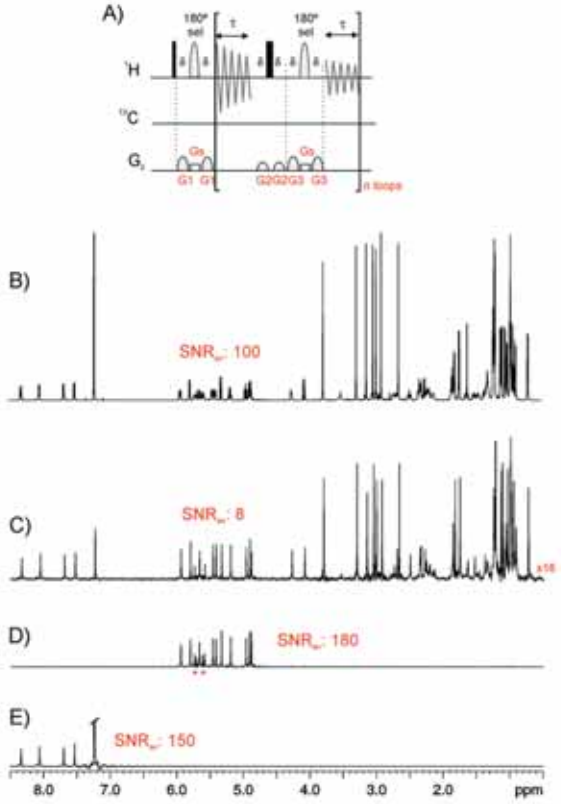

Figure 9. (A) General pulse scheme of the real-time 1D HOBB and HOBS experiments; (B) 600-MHz conventional ^{1}H spectrum of cyclosporine [3]; (C) 1D HOBB spectrum acquired with a REfocusing Band-selective Uniform-Response Pure-phase (RE-BURP) pulse of 5 ms for both excitation and decoupling and G_s = 1.1 G/cm. (D and E) 1D HOBS spectra acquired exactly as described for C but omitting the encoding gradient (G_s = off) and setting the frequency of the selective pulse on the H_α and NH regions, respectively. 8K data points were acquired using an acquisition time (*AQ*) of 576 ms [40 loops (*n*) were used with τ = 7.2 ms] and a recycle delay of 1 s. For an objective comparison of real sensitivities, the experimental averaged SNR is indicated for each 1D dataset. All spectra have been recorded with the same receiver gain, using a single scan, processed with a Fourier transformation without any additional window function and plotted with the same absolute vertical scaling factor.

magnetization is efficiently suppressed. It has been shown that a 100-fold enhancement of the satellite ^{1}H–^{13}C signals can be reached about 5–10 s after injection when compared with the normal thermal sensitivity (Fig. 10).

HOBS experiments

A very simple modification of the slice-selective 1D HOBB experiment allows one the collection of broadband homodecoupled spectra of specific regions of the ^{1}H spectrum without sacrificing sensitivity. As a major feature, this *homodecoupled band-selective* (HOBS) NMR method[118–120] does not use the spatial encoding gradient G_s applied simultaneously with the selective pulses, and therefore, pure shift 1D spectra can be quickly recorded without the sensitivity losses characteristic of the slice selection. The main limitation of this frequency-selective experiment is that only a particular part of the ^{1}H spectrum is monitored in a single-NMR spectrum. However, HOBS promises to have a potential use in spectra presenting a set of equivalent spin systems in well-separated and defined regions, such as the typical NH or H_α protons in peptides and proteins or those found in nucleic acids. In the case that mutually *J*-coupled protons resonate into the same selected region, they will display a splitting due to their mutual coupling.

Similar to the HOBB experiment, HOBS offers a very simple and fast experimental implementation (pulse scheme in Fig. 9A with G_s = off) and is particularly useful for small molecules. It will likely have an impact similar to that of routinely use of key frequency-selective 1D experiments such as selective 1D TOCSY and selective 1D NOESY. Only two parameters need to be defined and calibrated in a single-scan 1D experiment: the offset and the bandwidth of the 180° ^{1}H pulse as a function of the area to be analyzed. The best results in terms of selectivity and optimum relaxation are obtained using semiselective 180° RE-BURP pulses of 5–10 ms for both region-selective excitation and homodecoupling and applied at intervals of 2τ = 10–20 ms. Pulses of longer duration than 10–20 ms introduce important penalties in T_2 relaxation and FID interruption that generates sensitivity losses, line widths broadening and sidebands artifacts. From Figs 9D and 9E, it is shown that HOBS spectra corresponding to the H_α and NH region of cyclosporine are one order of magnitude more sensitive than the equivalent HOBB spectrum and they show even better sensitivity than the conventional ^{1}H spectrum because of the complete collapsing of conventional multiplets to full homodecoupled singlets.

An important advantage of the HOBS technique is its easy and reliable implementation for a large number of homonuclear and heteronuclear multidimensional experiments, as reported for HOBS-NOESY,[119,121] HOBS-ROESY,[116] HOBS-TOCSY,[118] HOBS-HSQC,[118,119] HOBS-HSQMBC,[122] HOBS-inversion-recovery (IR)[121,123] and HOBS-CPMG-PROJECT,[121] with particular applications for the measurement of heteronuclear coupling constants,[122] enantiodifferentiation studies,[124] discrimination of diastereoisomers[120] and the measurement of T_1 and T_2 NMR relaxation times.[121,123] In addition, it can be also attractive for biomolecular NMR applications, as reported for the effective elimination of *residual* HH *dipolar couplings* (RDCs) contributions to line broadening when working with partially oriented proteins in anisotropic media.[119]

Comparison of ZS methods

Both the pseudo-2D and real-time ZS experiments present a set of particular advantages/drawbacks that must be compared and evaluated for their proper use, as a function of the requirements/limitations of the sample or spin systems under study (Table 1).

First, a choice between broadband or selective ZS experiment must be carried out. The main advantage of broadband ZS experiments is that all signals can be fully homodecoupled in a single-NMR experiment although effective broadband homodecoupling cannot be fulfilled for all signals when using general conditions. In contrast, although the limitation of frequency-selective ZS methods is evident because only a set of signals can be monitored per experiment, sensitivity is maximized, and each experiment can be individually optimized.

In broadband homodecoupled NMR experiments, the price for the signal simplification is a considerable penalty in sensitivity. This loss of SNR depends on the homodecoupling block and the acquisition scheme used. As was mentioned before, the low sensitivity in slice-selective methods is due to the fact that the signal only coming from a thin slice of the sample (~1–5%), and

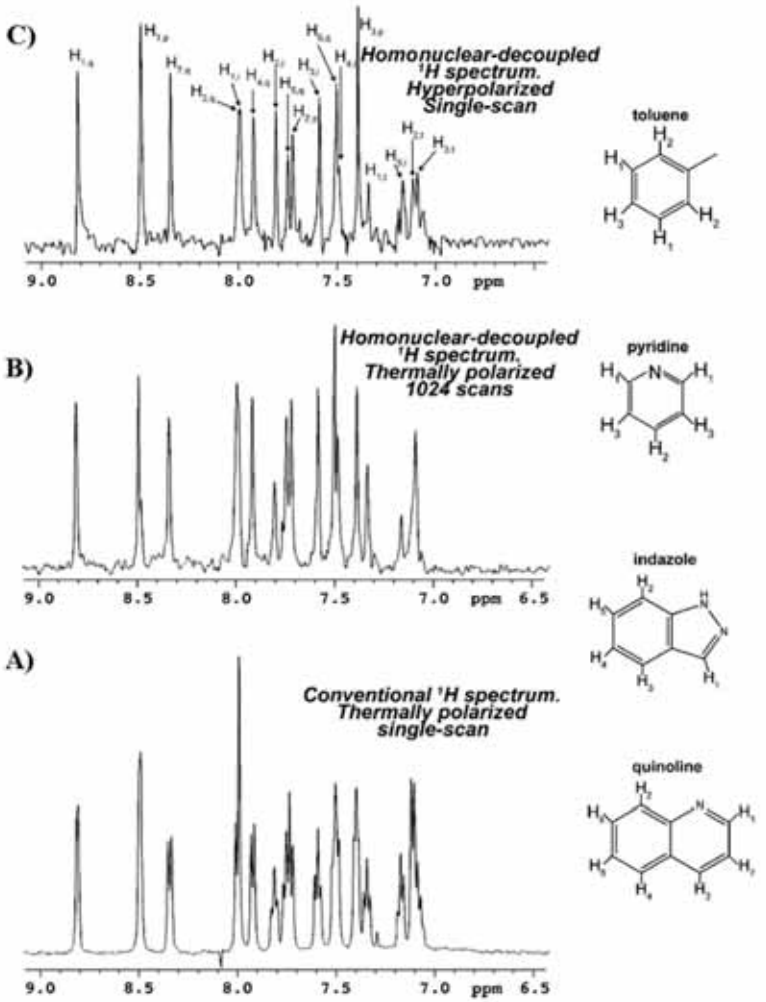

Figure 10. Application to the HyperBIRD experiment to the analysis of a mixture of heterocycle compounds. (A) Conventional ^{1}H spectrum with thermal polarization acquired with a single scan; (B) thermal polarized 1D homonuclear decoupled spectrum acquired with 1024 scans; (C) HyperBIRD spectrum after a single scan. More details can be found in the original publication. Reproduced with permission of reference.[27]

in BIRD-based experiments, it is due to the low natural abundance of ^{13}C (~1.1%). Additionally, pseudo-2D ZS experiments are more time consuming because a 2D dataset is required. When this acquisition scheme is incorporated into multidimensional experiments, the overall acquisition time can become extremely long because of the need for a 3D acquisition mode, decreasing even further the SNR per time unit. In contrast, the 1D acquisition mode of real-time ZS techniques improves the SNR per time unit although sensitivity still remains very low compared with conventional ^{1}H datasets (Fig. 11). The real-time homodecoupled HSQC experiment is the only exception of a broadband pure shift 2D experiment that does not suffers any sensitivity penalty compared with the conventional one.[20]

In terms of SNR per time unit, a single-selective HOBS method is more than one order of magnitude more sensitive than the aforementioned broadband (HOBB or pseudo-2D) ZS methods, which ensures that, for small molecules, recording series of individual selective 1D experiments can be faster and more effective than running a single-broadband experiment. As an example, the experimental SNR of each selective HOBS experiment is about 20 times higher than the equivalent HOBB experiment (Fig. 11C vs Fig. 11D). On the other hand, the theoretical SNR per time unit between the pseudo-2D and the HOBB experiments depends on $\sqrt{NE}$, where NE is the number of t_1 increments of the pesudo-2D experiment. In practice, the pseudo-2D experiment offers a better experimental behavior probably because of the narrower line widths.

In principle, pure shift NMR methods collapse J multiplet patterns irrespective of their complexity, leaving to a single peak for each chemical shift. The gain in spectral resolution can be almost of one order of magnitude, achieving a signal dispersion equivalent to those obtained in a hypothetical spectrometer of several gigahertz. For instance, chemical shift differences of ~1.5–2 Hz (~3 ppb) can be quickly distinguished in a 600-MHz spectrometer. Additionally, some differences are clearly observed when comparing the line widths of homodecoupled signals in different ZS

Table 1. Comparison of 1D ZS experiments to collect broadband homodecoupled ^{1}H NMR spectra

NMR method	Broadband *versus* band-selective	Signal selection	Parameter optimization	SNR	Acquisition mode	Line width	Implementation in nD experiments	Selective pulse	Data processing	Other features
Pseudo-2D ZS	Broadband	Spatial frequency encoding	Selective pulse and encoding gradient	1–5%	2D	Good	Requires 3D acquisition mode	Any shape and duration	Automation program[a]	Sensitivity enhancement by sequential or multiple offset excitation
Real-time 1D ZS (HOBB)	Broadband	Spatial frequency encoding	Selective pulse and encoding gradient	1–5%	1D	Medium	Ok	Pulses <10–15 ms	Conventional	Sensitivity enhancement by sequential or multiple offset excitation
Real-time 1D ZS BIRD	Broadband	^{13}C editing	Delay optimization	1%	1D	Medium	Only for $^1J_{CH}$ experiments, like HSQC	Not used	Conventional	Removes strong coupling effects; fails for CH_2
Real-time 1D HOBS	Band selective	Region selective	Region-selective pulse	Full sensitivity	1D	Medium	In band-selective 2D experiments	Pulses <10–15 ms	Conventional	Can be applied for single frequencies, fails for mutually coupled spins

[a]A data-processing script is available at Gareth Morris's group home page (nmr.chemistry.manchester.ac.uk).
ZS, Zangger–Sterk; HOBB, homodecoupled broadband; HOBS, homodecoupled band-selective.

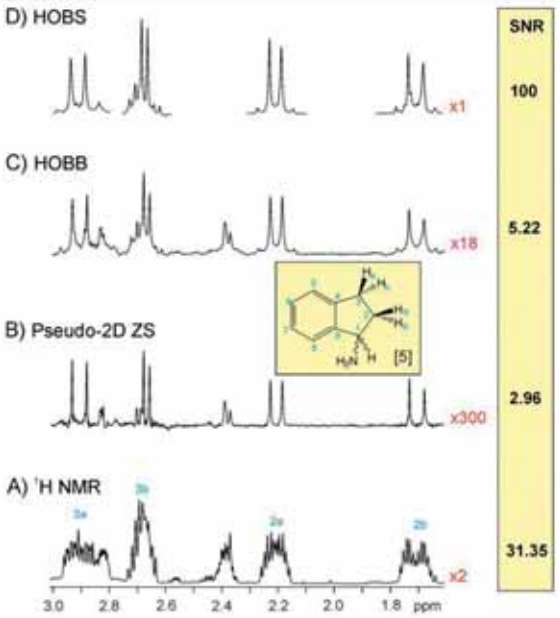

Figure 11. Relative sensitivity, signal resolution and spectral quality obtained in different ZS ^{1}H experiments at 600 MHz. Spectrum A corresponds to 50 mM (*RS*)-1-aminoindan[5] (1 : 1 proportion) in $CDCl_3$ after the addition of 4.5 equivalents of (*R*)-(−)-1-(9-anthryl)-2,2,2-trifluoroethanol (Pirkle alcohol) as chiral solvating agent. (B) Pseudo-2D ZS, (C) HOBB and (D) individual HOBS spectra for each group of signals. All four spectra were acquired within the same experimental time (~5 min) to obtain real and comparable SNR per time unit values. Spectra B–D used a 20-ms Gaussian-shaped pulse and a 2.1-G/cm encoding gradient, and a detailed description of all other acquisition and processing parameters can be found in the original publication. Reproduced with permission of reference.[124]

experiments (Fig. 11). As shown in Fig. 11B *versus* Fig. 11C and D, the pseudo-2D ZS method shows better line widths. In the pseudo-2D ZS experiment, line widths mainly depend on the number of increments used, and very good spectral resolution and excellent spectral quality are obtained collecting 16–32 increments. On the other hand, line widths in real-time HOBB and HOBS spectra are quite similar, and they are directly related with the number and duration of individual loops and the duration of the selective 180° ^{1}H pulse. As the time the FID is interrupted increases, correspondingly greater line widths are observed.

A serious challenge in all ZS experiments is the presence of strong coupling effects. It is not possible to obtain a perfect homodecoupled spectrum through ZS methods when protons are strongly coupled ($J > \Delta\delta$). When using slice selection, strong coupling effects are progressively minimized using more and more selective pulses but with a proportional decrease in sensitivity. In general, RE-BURP, rSNOB and Gaussian shapes give optimum results, and the correct choice of pulse shape and duration actually depends on the effective achievement of full homodecoupling for all signals present in the sample under study. Strong coupling effects are minimized using BIRD-based ZS experiments, but the incomplete homodecoupling for diastereotopic CH_2 groups and their decreased sensitivity must be also considered. Recently, the PSYCHE experiment has demonstrated an excellent complementarity between strong coupling effects and sensitivity. Experimentally, we have found that PSYCHE works perfectly with protons separated

by more than 50 Hz in a 600-MHz spectrometer but fails in extreme conditions, when strongly coupled signals are separated by less than 30–40 Hz. The PSYCHE approach can be implemented to improve the sensitivity in all homodecoupled experiments that will be discussed in the next sections, which were initially reported using slice selection with a selective 180° pulse.

Selectivity in slice-selective pseudo-2D ZS experiment can be enhanced as desired if the involved T_2 relaxation times allows the use of very long selective pulses. The main drawback of both HOBB and HOBS experiments is that they only accept selective pulses with a maximum duration of 10–20 ms. In general, all ZS experiments are susceptible to the presence of undesired artifacts in the form of sidebands. Practically, all real-time ZS version methods present a major number of artifacts because of the FID interruption whereas the pseudo-2D ZS method usually yields cleaner spectra where sidebands are only observed for concentrated samples.

Homodecoupled experiments and applications

All of the aforementioned ZS methodologies using BIRD or slice-selective homodecoupling have been implemented in different 1D and 2D NMR experiments (Table 2) according to the general schemes displayed in Fig. 12. A requirement for a success implementation of any ZS module is to have in-phase (IP) HH magnetization, because signals involving anti-phase (AP) components, like those found in conventional COSY or HMBC, cancel under homodecoupling conditions. The resulting pure shift spectra have a wide range of potential uses, as demonstrated for the analysis of diastereomeric[24,120,124] or complex mixtures,[105] to carry out structural elucidation studies,[6,20,22,24,25,102,104,112,113,116–119,122] to analyze diffusion[115] and molecular dynamic processes[121,123] or to measure heteronuclear coupling constants.[17,23,26,108,109,122]

Measurement of homonuclear coupling constants

A modified version of the 1D HOBB experiment has been reported to provide all J_{HH} coupling constants from a selected proton resonance. This experiment, which has been reported simultaneously by two groups,[125,126] yields a pseudo-broadband homodecoupled 1D ^{1}H spectrum where resonances coupled to the selected signal appear as doublets whereas the other remaining protons are fully homodecoupled singlets. The experiment provides information about multiple couplings analogous to that of an equivalent Gradient-encoded homonuclear SElective Refocusing Spectroscopy (G-SERF) technique[52] but in a few minutes rather than several hours. The key feature of this method is the application of an additional selective 180° ^{1}H pulse on a selected signal into the real-time homodecoupling element in order to retain specifically only those couplings from this selected proton. The main drawbacks of this technique are as follows: (i) poor selectivity because the duration of the selective 180° pulse is limited to ~10 ms, (ii) the experiment only works for well isolated resonances, (iii) there is a more pronounced presence of unwanted sideband artifacts than the original HOBB spectrum because of a major FID interruption, and (iv) the additional

Table 2. Summary of reported broadband homodecoupled 1D and 2D ^{1}H NMR experiments

NMR experiment		Homodecoupling			Acquisition mode		References
		BIRD	Slice selection	Band selection	Pseudo-2D	Real time	
1D	^{1}H NMR	✓			✓		[21], [26]
			✓		✓		[6], [24], [47], [55], [58], [105], [106], [108]
		✓				✓	[19], [27]
			✓			✓	[104]
				✓		✓	[118], [119], [120], [124]
	selTOCSY			✓		✓	[124]
	Quick-Serf		✓			✓	[125], [126]
	Inversion recovery			✓		✓	[121], [123]
	CPMG			✓		✓	[121]
2D	TOCSY		✓		✓		[112], [113], [114]
			✓			✓	[104]
				✓		✓	[118]
	DOSY		✓		✓		[105], [110], [111]
			✓			✓	[115]
	NOESY		✓		✓		[102]
				✓		✓	[119], [123]
	ROESY		✓			✓	[116]
				✓		✓	[116]
	HSQC/HSQCed		✓			✓	[117]
		✓			✓		[17], [18], [22], [23]
		✓				✓	[20], [24]
				✓		✓	[118], [119], [140]
	HSQC-TOCSY			✓		✓	[149]
	2D HSQMBC			✓		✓	[122]
			✓		✓		[109]

CPMG, Carr–Purcell–Meiboom–Gill.

180° pulse also causes more signal loss and transverse relaxation causing additional line broadening (~3 Hz), which sets the limit for the size of the couplings that could be measured. A similar pseudo-2D ZS method that improves the strong requirements on selectivity has been recently reported.[107]

Homodecoupled diffusion experiments

For the analysis of compound mixtures by NMR spectroscopy, it is important to identify and assign the different peaks belonging to each individual component. DOSY experiments are used to obtain signal separation depending on the molecular self-diffusion coefficient, which are determined by fitting the intensity decay of the NMR signal to a mono-exponential function.[127,128] However, signal overlap usually hampers a simple data analysis because the observed decays may be the result of superposition of several individual decays. In these cases, the use of more sophisticated methods, such as deconvolution, line fitting techniques or analysis of multiple-exponential decay, can be required to obtain correct values for each individual signal.

Several pure shift DOSY experiments based on the pseudo-2D ZS methodology were initially published to provide a much simplified spectrum, making the quantification of the diffusion coefficients easier and more accurate.[105,110] In principle, any diffusion pulse scheme could be adapted to the pseudo-2D ZS experiment, as represented in Fig. 12A. The resulting pure shift DOSY experiments represent a useful alternative to 3D-based DOSY experiments, which have been proposed to avoid signal overlapping and improve signal resolution. As a major drawback of these pure shift DOSY experiments is their 3D acquisition mode, requiring much longer measurement times and more elaborate data processing (Fig. 13). The pure shift DOSY experiment has been applied to the determination of the structure and solvation states of organolithium aggregates in complex solutions.[129]

Recently, an HOBB version of the popular BiPolar Longitudinal Eddy current Delay (BPLED) sequence has been also reported based on the scheme of Fig. 12B.[115] This HOBB-DOSY experiment uses the real-time acquisition, and therefore, it can be recorded and processed using the same automation protocols as for the standard DOSY experiments. The proposed method uses spatial selection, and therefore, reduced sensitivity is again the main drawback for its routine use. An equivalent sensitivity-enhanced HOBS-DOSY version that should be recorded with G_s = off has not been published, but it could be beneficial to analyze complex areas in particular cases.

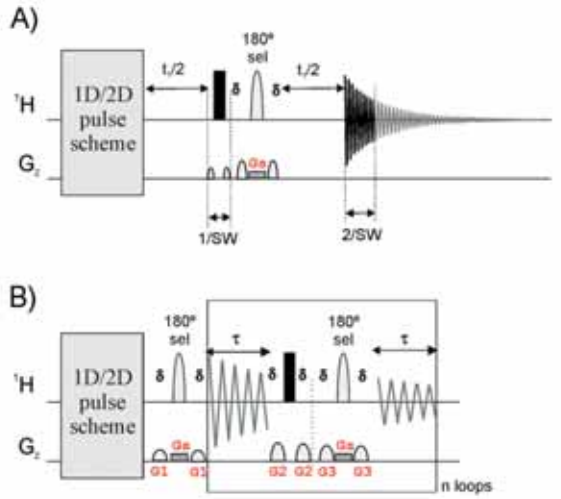

Figure 12. General pulse schemes showing the implementation of broadband homonuclear (A) pseudo-2D and (B) real-time ZS decoupling during the acquisition dimension in conventional 1D and 2D NMR experiments.

Homodecoupled T_1/T_2 relaxation experiments

The measurement of relaxation rates by NMR spectroscopy can provide important insights into the dynamics of molecules in solution. Longitudinal spin–lattice T_1 relaxation times are usually determined from the Inversion Recovery (IR) experiments[130,131] whereas transverse spin–spin T_2 relaxation times are measured from *Carr–Purcell–Meiboom–Gill* (CPMG) sequences.[132,133] One drawback of CPMG pulse trains is the presence of multiplet distortions due to J_{HH} evolution that can affect the accuracy of the measurement. An improved perfect CPMG sequence that achieves *periodic refocusing of J evolution by coherence transfer* (referred to as PROJECT) has been proposed to minimize the effects of *J* evolution during the echo periods, obtaining pure in-phase signals.[134] As mentioned previously, it has also been shown that the problem of signal overlapping can be solved through the implementation of the HOBS technique in standard IR and PROJECT experiments.[121]

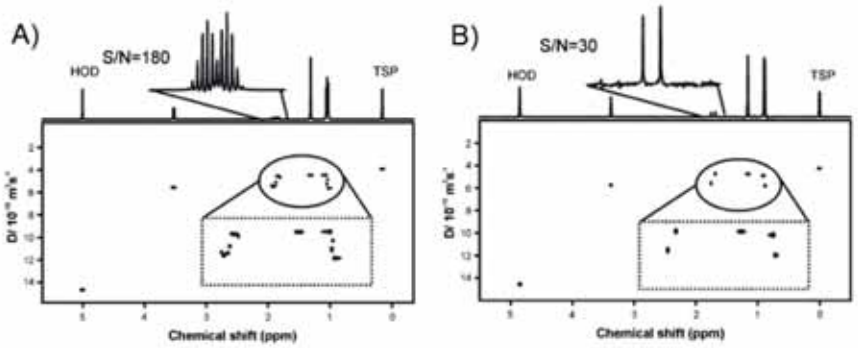

Figure 13. DOSY (A) and pure shift DOSY (B) spectra of a solution of 2-methyl-1-propanol, 2,3-dimethyl-2-butanol, and TSP in D_2O, acquired in 11 min and 2 h 10 min, respectively. Reproduced with permission of reference.[110]

Thus, T_1 and T_2 relaxation times can be accurately measured from the resulting singlet lines using conventional mono-exponential curve-fitting methods. Examples have been provided for the undecapeptide cyclosporine,[121] the small six-mer oligonucleotide d(GCCTGC) and the 16-mer d(CGACGCGTACGCGTCG)2 DNA duplex.[123] Figure 14A shows the basic scheme of the 1D HOBS-IR experiment where the conventional acquisition scheme has been replaced by an HOBS detection block. To obtain clean spectra, a selective echo element is inserted between the traditional IR block and the new acquisition block. The experimental T_1 data revealed good agreement between standard and HOBS-IR measurements (Fig. 14B vs Fig. 14C).

Figure 15A shows the pulse scheme of HOBS version of the PROJECT experiment designed to measure T_2 relaxation times or to be used as a T_2 filter. The features of the standard CPMG *versus* PROJECT are illustrated in spectra of Fig. 15C and D, and the further improvement and signal simplification achieved in the HOBS-PROJECT spectra are illustrated in Fig. 15E. Both HOBS-IR and HOBS-PROJECT experiments could be easily converted to their HOBB-IR and HOBB-PROJECT counterparts activating the encoding G_s gradient to monitor the complete ^{1}H spectrum. As noted previously, the major advantage of analyzing singlet peaks is the rapid and more accurate parameter determination using the same automatic T_1/T_2 data acquisition and processing protocols incorporated in standard NMR software packages (see exponential decay in Fig. 15F). This strategy can also be applied to other types of array experiments involving the analysis of the signal decays in severely overlapped

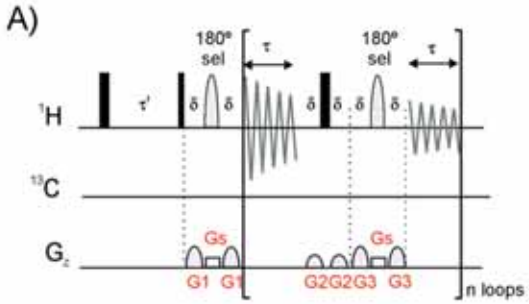

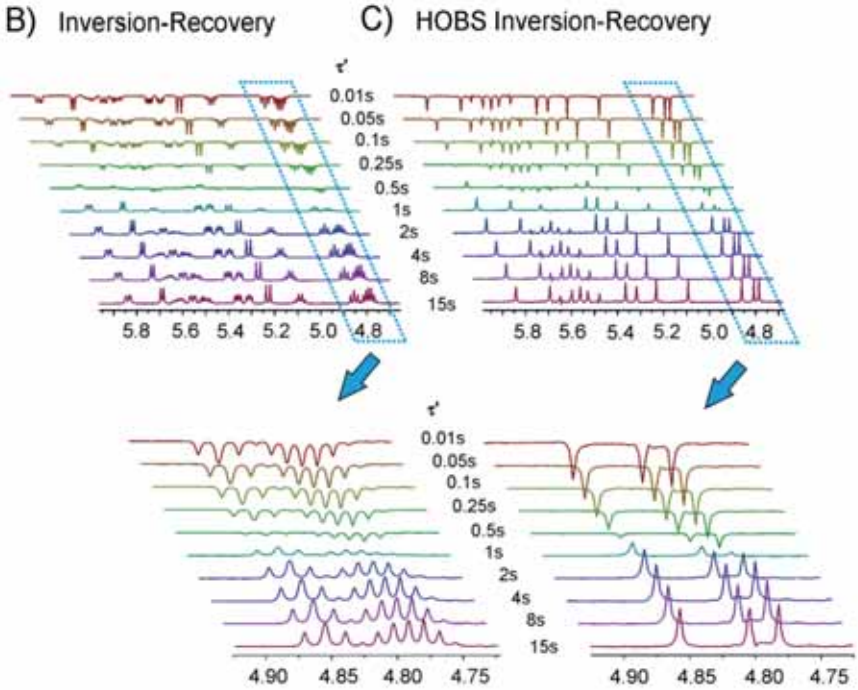

Figure 14. (A) NMR pulse scheme of the HOBB/HOBS-IR experiment designed to measure T_1 relaxation times in overlapped proton signals. 600-MHz (B) conventional and (C) HOBS IR ^{1}H NMR spectra showing the expanded area of the H_α protons corresponding to cyclosporine [3]. Homodecoupling was achieved using a 5-ms RE-BURP 180° ^{1}H pulse, $\tau = 8.9$ ms, $AQ = 569$ ms, $n = 32$ and the encoding gradient G_s switched off. Reproduced with permission of reference.[121]

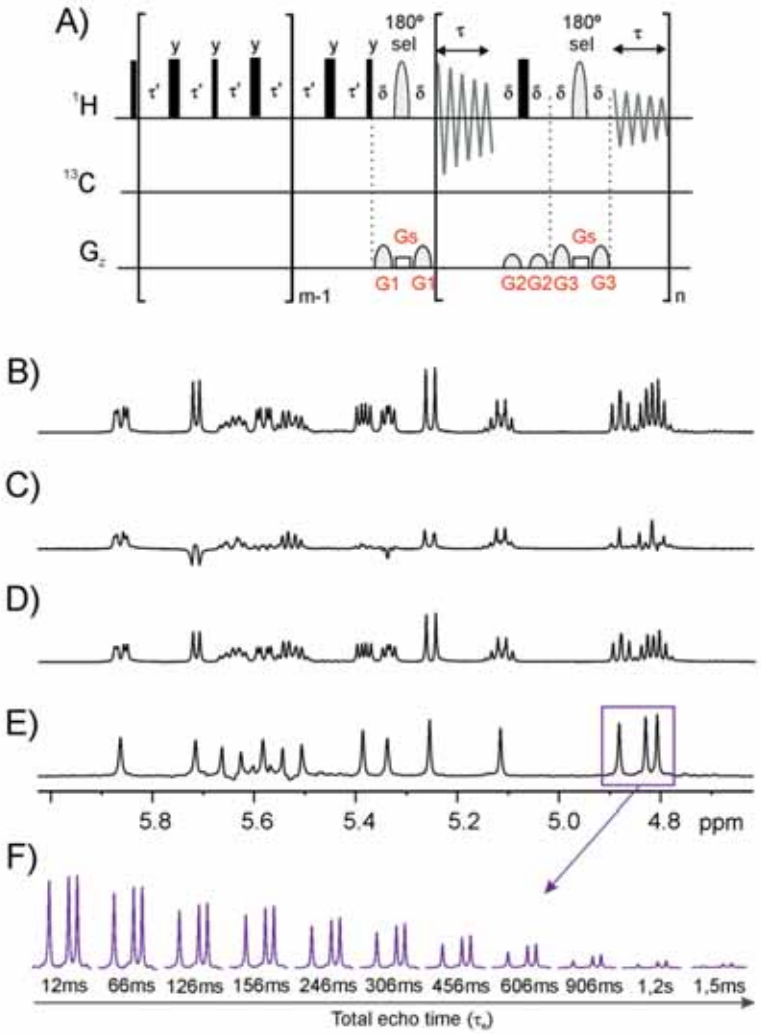

Figure 15. (A) NMR pulse scheme of the HOBB/HOBS-PROJECT experiment designed to measure T_2 relation in overlapped signals. 600-MHz (B) conventional ^{1}H, (C) standard CPMG, (D) PROJECT and (E) HOBS-PROJECT spectra of cyclosporine [3] acquired with a total echo time of τ_e = 156 ms (m = 26 and τ' = 1.5 ms) and G_z = 0. All spectra were collected under the same experimental conditions and are plotted at the same absolute vertical scale. (F) Signal T_2 decays for the H_5, H_8 and H_7 protons in the HOBS-PROJECT experiment. Reproduced with permission of reference.[121]

regions, such as the studies of kinetics or chemical reaction monitoring.

Homodecoupled homonuclear 2D experiments

The development of homodecoupled versions of the most popular 2D COSY, TOCSY, NOESY or ROESY experiments has been a topic of interest for many years. Homodecoupling in the indirect F1 dimension can be achieved by constant-time or BASHD methods, as discussed in Section on Classical Homodecoupling Techniques (Fig. 16B). In a complementary way, both pseudo-2D or real-time ZS homodecoupling methods can be incorporated along the acquisition dimension. The pseudo-2D ZS element can be included between the mixing time and the acquisition period (Fig. 16C), generating a pseudo-3D experiment that, in principle, would require long acquisition times. The HOBB/HOBS methods can be implemented changing continuous acquisition mode by the alternated-homodecoupling acquisition mode (Fig. 16D). Finally, real pure shift 2D experiments with broadband homodecoupling in both dimensions can be designed combining both approaches, as shown in the general schemes of Fig. 16E and F, respectively.

The 2D TOCSY experiment is a homonuclear NMR technique widely used to identify H–H correlations within networks of J-coupled spins. It has been reported that the resolution in the TOCSY spectrum can be improved by collapsing the in-phase multiplets to singlets for all cross-peaks, obtaining spectra where a single peak is seen for each connectivity. Homodecoupled TOCSY experiments have been proposed to simplify cross-peak appearance in the indirect F1[6] or the direct dimension using the pseudo-2D[112,113] or the real-time ZS modules,[104,118] which could be further enhanced by spectral aliasing in the indirect dimension.[135] Recently, an ultra high-resolved TOCSY experiment

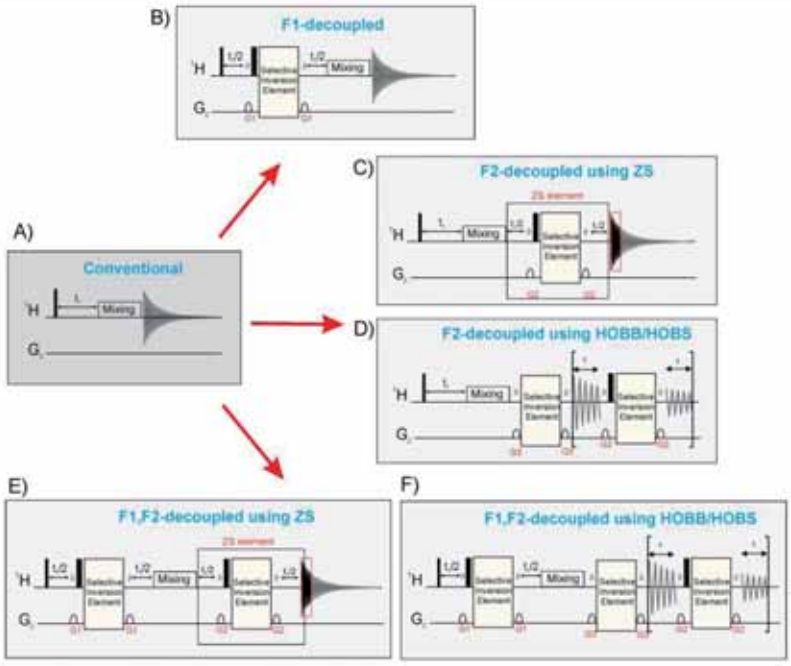

Figure 16. (B–E) General pulse schemes to obtain F1-homodecoupled, F2-homodecoupled or F1, F2-homodecoupled 2D spectra from the reference scheme of Figure A. The selective inversion element can be any building block described in Fig. 2 whereas the mixing time can be a standard TOCSY, ROESY or NOESY building block.

based on a PSYCHE scheme (Fig. 17A) affords broadband homodecoupling in the F1 dimension (Fig. 17C), and the use of covariance post-processing in the F2 dimension achieves pure shift cross-peaks in both dimensions (Fig. 17D).[112,114] This approach is an order of magnitude more sensitive than the previously published experiments.

Similar approaches have been reported to extract helpful distance restraints from simplified and well-resolved cross-peaks in broadband homodecoupled NOESY experiments based on the pseudo-2D ZS[102] and HOBS schemes.[119] This has been shown to be critical in the process of 3D structure determination of peptides, intrinsically disordered proteins[119] and nucleic acids.[123]

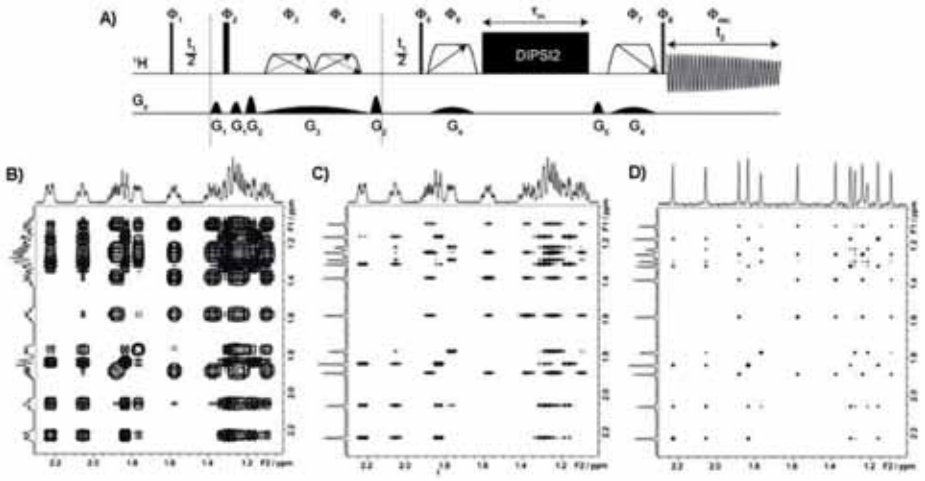

Figure 17. (A) Pulse scheme of the 2D F1-PSYCHE-TOCSY experiment; (B) expanded area of the conventional TOCSY spectrum of estradiol; (C) F1-homodecoupled PSYCHE-TOCSY spectrum acquired from sequence A; and (D) as (C) after applying covariance in the F2 dimension. Reproduced with permission of reference.[114]

Additionally, an exhaustive study comparing the performance of HOBB-ROESY *versus* HOBS-ROESY experiments has been reported for the analysis of medium-sized organic molecules (Fig. 18).[116]

Homodecoupled heteronuclear 2D experiments

The HSQC experiment is the most widely used NMR method for correlating the chemical shifts of directly bonded ^{13}C–^{1}H pairs. Conventional HSQC spectra show proton multiplet structures in the direct dimension, which can limit signal resolution when analyzing complex datasets. The pure shift methodology has been successfully implemented in HSQC experiments, as reported using the pseudo-2D ZS,[22] real-time HOBB,[117] HOBS[118] and BIRD-based[20,24] homodecoupling modules. A major breakthrough to obtain pure shift HSQC spectra of organic molecules at natural abundance is the recent development of the real-time BIRD-based HSQC experiment,[20] which does not present any additional sensitivity loss in comparison with the conventional HSQC (Fig. 19A) experiment. The resulting homodecoupled HSQC spectra show cross-peaks with collapsed multiplet J_{HH} structures for CH cross-peaks (Fig. 19D vs Fig. 19E). However, the method is not able to remove the geminal $^{2}J_{HH}$ splittings, and it is not suitable for fully ^{13}C-labeled compounds, in both cases because of the use of BIRD element. All of these advantages/inconveniences are also applicable to other related versions of the HSQC experiments, such as the reported pure shift versions of the sensitivity-improved HSQC using Preservation od Equivalent pathways (PEP) (Fig. 19B)[24] or the multiplicity-edited (ME) HSQC (Fig. 19C).[20] The performance of the pure shift HSQC and the ASAP-HMQC experiments has been compared for the rapid screening of natural products.[136] On the other hand, the pure shift HSQC has been also tested to characterize microgram samples of drug metabolites. For instance, using a 7.4-μg sample of the commercially available metabolite 3-hydroxy carbamazepine dissolved in 30 μl of deuterated solvent and a 600-MHz NMR equipped with a 1.7-mm cryogenic NMR probe, it was possible to acquire high signal-to-noise pure shift HSQC data in just over 30 min.[25] In the same study, high-quality pure shift HSQC data were recorded in slightly over 14 h for a 3-μg sample of a chromatographically isolated metabolite.

The implementation of ZS homodecoupling fails in heteronuclear correlation experiments involving anti-phase HH magnetization just prior to acquisition, like conventional HMBC/HSQMBC experiments. In addition, BIRD-based homodecoupling is not effective in heteronuclear hybrid experiments where J_{HH} is in-phase, such as HSQC-TOCSY or HSQC-NOESY, because the detected relayed ^{1}H–^{12}C magnetization is also coupled to ^{1}H–^{12}C protons. In these cases, pure shift spectra should be possible in refocused HMBC/HSQMBC, HSQC-TOCSY or HSQC-NOESY experiments applying slice selection but at expense of important sensitivity losses. On the other hand, it has been shown that pure in-phase cross-peaks with respect to J_{HH} can be obtained in refocused HSQMBC experiments using region-selective 180° ^{1}H pulses.[137] Based on this experiment, an HOBS-HSQMBC[122] experiment has been proposed to obtain band-selective pure shift long-range heteronuclear correlation spectra with a considerable enhancement in both resolution and sensitivity (Fig. 20). The major advantage of such an approach is that the selective 180° ^{1}H pulse is the same for the INEPT refocusing and homodecoupling, facilitating set-up and performance.

Measurement of heteronuclear coupling constants

It has been recognized since the early days of NMR that heteronuclear coupling constants (J_{XH}) contain very useful structural, conformational and configurational information. In the case of high-abundance nuclides ($X = {}^{19}F$, ^{31}P), the direct determination of heteronuclear couplings is often carry out through the analysis of conventional or *X*-decoupled ^{1}H multiplets, but the accurate measure of the J_{XH} can be problematic because of the simultaneous presence of large numbers of J_{HH} or because of the multiplet complexity. Several 1D and 2D pure shift experiments have been proposed to achieve simplified multiplet structures that allow the extraction of coupling values. For instance, it has been shown that J_{XH} can be directly extracted from simplified homodecoupled 1D multiplets obtained from pseudo-2D ZS spectra (Fig. 21).[108] Examples have been reported for J_{HF} and J_{HP} coupling constants, and similar results have been simultaneously reported using BIRD-based homodecoupling as a selective inversion element in the ZS experiment.[26] In Section on Efficient Measurement of Heteronuclear Coupling Constants, a simple and sensitive approach for the measurement of the sign and the

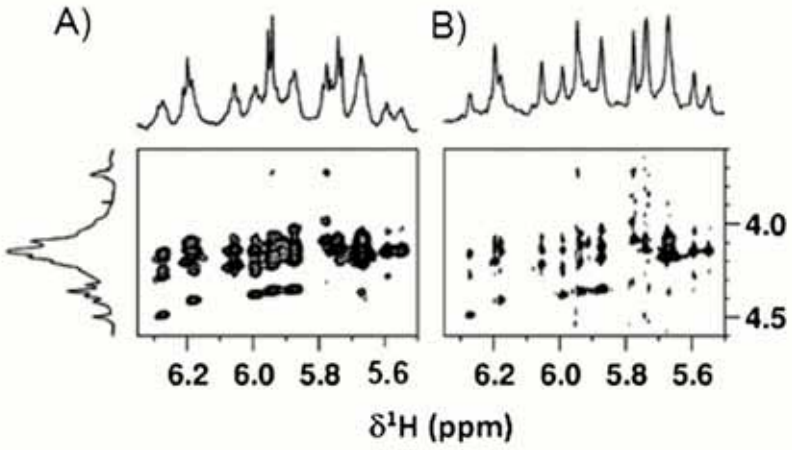

Figure 18. Expansions showing the H1'/H5 to H4'/H5'/H5" cross-peak region of the 600-MHz (A) standard NOESY; (B) HOBS-NOESY spectra for d(CGACGCGTACGCGTCG)2 in D_2O. Reproduced with permission of reference.[123]

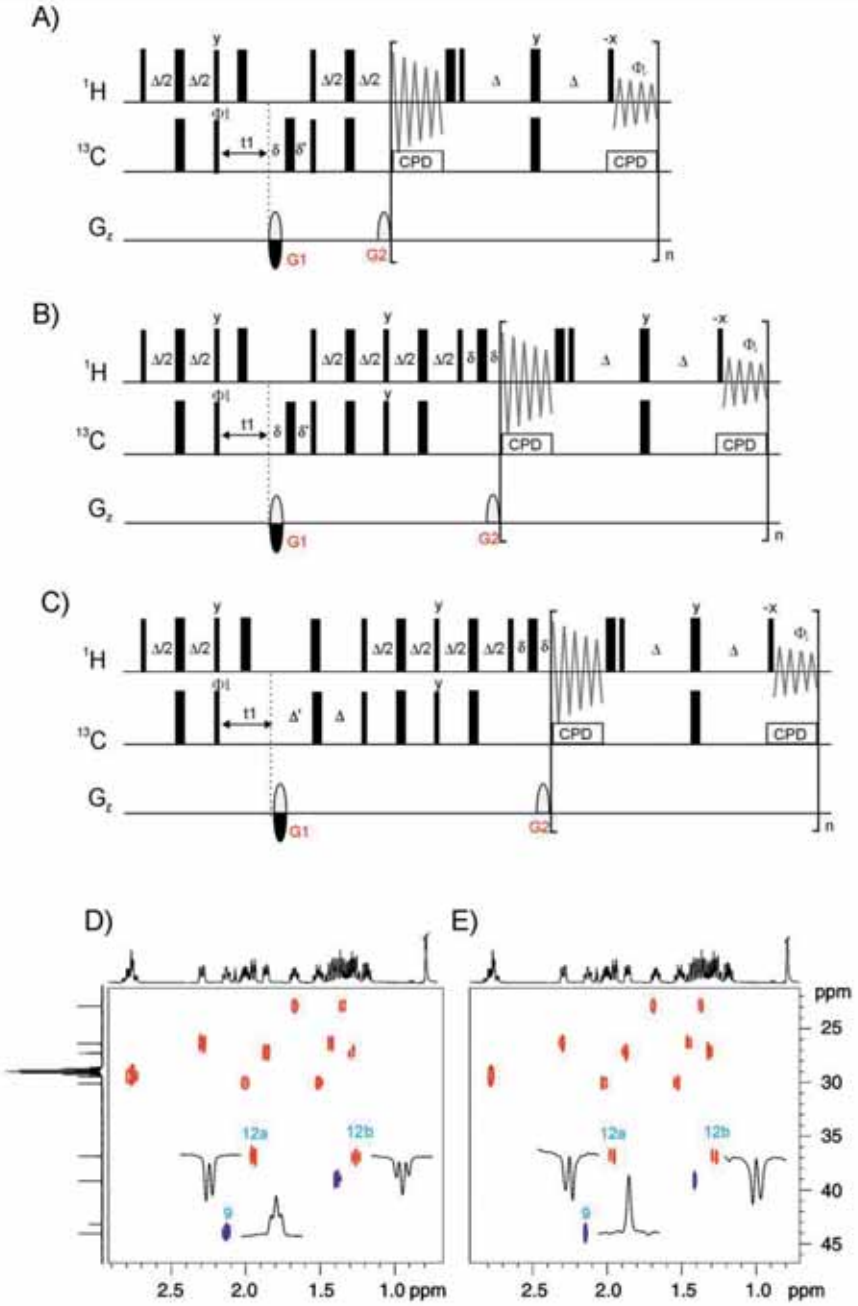

Figure 19. Basic pulse schemes of the broadband homodecoupled (A) HSQC, (B) HSQC-PEP and (C) multiplicity-edited HSQC-PEP experiments; (D and E) expanded area comparing CH and CH_2 cross-peaks in (D) conventional and (E) broadband homodecoupled multiplicity-edited HSQC-PEP spectra of estradiol [4] in $CDCl_3$.

magnitude of multiple coupling constants from high-resolved E.COSY cross-peaks in pure shift HSQC spectra is described.[138]

The measurement of one-bond scalar ($^1J_{CH}$) and residual dipolar ($^1D_{CH}$) coupling constants in isotropic and anisotropic media, respectively, can be easily carried out through F2-heteronuclear coupled HSQC-type spectra, for instance, using Clean-IP/Clean-AP (CLIP/CLAP) HSQC experiments.[139] Recently, two analog broadband homodecoupled CLIP/CLAP HSQC experiments have been simultaneously proposed, based on the implementation of the pseudo-2D ZS module (Fig. 22A).[17,23] Both approaches use the original RESET (Reducing nuclEar Spin multiplicitiEs to singuleTs)-HSQC pulse scheme as a basis,[22] where an optimum

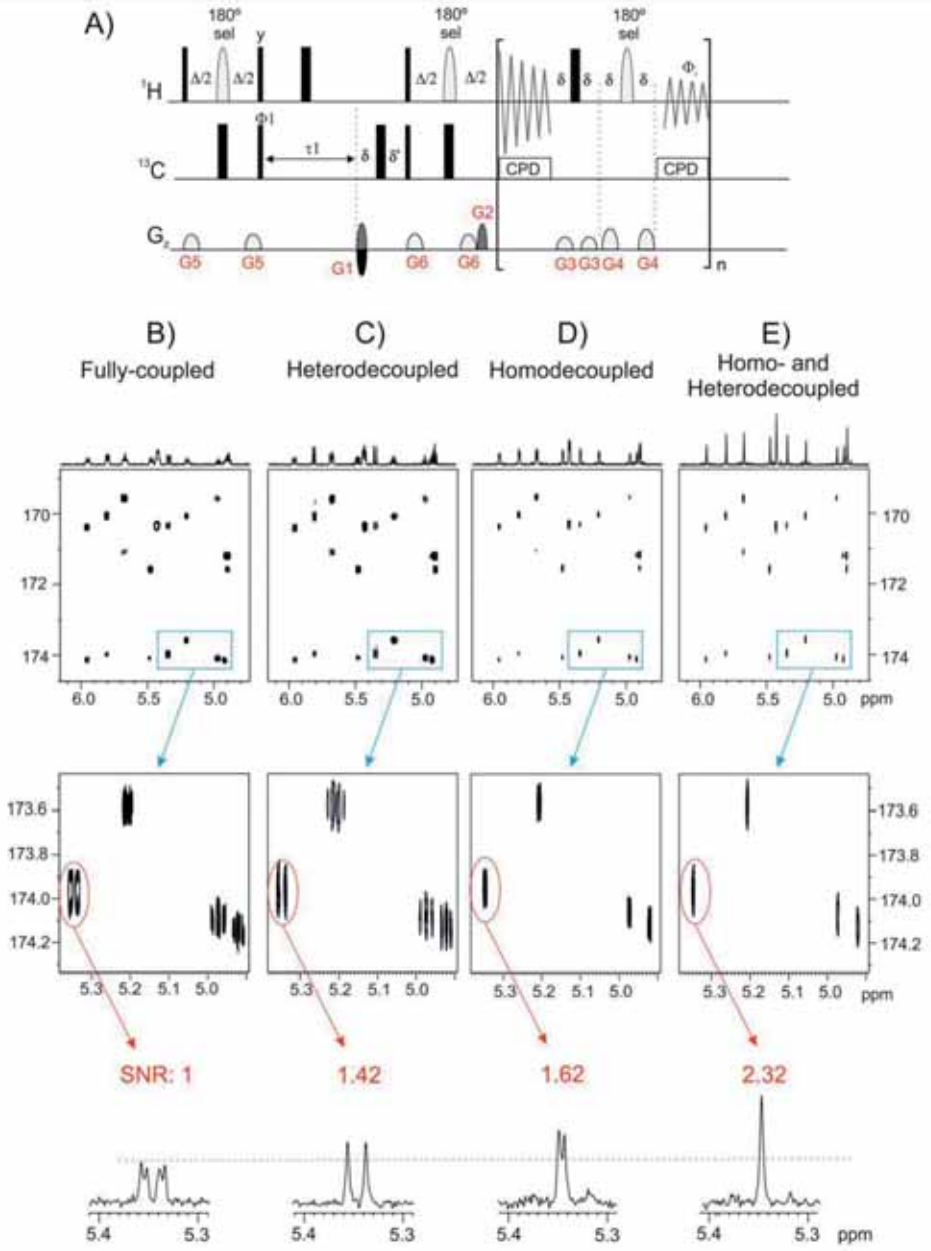

Figure 20. (A) Pulse scheme of the HOBS-HSQMBC experiment. (B–E) Resolution enhancement effects after incorporation of homonuclear or/and heteronuclear decoupling in region-selected $^1H\alpha-^{13}CO$ HSQMBC spectra of cyclosporine [3]: (B) 600-MHz conventional HSQMBC, (C) broadband ^{13}C-decoupled HSQMBC, (D) ^{1}H-decoupled and (E) ^{1}H and ^{13}C-decoupled HOBS-HSQMBC. The internal projection along the detected dimension is shown on top of each 2D plot, and all are plotted with the same absolute scale to compare the relative sensitivity and resolution. The experimental SNR for a selected 1D slice in each different HSQMBC spectra is shown taking the fully coupled peak (normalized value set to 1) as a reference. Reproduced with permission of reference.[122]

BIRD element allows the homonuclear decoupling while preserving heteronuclear coupling evolution. In these experiments, each homodecoupled CH cross-peak only exhibits a large doublet along the direct dimension because of $^1J_{CH} + {}^1D_{CH}$, allowing coupling constants to be extracted by measuring frequency differences between both singlets, instead of between the centers of complex multiplets (compare Fig. 22B vs Fig. 22C). These experiments lead to pure shift correlation spectra with enhanced resolution and offering interesting advantages for semi-automated peak picking or

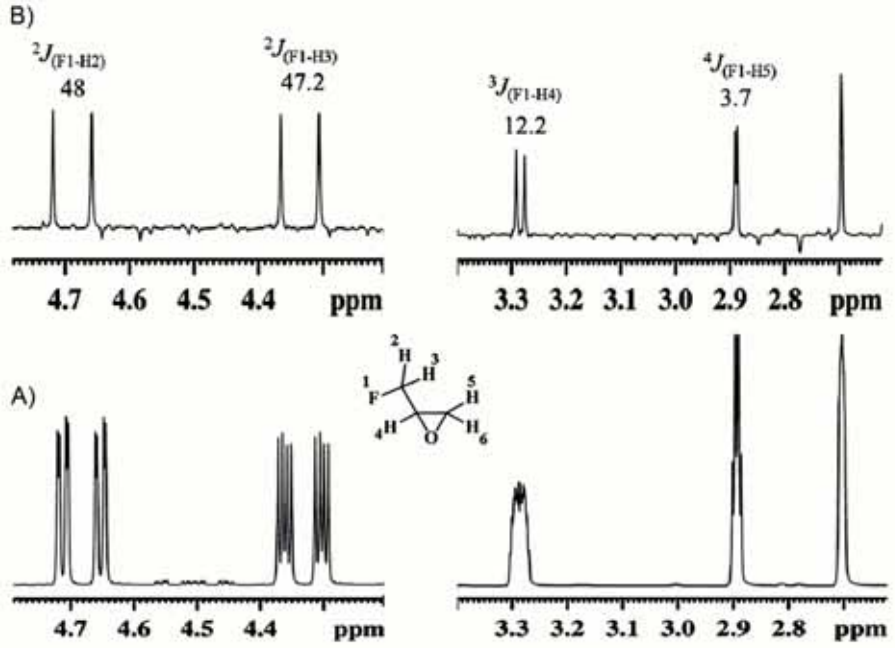

Figure 21. (A) ^{1}H NMR spectrum of the monofluorinated epiflurohydrin molecule in $CDCl_3$; (B) pseudo-2D ZS spectrum of the same molecule, depicting only $^nJ_{HF}$ couplings. Reproduced with permission of reference.[108]

automated intensity measurement. Again, the need for a 3D acquisition can limit its routine use.

Two novel but sophisticated modifications of the BIRD inversion element have been proposed to suppress the $^2J_{HH}+{}^2D_{HH}$ splitting in pseudo-3D ZS HSQC experiments: using a constant-time BIRD module[17] or a perfect-BIRD element (Fig. 23).[18] The constant-time approach necessarily limits the range of couplings accessible, while the perfect-BIRD method can accommodate a wide range of $^2J_{HH}+{}^2D_{HH}$, making perfect-BIRD particularly attractive for measurements on aligned samples. These new sequence elements provide full homonuclear broadband decoupling even in the case of diastereotopic methylene protons, but signal intensity losses can be more pronounced for aligned samples because overall sequence length becomes longer.

A ^{13}C–F2-coupled version of the sensitive HOBS-HSQMBC experiment depicted in Fig. 20A has been reported for the direct and simple measurement of small $^nJ_{CH}$ couplings.[122] The method retains the sensitivity of the original selHSQMBC experiment, and the resulting spectrum affords simplified pure in-phase doublets for all observed cross-peaks (Fig. 20C). A related multiplicity-edited approach has been reported to afford additional carbon multiplicity information by simple visual inspection of the resulting positive/negative cross-peak phases (Fig. 24A).[140] The IP pattern of the conventional selHSQMBC cross-peaks can be converted to doublets when using HOBS homodecoupling (Fig. 24C) and to singlets if additional broadband heteronuclear decoupling is applied (Fig. 24D), depending if the quantitative measurement of coupling constants or only the chemical shift assignment is of interest, respectively.

By analogy, a broadband homodecoupled version of the nonrefocused CPMG-HSQMBC experiment incorporating the pseudo-2D ZS module has been proposed to precisely measure long-range heteronuclear coupling constants from simplified anti-phase doublets. The 1D and 2D examples have been reported for the measurement of $^nJ_{PH}$, $^nJ_{SeH}$ and $^nJ_{CH}$ coupling constant in a series of compounds.[109] Long acquisition times and concentrated samples are required to achieve optimum SNR, but as mentioned in this study, sensitivity could be improved, for instance, using PSYCHE, and the determination of small J values from AP multiplets could be performed using multiplet fitting or by spin-state selective methods.

Ultra high-resolution NMR spectroscopy

Broadband ^{1}H homodecoupling in the acquisition F2 dimension is fully compatible with other resolution-enhanced techniques, such as spectral aliasing along the indirect F1 dimension[31,141–146] or nonuniform sampling,[147,148] opening the door to the design of ultra high-resolved 2D NMR experiments in reasonable acquisition times. A common feature of spectral aliasing is its general and very easy implementation in many routine experiments, improving the attainable resolution along the F1 dimension up to two orders of magnitude by a simple change of the ^{13}C spectral width in HSQC experiments. This approach has been recently reported in the development and application of ultra high-resolved HSQC experiments to analyze highly complex mixtures of similar isomers exhibiting near-identical ^{1}H and ^{13}C NMR spectra,[149] the determination of small chemical shift differences in enantiodifferentiation studies,[24] and for measuring the sign and the magnitude of multiple heteronuclear coupling constants from highly resolved 2D cross-peaks.[138]

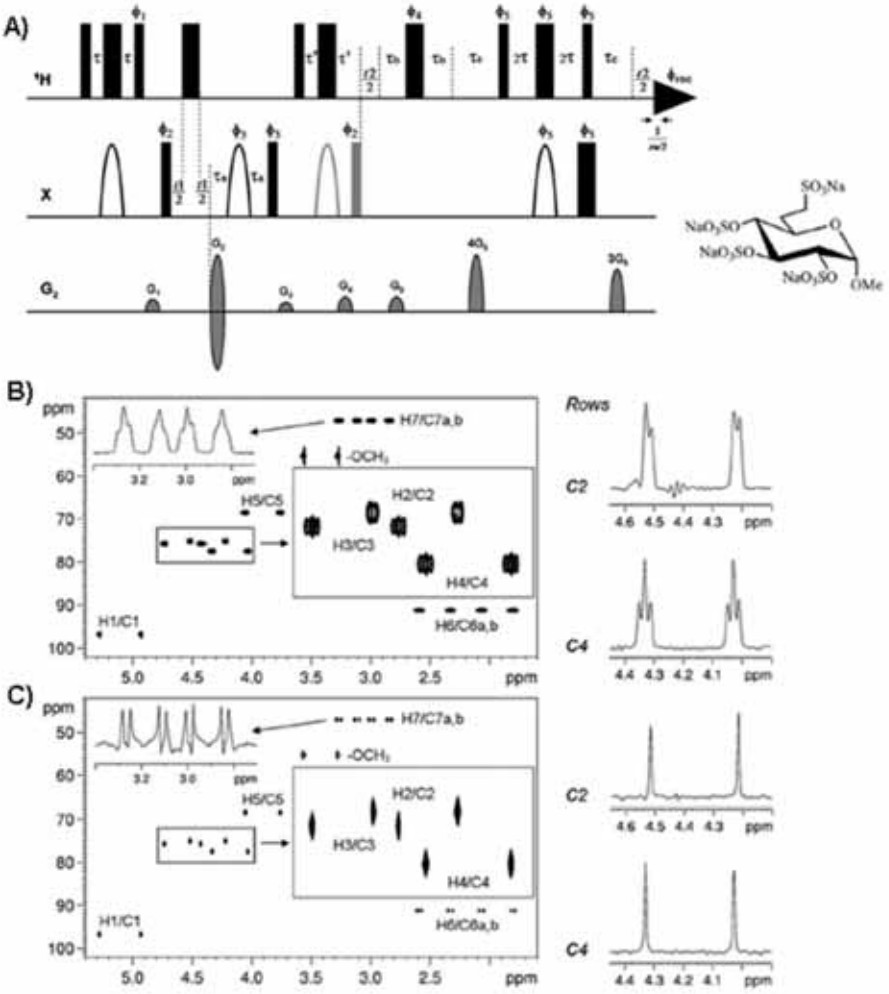

Figure 22. (A) Pulse scheme for the pseudo-3D homodecoupled CLIP/CLAP-HSQC experiment; expanded areas corresponding to the F2-coupled (B) conventional and (C) homodecoupled CLIP-HSQC spectra of tetra-sodium-(1-methyl-2,3,4-tri-O-sulfonato-6-deoxy-6-C-sulfonatomethyl-α-D-glucopyranoside dissolved in D_2O. Spectrum (C) was acquired with the pulse sequence of (A) using the same parameters as (B) and 16 FID data chunks. Reproduced with permission of reference.[23]

Analysis of near-identical ^{1}H and ^{13}C NMR spectra

Figure 25 outlines a schematic illustration showing how extremely high levels of signal dispersion can be achieved in a short range of frequencies by the simultaneous application of complementary resolution-enhanced NMR techniques. The whole ensemble of enhancements applied enables the *in situ* distinction and assignment of similar organic compounds exhibiting near-identical ^{1}H and ^{13}C NMR spectra in the same mixture.[149] Very small $\Delta\delta(^1H)$ and $\Delta\delta(^{13}C)$ have been distinguished and precisely determined, even in the presence of highly overlapped signals or severe chemical shift degeneracy in conventional 1D ^{1}H and $^{13}C\{^1H\}$ NMR spectra. Whereas $\Delta\delta(^1H)$ and $\Delta\delta(^{13}C)$ up to 3 and 17 ppb, respectively, can be established from the singlets obtained in 1D HOBS and ^{13}C NMR spectra, the high-signal dispersion achieved in spectral-aliased 2D HOBS-HSQC spectra allows an improvement in the level of detection to 1 and 5 ppb, respectively. This strategy combined with the use of HOBS versions of the HSQC-TOCSY and HSQMBC experiments has been used to unambiguously assign ^{1}H and ^{13}C chemical shifts for all peaks of different components of a complicated mixture. The proposed strategy proved to be very useful to facilitate the analysis of highly complex spectra, as found in many daily situations that exhibit high degeneracy of chemical shifts or severe signal overlap, such as the analysis of crude reactions, detection and characterization of intermediates, reaction monitoring or the analysis of complex mixtures.

Enantiodifferentiation studies

NMR has proved to be a valuable technique to determine enantiomeric purity using a great variety of auxiliary chiral sources, as, e.g. *chiral solvating agents* (CSAs). In the case of using CSAs,

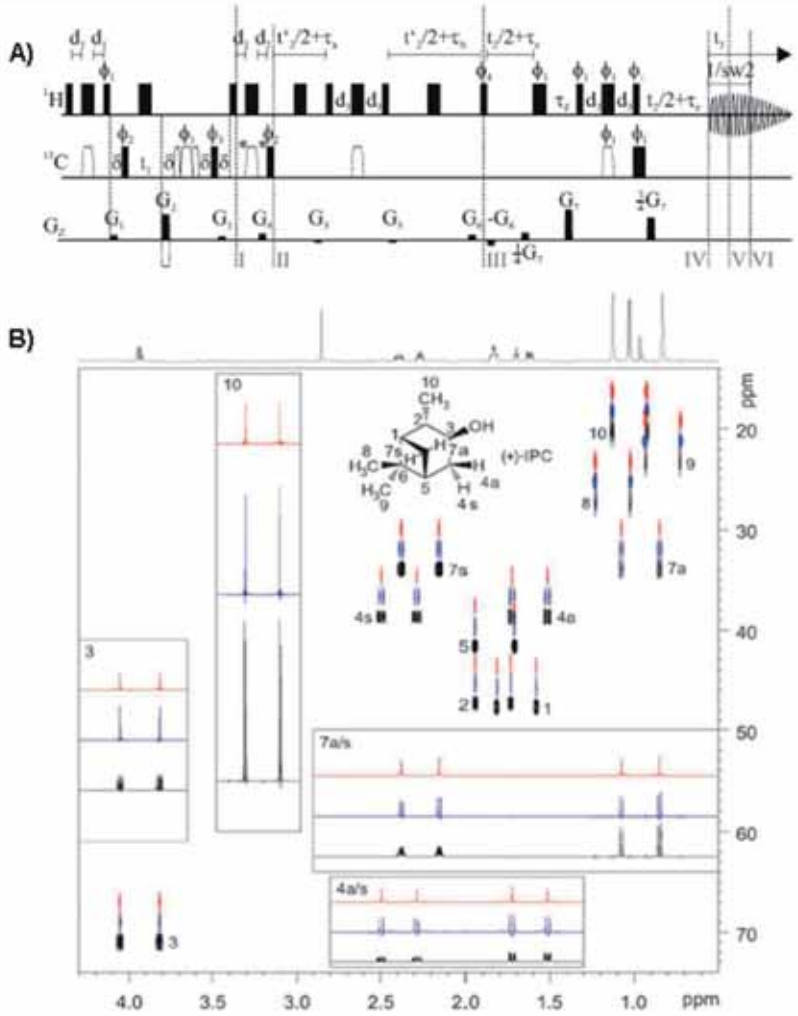

Figure 23. (A) Pulse scheme of the pseudo-3D homodecoupled CLIP-HSQC experiment incorporating a perfect BIRD inversion element. (B) F2-heterocoupled CLIP HSQC spectra without homonuclear decoupling (black) and with BIRD (blue) and with perfect BIRD (red) homonuclear decoupling during acquisition, collected for (+)-isopinocampheol in isotropic CD_2Cl_2 solution at 600-MHz proton frequency. Reproduced with permission of reference.[18]

theinitial indistinguishable mixture of enantiomers is converted into a chemical shift (δ)-resolved mixture of complementary diastereomeric complexes. As soon as there is enough chemical shift difference to achieve resolution between the signals of analogous nuclei in these diastereomeric complexes, the measure of enantiomeric purity can be carried out by direct signal integration. However, J_{HH} broadens ^{1}H NMR resonances, and accurate enantiomeric excess quantification is often hampered because of partial signal overlapping and low chemical shift. The features of homodecoupled experiments provide a great tool to avoid these overlapping problems.

Enantiodifferentiation studies involving chiral discrimination and the measurement of enantiomeric excess using some modern NMR methods, including pure shift NMR experiments, have been recently reviewed.[150] Two old classical experiments such as the conventional 1D $^{13}C\{^1H\}$ spectrum[151] or the use of the F2 projection in a 2D *J*-resolved experiments[86] offer simple set-up. An alternative method has been the distinction of different singlet lines along the indirect dimension of an F1-homodecoupled 2D spectra[152–154] or from the *z*-COSY experiment.[155]

Recently, two pure shift NMR approaches have been reported to carry out enantiodifferentiation studies using CSAs: (i) a fast determination from quickly acquired 1D HOBS spectra[124] and (ii) a 2D *spectral aliased pure shift* (SAPS) HSQC experiment.[24] In both cases, the relative sensitivity of standard 1D ^{1}H and HSQC experiments are retained and even improved because of the collapse of the signals to singlets (Fig. 26). In HOBS experiments, only the selected ^{1}H signals are studied but with full sensitivity. In practice, the experiment can be collected in a single scan, affording a powerful way to differentiate small chemical shift values into the same

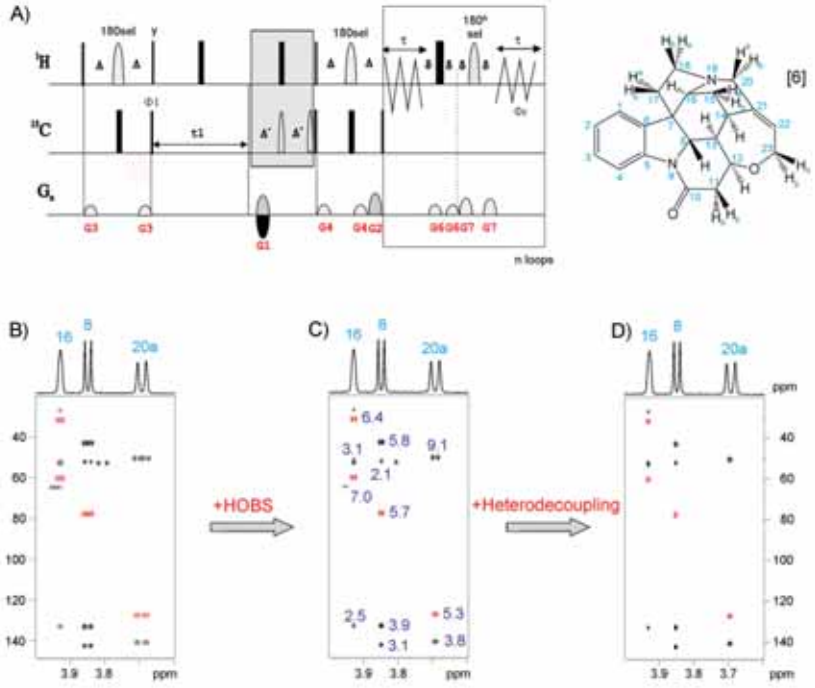

Figure 24. (A) Pulse scheme of the HOBS multiplicity-edited selHSQMBC experiment without heteronuclear decoupling during acquisition; (B) conventional ME-selHSQMBC experiment of strychnine [6] in $CDCl_3$ after selective excitation of the region around 4 ppm with a 12-ms RE-BURP 180° ^{1}H pulse; (C) HOBS-ME-selHSQMBC spectrum without ^{13}C heteronuclear decoupling showing a pure IP doublet pattern for all cross-peaks from which the magnitude of $^nJ_{CH}$ can be measured directly; (D) as (C) but with heteronuclear decoupling during acquisition, leading to a singlets for each individual cross-peak. Black and red cross-peaks represent C/CH_2 and CH/CH_3 multiplicities, respectively. Reproduced with permission of reference.[140]

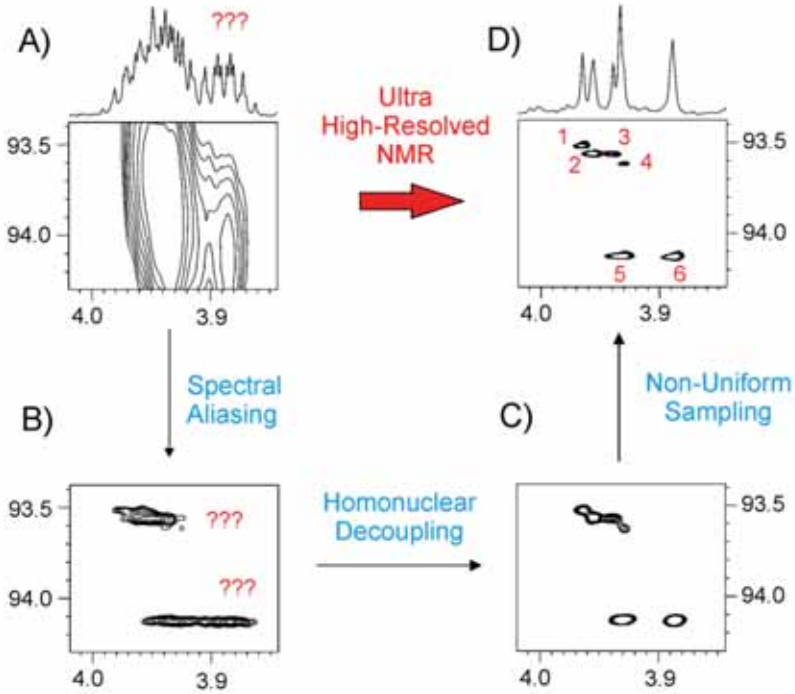

Figure 25. Schematic illustration of the resolution enhancements achieved after combining (B) spectral aliasing in the indirect dimension, (C) broadband homodecoupling in the detected dimension and (D) nonuniform sampling into a single ultra high-resolved HSQC experiment. Reproduced with permission of reference.[149]

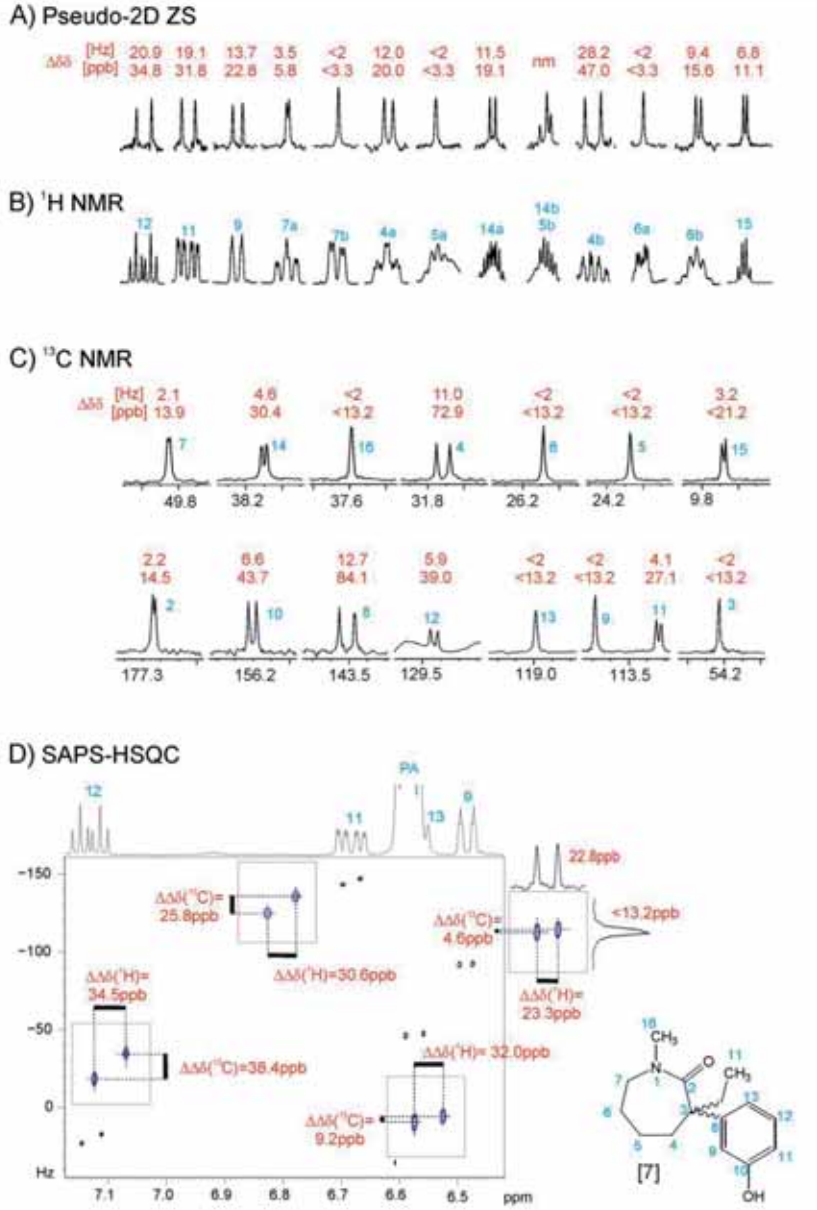

Figure 26. 600-MHz (B) conventional *versus* (A) pure shift ^{1}H multiplets; (C) ^{13}C{^{1}H} multiplets; (D) expanded aromatic area of the 2D SAPS-HSQC spectrum of racemic compound [7] complexed with 9.6 equiv. of *R*-PA in $CDCl_3$. Adapted with permission of reference.[24]

experimental time and using the same data processing as required for a conventional ^{1}H spectrum. It has been shown that the performance of the method can be improved by using multiple-frequency excitation simultaneously at different positions or appending a TOCSY transfer (1D HOBS-selTOCSY experiment) that can facilitate the analysis of signals in overcrowded areas, where conventional selective excitation could not be successfully applied. In Section on Comparison of ZS Methods, there is a comparative discussion on the results obtained from a pseudo-2D ZS, HOBB and HOBS spectra for a racemic mixture of (*RS*)-1-aminoindan complexed with Pirkle alcohol (Fig. 11). On the other hand, the combination of spectral aliasing and pure shift HSQC experiments represents an excellent routine tool for NMR enantiodifferentiation studies, yielding simultaneous ^{1}H and ^{13}C enantiodifferentiated data [$\Delta\Delta\delta(^{1}H)$ and $\Delta\Delta\delta(^{13}C)$] in short times and with high digital resolution and signal dispersion for both ^{1}H and ^{13}C nuclei. Signals that are not differentiated in conventional ^{1}H multiplets (Fig. 26A), pure shift 1D ^{1}H multiplets obtained from the pseudo-2D ZS experiment (Fig. 26B) or conventional ^{13}C peaks (Fig. 26C) can be distinguished in the SAPS-HSQC spectrum (Fig. 26D).[24] For instance, the excellent 2D dispersion of

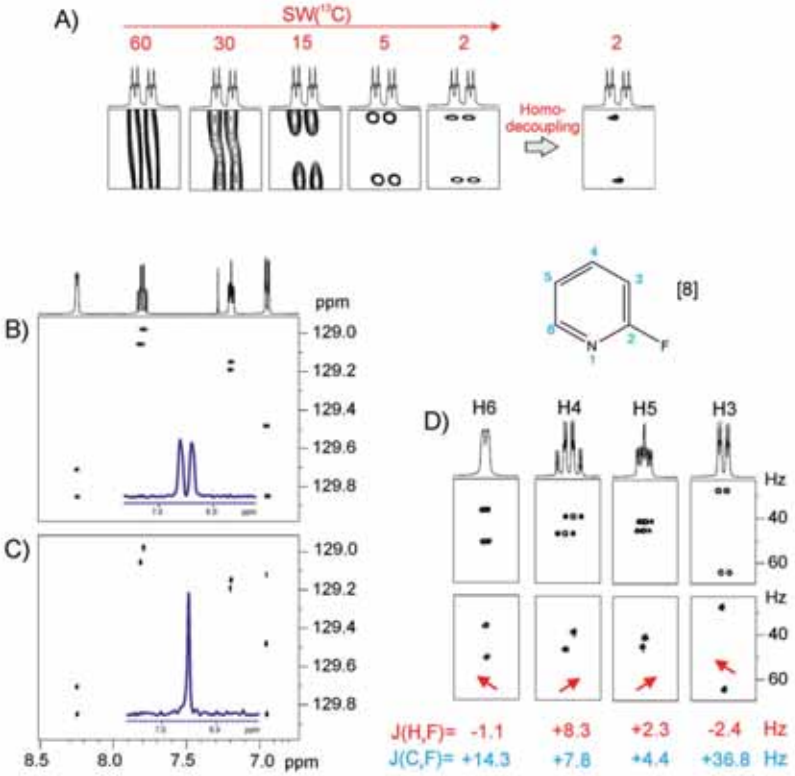

Figure 27. (A) Experimental effects on signal resolution after reducing SW(^{13}C) in HSQC experiments. In the right column, the additional benefits to add broadband ^{1}H homodecoupling along the detected F2 dimension can be appreciated. (B and C) 400-MHz 2D spectral-aliased ^{1}H-^{13}C HSQC spectrum of 2-fluoropyridine acquired with a reduced SW(^{13}C) of 2 ppm: (B) without and (C) with broadband BIRD-based ^{1}H homodecoupling in the F2 dimension. (D) Expanded cross-peaks showing the high levels of digitization and signal dispersion achieved for each experiment. Adapted from reference.[138]

the H9 protons (22.8 ppb) allows the separation of the two C9 carbons (4.6 ppb) in the SAPS-HSQC spectrum, which are indistinguishable in the 1D ^{13}C{^{1}H} spectrum.

Efficient measurement of heteronuclear coupling constants

It has been shown that the superb digital resolution achieved in SAPS-HSQC experiments allows the easy and simultaneous determination of the magnitude and the sign of J_{CX} and J_{HX} coupling constants (X = ^{19}F, ^{31}P or ^{2}H) from highly resolved E.COSY coupling patterns (Fig. 27).[138] The resulting 2D cross-peaks exhibit ultra-simplified multiplet patterns from which the measurement of the active J values is determined in a straightforward manner. As pointed out already, this general approach introduced in this study can be applicable in many experiments aimed at determining precise coupling constants along the indirect dimensions of 2D spectra.

Summary and outlook

In summary, a novel set of NMR experiments are now available for helping chemists to solve common problems encountered in their daily NMR activities. Modern pure shift NMR experiments afford simplified multiplet patterns that allow a much better analysis and interpretation of ^{1}H NMR spectra. Obtaining fully homodecoupled singlets for each proton resonance greatly minimizes the eternal problem of signal overlap. Several basic homodecoupling schemes have been evaluated, discussed and compared, and their implementation into the most standard 2D experiments has also been described. In addition, the combination with other complementary resolution-enhanced techniques tools excites the idea of ultra high-resolved NMR spectroscopy. The usefulness of these techniques have been demonstrated for a number of challenging practical applications, such as the determination of very small chemical shift differences, the analysis of highly crowded spectral regions, and the simplified and precise determination of relevant NMR parameters such as coupling constants, relaxation times or diffusion coefficients. Some challenges to improve even further the performance of these types of experiments will be of interest in the next future, such as the design of improved slice-selective methods that enhance absolute sensitivity, their robustness for a general and routine use, and the performance of perfect homodecoupling under strong coupling conditions, with a particular emphasis in the full collapse of diastereotopic CH_2 protons.

Acknowledgements

Financial support for this research provided by MINECO (project CTQ2012-32436) is gratefully acknowledged. We also thank the Servei de Ressonància Magnètica Nuclear, Universitat Autònoma de Barcelona, for allocating instrument time to this project.

References

[1] M. H. Levitt, R. Freeman, T. Frenkiel. *J. Magn. Reson.* **1982**, *47*, 328–330.
[2] A. J. Shaka, J. Keeler, T. Frenkiel, R. Freeman. *J. Magn. Reson.* **1983**, *52*, 335–338.
[3] A. J. Shaka, P. B. Barker, R. Freeman. *J. Magn. Reson.* **1985**, *64*, 547–552.
[4] E. Kupče, R. Freeman. *J. Magn. Reson.* **1995**, *115*, 273–276.
[5] R. Fu, G. Bodenhausen. *Chem. Phys. Lett.* **1995**, *245*, 415–420.
[6] K. Zangger, H. Sterk. *J. Magn. Reson.* **1997**, *489*, 486–489.
[7] N. H. Meyer, K. Zangger. *ChemPhysChem* **2014**, *15*, 49–55.
[8] R. W. Adams. *eMagRes* **2014**, *3*, 295–310.
[9] K. Zangger. *Prog. Nucl. Magn. Reson. Spectrosc.* **2015**, in press. DOI: 10.1016/j.pnmrs.2015.02.002.
[10] Y. Kown, S. Park, J. Shin, D. C. Oh. *Arch. Pharm. Res.* **2014**, *37*, 967–971.
[11] M. McCoy, L. Mueller. *J. Am. Chem. Soc.* **1992**, *114*, 2108–2112.
[12] J. Ying, F. Li, J. H. Lee, A. Bax. *J. Biomol. NMR* **2014**, *60*, 15–21.
[13] J. Farjon, W. Bermel, C. Griesinger. *J. Magn. Reson.* **2006**, *180*, 72–82.
[14] S. Paul, P. K. Madhu. *J. Indian Inst. Sci.* **2010**, *90*, 69–86.
[15] J. P. Garbow, D. P. Weitekamp, A. Pines. *Chem. Phys. Lett.* **1982**, *93*, 504–509.
[16] D. Uhrín, T. Liptaj, K. E. Kövér. *J. Magn. Reson.* **1993**, *101*, 41–46.
[17] T. Reinsperger, B. Luy. *J. Magn. Reson.* **2014**, *239*, 110–120.
[18] L. Kaltschnee, A. Kolmer, I. Timári, V. Schmidts, R. W. Adams, M. Nilsson, K. E. Kövér, G. A. Morris, C. M. Thiele. *Chem. Commun.* **2014**, *50*, 15702–15705.
[19] A. Lupulescu, G. L. Olsen, L. Frydman. *J. Magn. Reson.* **2012**, *218*, 141–146.
[20] L. Paudel, R. W. Adams, P. Király, J. A. Aguilar, M. Foroozandeh, M. J. Cliff, M. Nilsson, P. Sándor, J. P. Waltho, G. A. Morris. *Angew. Chem. Int. Ed.* **2013**, *52*, 11616–11619.
[21] J. A. Aguilar, M. Nilsson, G. A. Morris. *Angew. Chem. Int. Ed.* **2011**, *50*, 9716–9717.
[22] P. Sakhaii, B. Haase, W. Bermel. *J. Magn. Reson.* **2009**, *199*, 192–198.
[23] I. Timári, L. Kaltschnee, A. Kolmer, R. W. Adams, M. Nilsson, C. M. Thiele, G. A. Morris, K. E. Kövér. *J. Magn. Reson.* **2014**, *239*, 130–138.
[24] M. Pérez-Trujillo, L. Castañar, E. Monteagudo, L. T. Kuhn, P. Nolis, A. Virgili, R. T. Williamson, T. Parella. *Chem. Commun.* **2014**, *50*, 10214–10217.
[25] Y. Liu, M. D. Green, R. Marques, T. Pereira, R. Helmy, R. Thomas Williamson, W. Bermel, G. E. Martin. *Tetrahedron Lett.* **2014**, *55*, 5450–5453.
[26] J. A. Aguilar, G. A. Morris, A. M. Kenwright. *RSC Adv.* **2014**, *4*, 8278–8282.
[27] K. J. Donovan, L. Frydman. *Angew. Chem. Int. Ed.* **2014**, *54*, 594–598.
[28] R. Brüschweiler, C. Griesinger, O. W. Sørensen, R. R. Ernst. *J. Magn. Reson.* **1988**, *78*, 178–185.
[29] V. V. Krishnamurthy. *Magn. Reson. Chem.* **1997**, *35*, 9–12.
[30] K. Furihata, M. Tashiro. *Magn. Reson. Chem.* **2012**, *50*, 713–716.
[31] A. Cotte, M. Foroozandeh, D. Jeannerat. *Chim. Int. J. Chem.* **2012**, *66*, 764–769.
[32] W. L. Chuang, M. D. Christ, D. L. Rabenstein. *Anal. Chem.* **2001**, *73*, 2310–2316.
[33] J. Wang, D. Borchardt, D. L. Rabenstein. *Magn. Reson. Chem.* **2006**, *44*, 744–752.
[34] J. Wang, D. L. Rabenstein. *Anal. Chem.* **2007**, *79*, 6799–6803.
[35] K. Nguyen, D. L. Rabenstein. *Anal. Bioanal. Chem.* **2011**, *399*, 663–671.
[36] A. Kaerner, D. L. Rabenstein. *Magn. Reson. Chem.* **1998**, *36*, 601–607.
[37] K. Furihata, M. Tashiro. *Magn. Reson. Chem.* **2014**, *52*, 27–31.
[38] W. Kozmiński. *Pol. J. Chem.* **2000**, *1189*, 1185–1189.
[39] B. T. Martin, G. C. Chingas, O. M. McDougal. *J. Magn. Reson.* **2012**, *218*, 147–152.
[40] C. Mantel, P. A. Bayle, S. Hediger, C. Berthon, M. Bardet. *Magn. Reson. Chem.* **2010**, *48*, 600–606.
[41] P. Trigo-Mouriño, C. Merle, M. R. M. Koos, B. Luy, R. R. Gil. *Chem. Eur. J.* **2013**, *19*, 7013–7019.
[42] A. C. Pöppler, S. Frischkorn, D. Stalke, M. John. *Chemphyschem* **2013**, *14*, 3103–3107.
[43] J. Allen, K. Damodaran. *Magn. Reson. Chem.* **2015**. *53*, 200–202.
[44] T. Niklas, D. Stalke, M. John. *Chem. Commun.* **2014**, *51*, 1275–1277.
[45] B. Antalek. *Concepts Magn. Reson.* **2002**, *14*, 225–258.
[46] K. D. Park, Y. J. Lee. *Magn. Reson. Chem.* **2006**, *44*, 887–891.
[47] P. Sakhaii, B. Haase, W. Bermel, R. Kerssebaum, G. E. Wagner, K. Zangger. *J. Magn. Reson.* **2013**, *233*, 92–95.
[48] M. Vega-Vazquez, J. C. Cobas, M. Martin-Pastor. *Magn. Reson. Chem.* **2010**, *48*, 749–752.
[49] B. Sathyamoorthy, D. M. Parish, G. T. Montelione, R. Xiao, T. Szyperski. *Chemphyschem* **2014**, *15*, 1872–1879.
[50] G. E. Wagner, P. Sakhaii, W. Bermel, K. Zangger. *Chem. Commun.* **2013**, *49*, 3155–3157.
[51] N. M. Loening, M. J. Thrippleton, J. Keeler, R. G. Griffin. *J. Magn. Reson.* **2003**, *164*, 321–328.
[52] N. Giraud, L. Béguin, J. Courtieu, D. Merlet. *Angew. Chem. Int. Ed.* **2010**, *49*, 3481–3484.
[53] M. E. Di Pietro, C. Aroulanda, D. Merlet. *J. Magn. Reson.* **2013**, *234*, 101–105.
[54] S. Glanzer, E. Schrank, K. Zangger. *J. Magn. Reson.* **2013**, *232*, 1–6.
[55] L. Castañar, P. Nolis, A. Virgili, T. Parella. *Chem. Eur. J.* **2013**, *19*, 15472–15475.
[56] M. Foroozandeh, P. Giraudeau, D. Jeannerat. *Magn. Reson. Chem.* **2013**, *51*, 808–814.
[57] L. Frydman, T. Scherf, A. Lupulescu. *Proc. Natl. Acad. Sci. U. S. A.* **2002**, *99*, 15858–15862.
[58] N. Lokesh Suryaprakash. *Chem. Commun.* **2014**, *50*, 8550–8553.
[59] R. Freeman, E. Kupče. *Magn. Reson. Chem.* **2007**, *45*, 2–4.
[60] W. A. Anderson, R. Freeman. *J. Chem. Phys.* **1962**, *37*, 85–103.
[61] A. P. D. M. Espindola, R. Crouch, J. R. DeBergh, J. M. Ready, J. B. MacMillan. *J. Am. Chem. Soc.* **2009**, *131*, 15994–15995.
[62] D. Carnevale, T. F. Segawa, G. Bodenhausen. *Chem. Eur. J.* **2012**, *18*, 11573–11576.
[63] C. W. Vander Kooi, E. Kupče, E. R. P. Zuiderweg, M. Pellecchia. *J. Biomol. NMR* **1999**, *15*, 335–338.
[64] A. Hammarström, G. Otting. *J. Am. Chem. Soc.* **1994**, *116*, 8847–8848.
[65] E. Kupče, R. Freeman. *J. Magn. Reson. Ser. A* **1993**, 102, 364–369.
[66] J. P. Jesson, P. Meakin, G. Kneissel. *J. Am. Chem. Soc.* **1973**, *95*, 618–620.
[67] J. Weigelt, A. Hammarström, W. Bermel, G. Otting. *J. Magn. Reson.* **1996**, *110*, 219–224.
[68] V. D. M. Koroleva, N. Khaneja. *J. Chem. Phys.* **2012**, *137*, 094103.
[69] E. Kupče, H. Matsuo, G. Wagner. Homonuclear decoupling in proteins. in *Biological Magnetic Resonance, Volume 16: Modern Techniques in Protein NMR*, (Eds: N. R. Krishna, L. J. Berliner), **1999**, 149, 193–193.
[70] E. Kupče, G. Wagner. *J. Magn. Reson.* **1995**, *109*, 329–333.
[71] E. Kupče, G. Wagner. *J. Magn. Reson.* **1996**, *110*, 309–312.
[72] B. Vögeli, H. Kovacs, K. Pervushin. *J. Biomol. NMR* **2005**, *31*, 1–9.
[73] W. P. Aue, J. Karhan, R. R. Ernst. *J. Chem. Phys.* **1976**, *64*, 4226–4227.
[74] A. Bax, R. Freeman, G. A. Morris. *J. Magn. Reson.* **1981**, *43*, 333–338.
[75] A. J. Shaka, J. Keeler, R. Freeman. *J. Magn. Reson.* **1984**, *56*, 294–313.
[76] M. Woodley, R. Freeman. *J. Magn. Reson. Ser. A* **1994**, *109*, 103–112.
[77] M. Woodley, R. Freeman. *J. Magn. Reson. Ser. A* **1994**, *111*, 225–228.
[78] J. M. Nuzillard. *J. Magn. Reson.* **1996**, *118*, 132–135.
[79] S. Simanova, H. Sengstschmidt, R. Freeman. *J. Magn. Reson.* **1997**, *124*, 104–121.
[80] V. Mandelshtam, H. Taylor, A. J. Shaka. *J. Magn. Reson.* **1998**, *133*, 304–312.
[81] P. Mutzenhardt, F. Guenneau, D. Canet. *J. Magn. Reson.* **1999**, *141*, 312–321.
[82] M. J. Thrippleton, R. A. E. Edden, J. Keeler. *J. Magn. Reson.* **2005**, *174*, 97–109.
[83] A. J. Pell, J. Keeler. *J. Magn. Reson.* **2007**, *189*, 293–299.
[84] B. Luy. *J. Magn. Reson.* **2009**, *201*, 18–24.
[85] U. R. Prabhu, S. R. Chaudhari, N. Suryaprakash. *Chem. Phys. Lett.* **2010**, *500*, 334–341.
[86] S. R. Chaudhari, N. Suryaprakash. *Chem. Phys. Lett.* **2013**, *555*, 286–290.
[87] P. Sakhaii, B. Haase, W. Bermel. *J. Magn. Reson.* **2013**, *228*, 125–129.
[88] P. Sakhaii, W. Bermel. *J. Magn. Reson.* **2014**, *242*, 220–223.
[89] J. C. Cobas, M. Martin-Pastor. *J. Magn. Reson.* **2004**, *171*, 20–24.
[90] L. H. Lucas, W. H. Otto, C. K. Larive. *J. Magn. Reson.* **2002**, *156*, 138–145.
[91] C. Ludwig, M. R. Viant. *Phytochem. Anal.* **2010**, *21*, 22–32.
[92] A. J. Pell, R. A. E. Edden, J. Keeler. *Magn. Reson. Chem.* **2007**, *45*, 296–316.
[93] O. W. Sørensen, C. Griesinger, R. R. Ernst. *J. Am. Chem. Soc.* **1985**, *107*, 7778–7779.
[94] M. E. Girvin. *J. Magn. Reson. Ser. A* **1994**, 108, 99–102.
[95] F. J. M. van de Ven, M. E. P. Philippens. *J. Magn. Reson.* **1992**, *97*, 637–644.
[96] Y. Xia, G. Legge, K. Y. Jun, Y. Qi, H. Lee, X. Gao. *Magn. Reson. Chem.* **2005**, *43*, 372–379.

[97] M. Rance, G. Wagner, O. W. Sørensen, K. Wüthrich, R. R. Ernst. *J. Magn. Reson.* **1984**, *59*, 250–261.
[98] A. Bax, R. Freeman. *J. Magn. Reson.* **1981**, *44*, 542–561.
[99] A. G. Palmer, W. J. Fairbrother, J. Cavanagh, P. E. Wright, M. Rance. *J. Biomol. NMR* **1992**, *2*, 103–108.
[100] A. Bax, A. F. Mehlkopf, J. Smidt. *J. Magn. Reson.* **1979**, *35*, 167–169.
[101] B. T. Farmer, L. R. J. Brown. *J. Magn. Reson.* **1987**, *71*, 365–370.
[102] J. A. Aguilar, A. A. Colbourne, J. Cassani, M. Nilsson, G. A. Morris. *Angew. Chem. Int. Ed.* **2012**, *51*, 6460–6463.
[103] A. Bax. *J. Magn. Reson.* **1983**, *53*, 517–520.
[104] N. H. Meyer, K. Zangger. *Angew. Chem. Int. Ed.* **2013**, *52*, 7143–7146.
[105] J. A. Aguilar, S. Faulkner, M. Nilsson, G. A. Morris. *Angew. Chem. Int. Ed.* **2010**, *49*, 3901–3903.
[106] M. Foroozandeh, R. W. Adams, N. J. Meharry, D. Jeannerat, M. Nilsson, G. A. Morris. *Angew. Chem. Int. Ed.* **2014**, *53*, 6990–6992.
[107] S.R. Chaudhari, N. Suryaprakash. *ChemPhysChem* **2015**, *16*, 1079–1082.
[108] S. R. Chaudhari, N. Suryaprakash. *RSC Adv.* **2014**, *4*, 15018–15021.
[109] I. Timári, T. Z. Illyés, R. W. Adams, M. Nilsson, L. Szilágyi, G. A. Morris, K. E. Kövér. *Chem. Eur. J.* **2015**, *21*, 3472–3479.
[110] M. Nilsson, G. A. Morris. *Chem. Commun.* **2007**, 933–935.
[111] S. Islam, J. A. Aguilar, M. W. Powner, M. Nilsson, G. A. Morris, J. D. Sutherland. *Chem. Eur. J.* **2013**, *19*, 4586–4595.
[112] G. A. Morris, J. A. Aguilar, R. Evans, S. Haiber, M. Nilsson. *J. Am. Chem. Soc.* **2010**, *132*, 12770–12772.
[113] J. J. Koivisto. *Chem. Commun.* **2013**, *49*, 96–98.
[114] M. Foroozandeh, R. W. Adams, M. Nilsson, G. A. Morris. *J. Am. Chem. Soc.* **2014**, *136*, 11867–11869.
[115] S. Glanzer, K. Zangger. *Chem. Eur. J.* **2014**, *20*, 11171–11175.
[116] V. M. R. Kakita, J. Bharatam. *Magn. Reson. Chem.* **2014**, *52*, 389–394.
[117] N. H. Meyer, K. Zangger. *Chem. Commun.* **2014**, *50*, 1488–1490.
[118] L. Castañar, P. Nolis, A. Virgili, T. Parella. *Chem. Eur. J.* **2013**, *19*, 17283–17286.
[119] J. Ying, J. Roche, A. Bax. *J. Magn. Reson.* **2014**, *241*, 97–102.
[120] R. W. Adams, L. Byrne, P. Király, M. Foroozandeh, L. Paudel, M. Nilsson, J. Clayden, G. A. Morris. *Chem. Commun.* **2014**, *50*, 2512–2514.
[121] L. Castañar, P. Nolis, A. Virgili, T. Parella. *J. Magn. Reson.* **2014**, *244*, 30–35.
[122] L. Castañar, J. Saurí, P. Nolis, A. Virgili, T. Parella. *J. Magn. Reson.* **2014**, *238*, 63–69.
[123] J. M. McKenna, J. A. Parkinson. *Magn. Reson. Chem.* **2015**, *53*, 249–255.
[124] L. Castañar, M. Pérez-Trujillo, P. Nolis, E. Monteagudo, A. Virgili, T. Parella. *Chemphyschem* **2014**, *15*, 854–857.
[125] N. Gubensäk, W. M. F. Fabian, K. Zangger. *Chem. Commun.* **2014**, *50*, 12254–12257.
[126] N. Lokesh, S. R. Chaudhari, N. Suryaprakash. *Chem. Commun.* **2014**, *50*, 15597–15600.
[127] C. S. Johnson Jr. *Prog. Nucl. Magn. Reson. Spectrosc.* **1999**, *34*, 203–256.
[128] Y. Cohen, L. Avram, L. Frish. *Angew. Chem. Int. Ed.* **2005**, *44*, 520–554.
[129] G. Hamdoun, M. Sebban, E. Cossoul, A. Harrison-Marchand, J. Maddaluno, H. Oulyadi. *Chem. Commun.* **2014**, *50*, 4073–4075.
[130] P. B. Kingsley. *Concepts Magn. Reson.* **1999**, *11*, 29–49.
[131] P. B. Kingsley. *Concepts Magn. Reson.* **1999**, *11*, 243–276.
[132] H. Y. Carr, E. M. Purcell. *Phys. Rev.* **1954**, *274*, 630–638.
[133] S. Meiboom, D. Gill. *Rev. Sci. Instrum.* **1958**, *29*, 688–691.
[134] J. A. Aguilar, M. Nilsson, G. Bodenhausen, G. A. Morris. *Chem. Commun.* **2012**, *48*, 811–813.
[135] A. Cotte, M. Foroozandeh, D. Jeannerat. *Chimia* **2012**, *66*, 764–769.
[136] W. Reynolds, R. Breton, D. Burns. *Planta Med.* **2014**, *80*, IL26.
[137] S. Gil, J. F. Espinosa, T. Parella. *J. Magn. Reson.* **2010**, *207*, 312–321.
[138] N. Marcó, A. Fredi, T. Parella. *Chem. Commun.* **2015**, *51*, 3262–3265.
[139] A. Enthart, J. C. Freudenberger, J. Furrer, H. Kessler, B. Luy. *J. Magn. Reson.* **2008**, *192*, 314–322.
[140] J. Saurí, E. Sistaré, R. T. Williamson, G. E. Martin, T. Parella. *J. Magn. Reson.* **2015**, *252*, 170–175.
[141] D. Jeannerat. *Magn. Reson. Chem.* **2003**, *41*, 3–17.
[142] I. Baskyr, T. Brand, M. Findeisen, S. Berger. *Angew. Chem. Int. Ed.* **2006**, *45*, 7821–7824.
[143] D. Jeannerat. *J. Magn. Reson.* **2007**, *186*, 112–122.
[144] B. Vitorge, S. Bieri, M. Humam, P. Christen, K. Hostettmann, O. Muñoz, S. Loss, D. Jeannerat. *Chem. Commun.* **2009**, 950–952.
[145] G. B. B. Njock, D. E. Pegnyem, T. A. Bartholomeusz, P. Christen, B. Vitorge, J. M. Nuzillard, R. Shivapurkar, M. Foroozandeh, D. Jeannerat. *Chimia* **2010**, *64*, 235–240.
[146] M. Foroozandeh, D. Jeannerat. *ChemPhysChem* **2010**, *11*, 2503–2505.
[147] J. C. Hoch, M. W. Maciejewski, M. Mobli, A. D. Schuyler, A. S. Stern. *Acc. Chem. Res.* **2014**, *47*, 708–717.
[148] M. Mobli, J. C. Hoch. *Prog. Nucl. Magn. Reson. Spectrosc.* **2014**, *83*, 21–41.
[149] L. Castañar, R. Roldán, P. Clapés, A. Virgili, T. Parella. *Chem. Eur. J.* **2015**, in press, DOI: 10.1002/chem.201500521.
[150] S. R. Chaudhari, S. N. Suryaprakash. *J. Indian Inst. Sci.* **2014**, *94*, 485–516.
[151] M. Pérez-Trujillo, E. Monteagudo, T. Parella. *Anal. Chem.* **2013**, *85*, 10887–10894.
[152] N. Lokesh, S. R. Chaudhari, N. Suryaprakash. *Org. Biomol. Chem.* **2014**, *12*, 993–997.
[153] N. Nath, D. Kumari, N. Suryaprakash. *Chem. Phys. Lett.* **2011**, *508*, 149–154.
[154] N. Giraud, M. Joos, J. Courtieu, D. Merlet. *Magn. Reson. Chem.* **2009**, *47*, 300–306.
[155] U. R. Prabhu, N. Suryaprakash. *J. Magn. Reson.* **2010**, *202*, 217–222.

PULSE PROGRAMS
AND DATA SET EXAMPLES

In the following link are available all the Data Set Examples and the corresponding Pulse Program Code for Bruker of each Publication presented in this doctoral thesis.

http://sermn.uab.cat/2015/05/lauracastanar-phdthesis/